Development of an Improved Photometric Mode Identification formula for Pulsating Stars

GM. Mengistie

orcid.org/0000-0001-8053-2346

Msc. (University of Cape Town)

Msc. (Addis Ababa University)

BEd. (Jimma University)

Thesis submitted for the degree *Philosophiae Doctor* in *Physics*
at the Mahikeng Campus of the North-West University

Promoter: Prof Thebe Medupe

Graduation May 2018
Student number: 23981229

NWU®
NORTH-WEST UNIVERSITY
NOORDWES-UNIVERSITEIT
UNIBESITI YA BOKONE-BOPHIRIMA

Declaration of Authorship

I, Getachew Mekonnen Mengistie, declare that this thesis titled, "Development of an Improved Photometric Mode Identification Formula for Pulsating Stars" and the work presented in it are my own. I confirm that:

- This work was done wholly or mainly while in candidature for a research degree at the North-West University, Mafikeng campus.
- Where any part of this thesis has previously been submitted for a degree or any other qualification at this University or any other institution, this has been clearly stated.
- Where I have consulted the published work of others, this is always clearly attributed.
- Where I have quoted from the work of others, the source is always given. With the exception of such quotations, this thesis is entirely my own work.
- I have acknowledged all main sources of help.

Signed:
_____ Date:
_____

Abstract

Faculty of Natural and Agriculture Sciences
School of Physical and Chemical Sciences

by Getachew Mekonnen Mengistie

Stellar pulsations are found in stars that occupy different parts of the H-R diagram. Studying pulsations in stars is important in understanding the physics of their interiors. Identifying and studying the mode of pulsation of stars using photometry is crucial in understanding pulsating stars. We put more emphasis in studying pulsation modes because the information that we get from pulsating stars depends greatly on the number of modes identified.

In this thesis, a detailed review of stellar pulsation, mode identification techniques and radiative transfer equations are presented. Starting from the radiative transfer equations and by considering appropriate physical conditions and mathematical formulations, we derived a formula that describes the effect of pulsations in the light output of a star. We took into consideration the interaction of light with the different layers of the atmosphere. This is an improvement from previous studies where the atmosphere is treated as a single layer at $\tau = 2/3$. This thesis focused on improving the formula presented by Watson, ( ) and Watson, ( ) by using the idea introduced by Medupe, Christensen-Dalsgaard, and Phorah, ( ) due to the fact that treated the atmosphere of a pulsating star as a single layer and does not take into account the shape of the pulsation eigen function in the atmosphere. Thus high overtone pulsators that produces highly variable eigen functions in the atmosphere of A stars (Medupe, Christensen-Dalsgaard, and Phorah,) were not properly modeled. Therefore, in this thesis, we also investigated the depth dependence of eigen functions in the atmosphere of pulsating stars.

Our results demonstrate that the displacement eigen function $\frac{\delta r}{r}$, the temperature eigen function $\frac{\delta T}{T}$ and the opacity eigen function show great variability in the atmosphere of the equilibrium models studied. Our formalism is based on non-grey approximation where the pulsation equation and opacity depends on depth and frequency of observation. For a given stellar model, in general, luminosity variation caused due to pulsation is as a result of temperature, opacity perturbations and departure from radiative equilibrium ($I_\lambda - B_\lambda$). We also showed that the observed luminosity, for high overtone pulsators, comes from all the layers above the photosphere and the upper layer contributes the most. Moreover, from the equilibrium models considered in this study, the plots of the temperature eigen function as a function of depth demonstrated that, even with small T_{eff}, the atmosphere of a pulsating star will not be considered as a solitary and distinct layer as depicted by Watson, ( ) and Watson, ( ). In addition, this thesis also showed that the increase in temperature of the equilibrium models with high T_{eff}, the hydrogen ionization zone starts in the atmosphere of the pulsating stars. This thesis also shows the depth dependence of eigen functions in the atmosphere of pulsating stars.

Furthermore, we showed that our new formula reproduces Watson's formula at low frequencies. We caution that our model neglected convection and magnetic fields, thus our formula should be used with caution when applied to stars with strong magnetic fields such as $roAp$ stars or stars with sub-surface convection zone.

Acknowledgements

I would like to thank my supervisor Prof. Thebe Medupe for giving me this opportunity to work under him and introduced me to the field of Asteroseismology. I want to thank him for his many suggestions and constant support and guidance in each step of this work for successful completion. He taught me a lot from his wealth of experience in research. Words can not express my appreciation.

This journey was tough, rough and challenging in every aspect but with the help of God and people around me here in Mafikeng and back home in Ethiopia, I managed to push myself to the limit so as to get to this point. I want to thank every one who helped me in passing those hard times. God bless you all and thank you very much!!

I also want to thank the Department of Physics, Mafikeng Campus for all the assistances they provided me during my stay.

I would also like to thank my family: My mother W/ro. Asresie Kindie, brothers and sisters Addisu, Abebe, Muluken, Eng. Tefera, Dr. Demeke, Mimiye for your moral support, encouragement and prayers that kept me safe and gave me strength throughout my time. You are all gifts of God!! I thank you very much for every thing you did for me. My father (the late Ato Mekonnen Mengistie) you are and will be in my heart, you are the reason for being who I am now! I missed you! I love you all.

I would like to extend my appreciation to Prof. Eno Ebenso and MASIM research group for the support and encouragement during my stay in Mafikeng. It is worth mentioning the following colleagues from ESSTI, Prof. Solomon Belay, Ermias, Getinet, Wudu, Jerry, Alemiye, Dr. Birhan, Etsegenet, Firie, you are all wonderful thank you very much for the encouragement and your hospitality when I visited you.

It is worth mentioning and to thank Prof. Wassie and Sophonias Tsegaye for their moral support and encouragement during my time here in the Northwest University, Mafikeng, South Africa. I am also extremely grateful to the following people in the Mafikeng Campus, Dr. Chris Nditwani, Dr. Amare Abebe and his wife Dr. Maye Elmardi, Dr. Nahum Fajji, Mrs. Grace Fajji, Dr. Oyirowth Abedigamba, Dr. Bruno Letarte, Dr. Getinet Feleke, Mr. Solomon Makgamathe, Dr. Adedamola Shobo, Prof. Ashmore Mawire, Dr. Steven Katashaya, Dr. Dzinavatonga Dzina, Ms. Abigail Pori, Ms. Queen Molebatsi and Leratho (Science center) thank you very much, Daniel Nhlapo, Mr. Olebogeng Tlhapane, Ms. Tlotlo Lefenya who helped and encouraged me during my stay here in Mafikeng Campus. In addition, I would like to thank my colleagues: Heba, Joseph, Ndaba, Karabo, Phantsi and Katlego for the good times we had in 1042(46664!). I will not forget those sleepless nights! Thank you very much!

I want to extend my gratitude to my friends Kirubel, his wife (Sabina) and their son Kidus (Chonbie), I want to thank you for your support, encouragement and your unreserved hospitality, I am very lucky to have you as a family and friend. Thank you very much!!

Yidnek, his wife (Meski) and their son Yomi thank you very much for making the beginning of my study in Mafikeng interesting by providing me everything that I wanted God bless you all.

Kissenger, his wife (Geni) and their children, many thanks for all the things you helped me. Kissenger thank you very much for your unreserved hospitality. You are a wonderful person with an amazing personality many thanks and God bless you. This study would have not been possible without your assistance at the beginning.

The late Abebaw (RIP), his wife Kidist and their sons (Alazar and Joseph) thank you very much for the support, encouragement and everything you did for me God bless you all. Biniyam and his wife Mihret, Almi (what a kind person) (I am lucky to know you), Alex thank you very much for your support! God bless you all.

My friends Wubie, Teferi thank you very much for those wonderful times and your encouragements during those challenging times in Mafikeng. You are a wonderful people with a very nice personality. I am blessed to have you guys as friends and family. Tefie, I will never forget your contribution to my studies in all aspects, you have a heart that cares and Loves that is a gift from God. God bless you and your family! Esayas Sisay thank you very much for every thing you did for me. I also want to thank Dr. Yihunie Asres for the advice, friendship, assistance and good times we had in Mafikeng. Gashie Akushenshinew ena erat limita! Thank you!!

I also wanted to thank Tigistu Kifle and his wife Emu, Diakon Tefera Bizuneh, I can not find words to express my appreciation for your support, encouragements, hospitality and prayers. Thank you very much!!

I would like to thank the three examiners who took their precious time to read my work and gave their constructive criticism and complement my work and make it readable.

Last but not least, this is also a great opportunity to thank the Mafikeng St. Gebriel congregation for their unconditional support and prayers that gave me the courage and endurance that helped me to be stronger and work harder to this point. Thank you very much for your prayers.

"Medihanialem Abatie!!"

Contents

List of Figures

List of Tables

List of Abbreviations

HR diagram	Hertzsprung **R**ussell diagram
AAVSO	Association of **V**ariable **S**tar **O**bservers
MOST	Microvariability and **O**scillations of **S**tars
WIRE	**W**ide **F**ield **I**nfrared **E**xplorer
HST	Hubble **S**pace **T**elescope
TESS	**T**ransiting **E**xoplanet **S**urvey **S**atellite
PLATO	**P**lanetary **T**ransits and **O**scillations of **S**tars
RGB	**R**ed **G**iant **B**ranch
ZAMS	**Z**ero **A**ge **M**ain **S**equence
AGB	**A**symptotic **G**iant **B**ranch
LMC	**L**arge **M**agellanic **C**loud
SPB	**S**lowly **P**pulsating **B** star
CoRoT	**Co**nvection, **Ro**tation et **T**ransits **P**lanetaires
RoAp	**R**apidly **O**scillating **Ap** stars
TDC	**T**ime **D**ependent **C**onvection
PNNV	**P**lanetary **N**ebula **N**uclei **V**ariable
LAOL	**L**os **A**lmos **O**pacity
LLNL	**L**awrence **L**ivermore **N**ational **L**aboratory
ODF	**O**pacity **D**istribution **F**unction
LTE	**L**ocal **T**hermodynamic **E**quilibrium

This PhD. thesis is Dedicated to my family

Chapter 1

Introduction

1.1 Motivation

Different classes of stars pulsate in radial, non-radial and some in a combination of both (Gautschy and Saio, ; Joshi and Joshi,). A study of these pulsations is critical in understanding the detailed physics of the interior of stars in a way that is not possible by normal analysis of star light. This is because star light comes from the photosphere which is the shallow part of a star; the layers below the photosphere being opaque. The advantage of using stellar pulsations to probe the physics of stellar interiors is that they are caused by sesmic waves inside a star. These sesmic waves are primarily p-modes, g-modes and are sensitive to the different parts of a star through which they travel. Thus, by detecting and identifying the pulsation modes in a pulsating star we can infer the physics of the interior of a pulsating star. Furthermore, the larger the number of pulsation modes detected and identified in a star, the greater the amount of information that can be obtained.

This thesis looks at the commonly used formula for identifying pulsation modes from the multicolor photometry of stars. This formula was first presented by Dziembowski, ( ), Buta and Smith, ( ), Stamford and Watson, ( ) and Stamford and Watson, ( ), Watson, ( ) and Watson, ( ). Daszyńska-Daszkiewicz, Dziembowski, and Pamyatnykh, ( ) used this formula (which in this thesis we shall call Watson's formula) combined with radial velocity data to successfully identify modes in δ Scuti stars. In Chapter 3, we present this formula and show how it is derived. One of the challenges with Watson's formula is that it treats stellar atmosphere as a single layer. It therefore does not take into consideration the shape of the pulsation eigen functions in the atmosphere of pulsating stars. This ignores the fact that high overtone pulsations produce highly variable eigen functions in the atmosphere of A stars (Medupe, Christensen-Dalsgaard, and Phorah, ; Medupe, Kurtz, and Christensen-Dalsgaard,).

In this thesis, we investigate this depth dependence of eigen functions in the atmosphere of A stars to see how it changes the mode identification formula discussed above. This project is, therefore, designed in such a way that it fills the gaps and addresses the following objectives:

- Review critically mode identification methods.
- Calculate the opacity κ_ν of pulsating stars by using ATLAS9 to derive an improved mode identification formula.
- Test and compare the improved mode identification formula with that of Watson (1988) and other literature.

Hence, to address the aforementioned objectives and fill gaps, this project is structured in the following way:

The first part of the thesis, motivation and why we need to do this work is addressed. The introduction gives an overview of how the study of stellar pulsation started and gives a summary of how it has developed as a research field. The introduction also provides a detailed literature review of stellar pulsation across the HR diagram. Moreover, the introduction also provides a detailed explanation of pulsation across the HR diagram. In this section, pulsating stars across the HR diagram are explained in detail including their composition, temperature, mode of pulsation and causes of pulsation. In the second chapter, the theory of stellar pulsation is explained. In this chapter, stellar atmosphere, stellar structure is discussed in detail. Furthermore, both radial and non radial oscillations are summarized in this chapter. Also, linear adiabatic pulsation theory as well as stellar opacity and sources of stellar opacity are summarized. In addition, the summary of mode identification techniques are revised and presented. The third chapter presents the full derivation of Watson's flux variation formula. In chapter 4, we present the derivation of the new photometric mode identification formula. This chapter also presents the mathematical derivations of the new mode identification formula using the radiative transfer equations and intensity perturbations. This chapter is followed by the results of our new formula for photometric mode identification. We also show that the contribution for the observed flux comes not only from $\tau = 2/3$ as Watson, ( ) and Watson, ( ) stated but also from different regions of a pulsating star whereby the layer very close to the outer surface contributes more. In the last section of this chapter, we are going to present the conclusion of this work.

1.2 Brief History of Stellar Pulsation Studies

The oldest records of sky watching are dated 2000BC. and 1000BC. by people in the near and far East respectively (Percy,). During those times, human beings consciously or unconsciously watched the sun, the clear night sky and noticed the stars. They might also have an impression that stars are quite, dull and static objects. They also noticed the change in times (variation in day and night). Even out of curiosity, they might noticed variations of stars(change in brightness). There are also other evidences like paintings, rock carvings and bone carvings. In addition, alignments of giant stones, as evidenced using Archaeoastronomy, are also further evidences to prove humans' curiosity for observing stars (Percy,).

Peoples curiosity was further supported by the introduction of telescopes by Galileo Galilei $(1564 - 1642)$. Until that time there was no use of the telescope for astronomical studies. After Galileo Galilie, the use of telescopes to study astronomy became widely spread. Despite implementing telescopes for astronomical studies, the discoveries of variable stars surprisingly happened by random chance.

The study of pulsating stars started way back in 1572 when Tycho Brahe discovered his Stella Nova in the constellation of Cassiopeia and the discovery of the first known periodic variable star Mira in 1596 by the astronomer David Fabricius (1564-1617).

In the early stages of studying variable stars, astronomers took substantial amount of time to accept the existence of variable stars as there was a change in school of thought from Aristotelian to Copernicus (Gautschy,). Further in that line, between the 16^{th} and 17^{th} century, Galileo and Kepler enhanced the observations of variable stars, which were previously assumed to be novae or supernovae. Among the observational results, the first observation or discovery of the variable stars was made in 1784 by Goodricke. He was the pioneer to observe the periodic and asymmetric light variation of δ-Cephei stars; at the same time as he discovered eclipsing binaries (β-lgrae).

One of the great breakthroughs in the discovery of variable stars was associated with William Herschel (1738 – 1822) because of his innovative work on the development of large reflecting telescopes. He discovered two variable stars $44i$ Bootis and α Herculis Percy, ( ).

Further developments in studying variable stars grew when the British Astronomical Association created the variable star observers group in 1890. Similarly, in 1911 the American association of variable star observers (AAVSO) was established in Cambridge. Its main objective was to get observational results from members and collaborators across the world. The table below summarizes the early discoveries of variable stars with the year, type and spectrum of the stars.

TABLE 1.1: Summary of Early Variable Stars Discovered

Name	Year	Type	Period	Spectrum	Discoverer
OCeti	1596	Mira	372	M5e-M9e	Fabricius
β Persei	1667	EA	2.87	B8V	Montanari
ξcygni	1686	M	408	S6.2e-S10.4e	Kirch
R.Hydrae	1704	M	384	M6e-M9e	Maraldi
R.Leonis	1782	M	310	M6e-M9.5IIIe	Koch
β Lyrae	1784	EB	12.9	B8II-IIIep	Goodricke
η Aquilae	1784	δ Cep	7.18	F6IB	Pigott
δ Cephei	1784	δ Cep	5.37	F5-G1IB	Goodricke
R cr B	1795	RCB	–	GoIeP	Pigott
αHerculis	1795	SRC	–	M5Ib-II	W.Herschel
R Scuti	1795	RVa	147	G0Iae-K2pIbe	Pigott

As in the table shown, the star first discovered by Fabricius has a long period and is named O (Omicron) Ceti. Johann Bayer in 1603 proved that this star is found in the constellation of Cetus. In his first observational result from (August 3- August 21), Fabricius noticed the change in magnitude from 3 to 2 later in September 1596. It faded and completely disappeared in October (Clerke 1902). Due to this fact, he assumed the star was a nova but against all odds the star reappeared. Though this particular star had a strange behavior, it was forgotten for a long time until Johann Fokkesens Holward (1618 – 1651) observed and rediscovered it in 1638 and determined the period of oscillation to be 11 months. On November 7, 1639 Johannes Hevelius (1611 – 1678) discovered one of the variable stars and labeled it as Mira, *"The Wonderful Star"* in 1642 (Hoffleit,).

Studies of variable stars further continued due to the introduction of photography and later Spectroscopy (Spectral classification of stars for better understanding). The introduction of Spectroscopy by H. Draper in 1872 paved a way for enormous research in spectral studies. This analysis further helped to classify variable stars based on their temperature as well as their luminosity. Spectroscopy also played a major role to provide sufficient information to extract the chemical composition of the stars (Percy,). The following table, Table 1.2 summarizes the number of variable stars discovered from the early conception of variable stars observation.

When we discuss about the discovery of variable stars, the contribution from Fleming was a lot especially when she was studying variable stars at Harvard. Her study emphasized on the development of spectral analysis to classify stars. In her analysis, Fleming discovered the hydrogen line in emission for O Ceti as well as the absorption line for M-type spectra (Hoffleit,). During the early times of discovery of variable stars, the mere purpose was just to keep records. But during the turn of the century, there was plenty of efforts made to understand and study stars based on fundamental laws of physics. Using this as a stepping stone, Baker and Kippenhahn, ( ) presented the first numerical analysis result to explain the instability of Cepheid- type stars. Moreover, the

TABLE 1.2: Summary of variable star catalog showing the discovery of variable stars:courtesy to Cambell (1941)

Year	Authority	Variable
1786	Pigott	12
1844	Argelander	18
1866	Schoenfeld	119
1896	Chandler	393
1907	Cannon	1425
1920	*Müller* and Hartwig	2054
1930	Prager	4611
1936	Prager	6776
1941	Schneller	8445

use of computers as a tool to analyze stellar pulsation paved a way for more analysis. Due to this fact, the theory of stellar pulsation was developed and numerical solutions to differential equations describing the state of a pulsating star were obtained easily. All these developments contributed for the development of stellar pulsation theory, which is used as a tool to study stars, their structure, composition as well as pulsation modes. Following the introduction of numerical solutions for stellar theory equations, the research in the theory of stellar pulsation drastically increased (King and Cox,). More researches were conducted throughout the entire progress after the first discovery of the variable star. But there was an intriguing discovery which was the temperature variations of Cepheids which supports the pulsation hypothesis leading to the disapproval of Cepheids as binary systems Eddington, ( ) and Zhevakin, ( ). All these misunderstandings were cleared when Plummer and Shapely in 1914 proposed and devised mathematically the pulsation theory. Moreover, the confusion was cleared when Eddington, ( ) showed that the light changes or variations are due to pulsation of a single star. Furthermore, Eddington, ( ) wrote an article about stellar pulsation which plays a key role in establishing the theory of stellar pulsation. He also published papers which played a fundamental role in formulating the theory of conservative (adiabatic) free radial oscillations of gaseous spheres (Eddington, ; Zhevakin,). In addition, Eddington realized the driving mechanism which makes the star pulsate. It is a process that transforms thermal energy into mechanical energy and it consider the stars as thermodynamical engines (Zhevakin,). In this process, energy gain and dissipation complement each other and the process is governed by the equation given below:

$$W = -\int_M \oint \frac{\delta T}{T} dQ dm, \tag{1.1}$$

where W is the magnitude of the dissipation of mechanical energy of oscillation, $\frac{\delta T}{T}$ is the relative change of temperature at time t in the mass element dM and dQ is the quantity of heat put into dM in the time dt (Zhevakin,). The first integral is taken overall of the elements of the 'working body'. On the other hand, the closed integral is taken over the time of the oscillation.

Eddington, ( ) in his paper published about stellar pulsation theory and explained the problem regarding dissipation of pulsation energy which is associated to the oscillation of gaseous star decay. He also observed that the pulsation modes cannot last long from the energy generated from the compression. He also discussed phase lag and stated that the star's maximum brightness does not occur at maximum compression (contraction). In his subsequent works Eddington, ( ) associated this phenomenon with the non-adiabatic effect. He suggested that the temperature variation should be in phase with the variation in density and the variation in radius/velocity.

Rosseland, ( ) stated the possible cause of phase lag as dissipation of wave energy by viscosity and conduction. Further investigations by Castor, ( ) who developed analytical expression by considering the H-ionization zone (it is a region with constant temperature of T$\backsimeq 10^4$K where its contribution to instability is negligible). Castor, ( ) also considered the H-ionization zone as a discontinuity and by considering additional properties similar to the ones in the Cepheid instability strip, he concluded that the luminosity changes very closely in phase with the outward radial velocity.

According to Cox, ( ), the calculations in the phase lag between luminosity and outward velocity lacks a clear understanding of the cause of the phase lag. Because of the controversies, Castor, ( ) proposed a new theory for the phase lag. He suggested, especially for RR Lyrae and Cepheid stars, the cause of the phase lag is linear phenomenon or linear theory which is affected by non-linear effects with larger amplitudes. In addition, he also claimed that omission of convection inside the star can produce a better match with observations. Therefore, the results produced by Castor, ( ), the one which is widely accepted theory, where he indicated that the H-ionization zone is the cause of phase lag between light and radial velocity curve. Developments in studying stellar pulsation extended further when Edgar, ( ) calculated the solution for the standard model of pulsation and obtained the fundamental and first overtone solutions. Furthermore, Edgar, ( ) tried to separate the temporal component into $e^{i\delta_k t}$, where δ_k is the oscillation frequency which is a complex quantity. He also introduced a quasi-adiabatic approximation for stellar pulsation but did not realize the cause that makes stars unstable. More on the cause of stellar pulsation will be presented later in this thesis.

1.3 The Modern Age of Stellar Pulsation

Since the discovery of Mira variable stars, a lot had happened in developing theoretical formulations of stellar pulsations as well as observations by making use of both ground and space based observations. In this section, the emphasis is to give a brief overview of groups involved in observing stellar pulsation and studying them.

In addition to the introduction of computers for modeling and computing theoretical challenges in pulsation, observation with sophisticated techniques and softwares were conducted from ground based observatories. Furthermore, astronomers used space based telescopes to conduct studies on pulsations of stars. Introduction and advancement of astronomical spectroscopy and its implementations in studying variable stars also played a major contribution in understanding variable stars. The advancements of telescopes immensely contributed in studying stellar pulsation. Moreover, developments in optical telescopes and consortium of telescopes working together with high resolving power and observation for 24 hours to get complete and more reliable data played major role in enhancing studying variable stars.

Further developments and achievements in studying astronomy was to put optical telescopes in space (Percy,). One of the very important optical telescopes in space with high resolution till to date is the Hubble Space Telescope (HST).

In addition to Hubble telescope, Micro variability and Oscillation of Stars (MOST) satellite, and CoRoT are all providing necessary information about stars. All the data gathered from observation is analysed using super fast computers which enhances the design and modelling of variable stars that are physically complicated.

Variable star studies can be conducted from both ground based as well as space based observatories. In addition, observations from a single telescope may not give a complete follow up of the study target under consideration due to the daylight which literally brings a gap in the observation

Catelan and Smith, ( ). Astronomers use different ways to avoid this discrepancy and get time series data with no gaps. This is done by observations conducted in consortium whereby observatories are located in different places of the earth at separate longitudes which gives an opportunity to observe a target star for longer duration Catelan and Smith, ( ).

Researchers investigated several alternatives to avoid the gap created from ground based observations. Therefore, they come up with the idea of putting space based observatories. Due to the fact that space based observatories help to track and observe a variable star without any interruption. It is also possible to observe on different wavelengths which can not pass through the earth's atmosphere.

In addition to the Hubble Telescope, space based instruments designed to observe variable stars were launched. Among these, MOST (Microvariability and Oscillations of STars) Matthews, ( ) which was launched in June 2003, CoRoT (Convection, Rotation and Planetary Transits) Baglin et al., ( ) and Karoff et al., ( ) which was launched on 27^{th} December 2006 and can observe up to 150 days to do asteroseismic investigations. Even though its primary objective was to find earth like planets, KEPLER (Borucki and Koch, ; Koch et al., ; Koch et al.,) also contributes a lot in studying pulsations of stars.

According to Catelan and Smith, ( ) and Buzasi, ( ) a satellite called WIRE (Wide Field Infrared Explorer), where its primary target was not tracking variable stars failed after launch, but its star tracker contributed immensely in doing asterosesmic research.

The study of variable stars from space based observations grows tremendously and the future looks bright because further developments and building satellites are under way. Transiting Exoplanet Survey Satellite (TESS) is an all sky survey mission whose target is to monitor more than 500, 000 stars to look for earth sized planets. TESS is going to be launched in 2018 and will look for planets around bright stars. In this process, it will help astronomers analyze data and look for stellar pulsation. Moreover, the European Space Agency's PLATO2.0 (Planetary Transits and Oscillations of Stars) (Rauer et al.,) mission to be launched into space in the year 2022/24, will play a significant role in understanding variable stars. Its contribution is going to be high precision, long term photometric and astroseismic monitoring by covering 50% of the sky and monitoring millions of stars. These missions further enhances and paves a way for the advancement of space based asteroseismic studies.

1.4 KEPLER's contribution in studying stellar pulsation

KEPLER mission is a space telescope launched in 2009 with the sole purpose of finding Earth like planets in the habitable zone of solar-like stars. Due to its high quality instrumentation, *Kepler* contributed in the discovery of other stellar objects. Among other things, Kepler's contribution in discovering variability of stars is significantly high (Koch et al., ; Koch et al., ; Borucki and Koch,).

Prša et al., ( ) showed the first eclipsing binary stars catalog due to the fact that the contribution of binary stars, especially eclipsing binaries, in studying astrophysics to determine their mass and radius, which in turn help to study stellar evolution and study asterosesimology. Grigahcène et al., ( ) did asteroseismology for γDoradus and δ Scuti stars where they demonstrated that the former pulsates in high-order g-mode ($\approx$ 1day) and the latter pulsates with low order g and p modes ($\approx$ 2 hours) period. Moreover, using *Kepler's* observational data, they discovered hybrid stars. *Kepler* observation data also contributed in discovering some RR Lyrae stars. Some of the RR Lyrae stars, known as Rab showed Blazhko effect (periodic amplitude and phase modulation of light curves, with time range between $10 - 100$ days) (Kolenberg et al.,). Further studies

from *Kepler* mission by Stello et al., ( ) in the open cluster NGC6819 demonstrates the discovery of solar like pulsations. In their analysis, they managed to determine, $\Delta\nu$ (large frequency separation) and ν_{max} (frequency of maximum pulsation). Moreover, results obtained from asterosesmic analysis helped Stello et al., ( ) to determine cluster membership. *Kepler* mission significantly contributed in discovering Solar-like oscillations in red giants by using time series photometry Bedding et al., ( ). Furthermore, from the data obtained from Kepler, Bedding et al., ( ) demonstrated the strong relationship between $\Delta\nu$ and ν_{max}. More studies using data obtained from Kepler demonstrates the abundant capacity of *Kepler* in studying asteroseismology of red giants and Solar-like oscillators. On the other hand, Chaplin et al., ( ) used *Kepler* data to study G-type stars and demonstrated that all the G-type stars behave as Solar-like pulsators with high signal to noise. Moreover, from their analysis, mass, radii and age of the G-type stars were determined. Additional studies from *Kepler* data was done by Balona, ( ) to study long periods in roAp stars (KIC10483436) and (KIC10195926) with their frequency given as $\nu_{low} \approx \frac{1}{2}\nu_{rot}$, where ν_{low} is low frequency and ν_{rot} is rotational frequency. Furthermore, Balona et al., ( ) used *Kepler* data to study the open cluster NGC6819 and determined the age and distance of the cluster. In addition, they demonstrated that this cluster is made up of δScuti, γ-Dor and different kinds of eclipsing binaries. Moreover, Balona, ( ) also used Kepler's data to study rotation and variability in the cluster NGC6866. In general, despite the fact that its primary target was not to study variability, the Kepler asterosesmic investigation group contributed immensely in understanding variability and study asteroseismology for different kinds of stars. Kepler mission is also playing a fundamental role in understanding binary stars (especially eclipsing binary system) and their mode of pulsation. Recent investigations from *Kepler* data was done by Fox-Machado and Pérez Pérez, ( ) to do asterosesmic analysis of δ-Scuti star KIC6951642, that shows pulsation in both g mode (period between $0 - 4$ c/d), and it is a manifestation to γ-Dor stars and p mode (period between $8 - 20$ c/d), and it is a characteristic of δ-Scuti stars. These characteristics are manifestations of KIC 6951642 to be considered as a hybrid pulsator. More analysis and study to do asteroseismology of δ-Scuti stars in binary stars was also conducted by Liakos and Niarchos, ( ) using *Kepler* data. They investigated and compared the behavior of single δ-Scuti star and the δ-Scuti star in the component of binary system. They showed that their evolution and pulsation behavior differ substantially.

1.5 Why We Need to Study Pulsation in Stars?

Pulsating stars are classes of variable stars whose light is periodically changing due to intrinsically caused expansion and contraction of the star's surface. This is basically related to the wave propagated through the interior of the star (Zhevakin, ; King and Cox,). The study of pulsating stars is a very broad research area whereby studying pulsation instabilities enhances the possibility of deriving constraints on stellar physical mechanisms that would not be accessible by other methods. Moreover, it plays a fundamental role in analyzing the internal structure of stars and helps us to improve the fundamental issues in stellar structure theory and stellar evolution models (Aerts, Christensen-Dalsgaard, and Kurtz,). Investigating the fundamental principles of stellar astrophysics, especially in stellar evolution theory, relies heavily on the information gathered and analyzed from the physical processes in the stellar interiors.

In a book, The Internal Constitution of the stars by Eddington, ( ) stated: "*At first site it would seem that the deep interior of the sun and the stars is less accessible to scientific investigation than any other region of the universe our telescopes may probe farther and farther in to the depths of space; but how can we ever obtain certain knowledge of that which is hidden behind*

substantial barriers? What appliance can pierce through the outer layers of a star and test the conditions within?".

Through a lot of dedication and hard work, astronomers come up with an idea that can help not only to investigate stellar interiors but also to see the inside of a star. Such commitments lead to the introduction of a research area called Asteroseismology ("The real music of stars") emerged (Aerts, Christensen-Dalsgaard, and Kurtz,). Asteroseismology is the study of the internal structure of star by studying and analyzing the frequencies of oscillations of the stars caused by surface pulsation (Kurtz,). Asteroseismology works using spectroscopic or photometric observational data so as to get amplitudes, frequencies and phases of pulsations. By using the fundamental physical principles and models, asteroseismology can help determine the temperature, internal structure, chemical composition, pressure, density and mode of pulsation of stars (Kurtz, ; Aerts, Christensen-Dalsgaard, and Kurtz,). They described stars as noisy places, meaning they have sound waves. But the sound waves produced inside stars can not travel in a vacuum rather its effect in pulsating stars can make the stars contract and expand. The regular contraction and expansion of pulsating stars can be detected in the light output and the sound can be heard. Asteroseismology, as a matter of fact, plays a substantial role in understanding and studying the internal structure as well as the evolution of pulsating variable stars using their mode of pulsations (Handler, ; Kurtz, ; Aerts, Christensen-Dalsgaard, and Kurtz,).

1.6 Pulsation across HR Diagram

Stars go through several stages in their evolution period as shown in the HR diagram in Figure 1.1. The Hertzsprung-Russell (HR) diagram (Russell, .; Russell,) is one of the most powerful tools in astrophysics for studying the evolution of stars. It first originated in 1911 by Ejnar Hertzsprung, a Danish astronomer, who plotted the absolute magnitude of stars Vs Color (Effective temperature) and he used it to calibrate the period-luminosity relation and also to measure distance in Magellanic cloud. HR-diagram is a graph which shows the relationship between the stars' absolute magnitude against effective temperature which are the two fundamental properties of stars. Based on the initial mass, every star passes through specific evolutionary stage which is governed by its internal structure as well as how it generates energy. In every stage of the evolution, there is a change in luminosity and temperature which can be seen on the HR diagram. As stars pass through the different stages in their life time across the HR diagram, some stars will have pulsation properties as they pass across an instability strip. The instability strip for different classes of pulsating stars is shown in figure 1.1.

Pulsational variability either being radial or non-radial can be detected in different phases of stars' evolution. Different classes of pulsating stars are distributed and occupy different regions in the HR diagram (Gautschy and Saio,). Before going in to details about the pulsation of stars, it is worthwhile to mention something about stellar evolution. Stars can be classified into three major groups based on their initial mass, evolutionary history and their final destiny (Chiosi, Bertelli, and Bressan,). Based on these criterion, stars can be categorized as low mass , intermediate and massive stars.

- **Low mass stars**: are stars that spend billions of years burning hydrogen to helium inside their core by means of P-P nuclear reaction chain. As a star depletes hydrogen in its core, it will eventually have no hydrogen in its core. For a while, the core will not be hot enough to

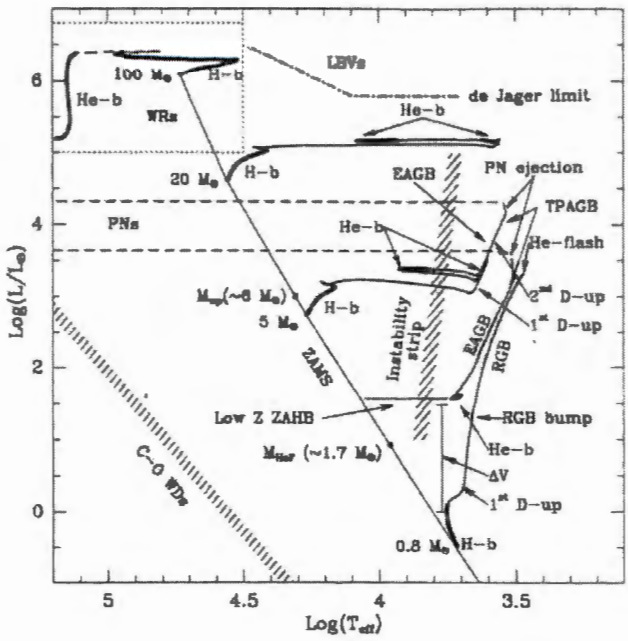

FIGURE 1.1: Schematic illustration of evolution of stars with different initial masses (Adapted from Chiosi and Bertelli (1992)). The hatched areas are instability strips.

produce energy. This leads to gravity overwhelming gas pressure, causing the core to contract and to become hot. The envelope and the core will expand in reaction to a contracting core, increasing the luminosity of a star.

These kinds of stars go to the red giant branch (RGB) immediately after leaving the main sequence. According to Chiosi, Bertelli, and Bressan, ( ), M_{He} the maximum initial mass for this process to happen is between $0.8 - 2.2M_{\odot}$ based on initial chemical composition. Taking into account the above argument, stars having more mass than M_{He} can be classified as intermediate mass or massive stars.

- **Intermediate Mass stars**: These types of stars, due to He-exhaustion inside the core, produce a highly degenerate Carbon-Oxygen (C-O) core and they also encounter helium shell flash or thermal pulses (Chiosi, Bertelli, and Bressan,).

- **Massive Stars**: are stars whereby carbon ignition is a preliminary process, which resulted in either producing iron core hence resulting in photo dissociation instability with core collapse and supernova explosion, or by undergoing several complex routes, core collapse and supernova explosion can take place.

The HR diagram shown in figure 1.1 shows the evolution of different stars with Helium abundance, Y=0.25, Metalicity, Z=0.008 and initial masses of $0.8M_{\odot}$, $5M_{\odot}$, $20M_{\odot}$ and $100M_{\odot}$. On the diagram shown, the quantities M_{HeF} and M_{up} are the two masses separating the low and intermediate mass stars and the second quantity M_{up} separates from high mass stars.

The HR diagram shows the evolution of stars with different initial masses and displays different stages of stellar evolution. Across the ZAMS line there are points labeled by H-b and He-b which refers to hydrogen and helium burning inside their core respectively. Further up in the evolutionary track on the right especially those having low initial mass is a region where there exists a stage of violent disturbance of He burning inside the core. This occurs at the end of the red giant branch

(RGB). Further representations in the HR diagram labeled by 1^{st}D-up and 2^{nd}D-up show external mixing. In addition, in the He-burning shell, the Asymptotic Giant Branch (AGB) is divided into early stages (EAGB) and thermally pulsating (TPAGB). Furthermore, the HR diagram also shows the instability strip of RR Lyrae and cepheid stars labeled by the vertical dashed lines. In the evolutionary track, the early stage of the evolution where the stage is assumed to be very slow is also distinguished from the remaining evolutionary stage by thick solid line as shown in fig. 1.1.

During the entire evolutionary process there is a time by which some stars start to pulsate or show some sort of pulsation. Pulsating stars are a subset of the class of intrinsic variable stars that shows some sort of instability and experience a periodic expansion and contraction in their outer layers. This in turn leads to concurrent variation of stars' luminosity which sometimes called vibration or oscillation. Theories of stellar evolution and location of variable stars on the Hertzsprung-Russell (H-R) diagram suggests that stellar variability is a transition phase in the evolution of some types of stars (Cox and Whitney, ; Cox,). Therefore, pulsation can occur from an instability to smaller oscillations which arises due to the movement of the stars from certain region of instability on the H-R diagram shown in fig. 1.2. Observation of different classes of pulsating stars shows that they populate in different regions of the H-R diagram (Gautschy and Saio,). One point that should be mentioned is that the study of pulsating stars is a very broad area of research because, during the evolution of a star, there is a possibility of stars crossing the instability strip, which can provide access to a unique opportunity to astronomers and researchers to learn and study about different constraints on stellar parameters which can not be obtained by other means (Gautschy and Saio,). Pulsating stars in general, based on their position across HR, can be divided into three groups:

1. Stars which evolved above the main sequence stars which can pulsate radially with fundamental modes and stochastically excited p-modes (lower-overtones).

2. Stars on or near the main sequence like Cepheids indicate self excited (predominantly) p-modes.

3. Stars evolved below the Zero Age Main Sequence (ZAMS)- indicate self-excited g-modes (Joshi and Joshi,)

The next three subsections deal with each of the above groups of stars. Furthermore, pulsating stars can be divided into three categories based on their amplitude of oscillation.

1. Large amplitude Cepheids, RR Lyrae and Cool red variables- These stars can pulsate in one or two radial modes.

2. Stars oscillating with low amplitude and pulsating in radial and non radial modes of pulsation. In this group white dwarfs, δ-Scuti stars, roAp stars, β Cephei stars, SPB stars and γDor stars are included.

3. Solar like stars whereby stars pulsate with μmag amplitudes. They are also main sequence stars, subgiants and giants. Pulsations in these stars are excited by stochastic processes due to convection.

The above discussion is summarized in fig. 1.2 which shows the distribution of different classes of pulsating stars in the H-R diagram.

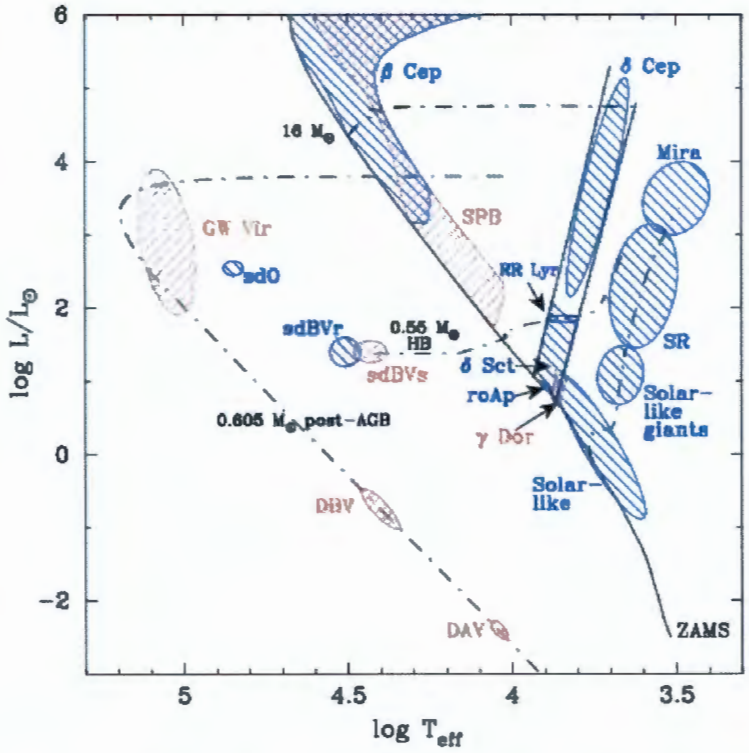

FIGURE 1.2: H-R Diagram with instability strips of various classes of pulsating stars. Adapted from (Christensen-Dalsgaard (2003))

1.6.1 Pulsating Stars above the Main Sequence in the HR Digram

In this section, we give a synopsis of pulsating stars that are on or above the main sequence.

1. **Mira Variable Stars**: Mira variable stars are pulsating stars and are best known as the end point in the AGB evolution. These kind of stars helps us understand the evolution of low and intermediate mass stars (Whitelock, 1990). In their evolutionary track, low and intermediate mass stars are in the advanced evolutionary stages (Joshi and Joshi, 2015). At very low surface temperatures, these pulsating stars are also cool red giants which are located near the tip of the Asymptotic Giant Branch. They are characterized by high luminosity, (luminosity above $10^3 L_{\odot}$ Gautschy and Saio, (1996a)). Their bolometric magnitude is shown in table 1.4. These variable stars have large amplitude, long pulsation period ranging from $80-1000$ days and low effective temperature ($2500 \leq T_{\text{eff}} \leq 3500$K) (Gautschy and Saio, 1995). Mira variables are also used as distance indicators (Feast, Whitelock, and Menzies, 2002). According to Bedding et al., (1998) and Joshi and Joshi, (2015), Mira variable stars with period $\geq$ 300d are usually subjected to high mass loss rates, with amplitude greater than 2.5mag in the V-band. Many Mira variables are luminous and bright, implying that some kinds of Miras are naked eye variables and are popular with many amateur astronomers (Zijlstra and Bedding, 2002).

   Feast, Whitelock, and Menzies, (2002) shows that Mira variable stars show a good infra red period-luminosity relations which can help to determine the distance modulus for Large Magellanic Cloud (LMC). But there are controversies regarding mass loss in these kinds of stars (Gautschy and Saio, 1996a). In addition, Mira variables have more stable periods

(Zijlstra and Bedding,) and shows irregularity in the shape of their light curves and amplitudes.

The cause of variability in Miras is associated with the thermal pulsating asymptotic Giant Branch, which is between partial hydrogen ionization and He-I ionization (Bedding et al., ; Gautschy and Saio, ; Joshi and Joshi,). These alterations occur in a star with degenerate Carbon/Oxygen core surrounded by hydrogen and helium burning shell. Pulsation occurs during the hydrogen burning phase in the shell where luminosity of the star is very high (Bedding et al.,). Moreover, pulsation of some stars may have Mira type of pulsation during helium shell flash (Wood and Zarro,).

TABLE 1.3: Mira Bolometric Magnitudes, Adapted from Zijlstra,(1995)

Population	M_{bol}	References
Galactic Centre	$-4.5 \rightarrow -6$	Jones et al. (1994)
Bulge	$-3.5 \rightarrow -5$	Whitelock et al. (1991)
Galactic Cup	$-3.5 \rightarrow -5$	Whitelock et al. (1994)
Metal-rich globular clusters	$-3.0 \rightarrow -4.5$	Menzies and Whitelock (1985)
LMC	≥ -7.2	Wood et al. (1992)

Studies proved that the driving mechanism for Mira variable stars are partial hydrogen ionization and He-I ionization (Gautschy and Saio,). Energy transport in the envelope is dominated by convection where the pulsation cycle obtained have the same order as the convective overturn. Hence, pulsation in Mira variable stars can be understood based on the relation between pulsation and convection (Gautschy and Saio,). In addition, our understanding also depends on the effect of convection on the equilibrium of the star (Gautschy and Saio,).

Energy transport by convection in stellar envelopes are not well explained and if included in the study of pulsation, it was treated in a wrong way (by mixing length theory). Balmforth, Gough, and Merryfield, ( ) investigated by including turbulent pressure to see its effect on the linear acoustic models. They concluded that the inclusion of turbulent pressure affects not only the equilibrium of the Mira stars but also the radial modes of pulsation which shows turbulent pressure that has a destabilizing effect. Moreover, they showed that the first overtone among others is dominantly excited mode. Determining the mode of pulsation for Mira variables is a challenge (Wood,) due to the fact that Miras lack sharp edges as the Sun and they gradually disappear unexpectedly as their angular diameter get bigger. There are still some disagreements whether Miras pulsate in their fundamental or first overtone (Wood, ; Ita et al., ; Balona,). Wood, ( ) stated that measurement of the angular diameter of solar neighborhood resulted in large radii in line with first overtone pulsation whereas pulsation velocity amplitudes of Miras turnout to be fundamental mode of pulsation.

In Miras, there is mass loss and according to Gautschy and Saio, ( ) observational evidences indicated that the rate of mass loss can be related to the pulsation periods. Further evidence in this regard was suggested by Whitelock, ( ) where at a given period those with the highest amplitudes will have high mass loss rates. Considering the evolutionary track, Mira variables (Whitelock,), are the end point of AGB. During their evolution, luminosity increases and period becomes longer and it is also associated with mass loss until it reaches a critical luminosity (Gautschy and Saio,). Furthermore, their evolution

might lead and end up in forming planetary nebula. Recent developments or observations from All Sky Automated Survey (ASAS) proved the category of 2875 stars as Miras and determined their period of pulsations (Vogt et al.,).

2. **Irregular (Irr) and Semi-regular (SR) Variables**: Stars which are found in the upper part of the giant branch in the HR diagram are commonly known by their light variability and are known to be Long period variable stars (Lebzelter and Obbrugger,). These types of stars (LPVS) include Miras, Semi-regular and irregular variable stars. Irr and SR basically have similar periods with Miras but lower amplitudes < 2.5mag in V. Those kinds of stars with smaller amplitudes are known as SRa (Aerts, Christensen-Dalsgaard, and Kurtz,). SRa are semi-regular late type giant stars with period $(35 - 1200$days), $T_{\text{eff}} > 3200$K and are different from Mira variables due to their small amplitude (Kerschbaum and Hron,). SRa kinds of stars are mixtures of 'intrinsic' Miras and SRb kinds. The second kind of variable stars in this category are SRb, which are a semi-regular late type giants with lower amplitudes but as compared to SRa's these kinds of variable stars have poorly defined periods, which is the semi-regularity in their light curves (Kerschbaum and Hron, ; Aerts, Christensen-Dalsgaard, and Kurtz,) with mean cycles $20 - 2300$d Kerschbaum and Hron, ( ).

   Among the SRb's, the O-rich ones create a homogeneous cluster based on amplitudes, temperature and periods of oscillation. SRb variable stars include 'blue' group without having hints of circumstellar shells. In the HR diagram, both Miras and SRa variable stars are found to the right of the instability strip at the lower temperature edge. The third group in this category is SRc. SRc stars are periodic supergiants and shows supergiant spectra (Kerschbaum and Hron,) with their amplitude <1.0 in V (Aerts, Christensen-Dalsgaard, and Kurtz,). Among the SRc stars, some are C-rich Asymptotic Giant Branch Stars (Kerschbaum and Hron,). The last group under this category is the SRd with spectral lines earlier than M and are metal poor (Kerschbaum and Hron,). In addition, these kinds of variable stars are double mode RR Lyrae stars (Aerts, Christensen-Dalsgaard, and Kurtz,).

3. **Cepheids**: During stellar evolution, stars with initial mass higher than $2.3M_{\odot}$ start to burn helium at the core (Gautschy and Saio,). At this stage of evolution the luminosity of these stars decreases, evolve and rise to the red giant branch in their first cycle. Those with masses $2.2 \leq M \leq 3M_{\odot}$ remain there with lower luminosity so as to burn the helium inside their core and start to move towards the giant branch for the second time (Gautschy and Saio,). But those stars with $M \geq 3M_{\odot}$ will follow a loop in the HR diagram (Gautschy and Saio,). Stars with initial mass $M \leq 5M_{\odot}$ will have blue loops where this loop prohibits reaching the instability strip (Gautschy and Saio, ; Aerts, Christensen-Dalsgaard, and Kurtz,). But stars with initial mass $M > 5M_{\odot}$ can cross the instability strip more than twice and become unstable in their pulsation (Gautschy and Saio,) and can be observed as Cepheids. Cepheids are yellow supergiant stars with spectra class F6-L2, very luminous with 500 to $300000L_{\odot}$ and pulsate with their period of pulsation varied from 1 day to 135 days (Joshi and Joshi,). Cepheid variables, sometimes known as distance indicators, play a prominent role in determining distances of stars by using the period-luminosity relation (Aerts, Christensen-Dalsgaard, and Kurtz,). Despite the fact that Cepheid variables shows periodic variation in radial velocity, it will not guarantee that the stars are binary (Eddington,). Further claims, on the other hand, by Madore, ( ) revealed that 20% of all Cepheids have companions and 7% have a great chance to have companions with the secondary companion with masses equivalent to Cepheids.

According to Chiosi, ( ), Cepheid variable stars can be categorized into two groups based on their metallicity.

(a) **Population I-Cepheids (Z>0.005)(Classical Cepheids)**: Classical Cepheids Δ Cepheid are the most nearly homogeneous type of pulsating stars (Cox, ; Cox,). Population I-Cepheids can have different categories

- Galactic population-I types are Cepheids which oscillate with periods ranging from 1 to 80 days (Chiosi,).
- Groups of population I-Cepheid variables located in the Large Magellanic Cloud (LMC) pulsate with periods close to 200 days.

The first groups, Galactic population-Cepheids, are focussed in the galactic plane in our galaxy having temperatures of $5500K \leq T_{\text{eff}} \leq 6600K$ with F5 to G5 spectral types. They are all giants or supergiants (Aerts, Christensen-Dalsgaard, and Kurtz,), summary is provided in table 1.4. In addition, their magnitudes also vary from -1 to -6 (Chiosi,). These groups of stars which are evolved from post-main sequence, helium burning phase from stars with masses $3M_{\odot}$ to $10M_{\odot}$, have well defined period-luminosity relation.

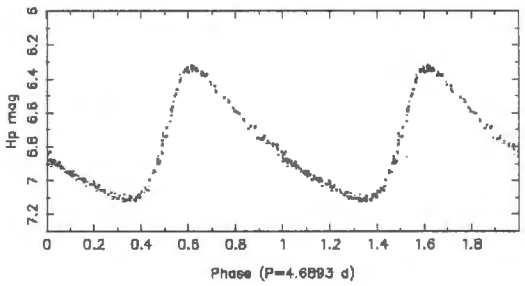

FIGURE 1.3: Light curve which shows an example of Cepheid pulsation HD112044. Adapted from (Aerts et al.2010).

The light curve shown in Fig. 1.3 is one example of a classical Cepheid HD 112044 which clearly shows the skewness and regular periodic oscillation, repeating over many periods, of such kinds of stars with 1m magnitude in average at a visual wavelength. These kinds of stars normally pulsate in the fundamental radial mode.

TABLE 1.4: Properties of Galactic classical Cepheids, Adapted from King and Cox,(1968)

Property	Range from	to
Period (II)	1 day	50 days
Mean Luminosity (L)	$300L_{\odot}$	$26000L_{\odot}$
Median Spectra type	F5	G5
Mean radius (R)	$14R_{\odot}$	$200R_{\odot}$
Mass (M)	$\leq 3.7M_{\odot}$	$\leq 14M_{\odot}$

Classical cepheids are yellow giants and supergiants leading to higher luminosity (Cox,). These kinds of stars were observed in more than 30 external galaxies.

Cepheids are very prominent kind of variable stars where the variations in their observational parameters such as (colour indices, radial velocity and magnitudes) help to calculate the stellar basic parameters of the stars such as Radius, temperature, mass and luminosity. Moreover, studying Cepheid variables can play a significant role in trying to understand the theory of stellar evolution (Bersier, Burki, and Burnet, 1994). Furthermore, Cepheids, double mode Cepheids, contributed in using Asteroseismology to determine stellar parameters and properties. The double mode pulsator Cepheids were used to determine the stellar parameters such as masses and radii by comparing theoretically determined period of oscillation with the observed ratio of first overtone to the fundamental mode of pulsation (Petersen, 1973). This discrepancy was further studied by developing Petersen diagram.

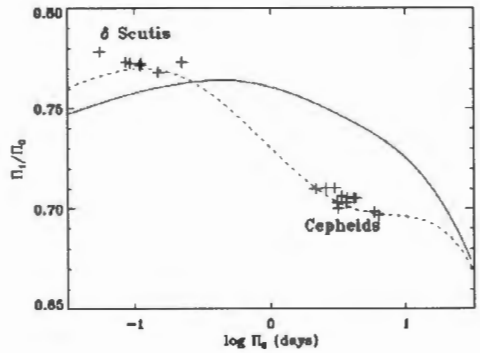

FIGURE 1.4: A graph, Petersen diagram, showing the ratio of first over tone and the logarithm of fundamental radial period (Π_0) (Aerts et al., 2010).

The Petersen diagram shown in Fig. 1.4 shows the ratio of the the firs overtone to the logarithm of the fundamental radial period. The points displayed on the graph as crosses represent observational values. The solid line on the plot shows the theoretical model computed by using the value of opacities determined by Cox and Tabor (1976). The graph presented in the Petersen diagram Fig. 1.4 by the dashed lines represents the model developed by using the OPAL opacity value Roger and Iglesias (1992). The values on the axes (Π_1) showing the period of the first radial overtone and (Π_0) represents the period of the fundamental mode.

(b) **Type II Cepheids (Population II Cepheids) (RV Tau, Stars, W-Vir Stars, BL Her Stars)**: Such kinds of variable stars are located between RR Lyrae, LPV and RV Tauri stars in the HR diagram and are governed by their own period-luminosity relation different from the population I Cepheids (Chiosi, 1990). As the stellar evolution progressed and He burning at the core continues, those with masses above $0.5M_{\odot}$ (Gautschy and Saio, 1996b) progressed and rise to the AGB. During the thermal pulse, there is a possibility of these stars crossing the instability strip which makes these kinds of stars to pulsate and be observed as Population II-Cepheids or type II-Cepheids. The following pictorial representation in Fig. 1.5 also shows the position of Population II Cepheids, RV Tau, Stars, W-Vir Stars and BL Her Stars. It also shows the evolutionary track of low mass stars. Population II-Cepheids have period of oscillation ranging from 0.8 days (Gautschy and Saio, 1996b) or 1 day for stars with luminosities similar to the RR Lyrae stars to 30 days at higher luminosities.

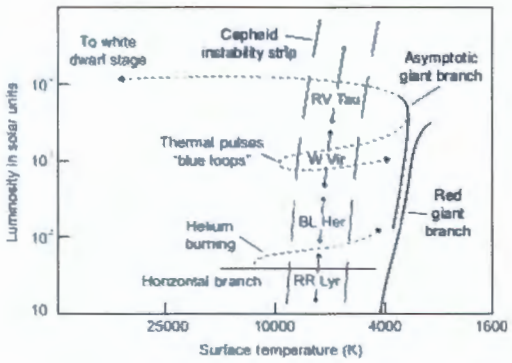

FIGURE 1.5: The location of Population II stars, BL Herculis, RV Tauri and W Virginis. The figure also shows the evolutionary track of low mass stars and their subsequent evolutionary stages. Adapted from (Percy, 2007).

Population II-Cepheids can easily be known based on their position which has a magnitude several classical cepheids scale heights in the galactic plane. It is also possible to locate population II-Cepheids using their space velocities which is two or more sigma higher than the young cepheid variable stars Wallerstein and Cox, (1984).

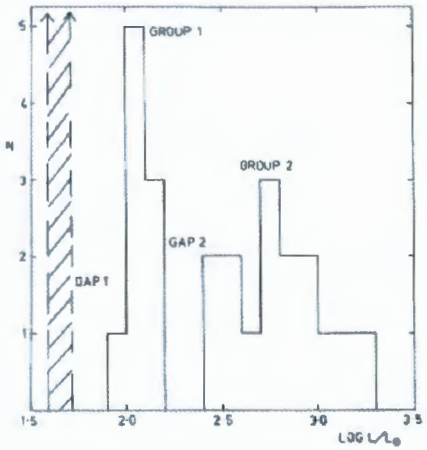

FIGURE 1.6: A Histogram showing the observed luminosity distribution of population II-Cepheids with periods <30days. The first bar graph on the left filled with hatched lines represent the RR Lyrae variables. Adapted from (Gingold, 1976).

The histogram shown above in Fig. 1.6 shows the number of globular clusters Cepheids within the intervals of 0.1 in $log\frac{L}{L_{\odot}}$. In the period interval between $3-6$ days, due to the lack of the presence of stars, there exists a gap which is gap2. On the other hand, Group 1 represents fainter stars and represent post horizontal branch stars that are going to the direction of the AGB. Furthermore, the second group represent the second GB stars crossing the instability strip. This happens when the envelope of the star reacts to the helium flash and lead to the latter stage of the star towards the white dwarf (Gingold, 1976)

The following table, Table 1.5, summarizes pulsating variables discussed above.

(c) **R-Coronae Borealis (RCB) Stars**:

TABLE 1.5: Summary of Pulsating Variables, Adapted from Cox(1968)

Kind of Star	Range of periods	Characteristic period	Range of Spectral Type
RR Lyrae	$1.5 - 24$ hr	0.5 d	A2-F6
Classical Cepheids	$1 - 50$d	$5 - 10$d	F6-K2
WVirigins stars	$2 - 45$d	$12 - 20$d	F2-G6
RV Tauri stars	$2 - 150$d	75d	G, K
Red Semi-regular variables	$100 - 200$d	K, M, R, N, S	-1 to -3
Long period variables	$100 - 700$d	Me, Re, Ne, Se	$+1$ to -2
βCephei stars (β)Canis Majoris stars	$4 - 6$hr	5hr	B1-B2
Dwarf Cepheids and δScuti stars	$1 - 3$hr	2hr	A2-F5

These are small group low mass, carbon and nitrogen rich F or G super giants (Feast, 1975), hydrogen deficient (Clayton, 1996a). Their effective temperature ranges between $T_{\text{eff}} = 5000 - 7000$K and Clayton, (1996a) and Clayton, (2012) famously observed and noticed by their asymmetrical decrement in their brightness which reveals the true characteristic of genuine irregular variables.

The RCB stars according to the light curve shown in Fig. 1.7 can be at constant brightness for at least months or even years. After that constant brightness time, there will be a dramatic decrement in brightness $\geq$ 3mag in a couple of days or might take weeks which is then followed by an increase in brightness to the highest point on the light curve, this might take a little bit longer time, needs months or even years, which makes it a slower event (Clayton, 2012). The decrease in brightness 8mag is due to the fact that carbon formation is dominant at a non-uniform interval (Clayton, 2009b). There are two ways for the formation of RCB stars, the first one is the product of a final helium shell flash due to the existence of Li in the atmospheres of four of the RCB stars (Clayton, 2009a). The other scenario for the formation of RCB stars is the merger of two white dwarfs Clayton, (2009a) and Clayton, (2009b), this is favoured because of huge abundance of 18O (Clayton, 2009a). RCB stars can be identified easily by looking at the light curves as shown below in Fig. 1.7:

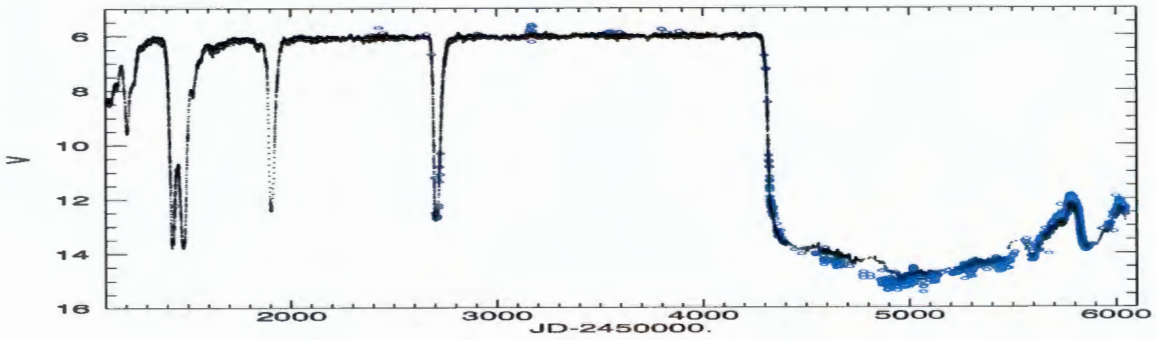

FIGURE 1.7: Sample light curve showing the uncharacteristic property of RCB stars where the light curve is generated using the AAVSO data from 1998 – 2012. Adapted from (Clayton, 2012).

The light curve of RCB stars is unique in its irregular variation in brightness, amplitude and no other type of stars show such an odd behavior (Clayton,).

All RCB stars pulsate (Feast,) and most of them are observed to have Cepheid-like pulsation. RCB stars play a fundamental role in understanding dust formation and evolution (Clayton, Whitney, and Lawson,).

(d) **RR Lyrae Stars**: Shapely and Bailey are the two astronomers who did observational investigations from Galactic globular clusters and discovered RR Lyrae variable stars (Bono and Marconi,). At the beginning, these stars were known to be cluster type variables. RR Lyrae variable stars are low mass stars roughly $(0.5-2.0M_{\odot})$ (Gautschy and Saio,) evolved away from the main sequence and burn helium inside their core (Kolenberg et al.,) and are classical radial pulsators (Aerts, Christensen-Dalsgaard, and Kurtz,). Those stars with initial mass $\leq 0.75M_{\odot}$ would become RR pulsators during their evolution while helium is burning inside their core (Gautschy and Saio,). RR Lyrae stars have A2-F6 spectral type on the horizontal branch Kolenberg et al., ( ) and Joshi and Joshi, ( ) with amplitudes $0.2-1.5/2$ mag in V. These kinds of stars occupy the region below the Cepheid variables in the instability strip of the HR diagram and pulsate with periods between $\sim 0.2-\sim 0.9$ days $(5-22\text{hrs})$ or up to 1 day (Kolenberg et al.,) or up to 0.5 days Joshi and Joshi, ( ) whereas according to Cox, ( ) the period of pulsation might vary from $1.5hr \leq \Pi \leq 1day$.

RR Lyrae pulsate and the driving or excitation mechanism is known to be the heat mechanism which is acting in the partial ionization region of HeII-HeIII (Aerts, Christensen-Dalsgaard, and Kurtz,) reference there in. According to Cox, ( ), RR Lyrae stars can be divided into three groups known as Bailey types a, b and c where the light curves of a and b types are asymmetric. In addition, they are radial fundamental mode pulsator variable stars as shown in the following light curves in Fig. 1.8 and Fig. 1.9. Whereas the light curves of c types are sinusoidal and pulsate in radial 1^{st} overtone (Cox, ; Gautschy and Saio, ; Kolenberg et al.,).

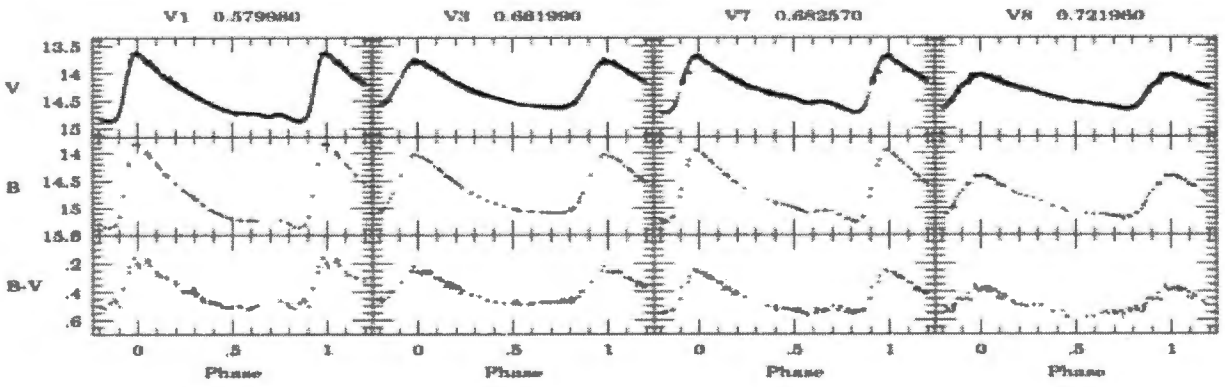

FIGURE 1.8: Light curve showing RRab Lyr stars in M55. Adapted from (Olech et al., 1999).

Some RR Lyrae stars on the other hand might have higher-order (double mode) radial overtone made of pulsation (Olech and Moskalik,). Furthermore, Dziembowski and Cassisi, ( ) and Olech et al., ( ) showed that RRab and RRac can have

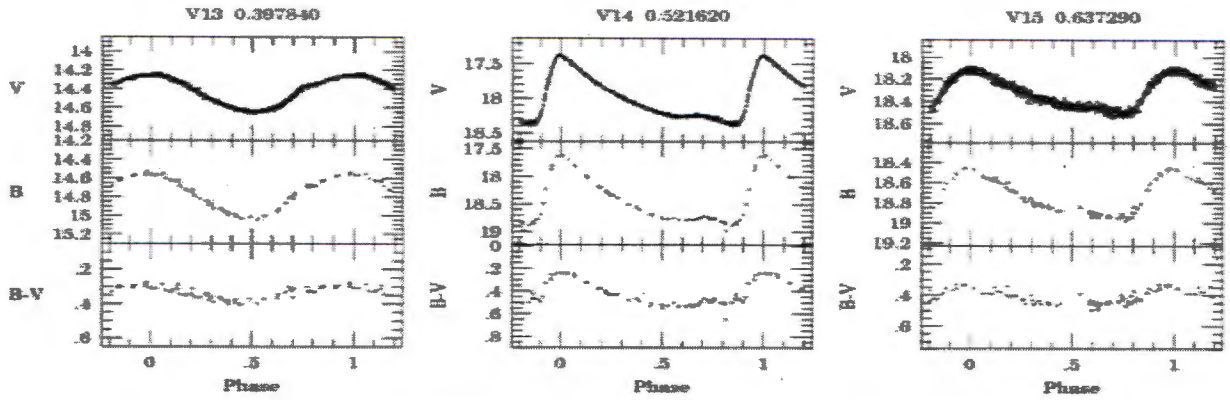

FIGURE 1.9: A light curve showing V, B, B-V RRc Lyr star from M55 and 2RRab Lyrae stars from Sagittarius dwarf galaxy.Adapted from (Olech et al., 1999).

unstable non-radial mode of pulsation which can be triggered by the opacity mechanism. More investigations on RR Layre stars demonstrated that a large fraction $\frac{1}{3}$ of RR Lyrae stars show long term, nearly periodic amplitude modulation known as *Blazhko effect* (Shibahashi and Takata,) which was named after Blazhko who observed this phenomenon first. Shibahashi and Takata, ( ) stated that Blazhko effect is a long standing, unresolved problem of stellar astrophysics.

1.6.2 Stars Near the Main Sequence and on the Main Sequence

(a) **β-Cephei Stars (β-Canis Majoris Stars)**:
Among the group of young population I, early B-type pulsators (Handler,), lie close to the main sequence and are called βCep stars. These stars have convective core surrounded by radiative envelope, their mass ranges from $8M_{\odot} - 18M_{\odot}$ (Joshi and Joshi,) or $10M_{\odot} - 20M_{\odot}$ compared to evolutionary tracks (Aizenman,). βCephei stars have short periods between $2 - 8$ hrs. (Joshi and Joshi, ; Gautschy and Saio,) oscillating in low order non radial p and g-modes. According to Stankov and Handler, ( ), these groups of stars include classes from dwarfs to giants. Cox, ( ) explained β Cephei stars as hot stars with mean spectral type between B0.5 and B2 (Aizenman,), amplitude < 0.3 mag in V (Moskalik,) and having $T_{\text{eff}} \sim 20,000 - 25,000$K which makes them the hottest pulsating stars observed. β Cephei stars are also known as '*β-Canis Majoris*' stars because of their multi-periodicity unlike β-Cephei (Percy,). Their periods are sometimes very close which can show ascending and descending in the amplitude, called *beat effect*. Most β Cephei stars can have multiple periods as well as variation in line profile (Pamyatnykh,).
If a non-rotating stationary spherical star is considered in a study of β Cephei star, the non radial periods becomes degenerate. But if the star rotates, the degeneracy will vanish, and makes the periods to be dissimilar which further enhances interference between periods that generates beats (Percy,). Since their discovery, the driving mechanism for their pulsation was a puzzle and lots of theoretical works were put forward to explain the phenomenon. Among these proposals, the one suggested by Moskalik and Dziembowski, ( ) is found to be acceptable. They demonstrated based on the idea

suggested by Stellingwerf, ( ) stating that in a non adiabatic linear pulsation the bump resulted is due to the HeII ionization edge caused by the opacity at T=1.5 $\times$ 10^5K which excites the fundamental radial mode (Moskalik and Dziembowski,). However, this effect was not sufficient to trigger the instability on both radial and non radial modes of pulsation (Saio and Cox, ; Moskalik and Dziembowski,). Further investigation to fill the gap was done by Simon, ( ) and Kiriakidis, El Eid, and Glatzel, ( ) by adding heavy elements and their effects on the opacity. Hence, pulsational instability is caused by κ mechanism (further explanation on this point will be presented latter in the thesis) which is initiated by the heavy metal opacity in a region at $T = 200000$K. The opacity of heavy elements such as iron at the specified temperature can trigger pulsation (Percy,). Moskalik and Dziembowski, ( ) emphasized this effect by considering the metal opacity table produced by Iglesias and Rogers and showed that the resulting opacity could be used to fill the gap created between the theoretical assumption and observational period of oscillation for β Cephei stars. Studying βCephei stars observationally was based on a single site observation till 2002 (Aerts, Christensen-Dalsgaard, and Kurtz,). These photometric observations lasted for a week or two which creates large discrepancy in the observational data. These discrepancies or gaps can lead to a lack of clear understanding of β Cepheid stars. Such discrepancies and gaps can be avoided by introducing multicite observation (both photometric and spectroscopic) of a certain target. Continuous follow up of a β Cephei target will result in having sufficient data which can help in detecting, analysing and interpreting modes of oscillation (Aerts, Christensen-Dalsgaard, and Kurtz,).
In addition to multi site observation, space based observations like, KEPLER, are implemented to get relevant data to study β Cephei stars. Balona et al., ( ) used Kepler data to analyse the light curves of B type stars and come up with 15 pulsating stars with low frequency (Slowly Pulsating B stars SPB). From these, 7 of them could be SPB or βCephei stars or hybrids.

(b) **Slowly Pulsating B (SPB) stars (53Per Stars)**:
Their name was proposed by Waelkens, ( ). Based on observational evidences, such kinds of stars are located along the main sequence in the HR diagram (De Cat,). They are B type variable stars which are pulsating in high radial order g modes (Waelkens, ; De Cat et al.,) and pulsate with periods $0.3 - 3$ days (Waelkens, ; De Cat et al.,) or $0.5 - 4$ days (De Cat,). Since they are found close to the main sequence, it is evident that their core is still dominated by hydrogen burning. These kinds of variables are massive and hot having spectral types B2-B9 (De Cat,) with $T_{\text{eff}} = 1.2 \times 10^4$ to 1.8×10^4K. SPB stars have masses between $3M_{\odot} - 7M_{\odot}$.
Slowly pulsating B stars (SPB) are very important types of stars to study Asterosesimology because g modes can penetrate deep into the interior or core of the star (De Cat,). SPB stars are first categorized based on their photometric variability during the observation conducted by (Waelkens,). These variabilities were analogous to the "53" $Persi$ stars (Smith et al., ; Waelkens,) which belongs to a group of OB type variable stars. Further investigations on such kinds of variable stars ("53" $Persi$) was done by Chapellier et al., ( ) by considering their observational characteristic and concluded that "53" $Persi$ variables are among the SPB.
Their oscillations are driven by κ mechanism triggered in the heavy metal (iron ionization zone) at a temperature of 2×10^5K (Dziembowski, Moskalik, and Pamyatnykh, ; Dziembowski and Pamiatnykh,).

(c) **δ-Scuti stars (53Per Stars)**: During stellar evolution, those stars with initial mass in the range between ($1.5 \leq \frac{M}{M_{\odot}} \leq 2.5$) during their hydrogen burning core and pass toward the base of the giant branch where their shell is dominated by hydrogen burning (Gautschy and Saio, 1996a). They are found at the intersection of classical instability strip and main sequence stars Breger, (2000) and slightly above main sequence stars (Daszyńska-Daszkiewicz, Dziembowski, and Pamyatnykh, 2003) as shown in Fig. .

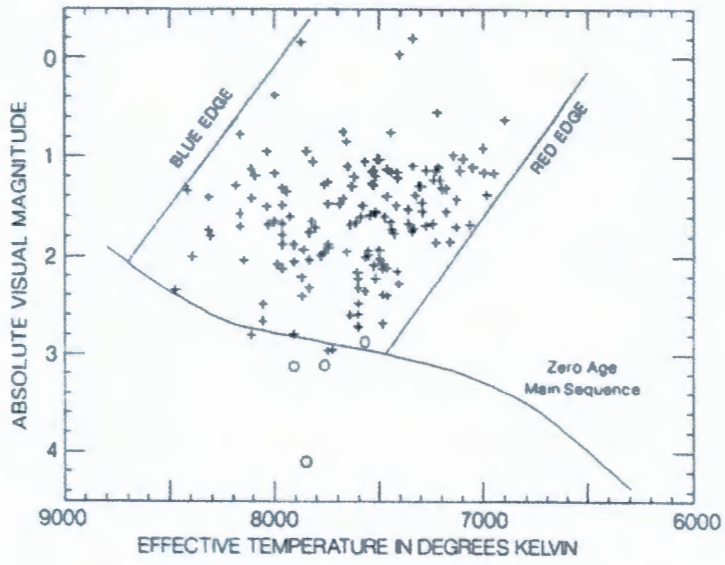

FIGURE 1.10: HR diagram showing the instability strip of δScuti stars of population I. Adapted from (Berger, 1995).

δScuti stars are intermediate stars belonging to population I pulsating stars whereas some of them belong to population II because of their metallicity and space velocity (Breger, 1979; Joshi and Joshi, 2015). Their spectral type ranges from A2-F5 in 1000K band (Breger, 1995) and luminosity between III-V (Breger, 1979; Joshi and Joshi, 2015) with period of oscillation from $0.25 - 0.3$d (Breger, 1979), $0.02 - 0.3$d (Percy, 2007; Balona, 2010) or $0.02 - 0.25$d (Breger, 2000). According to Breger, (1979), δ Scuti stars are the second abundant groups of pulsating stars in the galaxy next to pulsating white dwarfs. Breger, (1972) reference therein stated that δScuti stars can be found in pre-main sequence as evidenced in the young cluster NGC2264 and HR5999 that exhibits the property of δ Scuti stars (Kurtz and Marang, 1995). δ Scuti stars pulsate in either radial or non radial modes of pulsation with low order p modes having periods between 18minutes-8hrs (Aerts, Christensen-Dalsgaard, and Kurtz, 2010; Joshi and Joshi, 2015). Furthermore, δ Scuti stars have amplitudes ranging from mmag to $\frac{1}{10^{th}}$ magnitude. δ Scuti stars are in the class of pulsating variables and their causes of pulsations as discussed in Breger, (1979) is the HeII and H-ionization zones and κ mechanism is the driving mechanism especially in the HeII partial ionization zone without neglecting the influence of H-ionization (Balona, 2010). Some δ Scuti stars pulsate in pure radial whereas majority pulsate with non radial acoustic (p_{-}) modes which is triggered by opacity effects (Breger, 2000; Hareter et al., 2008; Joshi and Joshi, 2015). Therefore, many δ Scuti stars are multi periodic with small amplitudes $10^{-3} - 10^{-2} mag$ (Gautschy and Saio, 1996a; Percy, 2007; Jurcsik et al., 2006). Published results on such stars

also revealed that most δScuti stars are moderate or rapid rotators with $100 - 200km/s$ surface velocity (Joshi and Joshi,).

TABLE 1.6: Summary showing typical δ Scuti stars with their pulsation constant, period and period ratio, Adapted from Joshi and Joshi(2015)

Mode of Pulsation	Period	$\frac{P_i}{P_{i-1}}$	$\frac{p_i}{P_F}$	Q (days)	Reference
Fundamental, F	0.07861	–	1.000	0.0329	Berger et al., (1979)
1^{st}overtone, 1H	0.05950	0.761	0.757	0.0251	" "
2^{nd}overtone, 2H	0.04846	0.810	0.617	0.0203	" "
3^{rd}overtone, 3H	0.04095	0.845	0.521	0.0172	" "
4^{th}overtone, 4H	0.03533	0.862	0.449	—	" "
5^{th}overtone, 5H	0.03109	0.879	0.396	—	" "
6^{th}overtone, 6H	0.02774	0.882	0.353	—	" "

Table 1.6 shows the summary of a typical δ Scuti star with the following parameters $T_{\text{eff}} = 7800$K, M=$1.7M_{\odot}$, $L = 15L_{\odot}$ Y=0.28 and Z=0.02. Observational evidences also revealed that majority of δ Scuti stars pulsate with large number of simultaneously excited modes (Breger, ; Jurcsik et al.,). According to Breger, ( ) those δ Scuti stars whose rotational velocities are small display radial pulsation accompanied by large amplitudes whereas large number of δ Scuti stars are non radial pulsators with small amplitude p modes (Breger,). For the non radial pulsators of δScuti stars have low degree ($l \leq 3$) and low order p modes $n = 0$ to $n = 4$ Breger, ( )); $n = 0$ to $n = 7$ (Breger,)). Further spectroscopic investigations revealed the existence of high order non radial modes as high as $l = 20$ (Breger,) reference there in. Evidences for such high degree mode was revealed by Kennelly et al., ( ) while they were studying the pulsation of τ-pegasi using two dimensional least square cleaning algorithm and Fourier-Doppler imaging to identify frequencies and modes of oscillation and obtained spectrum up to $l = 20$ with small frequencies $\leq 35\frac{cycles}{day}$. Many δ Scuti stars FGVir are multi-periodic pulsators which makes them a prominent candidate to study asteroseismology (Breger, ; Joshi and Joshi,).
δ Scuti stars especially those with high amplitude which pulsate in fundamental or 1^{st}overtone as other kinds of pulsating stars follow a specific period-Luminosity or period-Luminosity-color relation in V-band that is given by:

$$M_v = -3.725logP(fundamental) - 1.969, \tag{1.2}$$

and used for distance determination (Petersen and Christensen-Dalsgaard,).
In addition to multi site ground based observations of δ Scuti stars, more efforts were placed on space based observations to further study and analyse δ Scuti stars. Among these, WIRE (Wide-Field Infra Red Explorer) satellite used to observe and study $\theta^2\tau$ where 12 independent frequencies with a small amplitude $0.5mmag$ (Poretti et al., ; Poretti et al.,) were observed. Further observations using MOST (Microvariabilty and Oscillations of STars) also revealed that HD209775 have more than 80 frequencies (Matthews,). In addition, other space based observations such as, CoRoT and KEPLER contributed immensely to asterosesmic study of δScuti stars. Balona, ( ) stated that doing asteroseismology using space based observation (MOST,

CoRoT and KEPLER) is better than ground based photometry as it lowers the threshold frequency of detection which was previously difficult to observe.

(d) **Rapidly Oscillating Ap (roAp) stars**

These stars are discovered by Kurtz, ( ). Since the first discovery in 1982, only 60 known roAp stars exist till 2015 where majority of them are found in the southern sky (Joshi and Joshi,). The rapidly oscillating Ap (roAp) stars are variable stars which are found in the sub group CP-A type with cool effective temperature ($T_{\rm eff} \sim 6.4 \times 10^3 - 8.5 \times 10^3$K) with spectral type B8-F2 (Percy,). These stars are cool magnetic Ap stars pulsating in a low degree ($l \leq 3$), high overtone $n \gg l$ p modes (Martinez and Kurtz,). Their period of pulsation varies from $4 - 21$ minutes with pulsation amplitude $\leq 16mmag$ and pulsate in high overtone, low degree, non radial p modes (Kurtz, ; Kurtz,). The roAp stars are hydrogen burning core objects of mass in the range $M \approx 2M_{\odot}$ with strong magnetic field of the order of few hundred to few KGauss (Kurtz,).

Aerts, Christensen-Dalsgaard, and Kurtz, ( ) stated that in addition to having strong dipole magnetic field, roAp stars are stars with spectral type A-F. The roAp stars also have unusual chemical surface composition due to the atomic diffusion. Further investigations of pulsation of roAp stars can lead to identifying and determining rotational inclinations, magnetic geometries, rotation periods, internal magnetic field strengths, masses, radii, luminosities and ages (Kurtz, ; Kurtz,). All these investigations can be achieved by asteroseismology. The main reason why roAp stars are fundamental role players in studying asteroseismology is because most roAp stars are multi periodic and non radial pulsators (Joshi and Joshi,). According to Kurtz, ( ), the pulsations observed in roAp stars are modeled using oblique pulsator model whereby the pulsation axis of roAp stars aligned with the magnetic field axis but inclined with respect to the rotation axis (Joshi and Joshi,) as shown in Fig. 1.11 and Fig. 1.12 which demonstrate old and new models of roAp stars.

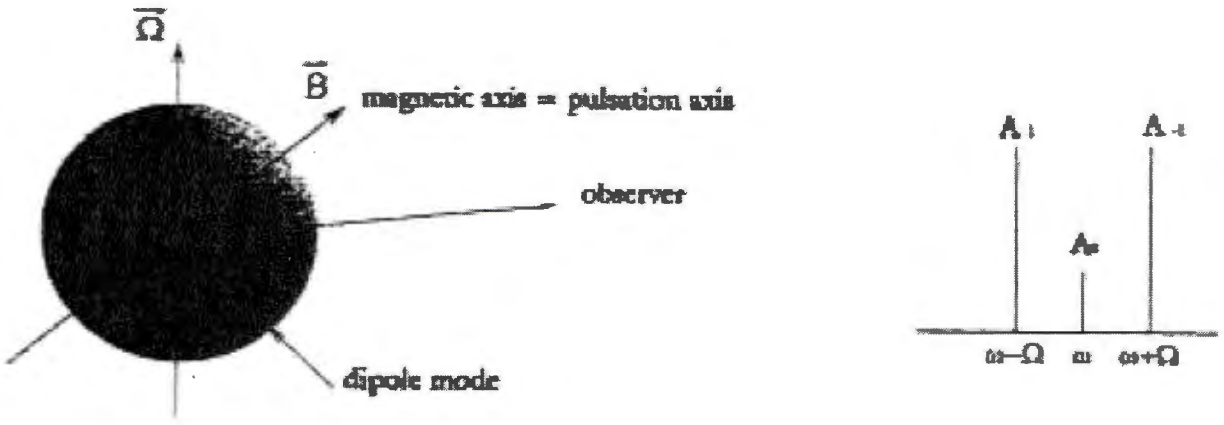

FIGURE 1.11: Oblique pulsator model as originally introduced by Kurtz (1982) where the right panel shows the two high frequencies separated by frequency of rotation (Ω). Adapted from (Bigot, 2003)

Oblique pulsator model proposed first by Stibbs, ( ), predicts the existence of modes in multiplets which are equidistant and separated the angular rotation frequency (Bigot and Dziembowski,). Their result contradicts with that of Kurtz, ( ) about the

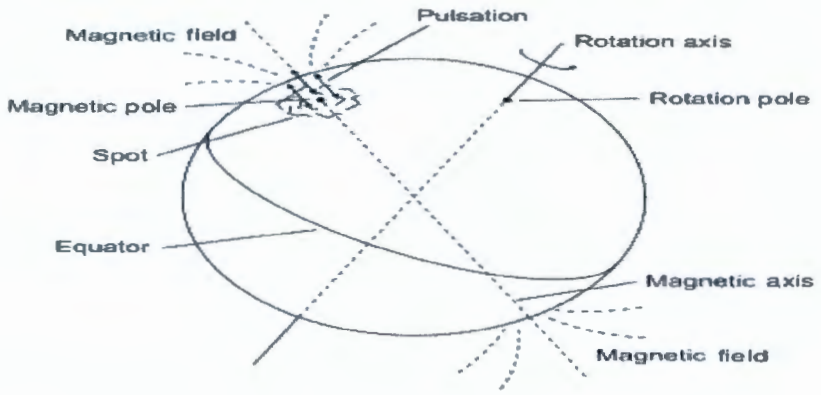

FIGURE 1.12: Pictorial representation of a roAp star. Adapted from (Percy, 2007).

oblique pulsator model where Bigot and Dziembowski, (2002) showed the pulsation axis of roAp stars does not align exactly with the magnetic field axis.
The oblique pulsator model introduced by (Kurtz, 1982) is used to describe roAp stars eigen mode using a single spherical harmonic when the magnetic axis is aligned with the pulsation axis. Due to this geometric setup, the eigen modes written as $2l + 1$ set of frequencies (Dziembowski and Goode, 1985) can be detected in the specified amplitude spectrum whereby each spectrum is distinguished from the existing by the amount which is equivalent to the rotational frequency (Cunha, 2002b).
The oblique pulsator model was further developed by Dziembowski and Goode, (1985) in order to accommodate the contribution of observed properties such as magnetic field and rotation in the oscillation of roAp stars. The inclusion of magnetic field in studying roAp stars is because its presence affects both the oscillation frequencies and eigen functions.
Since the presence of the magnetic field regulates the mode of pulsation, their period of oscillations are shorter as compared to the smaller order radial pulsation period (Percy, 2007). Short period of pulsation makes the measurement of small radial velocity variation difficult due to the fact that both time and velocity resolution play crucial role.
The presence of the magnetic field makes the study of roAp stars very complicated . This is because its importance is negligible towards the core whereas in the atmosphere, the importance is significant (Percy, 2007). Therefore, modeling of such kinds of stars should include the magnetic field rotation as well as the structure of the atmosphere.
Despite the fact that roAp stars pulsate, the cause of pulsation was controversial. But, due to their position in the HR diagram which is very close to or share the same position and cover the same range in temperature and luminosity as the δ Scuti star instability, researchers believe that the pulsation of such kind of stars can be triggered by κ mechanism in the H-ionization region (Houdek, 2003; Houdek and Gough, 2007; Houdek, 2012). But δ Scuti stars are low overtone pulsators as opposed to roAp stars, which makes roAp stars pulsation region to be confined in the upper layer of the stars. In this regard Matthews, (1988) recommended that κ mechanism acting on Si IV can be an effect to excitation mechanisms. But Matthews, (1988) suggestion in this regard faces a challenge because Si IV ionization region exists deep in the star where in roAp stars oscillation amplitudes are very low in that region. Further assumptions regarding their

pulsation mechanism were made based on their position in the HR diagram by considering the similarity of the roAp stars with the sun's pulsation period and suggested stochastic excitation as the cause of pulsation. But Houdek et al., ( ) stated that due to the large amplitude in roAp stars, it is hard to see the effect of stochastic mechanism to keep the pulsating going.

Magnetic field contributes a lot in the pulsation of roAp stars. Therefore, attempts were made to investigate its effect on the pulsation of roAp stars. One of the investigations was done by Dolez and Gough, ( ). Their emphasis was to study and calculate the growth rate by considering the equatorial region. Convection is untouched with chemically homogeneous stellar envelopes having H, He, heavy elements, and strong magnetic fields in the polar regions where convection is totally suppressed (Balmforth et al.,). Dolez and Gough, ( ) also considered the same stellar envelope with weaker magnetic field but their attempt failed in obtaining any excited high overtone modes.

More investigations were done by Gautschy, Saio, and Harzenmoser, ( ) regarding the excitation mechanism. They presented the excitation mechanisms by categorizing them into two broad groups: The first one is proposed by Shibahashi, ( ) which is resonant driving by observable convection with strong magnetic field in a super adiabatic zone close to the polar region. In this region, the convective motions are limited which makes the oscillation grow with time because of the heat exchange. Shibahashi, ( ) concluded that the global oscillations due to the over stability are going to be very high overtones. They are assumed to be the driving mechanism behind the rapid oscillation which in turn is also responsible for the change in the mean luminosity. The second is simply the classical κ mechanism acting in the H-ionization zone acting in the polar region (Dziembowski and Goode, ; Balmforth et al.,). In addition, Dziembowski and Goode, ( ) further investigated the driving mechanism by considering homogeneous equilibrium model and applying non adiabatic code. Pulsation in roAp stars is driven by κ mechanism which is acting in the hydrogen ionization zone. Further recommendations in their findings revealed that as compared to the radiative damping occurring beneath the hydrogen ionization zone, the driving mechanism is weak. One should notice that magnetic field was neglected while they did their modelling. More attempts were made to explain the driving mechanism by (Balmforth et al., ; Balmforth et al.,).

Recent developments in studying roAp stars was conducted by Holdsworth et al., ( ) by analyzing KEPLER data for KIC7582608. The star shows high pulsation frequency ($181.7324d^{-1}$) and low frequency rotational modulation with period of 20.4339d. Moreover, this star shows, from Kepler long cadence observation, a frequency quintuplet split by the rotational period of the star, typical for an oblique pulsator. Another result from *Kepler* observation is the discovery of a roAp star KIC4768731, a bright long period pulsator, which is a dipole pulsator whereby line profile variations are caused by rotation (Smalley et al.,).

(e) **γ-Doradus Stars** A new group of population I stars known as γ-doradus which was first discovered to be variable stars by Cousins and Warren, ( ) and further discoveries by Balona, Krisciunas, and Cousins, ( ). These groups of stars are recognized as new group of pulsating stars as F (F0-F2) type dwarf variables in a new group of population I stars. These stars are located close to the intersection of the red edge of δ Scuti instability strip and the main sequence partly overlap the cool edge of the δ Scuti

instability strip as shown in the Color-Magnitude diagram in Fig. 1.14.

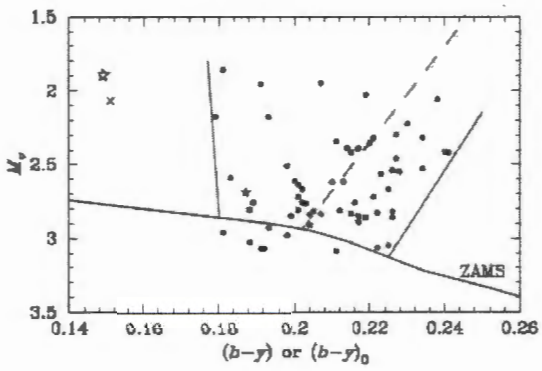

FIGURE 1.13: Location of γ-Doradus Stars in the HR diagram. Where the two lines represents the boundary of γ-Doradus instability strip, whereas the broken line is the cool edge of the δ Scuti instability. Where the dots represents γ-Doradus stars whereas the cross and the star represents γ-Doradus with unique features. Adapted from (Handler, 1999 modified by Percy, 2007).

Fig. 1.14, color-Magnitude diagram, shows the position of γ-Doradus Stars. The solid dot represents γ-Doradus. The cross and the star on the other hand represents γ-Doradus Stars with special features. The two solid lines running perpendicular to ZAMS are the limits of γ-Doradus instability strip where as the dotted line in between the two solid lines represents the colder edge of δ-Scuti instability strip. These stars are found in the HR diagram that is bound by a temperature range ($\sim 7200 \leq T_{\text{eff}} \leq 7550$K) on the ZAMS and $\sim 6900 - 7400$K near the end of the main sequence (Handler, ; Handler and Shobbrook,).

γ-Doradus stars have masses in the range between $1.5M_{\odot} - 1.8M_{\odot}$ and have periods of oscillations ranging between 0.3 days (De Cat et al.,) and $0.4 - 3$ days with amplitude 0.1 in V (Joshi and Joshi,). Furthermore, the absolute magnitude and their luminosities varies between $+1.93 - +3.07$ and $5 - 15L_{\odot}$ or $0.7 \leq \log \frac{L}{L_{\odot}} \leq 1.05$ respectively and luminosity classes V or IV-V. In addition, their effective temperature as stated in Percy, ( ) ranges between $6950 - 7375$K and radius $1.43 - 2.36R_{\odot}$ that makes them as one of the homogeneous groups of variable stars with convective cores and shallower convective envelope. γ-Doradus stars are considered to be very young with age $\leq$ 250Myr. (Kaye et al.,) which have metallicities similar to solar or subsolar stars.

γ-Doradus stars pulsate in multiple (double), non radial (Kaye et al.,), high order (n), low spherical degree (l) and non radial gravity modes (Kaye et al., ; Kaye et al., ; Percy,) pulsators of high radial overtone. The period of pulsation along with the g modes help to study asterosesmology and investigate the internal structure of the star. Specifically those stars having both p and g modes play a fundamental role in studying asterosesmology due to the fact that their multi-frequency pulsation can help to study both the outer/surface and the inside region of the stars.

Since our understanding towards γ-Doradus stars pulsation is obvious, research was focused on understanding their cause of pulsation. The cause of pulsation as discussed in Guzik et al., ( ) and Guzik et al., ( ) is due to the modulation at the base of deep convective envelope of radiative flux and flux blocking mechanism which is

introduced by Pesnell, ( ). Flux blocking is defined as a variation of the normal κ and γ mechanism in Cepheids. This mechanism was further investigated theoretically by Li, ( ) and Li, ( ).
Flux blocking mechanism is effective at a region whereby opacity increases and cause an unexpected transition from full radiative to full convective (Guzik et al., ; Guzik et al.,). In order for convective blocking to be considered as a driving mechanism, the γ doradus stars should have a deep envelope convection zone (Guzik et al.,). Convective blocking happens when the time of convection is either of the same order or longer than pulsation period. Radiative luminosity drops dramatically at the bottom of the convective zone due to the lack of adjustment during the pulsation cycle to transport the radiation energy which is coming from below the convective zone. At this phase of the cycle, the radiation luminosity will be blocked periodically whereby it is considered as a cause for oscillation (Dupret et al.,). This mechanism also plays a fundamental role to determine the exact position of the γ doradus stars in the HR diagram (Warner, Kaye, and Guzik,). On the other hand, the position of γ doradus stars in the HR diagram is between those stars having deep convective envelope and stars having radiative envelope. This implies that they are located at the position whereby depth of the convective envelope varies with the star's T_{eff} (Bouabid et al.,) and plays a preliminary role in the cause of pulsation of γ doradus stars.

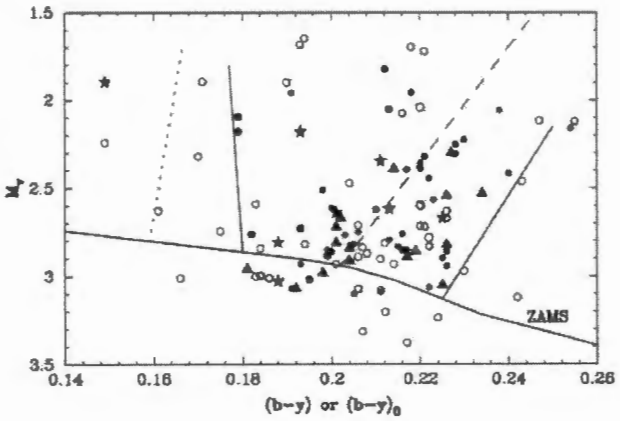

FIGURE 1.14: C-M diagram showing the location of γ-Doradus Stars. Where $\star$ shows bonafide γ-Doradus observed by Handler and Shobbrook. Filled triangles are bonafide γ-Doradus Stars from literature. • represents prime γ-Doradus candidates whereas ○ are other γ-Doradus candidates. The dotted lines are blue boundary of the γ-Doradus region. The dashed line on the other hand shows the red edge of the δ-Scuti instability strip. Adapted from (Handler and Shobbrook, 2002)

According to Balona et al., ( ) explanation, the calculation to find the instability strip for γ-doradus stars done by earlier researches (Warner, Kaye, and Guzik,) by applying frozen-in convection, found that the theoretical instability strip was far away from fitting with the observational results. To avoid such discrepancies, models were developed by implementing the theory of time dependent convection (TDC) to a specific star with known values of mass, modes of pulsation, which is assumed to be γ-doradus star. TDC proved that convective blocking is the fundamental cause of pulsation.

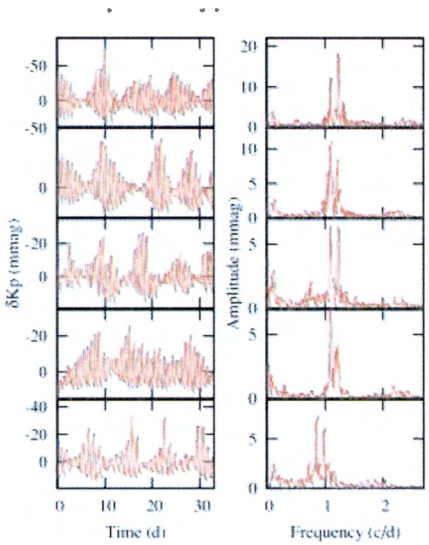

FIGURE 1.15: Light curves on the left and periodograms on the right panel for sampled γ-doradus stars from KEPLER observation. Adapted from (Balona et al., 2011)

Balona et al., (2011b) showed in Fig. 1.15 on the left panel asymetric light curves of selected γ-doradus stars from KEPLER observation. The right panel showed the periodograms of the stars under investigation from top to bottom in the following order KIC 3441414, 4547348, 4661223, 5000456 and 5021374. Significant contributions in the discovery of γ-doradus star was made by *Kepler* Balona et al., (2011b). They also emphasized the discovery of low frequency $3.412\frac{1}{d}$ and multi periodic γ-doradus pulsation detected in Ap star KIC8677585. Further discoveries of γ-doradus star pulsation were made by CoRoT in two pre-main sequence stars (Zwintz et al., 2013).

(f) **The Sun and Solar-like Stars (Oscillations excited stochastically by convection)**
The best example in discussing solar-like oscillation is the study of the closest star to us, the Sun. The position of solar-like oscillators in the HR diagram and the spectrum of the solar-like stars are shown in Fig. 1.16, Fig. 1.17 and Fig. 1.18.
The HR diagram shown in Fig. 1.16 clearly shows the position where the main sequence and stars with solar-like oscillations are positioned. The diagram also shows some of the solar-like oscillators observed using both ground and space based spectroscopy. The solid dots (filled circles) are observed from ground and open circles shows space based spectroscopic observations.

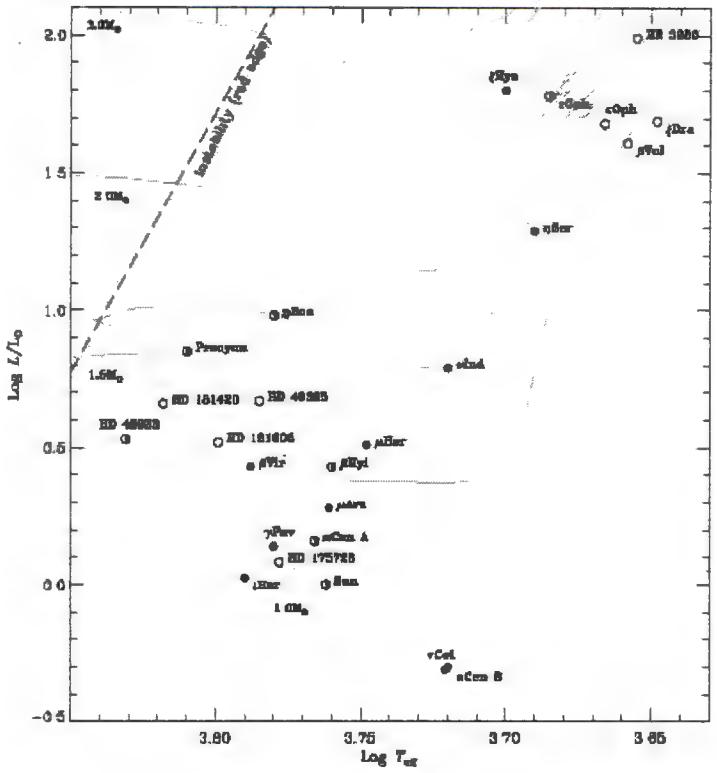

FIGURE 1.16: H-R diagram showing the position of stars with solar like oscillations. Adapted from (Bedding, 2014)

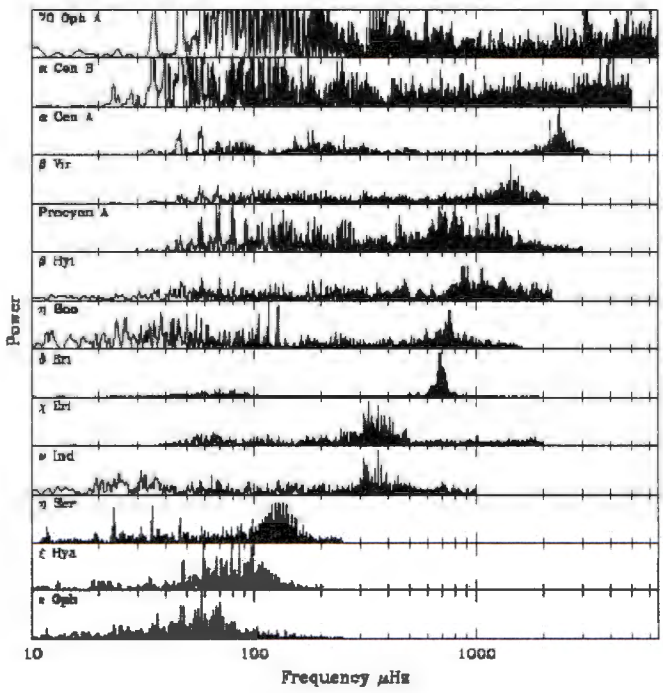

FIGURE 1.17: A diagram showing power spectrum of some of the solar-like stars throughout the whole range of spectrum. Adapted from (Aerts et al., 2010)

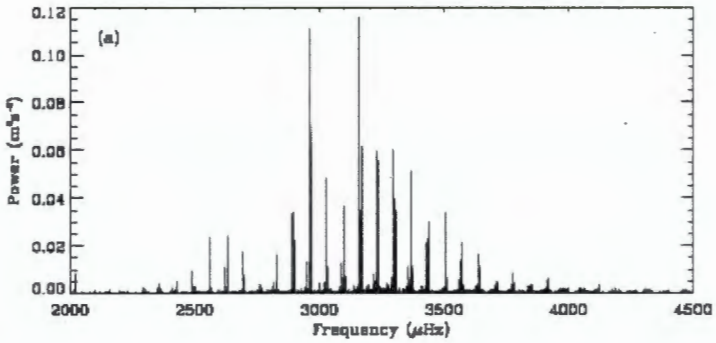

FIGURE 1.18: Power Spectrum of solar-like pulsators. Adapted from (Bedding, 2014).

Solar-like oscillations can easily be identified by studying their oscillation power spectrum as shown in the top panel of Fig. 1.17 and Fig. 1.18 and it shows p-mode in the Sun where it also shows the the peak power, ν_{max}.
The term solar-like is used to describe the pulsation of other kinds of stars where their pulsation is triggered by the same mechanism as the Sun does. The oscillation of the Sun is basically excited stochastically by convection (Ulrich, ; Christensen-Dalsgaard and Frandsen, ; Houdek et al., ; Toutain and Froehlich, ; Bedding,) and is intrinsically stable (Goode and Strous, ; Chaplin and Miglio,). These kinds of oscillations are expected in low mass MS stars, RGB, Asymptotic giant branch and sub giants. Their pulsation period is found to be around 5 minutes with frequency range (for the sun $1-4mhz$) to few days for main sequence (like the sun) and sub giants and giants respectively (Joshi and Joshi,). Theoretical investigations also revealed that their luminosity varies from $mmag-ppm$ (where this range is below the threshold of ground based photometric observation) in giants, MS, and sub giant stars respectively (Kjeldsen and Bedding,). For the cause of their pulsation, those stars with $T_{\text{eff}} \leq 7\times10^3$K usually in their outer region will have a convective layer which might be the cause for such stars to have solar like oscillation Kjeldsen and Bedding, ( ). It is even considered as a necessary condition for stars to have or show solar-like oscillation (Chaplin and Miglio,). In order for these stars to have a surface convective zone, the star under consideration should be cool (Bedding,).
The convective turbulence plays a fundamental role in exciting thousands of pulsation modes and confirmed both in photometric and spectroscopic observation in the sun (Percy,). The modes observed from solar like oscillations are high order, non radial acoustic p modes (Joshi and Joshi,). These pulsation modes helped in studying the interior of the sun and the subject is called Helioseismology.
Solar-like oscillations having period of oscillations with an hour or $\geq$ hours confirmed observationally in a lot of G and K giant stars. Bedding, ( ) also stated that solar like oscillations are observed in semi regular (M-giants) where the observation was conducted by amateur astronomers in AAVSO (Christensen-Dalsgaard, Kjeldsen, and Mattei,). Further evidences of solar like oscillations were detected in one δ Scuti some B type stars. CoRoT observations also revealed that one of the β Cephei star, V1449Aql exhibits solar like oscillation but investigations from Kepler on the same type of stars failed to prove stochastically excited oscillation (solar like oscillation) (Bedding,) reference there in.

Solar-like oscillations are standing waves which are called pressure (p) modes and are acoustic waves where pressure is the restoring force (Bedding and Kjeldsen, 2003). Such modes are always seen in the sun and other sun like stars (Bedding, 2014). Such modes can be characterised using 3 integers: namely n-representing radial order, l-which specifies the angular degree and m-represents the azimuthal degree. According to Bedding and Kjeldsen, (2003), it is always possible to write an approximation equation to describe the mode frequencies for lower p modes in main sequence stars. In pulsating stars, the asymptotic relations are very important if $n \gg l$ which is importnaat to interpret the results about stars. The asymptotic relation is given below in the following equation:

$$\nu_{n,l} = \Delta\nu(n + \frac{l}{2} + \epsilon) - l(l+1)D_0, \tag{1.3}$$

where $\Delta\nu$-large separation which shows the average stellar density, D_0-sensitivity to the sound speed near the core, ϵ-sensitivity to the surface layers.
Solar-like oscillations can easily be identified from their periodogram because of the existence of a comb like structure where the amplitudes show decrement from the maximum point at the middle as shown in Fig. 1.19 and Fig. 1.20.

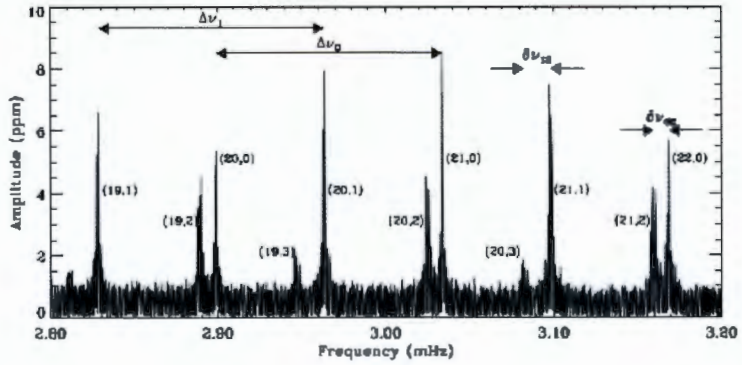

FIGURE 1.19: A small sample selected from a solar spectrum with specific (n, l) values for different modes.
Adapted from (Bedding and Kjeldsen, 2003)

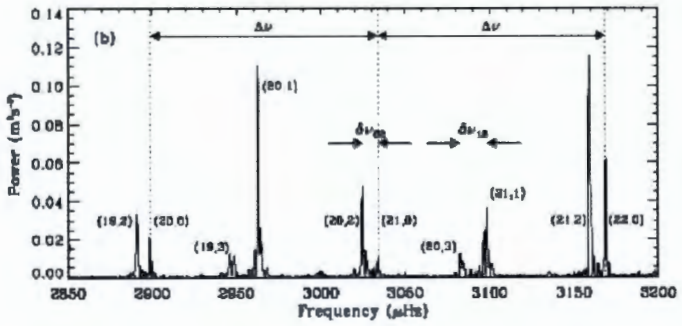

FIGURE 1.20: Figure showing Solar Spectrum for each mode with (n, l) values.
Adapted from (Bedding, 2014)

The power spectrum in Fig. 1.19 shows uniform and well structured design which clearly designates the property of the the oscillation of a spherical star (Bedding,). The two figures, Fig. 1.19 and Fig. 1.20 shows the power spectrum with specific values (n, l) which also shows $\Delta\nu$ (showing the space between successive radial tones) where,

$$\Delta\nu \propto \sqrt{\bar{\rho}}, \tag{1.4}$$

where $\bar{\rho}$ is mean stellar density.
Defining $\delta\nu_{02}$ in the following equation as the small separation (frequency spacing between neighboring modes with $l = 0$ and $l = 2$), where for a certain radial order n, the small frequency separations can be written as:

$$\delta\nu_{0,2} = \nu_{n,0} - \nu_{n-1,2}, \tag{1.5}$$

$$\delta\nu_{0,1} = \frac{1}{2}(\nu_{n,0} + \nu_{n+1,0}) - \nu_{n,1}, \tag{1.6}$$

$$\delta\nu_{1,3} = \nu_{n,1} - \nu_{n-1,3}, \tag{1.7}$$

$$\delta\nu_{0,4} = \nu_{n,0} - \nu_{n-2,4}. \tag{1.8}$$

All these values of small frequency separations are shown in Fig. 1.20.

1.6.3 Stars Below the Main Sequence Stars

(a) **EC**14026: Are also called pulsating sub dwarf B stars (sdBV). Pulsating sub dwarf B stars are groups of B stars along the main sequence star but are not young where in their evolutionary track they are passing at the end of their evolutionary stage (Percy,). Furthermore, these stars are low mass $0.5M_{\odot}$ (Aerts, Christensen-Dalsgaard, and Kurtz,), extreme horizontal branch found in the HR diagram where they are at the very hot end of the HB. Their structure consists of the core (centre) where He-burning is dominant and a shell which is found around the core where H-is deficient (Percy, ; Balona,).
A new class of sdB stars which are rapidly oscillating star EC14026 − 2647 were discovered by researchers at the South African Astronomical Observatory (SAAO)(Kilkenny et al.,). EC14026 has period of 134s with amplitude ~ 0.012mag having temperature $2.8 \times 10^4/(2.2 - 4) \times 10^4$(Green et al.,)/ $(2.3 - 3.2) \times 10^4$(Schuh et al.,)/3.6×10^4(Aerts, Christensen-Dalsgaard, and Kurtz,) and $5 \leq logg \leq 6$. Such kinds of stars are believed to pulsate and their pulsation is confirmed with their driving mechanism for pulsation. It is suggested that the driving mechanism for pulsation for such kinds of variables is deep in their envelope. κ mechanism is operating in the partially ionized iron atoms which causes the opacity bump (Percy,). Investigations on their evolution as Balona, ( ) claimed, such stars loses H from their envelopes during mass loss whereas the core gained some mass. As a result of an assumption made where sdB variables are considered as close binaries leading to the conclusion that mass loss is feasible.
Additional studies were conducted to investigate more on such kinds of stars and Green et al., ( ) accidentally discovered a new group PG1716 + 426 low amplitude, long

period multi mode sdB variable having period of the order of an hour which is longer than the previously discovered sdB stars (EC14026). Their investigation also revealed the longer period is because of the g-modes where it is common in cooler sdB stars. The new groups of stars have ten times longer period than EC14026 which is caused by g-modes. Moreover, Schuh et al., ( ) discovered a star with frequency spectrum of EC14026 HS0702+6043 where this star exhibits simultaneous g and p mode pulsations that makes such kinds of stars to contribute significantly in studying asteroseismology. Similar investigations were done by Brassard et al., ( ) for a star PG0014 + 067 which is an EC14026 star where they are confirmed to have low amplitude, short period, multi periodic variation. This star was further studied by Charpinet et al., ( ) and confirmed all the proposed findings in the previous study.

(b) **Planetary Nebula Nuclei Variable (PNNV)** These stars are pre-white dwarf which are populated at the center of the planetary nebula. PNNV stars are multiperiodic which pulsate with a period in the range between $10-35$ minutes having 0.1mag (Joshi and Joshi,). Planetary nebula according to Yungelson and Tutukov, ( ) are created by ejection of envelopes by AGB stars or by ejection of common envelops by close binaries. So, when one studies PNNV, it means the variability of stars contained at the center of planetary nebula where some have both spectroscopic and photometric variabilities up to 0.2 mag and pulsations with periods ranging from few hours to days and low T_{eff} between $(3-5)\times 10^4$K. The center of the planetary nebula is the hottest normal star and are located in the HR diagram in the temperature range $6\times 10^4-1\times 10^5$K. Their luminosity is found to be $(10-3000)L_{\odot}$. Investigations on such kinds of variables were conducted theoretically by Stothers, ( ). Photometric observational evidences also proved that the center of a planetary nebula nuclei is a variable. Among these variables, the first to be noted is Kohoutek/K1 $-$ 16 (Kaler,). The spectroscopic observation result of K1 $-$ 16 showed that the star is non-radial, multi periodic, g-mode pulsator with very high temperature ($T_{\text{eff}} \geq 1\times 10^5$K), high abundance of C, O and H-deficiency (Bond, Ciardullo, and Kawaler,). Bond and Meakes, ( ) showed that the planetary nebula Longmore 4(LO4) is non radial, multiperiodic pulsators with p-p amplitude 0.1mag. Both K1 $-$ 16 and LO4 showed strong optical spectra of He II, CIV and OVI. These results reveal that the PNNV are very hot $\sim T_{\text{eff}} \geq 10^5$ with stellar surface dominated by C and O but H-is deficient.

Further studies on observational evidences of PNNV was conducted and reported by Grauer and Bond, ( ) when they presented photometric evidences of the central star of Kohoutek/K1 $-$ 16. It was found out to be the first PNNV variable to be confirmed as a low amplitude pulsator. Non radial, non adiabatic pulsation models were performed on such PNNV stars K1 $-$ 16 by Starrfield et al., ( ) and demonstrated that K1 $-$ 16 is a family of the variable PG1159 $-$ 035 which is a bridge between OVI-CPN and hottest non DA WD. Moreover, Starrfield et al., ( ) modelled theoretically for such types of stars with $T_{\text{eff}} \geq 10^5 K$ with $M \approx 0.6 M_{\odot}$, hot, C-O pre WD pulsating in non radial g^+ mode and their pulsation is caused by ionization of C and O. The same mechanism works for K1 $-$ 16 variable star and are found in the same instability strip as the model done.

The light curves shown in Fig. 1.21 1a of the light curve K1 $-$ 16 which shows that the oscillation is sinusoidal with 0.01mag and period of 28 minutes (1680sec). Fig. 1.21 1b also shows the same behavior as Fig. 1.21 1a but observation was conducted on a different day but the period was still the same as the previous day. Furthermore, Fig. 1.21 1c

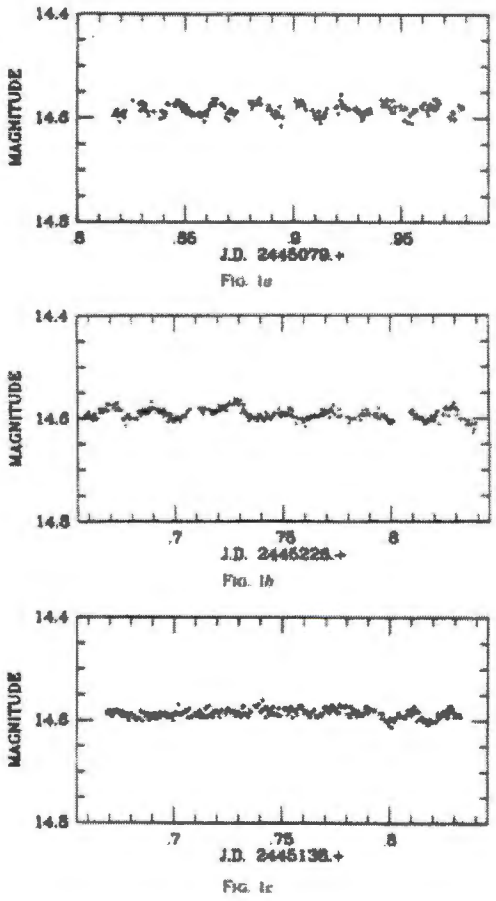

FIGURE 1.21: Light curves showing the variability of the central star in K1 − 16 (Planetary nebula) observed on 20^{th} April 1982. Adapted from (Grauer and Bond, 1984).

also shows results of the same target observed on a different day. It can be seen from the graph that there was no clear variability on the first part of the graph but a sudden change in variability can be seen on the latter stage of the observation (Grauer and Bond,).

Further evidences on PNNV variables also found in a planetary nebula IC418. Mendez, Verga, and Kriner, ( ) observed light variation with a period of a couple of hours (1 − 2hrs.) and amplitude of 0.1mag and suggested modulation in the outer flow as the cause for variation but they did not exclusively ignore non radial pulsation. More studies on the center of planetary nebula IC418, variable star, HD35914 classified as $07f$ Kuczawska and Zola, ( ) which is observed using multi site photometric observation (Handler et al.,).

Handler et al., ( ) observed two variabilities from their analysis:

- irregular light modulation (period$\sim$ order of days)
- cyclic variations (periods $\sim$ 6.5hrs) and its variations are semiregular.

Regarding the cause of their variabilities Hutton and Mendez, ( ) and Patriarchi and Perinotto, ( ) suggested variable stellar wind where as Zalewski, ( ) attributed stellar oscillation (non radial pulsation) as the cause for variability.

More theoretical modeling was done on variability of the centre of a planetary nebula (Kawaler et al.,). Kawaler et al., ( ) implemented full non adiabatic g-mode

pulsation to model the nucleus of the planetary nebula. They considered the nucleus of the PN to be H-deficient but possess a shell having dynamic He-burning. Kawaler et al., ( ) model predicted that the existence of He-burning shell triggers ε-mechanism to drive instabilities with periods $50 - 214$sec. These findings further enhances the suggestion that a number of g-modes might be unstable. In addition, Kawaler et al., ( ) for H-deficient and He-burning dominated shell showed that the PNNV stars show variability. Despite these suggestions, observation of the center of the PNNV using high speed photometry is a bit different due to the contamination occurred because of the nebular background brightness and error on the tracking of the telescopes used for observation. Due to this reason, Hine and Nather, ( ) suggested how to improve the contaminations and observe the PNNV variables by modifying a two-star photometer and letting channel-2 star to implement auto guide which helps small aperture ignoring contamination as well as decreasing the error caused by tracking. The problems are noticed in the period range suggested theoretically by (Kawaler et al.,).

1.7 Why Do Some Stars Pulsate?

Stars are usually approximated to have spherical shape where hydrostatic equilibrium is maintained between the pressure generated by the core and the force of gravity. Therefore, when we talk about stellar pulsation, it is about oscillation at this equilibrium position. Since the conception of the idea proposed by August Ritter in 1879 about variation of stars and prior to that, the cause of variation of stars was assumed to be rotation or eclipse. These assumptions were true till Harlow Shapely in 1914 demonstrated that pulsation was the cause of variation in δ Cephi stars. More studies for the cause of pulsation was done intensively and researchers came up with the idea that stars' pulsations are caused by κ-mechanism. Because in most stars, the opacity of the stellar gas decreases as temperature increases. On the other side, there are regions where this case gets weaker or might reverse. On the other hand, in Hydrogen and Helium ionization zones, opacity increases as temperature increases (Zhevakin, ; King and Cox,).

Stars are considered as giant hot ball of gas and as one moves from the outer surface to the core, one encounters different regions which vary in temperature and composition as shown in Fig. 1.22.

A non pulsating star having enough surface temperature, where the hydrogen ionization zone have large part of the envelope mass, and since helium has single electron bound to the nucleus, a small perturbation in a star can cause it to contract and hence resulted in an increase in the temperature. This makes the helium fully ionized which leads to an increase in the opacity of the layer. The increased opacity has the capacity to capture radiation emanating from the core of the star which causes the helium layer to expand, as a result the radius of the star increases due to the expansion. When a star expands, its temperature decreases and cools which in turn makes the electron to have a chance to recombine with nuclei which lowers the opacity and reduces the layer's ability to absorb the radiation. As a result, the layer shrinks and decreases the radius of the star. The second scenario which causes the stars to contract can also initiate the expansion. Therefore, this periodic contraction and expansion causes the stars to pulsate Percy, ( ). The above scenario is illustrated in Fig. 1.22 and Fig. 1.23 that shows the pictorial representation of a pulsating variable star's regions where hydrogen and helium ionization occurs.

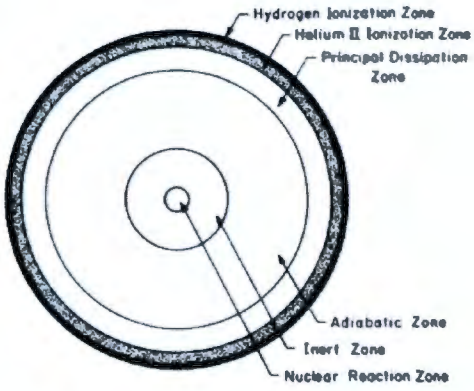

FIGURE 1.22: Schematic illustration of pulsating variable star showing the regions contributing for pulsation (Adapted from Christy (1967)

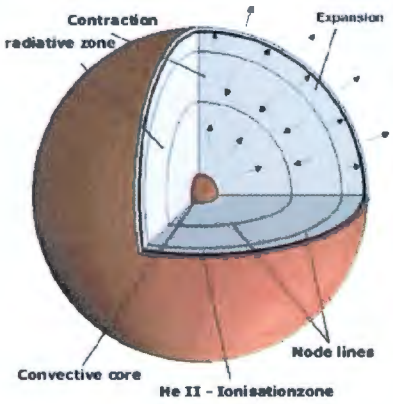

FIGURE 1.23: Schematic illustration of the node lines in the stellar interior for a radial pulsation with n=2 (Adapted from Zima (1999))

Since the first inception of the concept of driving mechanism for stellar pulsation by Eddington in 1926, a lot had happened to understand the mechanism that drives pulsation in stars. In this section, we summarize some driving mechanisms for pulsation. When one studies pulsation, it is fundamental to understand the contribution of opacity, denoted by κ. In studying stellar pulsation, the emphasis is to study and understand the mechanisms whereby the energy generated from stars by nuclear fusion is transferred to work. Eddington 1926 suggested a mechanism called *valve mechanism*, by considering stars as engines. The following are some of the driving mechanism in stellar pulsation.

(a) κ mechanism- is one of the mechanisms that excites pulsation in most stars. The reason behind this is that opacity's contribution to diffuse radiation in the star is higher. Opacity of a star depends mainly on mass, atoms, wave length and density. In order κ mechanism to have an effect in exciting pulsation, the layers in the star should gain energy and release it during pulsation (referring to compression and rarefaction). This gain and lose of energy is related to hydrogen and helium ionization zones (Catelan and Smith, 2015). κ mechanism is a heat engine mechanism for exciting pulsation through ionization dependent κ effect. κ mechanism provides a possible way of excitation of pulsation and mostly operate in both the partial ionization regions of hydrogen and helium.

(b) γ mechanism- when a star pulsates, in the partial ionization zone, a star contracts, the energy supposed to heat the region participates in κ mechanism to gain heat and increases ionization, this in turn increases κ and helps to hold more radiation. As a result an outward pressure dominates. This process gives rise to γ mechanism. γ mechanism can be explained based on the adiabatic components, Γ_3 refer section 2.2 of this thesis for further explanation of adiabatic components. Due to this fact, the region moves outwards resulting in cooling. Cooling triggers another combination of ionized elements. The position where this scenario happens, determines their contribution in exciting pulsation.

(c) Stochastic excitation- is a mechanism where pulsation in the Sun and other cool stars are excited. In such kinds of stars, especially close to the surface, there is a convective turbulence having a speed close to the speed of sound that causes acoustic radiation or noise which in turn leads to exciting normal modes or solar type oscillations (Aerts, Christensen-Dalsgaard, and Kurtz,).

Chapter 2

Theory of Stellar Pulsations in Stellar Atmosphere

2.1 Stellar Atmosphere

"Why in the world would any one want to study stellar atmospheres? They contain only 10^{-10} *of the mass of a typical star! Surely such a negligible fraction of a star mass cannot possibly affect its over all structure and evolution!"* question asked to Mihalas by Ed Salpeter during the $60's$ (Mihalas,).

A stellar atmosphere is a region or medium which is physically intact to a star where photons, which can provide clue and understand the star, emanate. It is also the outer part of the star which is visible from outside using our telescopes. The region can also be described as a region whereby electromagnetic radiation are released to space. Stellar atmosphere is also a transition between dense stellar interior and its stellar medium (Milne, ; Hubeny, ; Hubeny and Mihalas,). Stellar atmosphere can be divided into three regions (Milne,):

- Photosphere- One of the regions of the atmosphere of a star whereby the continuous spectrum from the star is given out where the energy transport mechanism changes from convective to be dominated by radiative transfer (Vögler, Bruls, and Schüssler,).
- Reversing Layer- is the region of the star where absorption-line spectrum are observed
- Chromosphere- It is the third region where flash spectrum is observed, when observed edge on. The chromosphere is studied in detail for the sun by different authors.

Understanding of the physics about the stars mainly depends on our conceptualization of the outer layers of the star, the atmosphere Mihalas, ( ). Deep inside the core of the star, density is higher that makes the photons to have shorter mean free paths whereas further outside the core of the star density drops drastically. These regions, where the photons coming from the core of the star pass through, interact with different physical conditions as well as combine with several atoms, gases, dust and molecules; and these encounters determine the spectral type observed from the stars. The atmosphere of the star is a very thin 10^{-10} of the mass of the star at the outer boundary of the star (Mihalas,). Despite the size of the atmosphere is very thin, studying it is crucial to understand the properties of stars using the information coming from it. The information regarding any astronomical objects (stars, galaxies) comes from the analysis of their radiation spectra emanating from their atmospheres. This makes the study of stellar atmospheres an important field in astrophysics.

Hubeny, ( ) credited the recent developments in the study of stellar atmosphere not only to the high quality earth and space based observatories but also to the development of trusted and reliable computer programs. In spite of all these promising research results, more should be done to unravel the necessary informations to understand the nature of stars. A stellar atmosphere, in general, is a plasma consisting of atoms, ions, free electrons, molecules, dust grains and photons where its temperature varies from $\leq 10^3$K for coolest stars to $\geq 10^5$K for hot stars and $10^6 - 10^7$K in the stellar corona. Their particle densities is in the range $10^6 \leq \rho \leq 10^6 cm^{-3}$ (Hubeny,). Hubeny, ( ), Mihalas, ( ), and Hubeny and Mihalas, ( ) summarized the importance of studying the atmospheres of the stars as:

- When one observes a star from a ground or spaced based observatory, the stellar atmosphere is the only visible part of the star. On the other hand, in the sun, where non radial modes of pulsations can be observed on its disk which can help to infer about the internal composition of the sun. The remaining stars, where the gas in the envelope of the star happen not to be transparent, getting information about the internal composition of the star would be difficult. Due to this fact, the data about the internal structure can only be obtained from the atmosphere. So it is fundamental to focus on studying the atmosphere of the stars.
- By implementing a reliable computer program to the analysis of the stellar spectra, it paves a way to analyse the stellar composition, internal structure and evolution history of the stars.
- The data that we get from observation of the atmosphere can help to change the observer's colour-magnitude to the theoretical Luminosity- Effective temperature graph ($L - T_{\text{eff}}$) where it can possibly lead to developing stellar evolution theory.
- To get information about any astronomical object, it is fundamental to study the spectra and analyse it, where it helps to study the dynamics of the astrophysical objects under investigation.
- Moreover, by studying the stellar atmosphere of stars, one can study stellar population in galaxies, ages and chemical compositions and evolutions. Furthermore, it provides plenty of information on testing the Big Bang.

2.2 Stellar Pulsation Theory

A gas inside a pulsating star is treated as a continuous matter and the pulsation of the stars are caused by the continuous perturbation of the fluid inside the star. The reason behind this assumption according to Cox, ( ) and Aerts, Christensen-Dalsgaard, and Kurtz, ( ) is to describe the properties as functions of position (r) and time (t). Some of the basic physical quantities required to describe the properties of the gas are $\rho(r,t)$, $P(r,t)$, $V(r,t)$ local density, pressure and instantaneous velocity respectively, $V(r,t) = \frac{dr}{dt}$. The introduction of these terminologies have an important role in the upcoming discussions on stellar pulsations. By using the basic hydrostatic equilibrium equations and implementing perturbations along with the physical quantities, we are going to lay foundation on developing the theory of stellar pulsation.

(a) **The continuity Equation**- During a stellar pulsation, mass is conserved and can be written as:

$$\frac{\partial \rho}{\partial t} + \nabla(\rho V) = 0, \tag{2.1}$$

where ∇ is the divergent, ρ, t are density and time respectively. The equilibrium equation stated above shows the equal rate of change of matter in a volume with the flux of the quantity into the volume which is the manifestation of standard conservation equation. The conservation equation can also be written in another form if one uses the time derivative,

$$\frac{d\rho}{dt} + \rho(\nabla \rho V) = 0, \tag{2.2}$$

where $\frac{d}{dt}$ is the material time derivative. Eqn.(2.2) describes the rate of change of density due to the motion.

(b) **Equations of Motion**- Stellar objects including the sun are governed by some factors which can affect their physical conditions. Among these factors, Aerts, Christensen-Dalsgaard, and Kurtz, ( ) mentioned the internal friction (viscosity) where this can be disregarded. The only force, on a given volume of gas, are the surfaces and body forces. This can lead to a new formalism of the equation of motion:

$$\rho \frac{dV}{dt} = -\nabla P + \rho f, \tag{2.3}$$

where $f = \frac{body\ force}{mass}$ and the gas pressure P can be defined as $-PndA$, where dA is the surface element and n is the normal. If one implements the time derivative relation ϕ,

$$\frac{d\phi}{dt} = \left\{ \frac{\partial \phi}{\partial t} \right\}_r + \nabla\phi . \frac{dr}{dt} = \frac{\partial \phi}{\partial t} + V.\nabla\phi, \tag{2.4}$$

then the equation of motion becomes:

$$\rho \frac{\partial V}{\partial t} = \rho V.\nabla V = -\nabla P + \rho f, \tag{2.5}$$

Aerts, Christensen-Dalsgaard, and Kurtz, ( ) take into account gravity and ignored

magnetic field where the gravitational acceleration $g = -\nabla\phi$, where ϕ is the gravitational potential which satisfies the poisson's equation $\nabla^2\phi = 4\pi G\rho$.

(c) **Energy Equations**- In order to get basic link among the two parameters p and ρ, one should consider the first law of thermodynamics:

$$\frac{dq}{dt} = \frac{dE}{dt} + P\frac{dV}{dt}, \tag{2.6}$$

where $\frac{dq}{dt}$ is rate of heat loss (gain), $E = \frac{Internal\,energy}{mass}$. Equn.(2.6) can also be written by assuming $V = \frac{1}{\rho}$ as:

$$\frac{dq}{dt} = \frac{dE}{dt} - \frac{P}{\rho^2}\frac{d\rho}{dt} = \frac{dE}{dt} + \frac{P}{\rho}\nabla V, \tag{2.7}$$

if one applies thermodynamic variables, the energy equation becomes:

$$\frac{dq}{dt} = \frac{1}{\rho(\Gamma_3 - 1)}\left[\frac{dq}{dt} - \frac{\Gamma_1}{\rho}\frac{Pd\rho}{dt}\right], \tag{2.8}$$

$$= c_p\left[\frac{dT}{dt} - \frac{\Gamma_2 - 1}{\Gamma_2}\frac{T}{P}\frac{dP}{dt}\right], \tag{2.9}$$

$$= c_\nu\left[\frac{dT}{dt} - (\Gamma_3 - 1)\frac{T}{\rho}\frac{d\rho}{dt}\right], \tag{2.10}$$

where c_p and c_ν are specific heat capacities respectively at constant pressure and at constant volume for a unit mass. Furthermore, the 1^{st}, 2^{nd} and 3^{rd} adiabatic indices are explained as: $\Gamma_1 = \frac{\partial P}{\partial \ln\rho}_{ad}$, $\frac{\Gamma_2 - 1}{\Gamma_2} = \frac{\partial \ln T}{\partial \ln P}_{ad}$, $\Gamma_3 - 1 = \frac{\partial \ln T}{\partial \ln\rho}]_{ad}$ where, the isentropic coefficients measures the ratio of the differentials dP, $d\rho$, dT that are responses to reversible isentropic changes in thermodynamic system (Cox, ; Prialnik,).

The foundations of theoretical stellar pulsations presented above can help to further enhance on studying stellar pulsation and develop additional information that contribute to the development of stellar modelling.

To this end, one should consider stars as spherical in shape and to be three dimensional (Kurtz,). Due to this fact, their pulsations modes have nodes in three orthogonal directions namely: radial direction (r), longitudinal direction (φ) and latitude (θ). So the general solutions of the equation of motion for a spherically symmetric star have components in three directions which are given by the following:

$$\xi_r(r,\theta,\varphi,t) = a(r)Y_l^m(\theta,\varphi)e^{i2\pi\nu t}, \tag{2.11}$$

$$\xi_\theta(r,\theta,\varphi,t) = b(r)\frac{\partial Y_l^m(\theta,\varphi)}{\partial\theta}e^{i2\pi\nu t}, \tag{2.12}$$

$$\xi_\varphi(r,\theta,\varphi,t) = \frac{b(r)}{\sin\theta}\frac{\partial Y_l^m(\theta,\varphi)}{\partial\varphi}e^{i2\pi\nu t}, \tag{2.13}$$

where ξ_r, ξ_θ and ξ_φ are displacements in the three orthogonal directions whereas the coefficients $a(r)$ and $b(r)$ are the amplitudes, ν is the frequency of oscillations and $Y_l^m(\theta, \varphi)$ are spherical harmonics given by Arfken and Weber, ( ) as:

$$Y_l^m(\theta, \varphi) = \sqrt{\frac{2l+1}{4\pi}\frac{(l-m)!}{(l+m)!}} P_l^m(\cos\theta) e^{im\varphi} \tag{2.14}$$

and $P_l^m(\cos\theta)$ are Legendre polynomials given by

$$P_l^m(\cos\theta) = \frac{(-1)}{2^l l!}(1-\cos^2\theta)^{\frac{m}{2}} \frac{d^{l+m}}{d\cos^{l+m}\theta}(\cos^2\theta - 1)^l, \tag{2.15}$$

where θ is measured from the pulsation pole which is the axis of symmetry (Kurtz,). The normalization constant after integrating the $|Y_l^m|^2$ over a unit sphere gives:

$$C_{lm} \equiv \sqrt{\frac{2l+1}{4\pi}\frac{(l-m)!}{(l+m)!}}, \tag{2.16}$$

The pulsation axis in most stars except the rapidly oscillating Ap stars coincides with the rotation axis. Since stars are considered as spherical, one needs three quantum numbers to clearly specify the modes of pulsation: n related to the number of radial nodes which is called the *over tone* of the pulsation mode; l the *degree* of the mode and specifies the number of surface nodes that are present; m the *azimuthal order* of the mode, here $|m|$ describes how many of the surface nodes are lines of longitude and the value of m will have a range $-l$ to $+l$ implying existence of $m = 2l + 1$ modes for each degree (Kurtz,).

2.3 Radial Oscillation

This type of pulsation is the simplest form of pulsation whereby a simple spherically symmetric in and out expansion and contraction occurs (Percy,). Radial oscillations are generally observed due to their effect in the change of the star's luminosity, which is due to photometric temperature change. Therefore, photometry is very effective in analysing radial pulsations. Stars are to the first order assumed to be spherical and the entire surface of the star has the same radius where it increases and decreases throughout the pulsation. Analysis of radial pulsations can provide information regarding the mean density. A star has an infinite number of radial modes and the simplest is called *fundamental radial mode* with $l = 0, n = 0$ (Kurtz,), where the entire atmosphere of the star expands and contracts together. First overtone, on the other hand, is caused when the outer zone of the star's envelope expand and the inner zone contracts and vice versa. Cepheids, RR Lyrae stars, and Mira stars primarily pulsate in radial modes. Radial pulsations produces significant changes in luminosity and temperature which in turn affects brightness and colour respectively, and radial velocity measurement that provides an evidence for a radial pulsation.

2.4 Non-Radial Pulsation

Non radial pulsation causes the star to change the shape by keeping volume constant. Non radial pulsation modes are typically characterized by three wave numbers n (number of nodes, radial quantum number (the number of shells between the centre and the surface of the star as previously

shown), m (azimuthal order of the mode) where $|m|$ specifies how many of the surface nodes are lines of longitude (Kurtz,), l (number of nodal lines on the surface of pulsator). During observation on a two dimensional surface, the lines which remain at rest while other parts of the star are oscillating are known as nodal lines. In non radial pulsation, the variation in brightness are not as strong as the radial oscillations due to the cancellation effects between parts of the star being out of phase in the pulsation cycle (Percy,). These cancellation effects are greater as the degree l of the pulsation is higher (Cunha et al.,) with one exception for $l = 1$, where the observable amplitude is greater than the radial mode (Kurtz,).

Non radial modes are more complex than the radial modes because these modes are caused by the movement of some parts of the star's surface inward while the other moves outward. Analysis of the pulsation modes in general will only give us information about l and m where these corresponds to the degree and azimuthal order of the spherical harmonics $Y_l^m(\theta, \varphi)$ that represents the dependence of the mode on the angular variables for a star assumed to be in spherically symmetric equilibrium. Pulsating white dwarfs, γ Doradus stars, slowly pulsating B stars, Beta Cepheids and Delta Scuti stars undergo non radial type of pulsation.

2.5 Modelling Stellar Pulsation

As any objects vibration mode, stars have patterns or modes of vibration. It is discussed earlier that asteroseismology depends critically on understanding of the physics from the observed phenomena. Stars including the sun, display different kinds of pulsation. When modelling a stellar pulsation, it is mandatory to study the basic stellar pulsation theories:

2.5.1 Linear Adiabatic Theory

This theory was first introduced by Eddington, ( ). It is one of the simplest pulsation theory models due to its inability to replicate the characteristics of pulsations. But, linear adiabatic pulsation theory can be implemented for simple radial mode pulsators. It also helps to obtain relations among some pulsation properties and some stellar physical parameters. In addition, this theory helps to coin the relationship between period and mean density (Christy, ; Cox,),

$$T \propto \frac{1}{\sqrt{\bar{\rho}}}. \tag{2.17}$$

It can also be written as : $\Pi\sqrt{\frac{\bar{\rho}}{\bar{\rho_\odot}}} = Q$, where $\bar{\rho_\odot}$ is the mean density of the sun, Q pulsation constant. The theory proposed by Eddington take into account the assumption that for an element of mass, the lagrangian variation in pressure δP and density $\delta\rho$ can be related as:

$$\frac{\delta P}{P} = \Gamma_1 \frac{\delta\rho}{\rho}, \tag{2.18}$$

where Γ_1 is the adiabatic exponent. This theory is based on the following assumptions:

- small amplitude oscillation about the equilibrium
- there is energy transfer between the zones in the star (*ADIABATIC*).

2.6 Modelling Stellar Atmospheres

The information one gets from the star comes from the light they emit that gives some clue about the source. However, to analyse and interpret the information gathered from stars, via the light they emit, it is prominent to have either a semi-empirical or theoretical stellar models of the atmosphere where the stellar radiation emanates (Magic et al.,). For this reason, modelling stellar atmosphere is a pillar in studying stellar atmospheres and stellar pulsations to do asteroseismology. For some kinds of stars like, the late type stars, modelling their atmospheres is very difficult due to convection, turbulence and magnetic field (Nordlund, Stein, and Asplund,). The spectral distribution and the atmospheric stratification are influenced by convection (Magic et al.,). Therefore, in order to make the modelling more efficient, one needs to include both radiative and convective energy transport methods. In this regard, the first grids of line blancketed model atmosphere was developed for late type stars (Querci, Querci, and Tsuji, ; Gustafsson et al., ; Kurucz,). Since then, a lot has been done to understand both atomic and molecular absorptions. Moreover, the introduction of Opacity Project (OP)(Seaton et al.,) contributed highly to study continuous opacities for heavy elements in the stellar envelope. Gustafsson et al., ( ) developed one of the grids of line blancketing atmosphere called MARCS (Model Atmospheres in Radiative and Convective Scheme) for late type stars (F, G and K) to model their atmospheres by considering the Opacity Distribution Function (ODF). Milne, ( ) defined line blancketing as the effects that the lines produced in the structure of the calculated atmosphere using only the continuum opacities and in the emergent spectrum. More advancements in modelling stellar atmosphere was done by Kurucz, ( ) and introduced ATLAS model atmosphere program Castelli and Kurucz, ( ). Carbon and Gingerich, ( ) introduced scaled solar models to study dwarfs of solar composition in the temperature range $4 \times 10^3 \leq T_{\text{eff}} \leq 6 \times 10^3$K where the scaled solar model is proved for such types of stars. Moreover, the Iron project (Bautista,) contributes immensely on the continuous absorption coefficient. Here, we only focus on ATLAS model atmosphere computer program.

2.6.1 ATLAS9 Model Atmosphere Program

ATLAS9 is a FORTRAN program, originally developed by Kurucz in 1970 by assuming LTE, hydrostatic equilibrium and plane parallel atmosphere, that is used to compute stellar atmospheres for a wide range of $T_{\rm eff}$, g, and metallicities. ATLAS9 model atmosphere computer program works for both radiative and convective equilibrium with Local Thermodynamic Equilibrium (LTE) assumptions (Kurucz, ; Kurucz, ; Castelli and Kurucz, ; Cugier,). The improvements in ATLAS code from ATLAS5, ATLAS8, ATLAS9 and ATLAS12 significantly improves modelling stellar atmospheres. The improvements include the inclusion of a large number of spectral lines by using Opacity Sampling (OS) or Opacity Distribution Function (ODF). The basic principles behind ODF is to sample the dependencies of the line opacities on frequency in order to form a monotonic function of the opacity with respect to frequency. Then, this function will be presented by a small number of frequencies in the derivation of stellar model atmosphere. The principles for OS is to statistically sample the real opacities of the lines averaged using very many frequencies within narrow bins to form again a monotonic function of the opacity or synthetic spectra for a given model atmosphere (Vögler, Bruls, and Schüssler, ; Castelli, ; Cardona, Simonneau, and Crivellari, ; Cugier,). ATLAS9 model atmosphere computer program takes the following assumptions:

- Homogeneous atmosphere where physical quantities vary with depth. The homogeneity reduces the problem to one dimension and ignores granulation and star spots,
- Plane parallel atmosphere where the thickness of photosphere is much less than the radius of the star and g is constant through the atmosphere,
- Hydrostatic Equilibrium where pressure stratification balances g,
- Steady state where all movements of matter, rotation, expanding envelopes, winds, shocks, variable magnetic field etc are ignored.

Based on the assumptions ATLAS, can implement iteration method to get the parameters needed to explain the model atmosphere (Kurucz,). For iteration, the starting point of temperature should be set first for a particular point in the atmosphere to calculate number density, pressure and opacity at these points. By using these outputs, one can determine the radiative and convective flux at a particular point. To this end, temperature variation will be done and successive iterations will also be concluded till we get constant total flux (Kurucz,). The importance in using the grids of stellar models according to Trampedach et al., ( ) is to analyse the stellar observations and obtain the fundamental properties. In this project, we are going to use ATLAS9 model atmosphere program to construct opacity tables and solve some of the parameters introduced in our mode identification formula. To develop opacity tables, one needs to include all sources of opacity while modelling stellar atmosphere. Therefore, in ATLAS9 possible sources of opacity are included. Castelli, ( ) stated that ATLAS9 was the last version for calculating model atmospheres using ODF whereas ATLAS12 uses OS for opacity sampling. ATLAS9 and ATLAS12 are similar except the inclusion, treatment and analysis of linear opacity. The models developed using ATLAS9 are restricted to microturbulent velocities and abundances so as to calculate the pre-tabulated line opacities (Castelli,). More detail information regarding ATLAS can be obtained from the following website (*http : //kurucz.harvard.edu* and *http : //wwwuser.oat.ts.astro.it/castelli*).

ATLAS9 model atmosphere program has been computed for temperature ranges $3500K \leq T_{\rm eff} \leq 50,000K$, $0 \leq \log g \leq 5$, $-4.0 \leq [\frac{Fe}{H}] \leq 0$. The values and parameters given are very important for RGB, SG (subgiant) and the LMS (lower main sequence stars). ATLAS9 model atmosphere program was developed with different subroutines that calculates the radiative transfer equations. Moreover, optical depth calculations, source functions, mean and specific intensities

calculating subroutines are well presented in the FORTRAN program. In addition, subroutines to compute radiation pressure, Roseland optical depth and opacities are included in the program (Kurucz,). ATLAS9 has also additional subroutines to include ionization, molecular equilibrium equations and thermodynamic derivatives which are very important in the construction of model atmospheres. Moreover, the inclusion of opacity is made by grouping all possible sources of opacities in 20 groups (Kurucz,).

The sources of opacities in ATLAS9 model atmosphere program are the following:

- HI bound-free and free-free transitions
- H_2^+ bound-free and free-free
- H^- bound-free and free-free
- HI Rayleigh scattering
- HeII bound-free and free-free
- HeI bound-free and free-free
- HeI Rayleigh scattering
- He^- free-free No bound state
- Low-temperature absorbers $(T \leq 1 \times 10^4 K)$ CI+MgI+SiI+AlI bound-free and free-free
- Intermediate temperature absorbers $(1 \times 10^4 \leq T \leq \times 10^4)$ SiII+MgII+CaII+NI+OI bound-free and free-free
- High absorbers:CII-IV+NII-V+OII-VI+NeI-VI bound-free for frequencies greater than the Lyman limit of hydrogen
- Electron scattering
- H_2 rayleigh scattering
- HI lines
- Line absorption distribution functions.
- Line scattering distribution function. Here, the line opacity is included as scattering as $S_\nu \simeq J_\nu$
- Experimental absorption line
- Experimental scattering line
- Experimental continuous absorption
- Experimental continuous scattering.

According to Kurucz, ( ) during modelling stellar atmosphere, it is not mandatory to know the exact values of opacities at every frequency, since the structure of the atmosphere of the star is composed from the integrals of the average quantities not on the details of the spectrum.

2.6.2 Stellar Opacity

Rosseland, ( ) and later Eddington, ( ) were the pioneers in studying stellar absorption coefficient known as opacity. Eddington, ( ) was the first to identify opacity as one of the two clouds which can make derivation of stellar parameters dubious and secondly, it contributes in the production of stellar energy. Opacities are one of the fundamental ingredients of stellar physics. Opacity, κ of a stellar material is the measure of how electromagnetic radiation interacts with the atoms, electrons, molecules and ions which are constituents of the stellar material. Opacity occurs due to photon absorption which is caused from energy dependent matter photon interaction (Cox,) where absorption depends on wavelength. The first real measurement of opacity was first

done by Rosseland, ( ) and proposed how to get the mean absorption over wavelength to get relationship between the total energy transport from hotter to cooler parts of the star with rate of change of temperature and local density known as Rosseland mean Opacity defined as:

$$\frac{1}{\kappa_R} = \int_0^\infty \frac{1}{\kappa_\nu} \frac{\partial B_\nu(T)}{\partial T} d\nu = \int_0^\infty \frac{\partial B_\nu(T)}{\partial T} d\nu = \frac{1}{B} \int_0^\infty \frac{B_\nu}{\kappa_\nu} d\nu, \tag{2.19}$$

where B is total brightness (intensity), B_ν specific brightness and κ_ν is specific opacity.

$$\frac{1}{\kappa_\nu} = \int \frac{1}{\kappa_\nu} \frac{\partial B(\nu, T)}{\partial T} \frac{d\nu}{B(T)}, \tag{2.20}$$

where $B(\nu, T)$ and $B(T)$ are the monochromatic and integrated black body specific intensities, κ_ν consists both effects of absorption and scattering (Carson,). The Rosseland opacity has significant advantage for analytical study of stellar structure, stellar atmosphere. The Rosseland opacity is familiar kind of opacity. Opacity (κ) can be calculated as a harmonic average of radiative (κ_r) and conductive (κ_c) opacities Carson, ( ) as:

$$\frac{1}{\kappa_\nu} = \frac{1}{\kappa_r} + \frac{1}{\kappa_c}. \tag{2.21}$$

Stellar opacity depends on temperature, density and composition of the stellar constituent. At quantum level when electrons change their quantum levels, photons with distinct frequencies can either be absorbed or emitted based on the transitions. Opacity is considered as an engine that signifies modelling of stellar atmosphere as well as other radiative domains (Alexander et al.,). One can also define opacity as the state or quality of being opaque or a measure of the absorption of photons on their way from stellar centre to the surface which depends on the frequency of radiation, κ_ν, the density, the chemical composition and thermodynamic state of the stellar gas. During the early developments of the study of stellar opacity, the contribution of bound-bound absorption towards the stellar opacity was considered to be minimal (Rogers and Iglesias, ; İbanoğlu,). The contribution of bound-bound transition on opacities was added on stellar models by Cox and Stewart, ( ), Cox, Stewart, and Lilers, ( ), Cox and Stewart, ( ), and Cox and Stewart, ( ) and was found to increase the Rosseland mean by three fold. The inclusion of this (Cox-Stewart opacity) significantly enhances stellar modelling. This formalism of opacity further improved and the effect was revised to construct more reliable and detailed stellar models. Cox, Stewart, and Lilers, ( ) and Cox and Stewart, ( ) introduced both conductive and radiative opacities and more researches lead to the development of opacity tables to obtain opacities for different compositions (from pure hydrogen (H) to compositions with heavy elements like (Fe)). Moreover, opacity calculations needs broad understanding and background facts about absorption, detailed knowledge of atomic structure where it gives a clue on matter and radiation interactions (Cox, Stewart, and Lilers,). Progress were made in advancing the study of opacities by Cox and Tabor, ( ) and at Los Almos Opacity (LAOL) in $1960's$ and $70's$ calculated radiative and conductive opacities. In addition, the opacity project introduced and led by Seaton University, OPAL led by LLNL (Lawrence Livermore National Laboratory) contributed significantly to the study of opacities. Despite the fact that the first generation of Los Almos opacities significantly improves and clears some aspects of stellar structures, there were a number of observational discrepancies which lacks clarification Rogers and Iglesias, ( ). More researches in OPAL increased the quality of studying opacity (Iglesias, Rogers, and Wilson, ; Iglesias, Rogers, and Wilson,). The theoretical Rosseland mean opacity increased by four folds for

temperature close to 3×10^5K due to the improvements and treatments of atomic physics. Moreover, the inclusion of iron or metallicity dependence on opacity calculations enhances in solving gaps between observations and theory (Rogers and Iglesias,).

Defining and studying opacity primarily focusses on studying the effects of photons on atoms, free electrons, ions and molecules during photon-matter interactions. The following are known to be the contributing factors for opacity calculations. All these contributing factors for opacity should be considered when modelling stellar atmosphere.

2.6.3 Sources of Opacity

1. **Bound-Bound Transition (Photo Excitation)**- Bound-Bound transition is a thermal process at temperatures $\geq 10^6$K and happens when a photon is absorbed by an electron in an atom where it transits from lower energy level to a higher energy level of an atom, molecules or ions which occurs due to one of the following:
   - Radiative Excitation
   - Spontaneous Radiation De-excitation
   - Collisional Excitation
   - Induced Radiation De-excitation and Collisional de-excitation

   At cooler temperature regions, Bound-Bound transitions is the dominant source of opacity. Bound-Bound transitions occur when a photon of particular frequency interacts with an electron of a definite atom at a particular quantum level. During such scenario it kicks the electron up to a higher bound energy level. Then, if the electron instantly comes back to its original quantum level, a photon of the same frequency as the incident photon will be released in an arbitrary direction. Bound-Bound transitions can also produce both the emissions and absorption lines which are observed in the stellar spectra.
2. **Bound-Free absorption (Photo ionization)**- Occurs when an interaction of a photon with sufficient energy to ionize an atom results in to a free electron. When the electron combines with an ion, bound-free absorption will occur where photon is radiated in a random direction. In this process, the frequency of the photon should be equal to or higher than the ionization energy of the orbit where the electron is currently placed.

$$h\nu \geq \chi \propto \frac{Z_i^2}{n^2}. \tag{2.22}$$

In the Bound-free absorption, it is fundamental to study the cross-section, the ionization and excitation conditions. For a particular H atom, the cross section for absorption from level n for ionization state i is given by:

$$\delta_\nu^{bf}(Z_{i,n}) \simeq 3 \times 10^{25} S_{nl}^4 \frac{1}{n^5} \frac{Z_i^4}{\nu^3} g_{bf} m^2, \tag{2.23}$$

where Z_i-atomic number, S-screening factor (due to electrons from lower orbits) and g_{bf} Bound-free gaunt factor (order of unity). Based on this cross section, the total Bound-free opacity becomes the total sum of all elements in all ionization and excitation stages, therefore the Bound-free opacity is given by:

$$\kappa_\nu = \sum_Z \sum_n \delta_\nu(Z_{i,n,l}) \left[\frac{n_{i,n}}{n_i}\right]_z \left[\frac{n_i}{\sum n_i}\right]_z. \tag{2.24}$$

Whereas the existence of an influential $i+1$ ionization state for a particular element,

$$n_i \simeq n_e \left(\frac{h^2}{2\pi m_e KT} \right)^{\frac{3}{2}} e^{\frac{\chi}{KT}}, \tag{2.25}$$

gives the number density which contributes to opacity.

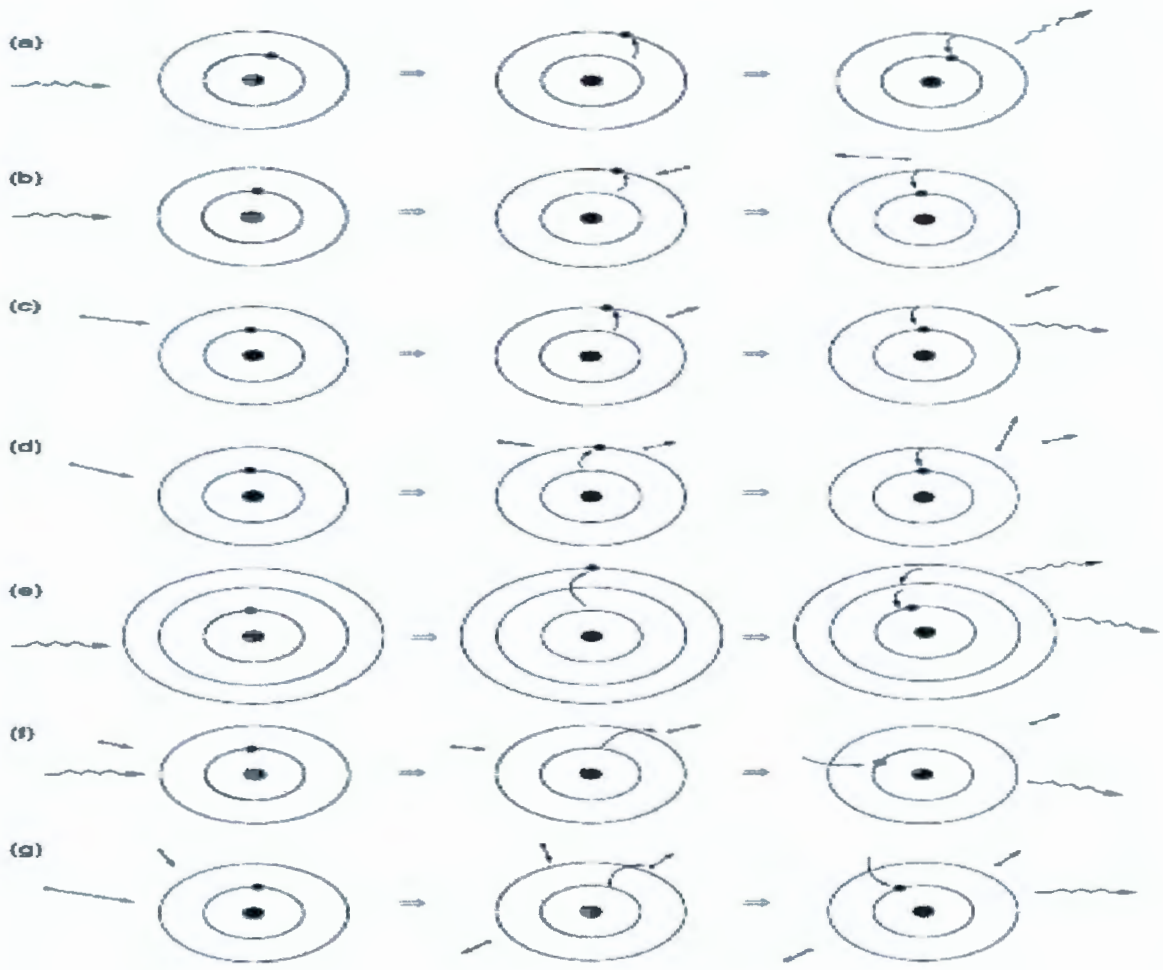

FIGURE 2.1: Figure demonstrating interaction of photon with matter. Adapted from ((LeBlanc, 2010)).

Fig. demonstrates interactions between matter and photon. From top to bottom is explained in the following order. The first figure (a) shows a radiation or photon assimilated by an atom and makes the electron to jump from its original state to the higher state later de-excited to come back to its original state by emitting photon. The second figure (b) the same as figure (a) where a photon interacts with an atom and makes the electron jump to the higher level but due to the collision with a free electron makes to de-excite the electron. The third figure (c) demonstrates an electron excites an atom by collision which triggers release of a radiation. Figure (d) shows an electron excites an atom then de-excitation occurs due to the collision from the second electron. Figure (e) on the other hand shows a photon ejecting an electron to the higher energy level then 2 successive radiative de-excitations occur. Figure (f) shows a photon changes the state of an atom then merge back to the electron. The last figure (g) demonstrates that an atom changes its state by collision of the atom with electron then recombine with the second electron triggering photon emission (LeBlanc, 2010).

3. **Free-Free Absorption**- This phenomena happens when an electron unbound or in (free state) orbit in the neighbourhood of an ion interacts with a photon but is not captured. This means,

the electron is free before and after interaction. During this process, the free electron experiences increased speed leading to an increase in kinetic energy as well as increased acceleration.The accelerated electron generates radiation. Free-Free radiation is sometimes known as Bremsstrahlung.
In a free-free, especially if the electron's velocity distribution is maxwellian, then the amount of electrons having $KE \simeq$ Boltzmann factor, which is $e^{\frac{-E}{KT}}$ that leads to the relation for frequency dependence to be $\propto e^{\frac{h\nu}{KT}}$. Moreover, the rate of emission $\propto n_i n_e$ (densities) therefore depends on n_i^2 ($\propto n_e^2, \propto \rho^2$) and the volume of emissivity becomes:

$$j_\nu \propto T^{\frac{-1}{2}} n_i^2 e^{\frac{-h\nu}{KT}}, \tag{2.26}$$

$$\propto T^{\frac{-1}{2}} \rho^2 e^{\frac{-h\nu}{KT}}, \tag{2.27}$$

this leads to the contribution of free-free opacity to become:

$$\kappa_\nu \propto \rho^2 \nu^{-3} T^{\frac{-1}{2}} (1 - e^{\frac{-h\nu}{KT}}). \tag{2.28}$$

In general, during a free-free absorption, the free electron travels across or along the electric field generated by the ion. During this time, the electron has very high acceleration and emits radiation as a result its acceleration decreases afterwards soaks up energy. This phenomena leads to the production of electron and ion with distinct/discrete dissimilar energy to the state where the system begins.

4. **Electron Scattering**- Electron scattering is a process that happens when a free electron interacts with a photon where the electron changes direction and losses its energy. When an incident photon interacts with an electron, prompts a force (Electromagnetic wave interacts with electrically charged particle (electron)). Due to this interaction, it begins oscillating or vibrating as a dipole since from electromagnetic theory, an oscillating dipole gives off radiation.
5. H^- **opacity**- When a free electron interacts with a neutral hydrogen, it can produce a dipole moment forming H^- and can absorb photons by either bound-free or free-free

$$H^- + h\nu \rightleftarrows H + e^- \tag{2.29}$$

$$H^- + e^- + h\nu \rightleftarrows H^- + e^-, \tag{2.30}$$

this can happen in regions where H can be neutral ($T_{\text{eff}} \leq 8000K$) in the photosphere.

TABLE 2.1: Summary of Dominant Sources of Opacities ((LeBlanc,)).

Types of Stars	Species	Types	
Cool stars (G-M) of Normal composition	H^-	Bound-Free	Dominant
	H^-	Free-Free	Secondary
Warmer (A-F) Stars	H	Bound-Free	Dominant
	H	Free-Free	Secondary
	H	Free-Free	

TABLE 2.2: More Sources of Opacities ((LeBlanc,)).

Sources	Bound-Free	Free-Free	Other
H I	Yes	Yes	Rayleigh
H2-	Yes	Yes	
H-	Yes	Yes	
He I	Yes	Yes	Rayleigh
He II	Yes	Yes	
He-	–	Yes	
Low Temperature Atomic : $T < 1 \times 10^4 K$ CI	Yes	Yes	
Mg I	Yes	Yes	
Si I	Yes	Yes	
Al I	Yes	Yes	
Intermediate Atomic: $1 \times 10^4 < T < 2 \times 10^4$ Mg II	Yes	Yes	
Si II	Yes	Yes	
Ca II	Yes	Yes	
N I	Yes	Yes	
O I	Yes	Yes	
Hot Atomic: T>2×10^4 C II-IV	Yes	Yes	
N II-V	Yes	Yes	
Ne I-VI	Yes	Yes	

2.7 Mode Identification

If we have a vibrating string, its mode of vibration can be expressed using a single integer, n. A two dimensional vibrating membrane requires two integer numbers to describe its vibration l, m. On the other hand, a three dimensional object, like a sphere, a star, requires three quantum numbers l, m, n to fully specify its mode of pulsation (Kurtz, ; Aerts, Christensen-Dalsgaard, and Kurtz,). To determine the mode of vibrations, one needs to study oscillation frequencies. Pulsation frequencies play a primary role in studying asteroseismology where their analysis can improve modelling of stellar physics. Therefore, we need to investigate which pulsation mode causes the frequency.

Mode identification is a method of identifying or determining the mode parameters n, l and m. The n is a measure of nodal lines in the radial direction, l number gives the total number of surface nodal lines. The azimuthal order m gives the number of surface nodal lines that are parallel to the longitudinal lines.

1. p (*pressure modes*): In this type of waves, the motion of the mass element is primarily dominated by radial motion where the restoring force is pressure. p-modes are acoustic waves that propagate by compression and rarefaction (Aerts, Christensen-Dalsgaard, and Kurtz,). p-modes have relatively high frequency and are designated with p_n where n represents the radial order: p_1, p_2, p_3.... From the designations, one can claim that p_1 mode relates to the radial fundamental mode and accordingly p_2 represents the first radial overtone.
2. g (*gravity modes*): The motion here on the other hand where the restoring force is negative buoyancy (Kurtz, ; Aerts, Christensen-Dalsgaard, and Kurtz,). g-modes have relatively low frequencies that do not have a radial analogue and shows deviations from a spherical symmetry (Cunha et al.,). This implies that g-modes do not exist for $l = 0$. Similar to the p-modes, g-modes can be labeled with g_n.

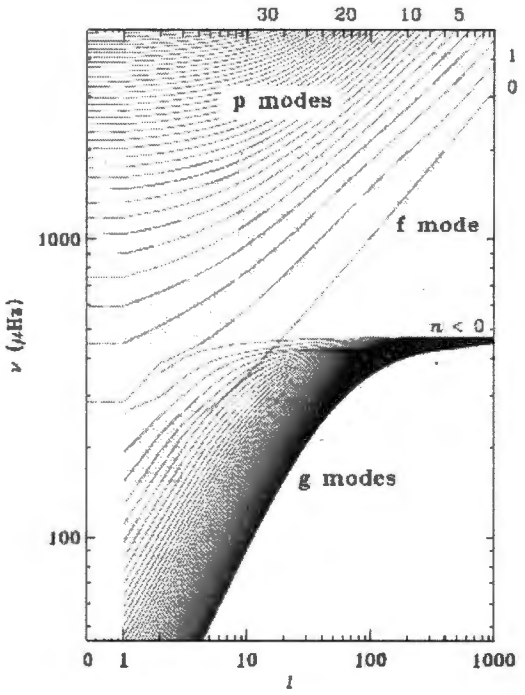

FIGURE 2.2: An illustration of various pulsation modes and their relation with frequency, l and n. Adopted from ((Aerts, Christensen-Dalsgaard, and Kurtz,)).

In addition to the aforementioned properties, the increase in the number of radial nodes leads to the increase in the frequency of p-modes whereas the frequencies in g-modes decrease with n (Kurtz,) as shown in figure 2.2.

Furthermore, p-modes are more abundant and are easily affected by the situation in the outer part of a star whilst g-modes are affected around the core of a star as it is shown in figure 2.3 (Kurtz, ; Aerts, Christensen-Dalsgaard, and Kurtz,) for the case of the Sun. Figure 2.3 (a) shows that a p-mode traveling inward from the surface is refracted as its speed increases with increasing stellar temperature. The refraction causes the p-mode to move towards the surface where it is reflected inwards by sharp drop in density. Figure 2.3(b) shows how in the Sun, g-modes, are trapped under the convection zone.

The classifications as p and g modes is based on the restoring force when a pulsating star comes back to its equilibrium position after the motion of the masses that causes pulsations (Handler,

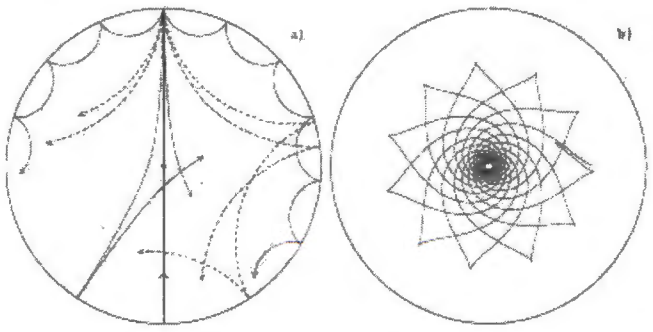

FIGURE 2.3: An illustration of solar interior showing the rays of p modes and g modes,in panel a and b respectively. Adopted from Cunha et al., (2007).

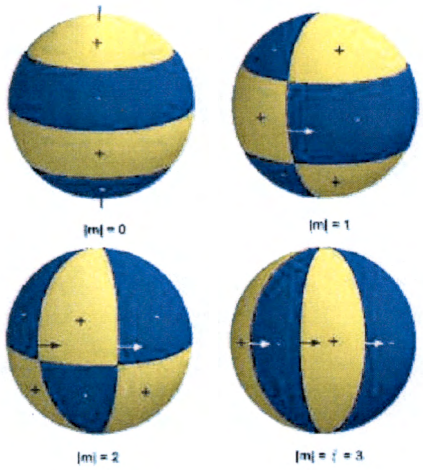

FIGURE 2.4: Figure showing the surface distortion caused by pulsation where the light colored areas moves outward whilst the darker shaded regions move inward. Adopted from Zima., (2010).

2006). Moreover, the division on pulsation waves (p or g) can also be done based on the shape caused after the deformation that can have an effect on the interior and surface of the star whereby the stellar surface has regions identified as contraction and expansion or heating and cooling as it is shown in Fig. 2.4. The figure also shows a three dimensional non-radial oscillation for $l = 3$.

Understanding the types of waves in stars can help to get information about the interior and the stellar surface where they travel. Besides, asteroseismology plays a significant role in identifying and studying modes of pulsation in stars.

The light coming from the stellar object carries plenty of information about the physical conditions of its origin. Therefore, in order to decode relevant information, astronomers invest a lot of time in determining the pulsation modes due to the fact that the amount of astrophysical information that can be obtained from observed pulsations depends on the number of modes identified from the pulsating star (Aerts and Eyer, 2000a).

For slowly rotating pulsators like the Sun and solar like pulsators, derivation of frequency or period spacing is sufficiently enough to identify modes of pulsation (Aerts, Christensen-Dalsgaard, and Kurtz, 2010). However, mode identification using the information from frequencies will be inefficient if

- the number of modes excited are too small or
- the number of modes excited do not have a particular trend in their frequency separation or
- the estimated frequency spectrum is too dense to identify (Aerts, Christensen-Dalsgaard, and Kurtz, 2010; Cunha et al., 2007).

According to Cunha et al., (2007), for such complex scenarios, asteroseismic modelling is possible by taking all possible values of (n, l, m) into account for all pulsation frequencies observed. Although its modelling is time consuming, it is possible to shorten the computation time by considering mode values $l \leq 3$, $m = 0$ and ignoring rotational splitting. The reason behind this is that stellar rotation can result in non-equidistant splitting which in turn leads to merging of frequency

multiplet that makes the procedure not satisfactory for frequency analysis. The challenges in the method is that some classical pulsators show evidence for modes with $l \geq 3$ from spectroscopy, where partial cancellation has a different effect than photometry. This makes the assumption $l \leq 2$ or $m = 0$ baseless or unreasonable. Due to the complexity of obtaining modes of oscillations, researchers introduced different techniques for mode identification. In the upcoming sections of the thesis, I will summarize some of the techniques used for mode identification.

2.7.1 Mode identification from Multi-Colour Photometry

The two major inputs for asteroseismology are frequencies of pulsation and mode identification where the data to perform all these are collected using photometry and spectroscopy:

- **Photometry**- It is a technique used to measure variability in stellar flux or intensity of a stellar object's electromagnetic radiation. This observational method measures changes in temperature which are triggered by pulsation of the stellar object. Stellar photometry plays a fundamental role in getting stellar pulsation frequency for asteroseismology which in turn contributes significantly for mode identification.
- **Spectroscopy**- When stars pulsate, surface elements of the star move, which causes velocity variations that can be observed spectroscopically from periodic shifts in spectral lines and changes in line profiles.

The two observational techniques supply relevant information for doing asteroseismology. Variations in shape, geometry and temperature of a star which are caused by pulsation can affect the observed luminosity further affecting the spherical harmonic of the mode of oscillation (Aerts, Christensen-Dalsgaard, and Kurtz,). Photometric observations obtained from ground based observatories measure the intensity of the light that is coming from the star using different filters and measures the variations in different wavelength range. Due to the fact that temperature variations are wavelength dependent and impacts light variability from pulsation, mode identification for pulsating stars specifically spherical degree l, can be obtained from the observed pulsation amplitude as well as phases observed using different filter bands. The technique which uses photometric amplitudes to determine the mode of pulsation is the emphasis of this section.

Theoretical derivations of light and velocity variation and its implication on identification of oscillation modes was derived by Dziembowski, ( ). His theory and derivation were extended by Balona and Stobie, ( ) and Balona and Stobie, ( ). Moreover, their work implemented this method for the determination of an observational data for 53 Persi variables by Buta and Smith, ( ). Furthermore, the idea presented in the previous works was extended by Stamford and Watson, ( ) who mentioned the concept of photometric mode identification. Moreover, Cugier, Dziembowski, and Pamyatnykh, ( ) were the first to use non adiabatic computation for photometric mode identification. Heynderickx, Waelkens, and Smeyers, ( ) and Heynderickx and Haug, ( ) further extended the theoretical work by including perturbation in limb darkening to derive an expression for surface variation for non radially pulsating stars in a Lagrangian formalism. They applied the method to determine the pulsation mode l (spherical mode) for β Cephei stars. During their derivations of the theoretical expression, the foundation of the theoretical derivations of the pulsation equations are all adiabatic but the non adiabatic theory is included as a special criterion in the external stellar atmosphere (Aerts, Christensen-Dalsgaard, and Kurtz,). Mode identification using photometric amplitudes and phases of the stellar magnitude measured using filter bands helps to determine the spherical degree l. Dupret et al., ( ) improved the theoretical work which was developed by Heynderickx, Waelkens, and Smeyers,

( ) by including non adiabatic eigen function in the outer stellar atmosphere where the photometric modal discrimination is independent of the adhoc parameter for non adiabatic oscillation behavior. Dupret et al., ( ) and Dupret et al., ( ) implemented their improved photometric mode identification on SPB stars, HD74560, HD138764 and βCephi star EN(16)Lac and obtained reliable solutions. Moreover, their equation contributed in determining the degree l as well as understanding the atmosphere and the internal structure of stars by introducing additional parameters such as metallicity ($\frac{Fe}{H}$).

Photometric mode identification method in Garrido, Garcia-Lobo, and Rodriguez, ( ) and Garrido, ( ) are all developed based on flux changes on a pulsating star introduced by Watson, ( ) but ignoring the effect of the limb darkening for $l \leq 2$ on the flux changes. Garrido, Garcia-Lobo, and Rodriguez, ( ) and Garrido, ( ) used the Kurucz model atmosphere to evaluate some terms from the flux change equation and implemented the flow chart given in Fig. 2.5 to determine the required mode of pulsation. The flow chart shows the procedures to follow to determine the values of l for γ-Doradus and δ-Scuti type stars. Some of the variables T_{eff} and $logg$ can be acquired from model atmospheres. Moreover, estimated values of R (deviation from adiabaticity), Ψ^T (phase lag) and $[\frac{M}{H}]$ metallicities are used. Furthermore, pulsation constant Q was used which is calibrated using Garrido, ( ) as:

$$logQ = -6.456 + logP + 0.5logg + 0.1M_{bol} + logT_{eff}. \tag{2.31}$$

Limb darkening and others such as ∂x, $\frac{\partial b_{l,\lambda}}{\partial T_{eff}}$, $logg$ can also be obtained from model atmospheres. The values of R and ψ^T can be selected from the ranges of $0.25 < R < 1$ and $90^o < \psi^T < 135^o$ respectively. Then, one can determine the region of interest for several l values.

Later Garrido, ( ) used the same idea of Watson, ( ) formalism which is literally the same as their previous argument in Garrido, Garcia-Lobo, and Rodriguez, ( ). They started by using the following photometric variation equation introduced by Watson, ( ) to describe changes in luminosity due to stellar pulsation.

$$\delta x(t) = -1.086\epsilon P_{l|m|}(\cos\theta) \times [(T_1 + T_2)\cos(\omega t + \psi_T) + (T_3 + T_4 + T_5) \times \cos(\omega t)], \tag{2.32}$$

where,

- $T_1 = b_{l,\lambda} B \frac{\partial x(t)}{\partial \log T}$,
- $T_2 = \frac{B}{2.3026} \frac{\partial b_{l,\lambda}}{\partial logT}$,
- $T_3 = b_{l,x}(2 + l)(1 - l)$,
- $T_4 = -b_{l,\lambda} P^* C \frac{\partial x(t)}{\partial \log g}$,
- $T_5 = \frac{-P^* C}{2.3026} \frac{\partial b_{l,\lambda}}{\partial logg}$ and
- $b_{l,x} = \int_0^1 h_\lambda(\mu)\mu P_l(\mu) d\mu$, where h_λ follows quadratic law.
- $P^* = (\frac{\partial \log g}{\partial \log p})_{\tau=1}$ shows the relation between p and g. Its value can be obtained from model atmosphere.
- $B = R(1 - \frac{\Gamma}{\Gamma_2})C$, where $C = (4 + \frac{1}{\alpha_H}) - l(l+1)\alpha_H$ and $\alpha_H = G\frac{\rho_\odot Q^2}{3\pi}$, where Q and Γ_2 are pulsation constant and adiabatic exponent respectively.

$P_{l,m}$ is associated Legendre polynomial, $b_{l,x}$ is weighted limb darkening, ψ_T is the phase lag. [N.B. Derivation and detailed discussion of Watson's formula is presented in Chapter 3.]

According to Garrido, Garcia-Lobo, and Rodriguez, ( ), Dupret et al., ( ), Dupret et al., ( ), Cunha et al., ( ), and Aerts, Christensen-Dalsgaard, and Kurtz, ( ), one can

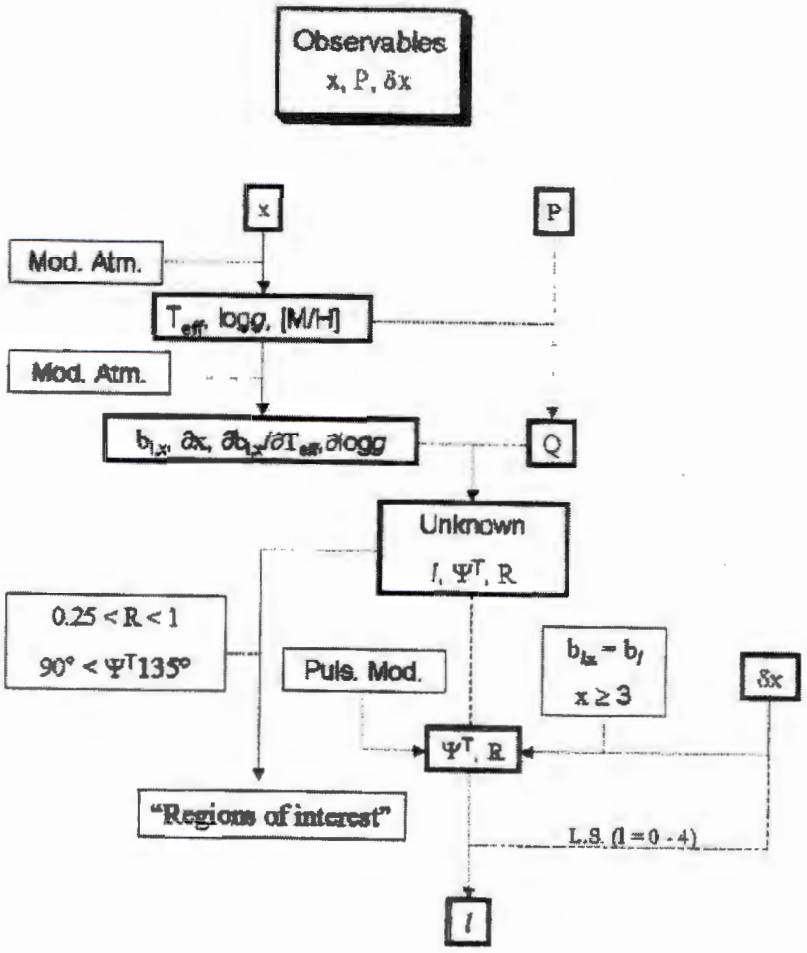

FIGURE 2.5: Flow chart summarizing the input and the procedure to determine the modes of pulsation l. Adopted from (Garrido,)

determine the mode of pulsation l by comparing the amplitude ratios and phase differences measured in different filters. Fig. 2.6 from Garrido, Garcia-Lobo, and Rodriguez, ( ) shows the ratio of phase shift versus amplitudes to determine the mode of pulsations for different filter bands, temperature range and surface gravity. They also compared their formalism with photometric amplitude ratio versus phase difference for $l = 0, 1, 2$. Fig. 2.6 shows the amplitude ratios for different colours and their phase differences for δ-Scuti stars. It also shows the values of R (magnitude showing deviations from adiabaticity) as well as Ψ^T phase lag. Particular values of (R, Ψ^T), $l = 0, 1, 2$ are used to construct the loci for a given $T = 8000$K and $logg = 4$ for the six plots shown. The only difference among the plots is the filters used (u, b, v, y). The combination of u filter with others shows significant variations in the phase $(2^o - 10^o)$ as it is shown in the first three plots of Fig. 2.6. But their separation among radial and non radial pulsations for values of $l = 0, 1, 2$ is not clear. This is because $\frac{\partial u}{\partial logg} < 0$ for u filter is positive for other filters. Therefore, mode identification is an impossible task when using u and its possible combinations (Garrido, Garcia-Lobo, and Rodriguez,). But mode identification can be improved by implementing other filter combinations. The challenge in this case is the lack of significant phase shifts. Particularly for filter combination $(v - b)$, it is hard to see the phase shift whereas for $(v - y)$ and $(b - y)$, one can see radial (positive phase shift) and non radial (negative phase shifts) as clearly shown in the last three plots of Fig. 2.6.

The procedure to achieve the main objectives in photometric mode identification is summarized in the flow chart shown in fig. 2.5 . Garrido, ( ) stated that the flow chart takes parameters from a model atmosphere and it also takes into account R and ψ_T to get l where the value is chosen using the least squares method fit to photometric amplitude and phase difference.

To find the values of l, one needs to calculate the theoretical equilibrium model by using the relevant values $T_{\rm eff}$, luminosity and M. The non adiabatic code developed by Dupret et al., ( ) and Dupret et al., ( ), gives the values for f_T (amplitude of local effective temperature variation), f_g (amplitude of local effective gravity variation) and ψ_T (the phase difference between $T_{\rm eff}$ and radial displacement). Then, the amplitude is calculated for every filter j and mode l by using:

$$A_{j,th} = |b_{l,j}||(1-l)(l+2) + f_T e^{i\psi_T}(\alpha_{Tj} + \beta_{Tj}) - f_g(\alpha_{gj} + \beta_{gj})|, \tag{2.33}$$

where, $b_{lj} \equiv \int_0^1 h_\lambda \mu P_l d\mu$, $\beta_{Tj} \equiv \frac{\partial \ln b_{l\lambda}}{\partial \ln T_{\rm eff}}$ and $\beta_{gj} \equiv \frac{\partial \ln b_{l\lambda}}{\partial \ln g}$.

Moreover, reference filters (A_{ref}) were chosen with maximum amplitude having maximum $\frac{Signal}{Noise}$ afterwards, $(\frac{A_{j,th}}{A_{1,ith}})_{theoretical}$ is compared to $(\frac{A_{j,obs}}{A_{1,obs}})$ which leads to the required values of the mode l which decreases the values of the chi-square (χ^2) according to the following expressions:

$$\chi^2(l) = \sum_{j=1}^{N} \left[\frac{A_{j,th}}{A_{1,th}} - \frac{A_{j,obs}}{A_{1,obs}} \right]^2, \tag{2.34}$$

$$\chi^2(l) = \sum_{j=1}^{N} \left[\frac{\frac{A_{j,th}}{A_{ref,th}} - \frac{A_{j,obs}}{A_{ref,obs}}}{\delta_{j,0bs}} \right]^2, \tag{2.35}$$

where N is the number of filters and $\delta_{j,obs}$ is the propagated standard error of the observed amplitude ratio for filter j which is defined as follows:

$$\delta_{j,obs} = \frac{A_{j,obs}}{A_{ref,obs}} \sqrt{\left[\frac{S_{Aj,obs}}{A_{j,obs}}\right]^2 + \left[\frac{S_{Aref,obs}}{A_{ref,obs}}\right]^2}, \tag{2.36}$$

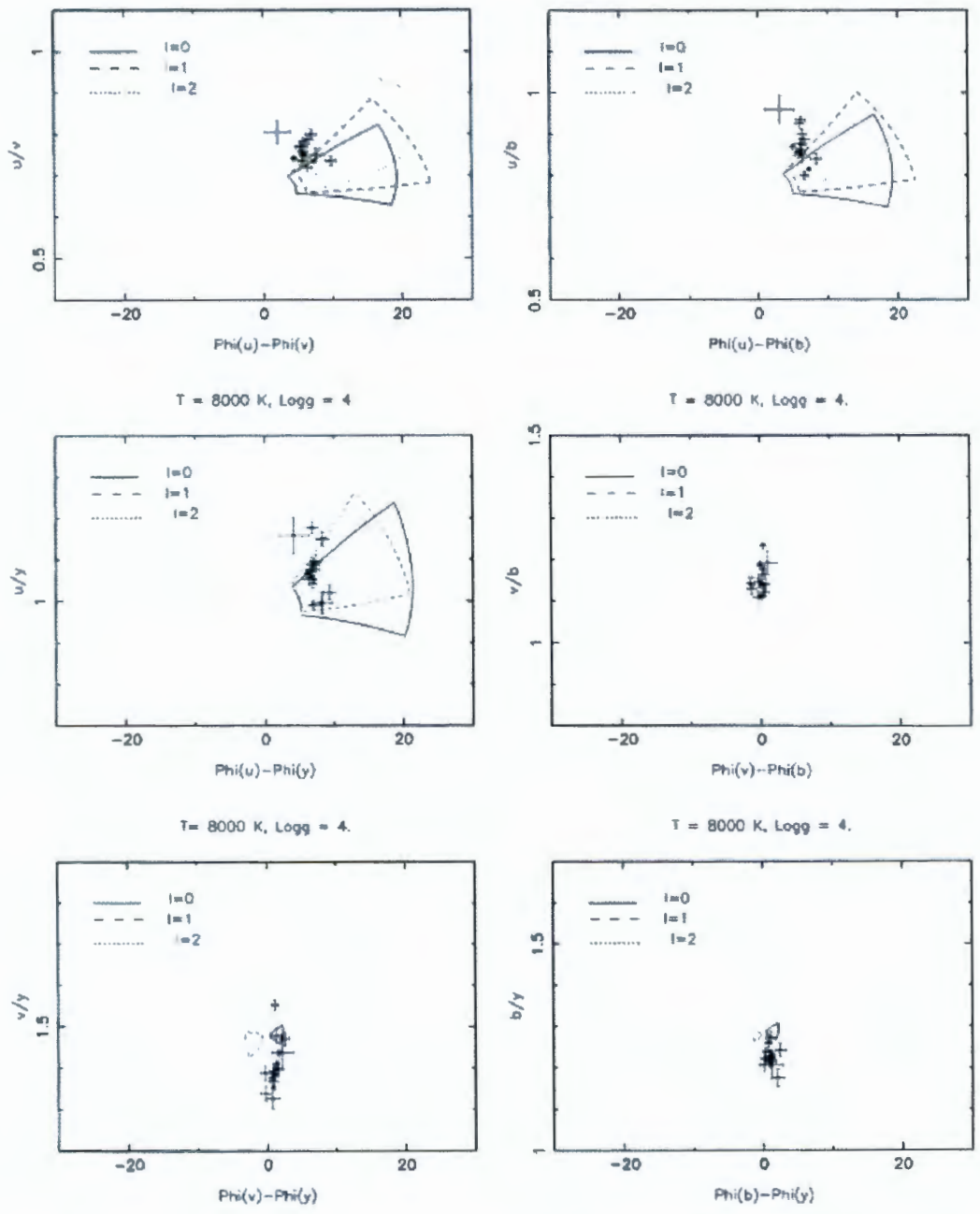

FIGURE 2.6: Amplitude ratios versus Phase shift for different filters. u, v, b and y are *Strömgen* filters The solid lines are the locii for different fits for l values. More explanations are given in the text. Adopted from (Garrido, Garcia-Lobo, and Rodriguez, 1990).

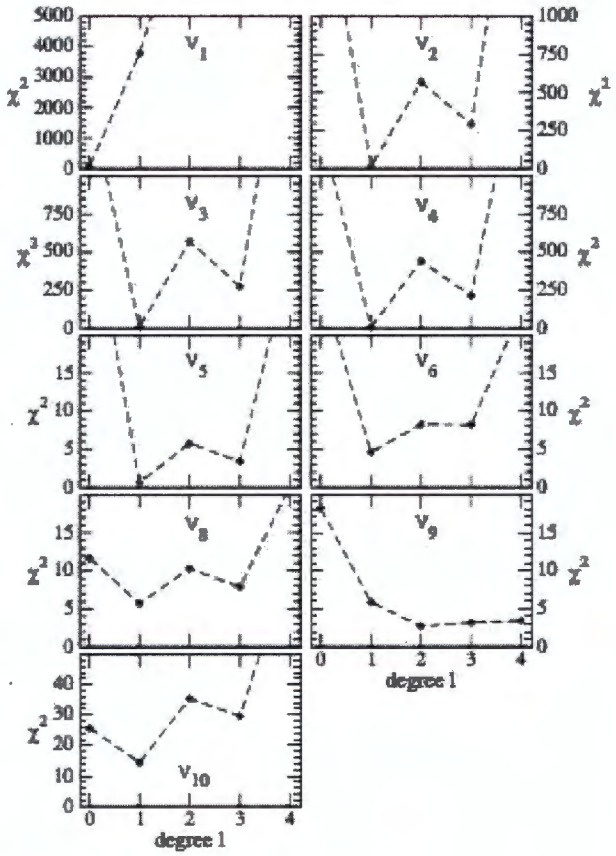

FIGURE 2.7: χ^2 as a function of l for best fit parameters of a model developed using $M = 9M_{\odot}$, $Z = 0.016$ and $T_{eff} = 2.25 \times 10^4$K for frequencies $(\nu_1, \nu_2 ... \nu_{10})$ found in β-Cephei star νEri stars (Adapted from (De Ridder et al.,)).

where, $S_{A,j,obs}$ is standard error in the observed amplitude in filter j. More studies on mode discrimination using photometry amplitude ratio was done. Improved suggestions were made by Randall et al., ( ) especially on the χ^2 minimization by introducing a scaling factor f_l where it is considered as a free parameter. Then the minimization equation becomes:

$$\chi^2(l) = \sum_{j=1}^{N} \left[\frac{\frac{f_l^* A_{ref,obs}}{A_{ref,th}} A_{j,th} - A_{j,obs}}{\delta_{j,obs}} \right]^2, \tag{2.37}$$

$$= \sum_{j=1}^{N} \left[\frac{f_l A_{j,th} - A_{j,obs}}{\delta_{j,obs}} \right]^2. \tag{2.38}$$

The implementation of the χ^2 minimization and its contribution for mode identification is illustrated in Fig. 2.7 and Fig. 2.8. The advantage of using the latter χ^2 minimization Eqn.(2.37) and Eqn.(2.38) is the introduction of free parameter where amplitude ratios are still significant without taking a particular filter to calculate the amplitude ratio. This implies that the latter formalism Eqn.(2.38) treats all filters equally. But one thing that should be noted is the introduction of an extra free parameter to be selected for every l.

Figure 2.7 shows best fit photometric observation in the χ^2 field for different frequencies. The model plotted in figure 2.7 has a mass $M = 9M_{\odot}$, $Z = 0.016$ and $T_{\rm eff} = 2.25 \times 10^4$K.

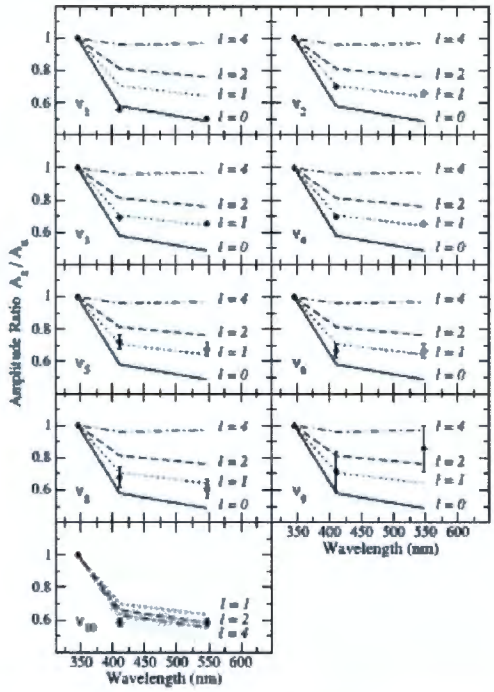

FIGURE 2.8: Theoretical amplitude ratios for νEri stars for different l values and frequencies for different filters (Adapted from (De Ridder et al., 2004))

The χ^2 plot shows an alternative way of obtaining the modes of pulsation unlike in figure . According to the χ^2 plot as a function of the spherical degree l, ν_1 is a radial mode. The rest ($\nu_2 - \nu_8$) are dipole modes whereas ν_9 can be considered to be a higher order greater than 1. The significant differences between the two figures presented as photometric mode identification is how one chooses the modes. Figure heavily relies on comparison of theoretical and observational photometric amplitude ratios, only where unstable modes are used. Whereas the χ^2 map uses unstable modes only, excluding ν_{10}. Because of ν_{10} has stable modes (De Ridder et al., 2004).

Figure shows the comparison of theoretical and observational amplitude ratios of β-Cephei star νEri for nine different frequencies. The theoretical amplitude ratios (represented with solid lines) and observed ones are shown in full circles with error bars. The solid lines in the plot shows radial modes, the dotted lines ($l = 1$), dashed lines ($l = 2$) and the lines shown as a combination of dots and dashed lines represent ($l = 3$). Moreover, the region represented by shaded grey shows the minimal uncertainty for the amplitude ratio obtained theoretically using the root mean square. Among the nine amplitude ratio plots for different frequencies ($\nu_1, \nu_2 ... \nu_{10}$), ν_1 is radial mode whereas ν_2, ν_3 and ν_4 are elements of $l = 1$ and ν_5 is an $l = 1$ mode. In addition, ν_6 and ν_8 are $l = 1$. But due to the fact that the amplitude is too small and huge error bar for ν_9, photometric mode identification is hard to implement. For the last frequency, ν_{10} the amplitude ratio and root mean square is large for higher values of l. Therefore, the regions of uncertainty for $l = 1, l = 2$ are detached whereas the regions of uncertainty (grey shaded region) in Fig.2.8 for $l = 4$ lie over both regions of $l = 1$ and $l = 2$. Therefore, mode selection for this particular case was done by comparing theoretical and observational amplitude ratios that lead to $l = 2$ or $l = 4$ though $l = 1$ can't be ignored as a possible solution (De Ridder et al., 2004).

2.7.2 Mode Identification from Line Profile variation

Since the breakthrough published by Osaki, ( ) about non radial oscillation where its oscillation generates a velocity field in the line forming regions which are revealed as a disturbance in the profiles of the spectral lines, a lot of progress has been made on calculating line profile variations. The pulsation velocity field creates regular change in the profiles of the spectral lines which contributes to the study of mode identification. The main reason behind using spectroscopically observed data is that it provides a fine detail of pulsational velocity field created in the photosphere that helps to find the mode of oscillation (l, m) (de Pauw, Aerts, and Waelkens,). Spectroscopic mode identification, which primarily uses the time changes of a line profile, play a significant role in determining not only the azimuthal order m but also intrinsic displacement, amplitude or the inclination angle (Zima,). Based on the ideas of Osaki, ( ), Balona, ( ) expanded and proposed a quantitative method that should provide an objective criterion to determine both l and m based on spectroscopy known as *the moment method*. Finding the mode of pulsation from observational data of variables from non radially pulsating stars is a primary step leading to asteroseismology. The emphasis on using high resolution spectroscopy is that it paves a way of determining radial and non radial modes of pulsations as it can be seen from the oscillations and it appears on the line profile (Mantegazza,). Based on the the theoretical work introduced by Osaki, ( ), to develop the theoretical line profile for non radially pulsating stars, one needs to write the pulsation velocity vector using spherical coordinates (R, θ, ϕ) in to components:

$$V_{osc}(R, \theta, \phi, t) = (v_r, v_\theta, v_\phi, t), \tag{2.39}$$

The velocity of the second harmonic oscillation at the surface is given for $m \pm 2$ as.

$$v_r = A^{(2)} \sin^2 \theta \cos \phi, \tag{2.40}$$

$$v_\theta = A^{(2)} K \sin 2\theta \cos \phi, \tag{2.41}$$

and

$$v_\phi = \pm 2A^{(2)} K \sin \theta \sin \phi, \tag{2.42}$$

where $A^{(2)}$ and $2A^{(2)}k$ are radial and the azimuthal velocity amplitude of the star's equator.

For $m = \pm 1$

- $v_r = A^{(1)} \sin 2\theta \cos \phi$,
- $v_\phi = \pm 2A^{(1)} k \cos \theta \sin \phi$,
- $v_\theta = 2A^{(1)} k \cos 2\theta \cos \phi$,

For $m = \pm 0$

- $v_r = A^{(0)}(\frac{3}{2} \cos 2\theta - \frac{1}{2}) \cos \delta t$,
- $v_\phi = 0$,
- $v_\theta = -3A^{(0)} \sin \theta \cos \theta \cos \delta t$.

More descriptions on the terminologies can be found in Osaki, ( ). Aerts, Christensen-Dalsgaard, and Kurtz, ( ) expanded the formalism and wrote the equation by neglecting the rotational effect.

$$v_{osc}(R, \theta, \phi, t) = (v_r, v_\theta, v_\phi, t) \tag{2.43}$$

$$= \Re\left\{ -i\omega\xi_r(R)(1, K\frac{\partial}{\partial\theta}, \frac{K}{\sin\theta}\frac{\partial}{\partial\phi})Y_l^m(\theta,\phi)e^{-i\omega t}\right\}, \tag{2.44}$$

where $\Re$ referring the real part of the given expression, $Y_l^m(\theta,\phi)$ is spherical harmonics, ω is the pulsation frequency and K is ratio between the radial and horizontal components of the displacement. For a real stellar pulsation, it is important to write the total velocity as the combination of surface oscillation velocity and rotational velocity as follows:

$$v(R,\theta,\phi,t) = v_{osc}(R,\theta,\phi,t) + v_{rot}(R,\theta,\phi,t), \tag{2.45}$$

where $v_{rot}(R,\theta,\phi,t) = \Omega R_{a\phi}$, Ω is the angular velocity of rotation, R is the radius and $R_{a\phi}$ is rotational surface velocity. The first step towards line profile method is to determine the observed line profile, $P(\lambda,t)$ which is related to the velocity field by,

$$P(\lambda,t) = \frac{\int_{\theta'=0}^{\frac{\pi}{2}}\int_{\phi'=0}^{2\pi}\left[dA(R,\theta',\phi',t).a_z'\right] I_\lambda(R,\theta',\phi',t,a_z')}{\int_{\theta'=0}^{\frac{\pi}{2}}\int_{\phi'=0}^{2\pi}\left[dA(R,\theta',\phi',t).a_z'\right] I_\lambda^{cont}(R,\theta',\phi',t,a_z')}, \tag{2.46}$$

where, dA is the local surface area, I_λ and I_λ^{con} are the intensity and continuum intensity respectively where the continuum intensity is detected if spectral lines are missed. The integrals in equation (2.46) are evaluated by slicing the surface of the star by contour lines. The changes in the velocity field as a result of both oscillation and rotation causes Doppler shift at the specified coordinates. Therefore, to solve the above equation, I_λ should be assumed constant. The numerical solutions for $P(\lambda,t)$ can be achieved if one considers the following effects:

- Intensity perturbation
- Flux perturbation
- Atomic broadening
- Pressure broadening
- Thermal broadening
- Rotational broadening
- Periodic broadening of the line profile caused by stellar oscillation.

For line profile variation calculation based on the previous equation (Eqn.2.46) and its numerical calculation, one can write λ_{ij} as:

$$\frac{\lambda_{ij}-\lambda_0}{\lambda_0} \equiv \frac{\lambda(R,\theta_i',\phi_j',t)-\lambda_0}{\lambda_0} = \frac{\Delta\lambda(R,\theta_i',\phi_j',t)}{\lambda_0} = \frac{v(R,\theta_i',\phi_j',t)}{\tilde{c}}, \tag{2.47}$$

Aerts, de Pauw, and Waelkens, ( ) and Aerts and Eyer, ( ), where λ_{ij} is Doppler corrected wavelength. Then, after coordinate transformation, $Y_l^m = \sum_{k=-l}^{l} a_{lmk}(i)Y_l^k(\theta',\phi')$ where v is the sum of the velocities of pulsation and rotation, that can be written as:

$$v(R,\theta_i',\phi_j',t) = -v_\Omega \sin\theta' \sin\phi' + v_p \sum_{k=-l}^{l} a_{lmk}(i)\left[\cos\theta' P_l^k - K\sin\theta'\frac{dP_l^k}{d\theta'}\right]\times\sin\left[(\omega - m\Omega)t + k\phi'\right], \tag{2.48}$$

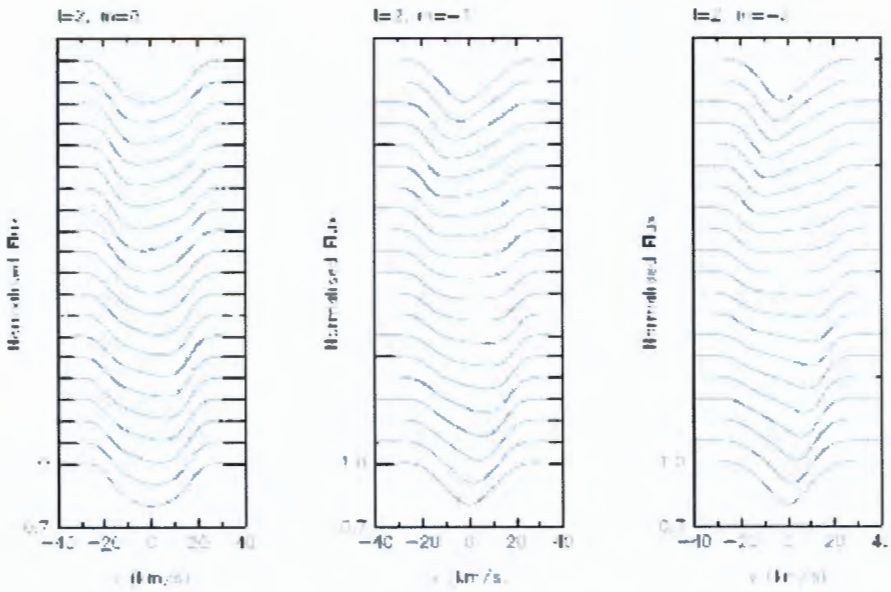

FIGURE 2.9: Illustration showing theoretical line profile variations presented with Normalized flux Vs velocity for various values of l, m. Adopted from (Aerts and Eyer, 2000b)

where v_p and $v_\Omega = v \sin i$ are velocity amplitude and projected rotation velocity respectively. Hence, the line profile becomes:

$$p(\lambda, t) = \frac{\sum_{i,j} \frac{I_0 h_\lambda(\theta_i')}{\sqrt{2\pi} v_{int}} e^{[\frac{-(\lambda_{i,j}-\lambda)^2}{2v_{int^2}}]} R^2 \sin\theta_i' \cos\theta_i' \Delta\theta_i' \Delta\phi_j'}{\sum_{i,j} I_0 h_\lambda(\theta_i') R^2 \sin\theta_i' \cos\theta_i' \Delta\theta_i' \Delta\phi_i i}. \tag{2.49}$$

Based on the equations presented earlier, Aerts and Eyer, (2000b) produced theoretical line profile variations shown in Fig. 2.9.

The theoretical line profile variation shown in Fig. 2.9 is calculated using the line profile variations given above by considering $m = -2$ and $l = 2$ presented on the right, $l = 2$, $m = -1$ for the centre figure and $l = 2$, $m = 0$ presented on the left figure. Moreover, for the calculations of the variations on the line profile $v_p = 5km/s$, is the pulsational velocity amplitude, $v_\Omega = v \sin i = 30km/s$, $v_{int} = 4km/s$ and $i = 55^o$. Further assumptions regarding the θ' and ϕ' where $0^o \leq \theta' \leq 90^0$ and $0^o \leq \phi' \leq 360^0$, this further reveals the assumption of surface normal and stellar surface constant. Getting the line profiles by implementing the equation provided earlier alone wont make mode identification feasible therefore, researchers introduced techniques that will complete the mode identification process by using line profile variations.

2.7.2.1 Line Profile Fitting

The introduction of theoretical work on line profile calculations by Osaki, (1971) was the first attempt to use line profile variation for mode identification on a trial and error basis. The idea of using trial and error method is based on the comparison between the theoretically calculated, using eqn.(2.49) and the observed ones (Campos and Smith, 1980a; Campos and Smith, 1980b; Aerts and Eyer, 2000b). Campos and Smith, (1980b) used the line profile fitting to identify the

mode of pulsation for δ Scuti ρ Puppis stars. Moreover, the line profile fitting was implemented for δScuti stars by Campos and Smith, ( ), βCephei stars Smith, ( ). In spite of the fact that the implementation of line profile fitting by trial and error has played a major contribution, there are drawbacks in the technique due to the high number of free parameters in the fitting model. Another drawback is that it is limited to a single period oscillators (Aerts, Christensen-Dalsgaard, and Kurtz,).

2.7.2.2 The Moment Method

Due to the large number of parameters that makes the computational work for line profile fitting more time consuming, researches were conducted to improve on the techniques of mode identification using line profile method. Balona, ( ) developed a new quantitative method for determining the modes using the first, second and third moments of a line profile, where these moments measure line width, centroid and skewness. The method introduced works based on time variations of the moment. Moreover, Balona, ( ) extended his own formalism and developed a quantitative least-square algorithm which is used as a tool in obtaining parameters that are relevant in identifying the required modes of pulsation. In his first paper, Balona, ( ) defined the n^{th} moment as:

$$M_n = \int_{-\infty}^{\infty} x^n f(x) dx, \tag{2.50}$$

where $f(x)$ is frequency distribution.

Definition: A line profile is "*a convolution of the intrinsic profile and the component of the velocity field in the direction of the observer* (Aerts, de Pauw, and Waelkens,)".

A line profile as described in the definition can be written as:

$$p_{theor}(v) = (f * g)(v), \tag{2.51}$$

where the equation stands for convolution of the intrinsic profile $g(v)$, the velocity $v = v(R, \theta', \phi', t)$, and $f(v)$ stands for flux towards the the observer given by:

$$F_\lambda(R, \theta', \phi') = I_0 h_\lambda(\theta') R^2 \sin\theta' \cos\theta' d\theta' d\phi', \tag{2.52}$$

where I_0 is the continuum intensity at $\theta' = 0$ and h_λ is limb darkening law.

A formal approach to the moment method is to write:

$$< x^n >_{f*g} = \frac{M_n}{M_0}, \tag{2.53}$$

and the n^{th} moment for a line profile $(f * g)(v)$ is

$$< v^n >_{f*g} = \frac{\int_{-\infty}^{\infty} v^n f(v) * g(v) dv}{\int_{-\infty}^{\infty} f(v) * g(v) dv}. \tag{2.54}$$

From a Fourier transform equation, the centroid of a convolution is equivalent to the sum of the centroids of the functions being convolved. Therefore, one can write the above convolution equations for the first three moments where they can provide substantial facts about the spectral lines (Aerts, de Pauw, and Waelkens,) as:

$$< v >_{f*g} = < v >_f + < v >_g, \tag{2.55}$$

$$< v^2 >_{f*g} = < v^2 >_f + 2 < v >_f < v >_g + < v^2 >_g, \tag{2.56}$$

$$< v^3 >_{f*g} = 3 < v^2 >_f < v >_g + 3 < v >_f < v^2 >_g + < v^3 >_f + < v^3 >_g, \tag{2.57}$$

where the first moment $< v >$ is the centroid of the line profile in a reference frame with origin at the stellar centre, the second moment $< v^2 >$ is the measure of the width of the line profile and the third moment $< v^3 >$ is a measure of the skewness of the line profile. Balona, ( ) further derived the velocity fields due to rotation and pulsation by using a spherical coordinate (r, θ, ϕ) where the Z-axis directs towards the observer and the rotational axis is tilted at angle i^o with respect to the Z axis, so the rotation velocity is given by:

$$V_{rot} = \Omega \times r, \tag{2.58}$$

where $\Omega = \Omega(x \sin i + 2 \cos i)$ is the angular velocity of rotation and $r = R(x \sin\theta \cos\phi + y \sin\theta \sin\phi + z \cos\theta)$ is position vector with $\dot{x}, y$ and z as unit vectors. He considered a single oscillation having modes of oscillations l, m and spherical harmonic $Y_l^m(\theta, \phi)$ and Legendre polynomial $P_l^m(\cos\theta) = \frac{(1-m)}{2^l(l!)^2} \sin^m\theta \frac{d^{l+m}}{d\mu^{l+m}}(\mu^2 - 1)$, where $\mu = \cos\theta$, and $P_{l,-m} = (-1)^m P_l^m$ and came up with the equation that shows the total velocity as detected by the observer as:

$$v = -v_\Omega \sin\theta \sin\phi + \sum_{lm} v_{lm} \sum_k a_{lmk} F_{lk} \cos(\delta_{lm} + k\phi), \tag{2.59}$$

where $\delta_{lm} = \omega_{lm} t + \chi_{lm}$, where ω_{lm} and χ_{lm} are observed angular frequency of oscillations and phase constant respectively. More discussions on total velocity can be found in Balona, ( ). Moreover, he calculated the zeroth moment which represents the observed luminosity at a certain wavelength, λ, f_λ. In addition, Balona, ( ) and Balona, ( ) calculated the first, second and third moments of the line profile in reference to the centre of mass (CM) as a stepping stone for mode identification. The first moment $< v >$, second moment $< v^2 >$ and the third moment $< v^3 >$ stands for the centroid of the line profile, measure of the width and skewness of the line profile respectively (Aerts, de Pauw, and Waelkens, ; de Pauw, Aerts, and Waelkens, ; Aerts,). Based on the work of Balona, ( ) and Balona, ( ); Aerts, de Pauw, and Waelkens, ( ) extended to implement the formalism to observed line profiles. In addition, by writing the determinant as a function of l, m, i and v_p, it allows mode identification possible. Mode identification by the moment method is usually done by implementing a simple comparison of the Fourier components obtained from line profile variation with the Fourier values obtained theoretically (de Pauw, Aerts, and Waelkens,). The first three moments of the line profile are given by the following equations (Balona, ; Aerts, de Pauw, and Waelkens, ; de Pauw, Aerts, and Waelkens,):

$$< v >= v_p A(l, m, i) \sin[(\omega - m\Omega)t + \psi], \tag{2.60}$$

$$\begin{aligned} < v^2 > = {} & v_p^2 C(l, m, i) \sin[2(\omega - m\Omega) + 2\psi + \frac{3\pi}{2}] + v_p v_\Omega D(l, m, i) \sin[(\omega - m\Omega)t + \psi + \frac{3\pi}{2}] \\ & + v_p^2 E(l, m, i) + \delta^2 + b^{22} v_\Omega^2, \end{aligned} \tag{2.61}$$

$$< v^3 >= v_p^3 F(l,m,i)\sin[3(\omega - m\Omega) + 3\psi] + v_p^2 v_\Omega G(l,m,i)\sin[2(\omega - m\Omega)t + 2\psi + \frac{3\pi}{2}]$$
$$+ [v_p^3 R(l,m,i) v_p v_\Omega^2 S(l,m,i) + v_p \delta^2 T(l,m,i)] \times \sin[(\omega - m\Omega)t + \psi], \quad (2.62)$$

where Ω, ω are rotation and pulsation frequencies, v_p and v_Ω are pulsation amplitude and projected rotation velocity, ψ and δ(Gaussian) are phase constant and width of the intrinsic profile. $A, C, D, E, F, G, R, S, T$ are dimensionless normalized functions that depends on types of modes and inclination. These terms along with the pulsation velocity v_p consists of the full physical information connected with the theoretical expressions of the non radial pulsation modes. From the theoretical expressions of the three line moments given above in Eqns.(2.60), (2.61) and (2.62), the terms which are significant in the mode identification are those with frequency variables like ω, 2ω, and 3ω for that they are influenced by the star's pulsation. For the purpose of mode identification, de Pauw, Aerts, and Waelkens, ( ) and Aerts, ( ) defined the discriminant as:

$$\begin{aligned}\Gamma_l^m(v_p, i, v_\Omega, v_{int}) = {} & [|A_{obs} - v_p|A(l,m,i)||^2 f_A^2 \\ & + (|C_{obs} - v_p^2|C(l,m,i)||^{\frac{1}{2}} f_c)^2 + (|D_{obs} - v_p v_\Omega|D(l,m,i)||^{\frac{1}{2}} f_D)^2 \\ & + (|E_{obs} - v_p^2|E(l,m,i)| - V_{int}^2 - b_2 v_\Omega^2|^{\frac{1}{2}} f_E^2)^2 \\ & + (|F_{obs} - v_p^3|F(l,m,i)||^{\frac{1}{3}} f_F)^2 + (|G_{obs} - v_p^2 v_\Omega|G(l,m,i)||^{\frac{1}{3}} f_G)^2 \\ & + (|T_{obs} - v_p^3|R(l,m,i)| - v_p v_\Omega^2|S(l,m,i)| - v_p v_{int}^2|T(l,m,i)||^{\frac{1}{3}} f_T)^2]^{\frac{1}{2}},\end{aligned} \quad (2.63)$$

where the terms with *obs* are observed values of the functions, $A, C, D, E, F, G, R, S, T$ are all dependent on l, m and the inclination angle i. In addition, the respective terms $f_A, f_B, f_c ... f_T$ are averaged weights. The quantity $\Gamma_l^m(v_p, i, v_\Omega, v_{int})$ has a dimension of velocity. Mode identification using the discriminant can be done by minimizing $\Gamma_l^m(v_p, i, v_\Omega, v_{int})$ for every set of value (l, m) and determine the values of i and v_p. Therefore, by defining another function, $\gamma_l^m \equiv min_{v_p, i, \Gamma_l^m(v_p,i)}$ where the best values for l and m are those values which gives minimum values for γ_l^m (de Pauw, Aerts, and Waelkens, ; Aerts,). de Pauw, Aerts, and Waelkens, ( ) discussed that the least value of γ_l^m to be considered as an uncertainty for the values v_p and i which implies γ_l^m is assumed to be a lower boundary on the pulsation amplitude. Rigorous theoretical work was conducted by both Aerts, ( ) and de Pauw, Aerts, and Waelkens, ( ) to check the ability of the discriminant with significant noise level. The technique to use mode identification is more reliable for low degree modes ($l \leq 4$) and more advantageous than the photometric counterpart since the factors considered in this case are only dependent on the velocity terms given earlier in this section. Although the moment method plays a major role in identifying the mode of pulsations, there are still drawbacks. The values obtained are accurate by implementing a statistically significant test where one does not have a proof to decide whether the minimum value from γ_l^m is the best choice from the immediate neighbor.

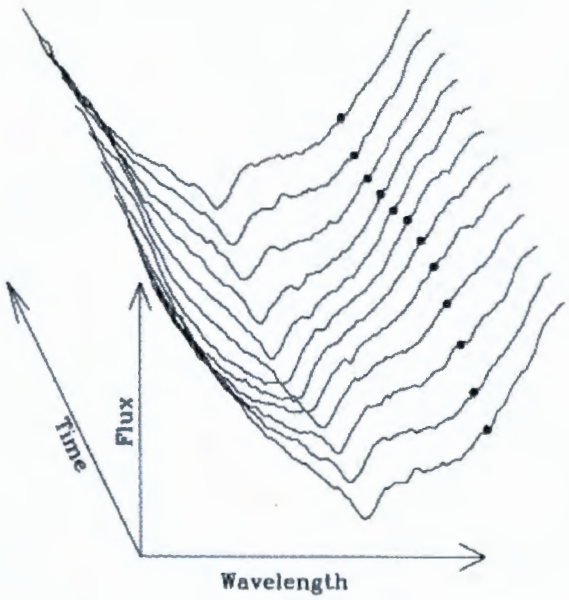

FIGURE 2.10: An observational line profile of a star X caeli at $\lambda = 4501 \times 10^{-10} m$. Adopted from (Mantegazza, 2000)

2.7.2.3 The Pixel- by- Pixel Method

Despite the fact that the moment method played significant role in identifying (l, m), the lack of statistical inference on the values and contradictions between several values of (l, m) lead researchers to look for a better alternative for mode identification. According to Aerts, Christensen-Dalsgaard, and Kurtz, (2010), if one observes a $(1, 1)$ mode of pulsation from the equator and a $(1, 0)$ mode of pulsation from the poles, it is impossible to identify them from the radial modes of pulsation due to the similarities in their line profiles for possible permutations of (l, m, v_p, i). As a matter of fact, these discrepancies can be corrected using pixel-by-pixel method that helps to unfold modes with similar line profiles. Pixel-by-Pixel method relies heavily on the characteristics of both phase distribution and amplitude of the pulsation frequency as well as the first harmonic of the whole line profile (Mantegazza, 2000). This technique usually takes into account the flux measured in the same pixel of the line profile at the same wavelength that varies with the same period throughout the pulsation cycle of the star's pulsation.

Figure 2.10 shows the observational line profile for a star X Caeli at $\lambda = 4501 \mathring{A}$ and phased at the dominant period $7.36 c/d$ where the dots on the line profile shows the flux at a fixed pixel. Among the fluxes, with identical pixels, one should obtain all the matching line profiles in time series so as to analyse and understand the 1D time series (Mantegazza, 2000). Furthermore, Mantegazza, (2000) stated that in order to implement pixel-by-pixel for mode identification, the line profile should be devoid of observer's velocity which is caused by the spinning of the Earth. This helps to select particular pixel time series.

The two figures, Fig. 2.11, top left panel, shows the average line profile in $FeII4508$ line of BV Cir star where the top right panel shows the pixel-by-pixel spectra calculated using the least square and the lower one displays the global least square spectrum which is identical to the weighted mean of the separate pixel-by-pixel spectra. Fig. 2.12, bottom, shows detailed line profile and reveals the real pulsation spectrum (mean of pixel-by-pixel CLEAN spectra) computed

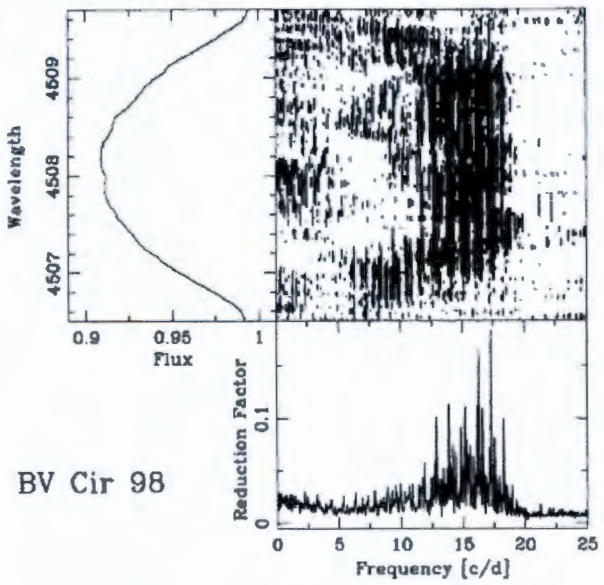

FIGURE 2.11: Analysis of frequency using the pixel-by-pixel least-squares for BV Cir star at $\lambda = 4508\mathring{A}$. Top left: Averaged profile, Top right: Pixel-by-pixel least squares power spectra devoid of known quantities and Bottom right: Global least squares power spectrum. Adopted from (Mantegazza, 2000)

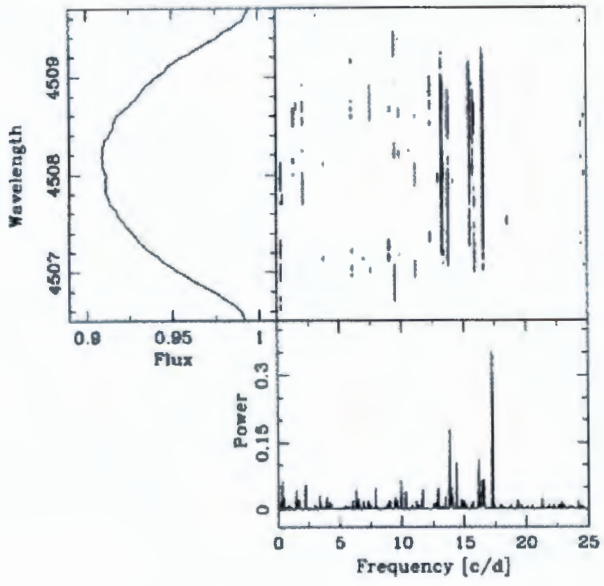

FIGURE 2.12: Analysis of frequency using pixel-by-pixel CLEAN spectra for BV Cir star at $\lambda = 4508\mathring{A}$ Top left: Average profile, Top right: Pixel-by-pixel CLEAN power spectra and Bottom: Average of the pixel-by-pixel CLEAN spectra. Adopted from (Mantegazza, 2000)

using the CLEAN algorithm. As compared to the least square power spectrum, the one obtained using CLEAN algorithm is more clear that it can easily be seen on the frequency analysis shown in Fig. 2.12 (Mantegazza,). CLEAN algorithm has an advantage over least square power spectrum because it takes prior knowledge, like the period of oscillations, from the light curves. More researches were conducted in this regard among these are the one by Zima et al., ( ) who extended Mantegazza, ( ) idea of pixel-by-pixel method by incorporating a statistical significance test and used it to identify the mode of pulsation. He implemented the technique to detect line profiles for δScuti and FG Vir and observed 11 modes in the line profiles similar to those found in multi colour photometry.

Zima et al., ( ) examined for every observed frequency by using pixel-by-pixel technique and he calculated changes in the phase as well as the amplitude. He also showed the two best fits for FG Vir amplitudes and phase changes using spectroscopic analysis. In addition to getting the best fits, this method has more advantages than the moment method because one should not bother about mode coupling in the linear approximation and analyse the modes individually. Moreover, Telting and Schrijvers, ( ) did simulations on line profile variations for non radial oscillations with several l and m values as a means of mode identification. The Montecarlo simulations implemented in their analysis takes into account coriolis force in the velocity eigen function, several pairings of the parameters $(l, m, v_p, i, v_\Omega, v_{int})$, $0 \leq l \leq 15$, and $-l \leq m \leq l$. By using these parameters, Telting and Schrijvers, ( ) created a set of time series spectra and then applied Fourier transform of the time series so as to examine the amplitude and phases. They also found a relationship between the red and blue phase differences and the mode of pulsations l and m. For particular frequency, $\Delta\psi_0(l)$ and its first harmonic$(\Delta\psi_1(m))$ with frequency of oscillation ω, then the approximate value for l is given by:

$$l \approx [0.1 + 1.09\frac{\Delta\psi_0}{\pi}] \pm 1, \tag{2.64}$$

Furthermore, Telting and Schrijvers, ( ) also showed the weak relationships between $\Delta\psi_1$ from blue to red for 1^{st} harmonic with 2ω frequency and m. Then they came up with the relationship:

$$m \approx [1.33 + 0.54\frac{\Delta\psi_1}{\pi}] \pm 2. \tag{2.65}$$

They implemented the method to analyse the spectroscopic data for ξ Oph and ϵ Per and suggested pulsation mode values of l and m. The two equations Eqn.(2.64) and Eqn.(2.65) above can be used if the oscillation frequencies are determined (Telting and Schrijvers, ; Cunha et al.,). The pixel-by-pixel method discussed above helps to identify m value using spectroscopy. But the method has a drawback. The drawback is the inability to determine the pulsation l value for the example considered FG Vir and δ Scuti variables

2.7.3 Mode Identification from Combined Photometry and Spectroscopy

As discussed in previous section pixel-by-pixel method has certain pitfalls. In order to avoid such problems and to identify both l (multicolour photometry) and m (line profile variations), it is advised to implement both photometric and spectroscopic identification due to the fact that one complements the other.

De Cat et al., ( ) studied slowly pulsating B stars (SPB) and main sequence g mode pulsators. They combined and implemented photometric amplitudes, moment method using phase and amplitude variations to determine the modes of pulsations. The summary of the significance

of photometric mode identification is to determine l, spectroscopy to determine both l, m values was given in the section before. Combining both techniques was done by De Ridder, Aerts, and Dupret, ( ) using the two as a means for identifying the methods of pulsation. They used the photometric amplitude ratios ($\frac{A_{j,th}}{A_{1,th}}$) to the observed ($\frac{A_{j,obs}}{A_{1,obs}}$) then implemented χ^2 minimization to identify the degree l:

$$\chi^2 = \sum_{j=2}^{k} \left[\frac{A_{j,th}}{A_{1,th}} - \frac{A_{j,obs}}{A_{1,obs}} \right]^2, \tag{2.66}$$

where k is the number of filters. To determine the values of l, they used spectroscopic technique followed by photometry (cyclic implementations of both photometric and Spectroscopic techniques). Then they did photometric amplitude fitting so as to get the possible values of l and m. De Ridder, Aerts, and Dupret, ( ) tested their methods to β Cephei, 16 Lac and SPB star HD123515 as shown in Fig. 2.13 for 16Lac.

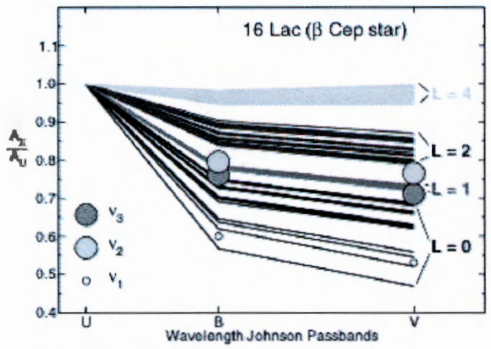

FIGURE 2.13: Illustration showing the photometric amplitude ratios for 16Lac where, lines(Theory) and Circles(Observation). Adopted from (De Ridder, Aerts, and Dupret, 2004)

Figure 2.13 shows the amplitude ratios for different filters U, B, V where the data points represented with circles are observational amplitude ratios. Moreover, the largeness of these circles is related to the uncertainty of the measurements. For different values of l, the solid lines shown in the figure are theoretical amplitude ratios. From Fig. 2.13, one can also see that for the 1^{st} frequency, the amplitude ratios are directed to a radial mode of pulsation (De Ridder, Aerts, and Dupret, 2004).

Chapter 3

Watson's Flux Variation Formula

3.1 Derivation of Watson, ( ) and Watson, ( )'s Formula

By considering a non radial pulsating star, Watson, ( ) and Watson, ( ) developed an equation to describe observed flux. In his formula, he presented the contribution of geometry, pressure, local temperature and limb darkening in the observed flux variations. He also showed the contribution of these factors on light variability that helps to determine the modes of pulsation.

3.2 Basic Assumptions and Principles

In this section we are going to explain the fundamental principles and assumptions that are taken into consideration while deriving the new mode identification formula. Before going into detail, one needs to know the physical parameters that affect stellar spectra:

- Surface temperature (T_{eff})
- Surface gravity
- Stellar composition
- Rotation
- Magnetic field

where the last factor has a very weak effect except for roAp stars. In order to derive the mode identification formula, there were assumptions considered.

These assumptions are:

- A star spherically symmetric in hydrostatic equilibrium,
- Local Thermodynamic equilibrium (LTE)
- that the pulsations are linear adiabatic
- The star has a plane parallel atmosphere

Where the last assumption is applied when the thickness of the atmosphere of the star is less than the radius of the star. Moreover, rotation and magnetic field are ignored in this calculation. Our formalism is based on the works done by (Dziembowski, ; Buta and Smith, ; Watson, ; Watson, ; Heynderickx, Waelkens, and Smeyers, ; Medupe, Christensen-Dalsgaard, and Phorah,). Based on the aforementioned articles, stellar pulsations give rise to perturbations on both surface temperature and gravity, that contribute to the variation in the observed flux.

Using the approach by Dziembowski, ( ) and Buta and Smith, ( ), we develop a theoretical expression that explains the observed light variations of non radial pulsators. Non radial pulsations are described by spherical harmonic functions $Y_l^m(\theta, \phi)$. Therefore, by assuming a very small radius variation ($\ll 1$), small amplitude oscillation causes linear pulsation in:

- **Surface Normal**- When there is a non radial pulsation, the surface normal will point in different directions. This effect occurs as a result of periodic variations in the direction of the normal of the small area.
- **Surface area**- Pulsations in a star cause the radius to vary periodically in time. Thus, the surface area of the star will vary. This affects the variation in light output which is caused by change in the projected small area element considered.
- **Temperature**- this effect is caused by the regular pulsation or contraction and expansion of the stellar material which leads to variations in the surface brightness.

In addition, when a star pulsates, the following variations will happen:

- Radius of the star from its equilibrium (r_0) will be perturbed as $r_0 + \delta r$,
- Temperature and Pressure will be perturbed,
- Surface area will be disturbed $da = da_0 + \delta da$,
- Variation in the surface normal will happen,
- Perturbation in the limb darkening and
- Variations in the observed surface flux.

Therefore, Watson, ( ) and Watson, ( ) took into account all the effects while deriving his famous equation for observed flux. His formalism is an extension of the work done by (Dziembowski, ; Buta and Smith, ; Stamford and Watson,). Watson, ( ) and Watson, ( ) considered a non radial pulsating star and used a linear approximation to calculate the changes in the observed flux. In this part of the thesis, the emphasis is to revisit how he came up with his equation:

$$\Delta m(\lambda, t) = -1.086 P_{|l|,m}(\mu_0)[(T_1 + T_2)\cos(\omega t + \psi_T) + (T_3 + T_4 + T_5)\cos(\omega t)], \qquad (3.1)$$

where

- T_1 is the local temperature change due to pulsation,
- T_2 and T_5 are variations in the limb darkening ($T_e, logg$), where these terms are not important if $l \leq 2$ is considered but if one considers $l > 2$ both terms are very important (Watson,),
- T_3 is the term that stands for local geometry change,
- T_4 refers to local surface pressure changes.

The terms $T_1 ... T_5$ are shown below but later we are going to present the detailed derivations of the equations.

$$T_1 = \epsilon Y_l^m(\theta_0, \phi_0)\alpha_T B b_{l\lambda},$$

where, $b_{l\lambda} = \int_0^1 h_\lambda \mu p_l d\mu$ is the weighted limb darkening.

$$T_2 = \frac{\epsilon Y_l^m(\theta_{0,0})}{2.3026} B \frac{\partial b_{l\lambda}}{\partial \log T_{\text{eff}}}.$$

$$T_3 = \epsilon Y_l^m(\theta_0, \phi_0)[(2 + l)(1 - l)b_{l\lambda}].$$

$$T_4 = -\epsilon P^* C Y_l^m(\theta_0, \phi_0) b_{l\lambda} \alpha_g.$$

and

$$T_5 = \frac{-\epsilon p^* C}{2.3026} \frac{\partial b_{l\lambda}}{\partial \log g} Y_l^m(\theta_0, \phi_0).$$

3.3 Derivation of Watson's Formula

To derive Watson, ( ) equation, one can start by writing the perturbed flux of stellar pulsation and taking in to account the assumptions introduced in section 3.2 as:

$$F'_\lambda = F_{0\lambda} + \delta F_\lambda, \tag{3.2}$$

since the formalism in his expression is in terms of predicted flux magnitude (Δm), it is easy to write the magnitude as:

$$\Delta m_\lambda = -2.5ln(1 + \frac{\delta F_\lambda}{F_\lambda}) \tag{3.3}$$

To make the calculation easy, it is important to write the equation as follows:

$$\Delta m_\lambda = -1.086ln(1 + \frac{\delta F_\lambda}{F_\lambda}), \tag{3.4}$$

where $\frac{2.5}{ln10} = -1.086$ and for small values of x, one can take linear approximation as $ln(1+x) \approx x$, then the magnitude reduces to:

$$\Delta m_\lambda = -1.086\frac{\delta F_\lambda}{F_\lambda} \tag{3.5}$$

The flux for a star in equilibrium is given by,

$$F_\lambda = \int_s I_\lambda \frac{da_0}{r_0^2}, \tag{3.6}$$

where r_0 and I_λ are the radius of the star in equilibrium, da_0 is the projected surface area and intensity respectively, the integration is done over the surface. Then, $I_\lambda = I_{0\lambda} g_\lambda(\mu)$, where g_λ and $I_{0\lambda}$ are limb darkening and intensity at the centre, $\mu = \cos\theta$. As stated earlier, during pulsation the surface normal is perturbed as $\mu' = \mu + \delta\mu$ which further affects the limb darkening $g_\lambda(\mu)$ and intensity $I'_\lambda = I_{0\lambda} + \delta I_\lambda = I_{0\lambda}(1 + \frac{\delta I_\lambda}{I_{0\lambda}})$. Since the perturbation is assumed to be very small (when linear approximation is applied), the perturbation in the limb darkening can be written by implementing Tylor's expansion like (Buta and Smith,),

$$g_\lambda(\mu') = g_\lambda(\mu) + (\mu' - \mu)\frac{\partial g_\lambda}{\partial \mu}, \tag{3.7}$$

therefore, if one perturbs the flux introduced earlier in eqn.3.6:

$$F'_\lambda = \int_s I'_\lambda g\lambda(\mu')da', \tag{3.8}$$

$$F'_\lambda = \int_s I_{0\lambda}(1 + \frac{\delta I_\lambda}{I_{0\lambda}})\left[g_\lambda(\mu) + (\mu' - \mu)\frac{\partial g_\lambda}{\partial \mu}\right](\frac{da_0 + \delta a}{r_0^2}), \tag{3.9}$$

where g_λ is the unperturbed limb darkening. By doing simple algebra to simplify the perturbation in the surface flux, one can get:

$$F'_\lambda = \int I_{0\lambda}\left[\left(g_\lambda(\mu) + (\mu' - \mu)\frac{\partial g_\lambda}{\partial \mu}\right)\frac{da_0}{r_0^2} + \frac{\delta da}{r_0^2} + \frac{\delta I_\lambda}{I_{0\lambda}}\frac{\delta da}{r_0^2}\right], \tag{3.10}$$

then, eqn.3.10 becomes:

$$F'_\lambda = \int \left[I_{0\lambda} g_\lambda(\mu) \frac{da_0}{r_0^2} + (\mu' - \mu) I_{0\lambda} \frac{\partial g_\lambda}{\partial \mu} \frac{da_0}{r_0^2} + \frac{\delta da}{r_0^2} I_{0\lambda} + I_{0\lambda} \frac{\delta I_\lambda}{I_{0\lambda}} \frac{\delta da}{r_0^2} \right], \tag{3.11}$$

$$F'_\lambda = \int I_{0\lambda} g_\lambda(\mu) \frac{da_0}{r_0^2} + \int (\mu' - \mu) I_{0\lambda} \frac{\partial g_\lambda}{\partial \mu} \frac{da_0}{r_0^2} + \int I_{0\lambda} \frac{\delta da}{r_0^2} + \int I_{0\lambda} \frac{\delta I_\lambda}{I_{0\lambda}} \frac{\delta da}{r_0^2} \tag{3.12}$$

To simplify eqn. 3.12, let us introduce terms that can help us achieve what we need and derivation of the following terms:

$$\frac{a_0}{r_0^2} = \omega_0, \tag{3.13}$$

$$\frac{\delta da}{r_0^2} = \delta\omega \tag{3.14}$$

In order to solve the change in the solid angle, one needs to calculate the area of the surface element $\overrightarrow{dA}$. The rest of this section is done based on Buta and Smith, (1979). Hence, for the derivation of the equation, we consider an infinitesimal area element, dA on the surface of the sphere of radius r shown in fig. 3.1 . Any vector $\overrightarrow{r}$ in spherical coordinate can be written as:

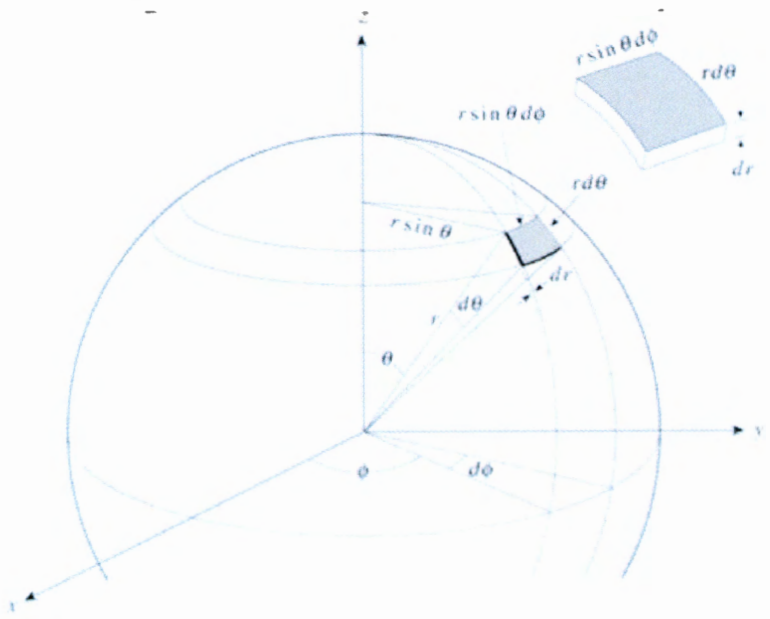

FIGURE 3.1: Area element from a sphere with spherical coordinate. Credit: University of California Davis Lecture, 2012

$$\overrightarrow{r} = r\sin\theta\cos\theta\hat{e_r} + r\sin\theta\sin\phi\hat{e_\theta} + r\cos\theta\hat{e_\phi}, \tag{3.15}$$

where $\hat{e_r}, \hat{e_\theta}, \hat{e_\phi}$ are the unit vectors. Buta and Smith, (1979) considered a spherically symmetric non radial pulsation that change in the observed light which is caused by a little perturbation

from the equilibrium position. The little change in the radius of the star is expressed using the Lagrangian expression as:

$$\delta r(\theta, \phi, t) = b(r) Y_l^m(\theta, \phi) e^{-i\omega t}, \tag{3.16}$$

where $b(r)$ and Y_l^m are radial amplitude and spherical harmonics function respectively, and ω is frequency of oscillations. Then, Buta and Smith, ( ) calculated the area $d\vec{A}$ by taking the instantaneous radius during pulsation given as $r = (r_0 + \delta r)\hat{e_r}$. Then

$$d\vec{A} = (\frac{\partial \vec{r}}{\partial \theta} \times \frac{\partial \vec{r}}{\partial \phi}) d\theta d\phi, \tag{3.17}$$

where

$$\frac{\partial \vec{r}}{\partial \theta} = r\hat{e_\theta} + \frac{\partial \delta r}{\partial \theta}\hat{e_r} \tag{3.18}$$

and

$$\frac{\partial \vec{r}}{\partial \phi} = r \sin\theta \hat{e_\phi} + \frac{\partial \delta r}{\partial \phi}\hat{e_r}, \tag{3.19}$$

therefore, the surface area vector is given as:

$$d\vec{A} = \begin{pmatrix} \hat{e_r} & \hat{e_\theta} & \hat{e_\phi} \\ \frac{\partial \delta r}{\partial \theta} & r & 0 \\ \frac{\partial \delta r}{\partial \phi} & 0 & r\sin\theta \end{pmatrix},$$

which implies that

$$d\vec{A} = (r^2 \sin\theta \hat{e_r} - r\sin\theta \frac{\partial \delta r}{\partial \phi}\hat{e_\theta} - r\frac{\partial \delta r}{\partial \phi}\hat{e_\phi}). \tag{3.20}$$

This can be simplified further to be:

$$d\vec{A} = r^2 \sin\theta [\hat{e_r} - \frac{1}{r}\frac{\partial \delta r}{\partial \theta}\hat{e_\theta} - \frac{1}{r\sin\theta}\frac{\partial \delta r}{\partial \phi}\hat{e_\phi}]. \tag{3.21}$$

This is one of the equations that is going to be used later in our derivation so as to get the variation in the solid angle.

The unit vector towards the observer is $\vec{n} = \cos\theta \hat{e_r} - \sin\theta \hat{e_\theta}$. The magnitude of $d\vec{A}$ gives the actual area of the surface element. The direction of $\vec{dA}$ is that of the surface normal and $\vec{n}$ is the unit vector. Moreover, one needs to write the radius of the star in terms of the unperturbed radius r_0 and the displacement δr as:

$$r = r_0 + \delta r. \tag{3.22}$$

Then, the dot product between $\vec{n}$ and $d\vec{A}$ is:

$$\vec{n} \bullet \vec{dA} = \left[\cos\theta \hat{e_r} - \sin\theta \hat{e_\theta}\right] \bullet \left[r^2 \sin\theta d\theta d\phi \hat{e_r} - \frac{1}{r_0}\frac{\partial \delta r}{\partial \theta}\hat{e_\theta} - \frac{1}{r_0 \sin\theta}\frac{\partial \delta r}{\partial \phi}\hat{e_\phi}\right], \tag{3.23}$$

which leads to:

$$\vec{n} \bullet \vec{dA} = r^2 \sin\theta d\theta d\phi \cos\theta + \sin\theta \frac{1}{r_0}\frac{\partial \delta r}{\partial \theta},$$

If we put the radius in terms of $r = r_0 + \delta r$, then $r^2 = r_0^2(1 + \frac{2\delta r}{r_0})$. Therefore,

$$\vec{n} \bullet \vec{dA} = r_0^2 \sin\theta d\theta d\phi \left[\cos\theta + \sin\theta \frac{1}{r_0}\frac{\partial \delta r}{\partial \theta} + \frac{2\delta r}{r_0}\cos\theta + 2\sin\theta \left[\frac{\delta r}{r_0}\right]^2 \frac{\partial \delta r}{\partial \theta}\right]. \tag{3.25}$$

If we rearrange the second and the fourth terms of eqn.(3.25), then

$$\vec{n} \bullet \vec{dA} = r_0^2 \sin\theta d\theta d\phi [\cos\theta + \frac{2\delta r}{r_0}\cos\theta + \sin\theta \frac{\partial}{\partial\theta}(\frac{\delta r}{r_0})]. \tag{3.26}$$

Multiplying and distributing the term $r_0^2 \sin\theta d\theta d\phi$ throughout, then

$$\vec{n} \bullet \vec{dA} = r_0^2 \sin\theta\cos\theta d\theta d\phi + r_0^2 \frac{2\delta r}{r_0}\sin\theta\cos\theta d\theta d\phi + r_0^2 \sin^2\theta d\theta \frac{\partial}{\partial\theta}(\frac{\delta r}{r_0})d\phi. \tag{3.27}$$

By implementing the definition $\mu = \cos\theta$ and $d\mu = -\sin\theta d\theta$, the above equation becomes

$$\vec{n} \bullet \vec{dA} = -r_0^2 \mu d\mu d\phi - r_0^2 \frac{2\delta r}{r_0}\mu d\mu d\phi + r_0^2(1-\mu^2)\frac{\partial}{\partial\mu}(\frac{\delta r}{r_0})d\phi, \tag{3.28}$$

where we used the trigonometric identity $\sin^2\theta + \cos^2\theta = 1$ and $\sin^2\theta = 1 - \cos^2\theta$.

$$\vec{n} \bullet \vec{dA} = -r_0^2 \mu d\mu d\phi - r_0^2 \frac{2\delta r}{r_0}\mu d\mu d\phi + r_0^2(1-\mu^2)\frac{\partial}{\partial\mu}(\frac{\delta r}{r_0})d\phi d\mu, \tag{3.29}$$

where the first term, $da_0 = -r_0^2 \mu d\mu d\phi$, is the unperturbed area and the rest of the terms represents perturbations in surface area:

$$\delta dA = -r_0^2 \frac{2\delta r}{r_0}\mu d\mu d\phi + r_0^2(1-\mu^2)\frac{\partial}{\partial\mu}(\frac{\delta r}{r_0})d\mu d\phi. \tag{3.30}$$

The perturbed solid angle can be derived from:

$$d\delta\Omega = \frac{d\delta A}{r_0^2}. \tag{3.31}$$

Therefore, the perturbed solid angle becomes:

$$d\delta\Omega = \frac{1}{r_0^2}[-r_0^2 \frac{2\delta r}{r_0}\mu d\mu d\phi + r_0^2(1-\mu^2)\frac{\partial}{\partial\mu}(\frac{\delta r}{r_0})d\mu d\phi], \tag{3.32}$$

$$d\delta\Omega = \frac{-2\delta r}{r_0}\mu d\mu d\phi + (1-\mu^2)\frac{\partial}{\partial\mu}(\frac{\delta r}{r_0})d\mu d\phi, \tag{3.33}$$

Intensity and limb darkening are the factors contributing to the spectrum of a pulsating star and are functions of $(T_{\text{eff}}, logg)$. Therefore, a small perturbation on both temperature and gravity has an impact on the perturbation of intensity that can be written as:

$$\frac{\delta I_\lambda}{I_{0\lambda}} = \alpha_T \frac{\delta T_{\text{eff}}}{T_{\text{eff}}} + \alpha_g \frac{\delta g}{g}, \tag{3.34}$$

where, $\alpha_T = \frac{\partial log F_\lambda}{\partial log T_{\text{eff}}}$ and $\alpha_g = \frac{\partial log F_\lambda}{\partial log g}$. In addition, the perturbation in the limb darkening is written as:

$$\frac{\delta g_\lambda}{g_\lambda} = \beta_T \frac{\delta T_{\text{eff}}}{T_{\text{eff}}} + \beta_g \frac{\delta g}{g}, \tag{3.35}$$

where $\beta_T = \frac{1}{2.3026} \frac{\partial ln g_\lambda}{log T_{\text{eff}}}$ and $\beta_g = \frac{1}{2.3026} \frac{\partial ln g_\lambda}{log g}$.

Then, the perturbation in flux can also be written as $F'_\lambda = F_{0\lambda} + \delta F_\lambda$.

$$F_{0\lambda} + \delta F_\lambda = F_0 + \int_s I_{0\lambda} g_\lambda(\mu) d\omega_0 + \int_s I_{o\lambda}(\mu' - \mu) \frac{\partial g_\lambda}{\partial \mu} d\omega_0 + \int_s I_{0\lambda} g_\lambda \delta d\omega + \int_s I_{0\lambda} \frac{\delta I_\lambda}{I_{0\lambda}} g_\lambda d\omega_0 \tag{3.36}$$

$$\int_s I_{0\lambda} g_\lambda (\frac{\delta g_\lambda}{g_\lambda}) d\omega_0 + \int_s I_{0\lambda}(\mu' - \mu) \frac{\partial g_\lambda}{\partial \mu} d\omega_0 + \int_s I_{0\lambda} g_\lambda \delta d\omega + \int_s I_{0\lambda} \frac{\delta I_\lambda}{I_{0\lambda}} d\omega_0. \tag{3.37}$$

By introducing the values of $\frac{\delta g_\lambda}{g_\lambda}$ and $\frac{\delta I_\lambda}{I_{0\lambda}}$ in the previous equation, eqn.(3.37) becomes:

$$\delta F_\lambda = \int_s I_{0\lambda} g_\lambda \left[\beta_T \frac{\delta T_{\text{eff}}}{T_{\text{eff}}} + \beta_g \frac{\delta g}{g} \right] d\omega_0 + \int_s I_{o\lambda}(\mu' - \mu) \frac{\partial g_\lambda}{\partial \mu} d\omega_0 + \int_s I_{o\lambda} g_\lambda \delta d\omega + \int_s I_{0\lambda} [\alpha_T \frac{\delta T_{\text{eff}}}{T_{\text{eff}}} + \alpha_g \frac{\delta g}{g}] d\omega_0 \tag{3.38}$$

After a simple algebra, eqn.3.38 becomes:

$$\begin{aligned} &= \int_s I_{0\lambda} g_\lambda \beta_T \frac{\delta T_{\text{eff}}}{T_{\text{eff}}} d\omega_0 + \int_s I_{0\lambda} g_\lambda \beta_g \frac{\delta g}{g} d\omega_0 + \int_s I_{0\lambda}(\mu' - \mu) \frac{\partial g_\lambda}{\partial \mu} d\omega_0 + \int_s I_{o\lambda} g_\lambda \delta d\omega \\ &+ \int_s I_{0\lambda} \alpha_T \frac{\delta T_{\text{eff}}}{T_{\text{eff}}} d\omega_0 + \int_s I_{0\lambda} \alpha_g \frac{\delta g}{g} d\omega_0. \end{aligned} \tag{3.39}$$

If we introduce the following terms to simplify eqn.(3.39) above:

$$\beta_g = \frac{1}{2.3026} \frac{\partial ln g_\lambda}{\partial log g} = \frac{1}{2.3026} \beta'_g, \tag{3.40}$$

$$\beta_T = \frac{1}{2.3026} \frac{\partial \ln g_\lambda}{\partial log T_{\text{eff}}} = \frac{1}{2.3026} \beta'_T, \tag{3.41}$$

then using the two terms, eqn. (3.39) reduces to:

$$\begin{aligned} \delta F_\lambda = &\frac{1}{2.3026} \int I_{0\lambda} g_\lambda \beta'_T \frac{\delta T_{\text{eff}}}{T_{\text{eff}}} d\omega_0 + \frac{1}{2.3026} \int_s I_{0\lambda} g_\lambda \beta'_g \frac{\delta g}{g} d\omega_0 + \int_s I_{0\lambda}(\mu' - \mu) \frac{\partial g_\lambda}{\partial \mu} d\omega_0 \\ &+ \int_s I_{0\lambda} g_\lambda \delta d\omega + \int_s I_{0\lambda} \alpha_T \frac{\delta T_{\text{eff}}}{T_{\text{eff}}} d\omega_0 + \int_s I_{0\lambda} \alpha_g \frac{\delta g}{g} d\omega_0. \end{aligned} \tag{3.42}$$

As it is defined earlier, $F_{0\lambda} = \int_s I_{0\lambda} g_\lambda d\omega_0$, if we divide the previous eqn. (3.42) with F_0, we will get:

$$\frac{\delta F_\lambda}{F_{0\lambda}} = \frac{1}{2.3026}\frac{\int I_{0\lambda} g_\lambda \beta' \frac{T_{\text{eff}}}{T_{\text{eff}}} d\omega_0}{\int I_{0\lambda} g_\lambda d\omega_0} + \frac{1}{2.3026}\frac{\int I_{0\lambda} g_\lambda \beta'_g \frac{\delta g}{g} d\omega_0}{\int I_{0\lambda} g_\lambda d\omega_0} + \frac{\int I_{0\lambda}(\mu' - \mu)\frac{\partial g_\lambda}{\partial \mu} d\omega_0}{\int I_{0\lambda} g_\lambda d\omega_0} + \frac{\int I_{0\lambda} \delta d\omega}{\int I_{0\lambda} g_\lambda d\omega_0} + \frac{\int I_{0\lambda} \alpha_T \frac{\delta T_{\text{eff}}}{T_{\text{eff}}} d\omega_0}{I_{0\lambda} g_\lambda d\omega_0} + \frac{\int I_{0\lambda} \alpha_g \frac{\delta g}{g} d\omega_0}{\int I_{0\lambda} g_\lambda d\omega_0}, \tag{3.43}$$

Since I_0 is constant, one can factor it out and cancel with the term in the denominator. This leads us to the following simplified equation, where simplifications are done term by term as follows:

- First term on RHS of eqn. (3.43):

$$\frac{1}{2.3026}\frac{\int g_{\lambda\beta'_T} \frac{\delta T_{\text{eff}}}{T_{\text{eff}}} d\omega_0}{\int g_\lambda d\omega_0}, \tag{3.44}$$

$$= \frac{1}{2.3026}\int \frac{g_\lambda}{\int g_\lambda d\omega_0} \beta'_T \frac{\delta T_{\text{eff}}}{T_{\text{eff}}} d\omega_0, \tag{3.45}$$

$$= \frac{1}{2.3026}\int h_\lambda \frac{\partial lng}{\partial log T_{\text{eff}}} \frac{\delta T_{\text{eff}}}{T_{\text{eff}}} d\omega_0, \tag{3.46}$$

where we used $h_\lambda(\mu) = \frac{g_\lambda}{\int g_\lambda d\omega_0}$ is the normalized limb darkening and $\beta'_T = \frac{\partial lng}{\partial log T_{\text{eff}}}$. Then by using $\frac{\partial lng_\lambda}{\partial log T_{\text{eff}}} = \frac{1}{g_\lambda}\frac{\partial g_\lambda}{\partial log T_{\text{eff}}}$, the first term becomes:

$$= \frac{1}{2.3026}\int \frac{\partial h_\lambda}{\partial log T_{\text{eff}}} \frac{\delta T_{\text{eff}}}{T_{\text{eff}}} d\omega_0. \tag{3.47}$$

- Second term on RHS of eqn. (3.43):

$$= \frac{1}{2.3026}\frac{g_{\lambda\beta'_g} \frac{\delta g}{g} d\omega_0}{\int g_\lambda d\omega_0}, \tag{3.48}$$

Appplying the same procedure as we did in the first, this equation becomes:

$$\frac{1}{2.3026}\int \frac{g_\lambda}{\int g_\lambda d\omega_0} \frac{\partial \ln g_\lambda}{\partial log g} \frac{\delta g}{g} d\omega_0, \tag{3.49}$$

where $\beta'_g = \frac{\partial \ln g_\lambda}{\partial log g}$. Therefore the equation above reduces to the following:

$$\frac{1}{2.3026}\int \frac{\partial h_\lambda}{\partial log g} \frac{\delta g}{g} d\omega_0. \tag{3.50}$$

- Third term on RHS of eqn. (3.43)

$$= \frac{\int (\mu' - \mu)\frac{\partial g_\lambda}{\partial \mu} d\omega_0}{\int g_\lambda d\omega_0}, \tag{3.51}$$

then it reduced to

$$\int (\mu' - \mu) \frac{\partial h_\lambda}{\partial \mu} d\omega_0. \tag{3.52}$$

- Fourth Term on RHS of eqn. (3.43)

$$\frac{\int I_{0\lambda} \delta d\omega}{\int I_{0\lambda} g_\lambda d\omega_0}, \tag{3.53}$$

$$= \int h_\lambda \delta d\omega. \tag{3.54}$$

- Fifth term on RHS of eqn. (3.43)

$$\frac{I_{0\lambda} \alpha_T \frac{\delta T_{\text{eff}}}{T_{\text{eff}}} d\omega_0}{\int I_{0\lambda} g_\lambda d\omega_0}, \tag{3.55}$$

$$\int \alpha_T \frac{\delta T_{\text{eff}}}{T_{\text{eff}}} h_\lambda d\omega_0 \tag{3.56}$$

- Sixth term on RHS of eqn. (3.43)

$$\frac{I_{0\lambda} \alpha_g \frac{\delta g}{g} d\omega_0}{\int I_{0\lambda} g_\lambda d\omega_0}, \tag{3.57}$$

$$\int \frac{\alpha_g \frac{\delta g}{g} d\omega_0}{\int g_\lambda d\omega_0} = \int \alpha_g \frac{\delta g}{g} h_\lambda d\omega_0. \tag{3.58}$$

By combining the simplified individual terms done previously, the variation in the surface flux becomes:

$$\begin{aligned} \frac{\delta F}{F_0} = {} & \overbrace{\frac{1}{2.3026} \int \frac{\partial h_\lambda}{\partial \log T_{\text{eff}}} \frac{\delta T_{\text{eff}}}{T_{\text{eff}}} d\omega_0} + \underbrace{\frac{1}{2.3026} \int \frac{\partial h_\lambda}{\partial \log g} \frac{\delta g}{g} d\omega_0} \\ & + \overbrace{\int (\mu' - \mu) \frac{\partial h_\lambda}{\partial \mu} d\omega_0 + \int h_\lambda \delta d\omega} + \underbrace{\int \alpha_T \frac{\delta T_{\text{eff}}}{T_{\text{eff}}} h\lambda d\omega_0} + \overbrace{\int \alpha_g \frac{\delta g}{g} h\lambda d\omega_0}, \end{aligned} \tag{3.59}$$

where, the terms in the integral above respectively stands for T_2, T_5, T_3, T_1 and T_4 of the Watson's formula. Then, one can see that the variations in flux is the combinations of all the five terms derived above. Where these terms account for:

- Perturbation in the surface normal,
- Perturbations or Effects of the surface area/ variation in the surface area,
- Variation in the surface brightness.

In addition, Watson, ( ) equations account for limb darkening (g_λ and h_λ). For more simplification of terms in the equation above by using some of the equations derived in the earlier section including the following:

- The solid angle: $d\omega_0 = -\mu d\mu d\phi$,
- The variation in the surface normal: $\mu' - \mu = -(1 - \mu^2) \frac{\partial}{\partial \mu} (\frac{\delta r}{r_0})$ derived as follows:
  the variation in the surface normal $\frac{\delta \mu}{\mu} = \frac{1-\mu^2}{\mu} \frac{\partial Y_l^m}{\partial \mu} \frac{\delta \tilde{r}}{r}$ can be derived as follows:
  by definition

$$\cos\theta = \hat{\imath}.\hat{n}_i = \mu, \tag{3.60}$$

and

$$\delta\mu = \mu' - \mu = \hat{n}.\delta\hat{n}_s, \tag{3.61}$$

where the unit vectors

$$\hat{n} = \cos\theta\hat{e_r} - \sin\theta\hat{e_\theta} \tag{3.62}$$

and

$$\hat{n_s} = \hat{e_r} - \frac{1}{r_0}\frac{\partial\delta r}{\partial\theta}\hat{e_\theta} - \frac{1}{r_0\sin\theta}\frac{\partial\delta r}{\partial\phi}\hat{e_\phi}. \tag{3.63}$$

By using the definitions, one can write:

$$\delta\hat{n_s} = \hat{n_s} - \hat{e_r} = \frac{-1}{r_0}\frac{\partial\delta r}{\partial\theta}\hat{e_\theta} - \frac{1}{r_0\sin\theta}\frac{\partial\delta r}{\partial\phi}\hat{e_\phi}, \tag{3.64}$$

and,

$$\hat{n}.\delta\hat{n_s} = \frac{-\sin\theta}{r_0}\frac{\partial r}{\partial\theta} = \delta\mu, \tag{3.65}$$

but $\mu = \cos\theta$, therefore $\partial\mu = -\sin\theta d\theta$. Hence leads to:

$$\delta\mu = \frac{-\sin^2\theta}{r_0}\frac{\partial r}{\partial\mu}, \tag{3.66}$$

but from trigonometry $\sin^2\theta = 1 - \cos^2\theta = 1 - \mu^2$. Using this identity our equation for $\delta\mu$ becomes:

$$\delta\mu = \frac{(\mu^2-1)}{r_0}\frac{\partial r}{\partial\mu} = (\mu^2-1)\frac{\partial}{\partial\mu}(\frac{\delta r}{r_0}), \tag{3.67}$$

- The variation in the solid angle: $\delta\omega = -2\frac{\delta r}{r_0}\mu d\mu d\phi + (1-\mu^2)\frac{\partial}{\partial\mu}(\frac{\delta r}{r_0})d\mu d\phi$,
- $\frac{\delta r}{r} = \epsilon Y_l^m(\theta,\phi)e^{i\omega t}$, where $\epsilon << 1$ is amplitude parameter.

Therefore, inorder to simplify the terminologies introduced above, we need additional terms so as to come up with the final expressions that we are looking for. For such simplifications, one can relate the variation in effective temperature with radius and variation in local gravity with variation in local pressure given below as:

$$\frac{\delta T_{\text{eff}}}{T_{\text{eff}}} = B\frac{\delta r}{r} = B\epsilon Y_l^m(\theta,\phi)e^{i\omega t}, \tag{3.68}$$

and

$$\frac{\delta g}{g} = \frac{\partial\log g}{\partial\log P}\Big|_{\tau=1}\frac{\delta P}{P}. \tag{3.69}$$

Applying these terms to the different components labelled T_1, T_2, T_3, T_4 and T_5, then Watson's terms become:

$$T_1 = \int \alpha_T\frac{\delta T_{\text{eff}}}{T_{\text{eff}}}h_\lambda d\omega_0, \tag{3.70}$$

$$T_1 = \int_0^{2\pi}\int_0^1 \alpha_T B\epsilon Y_l^m(\theta,\phi)e^{i\omega t}h_\lambda\mu d\mu d\phi, \tag{3.71}$$

$$T_2 = \frac{1}{2.3026}\frac{\partial h_\lambda}{\partial \log T_{\rm eff}}\frac{\delta T_{\rm eff}}{T_{\rm eff}}d\omega_0, \tag{3.72}$$

$$T_2 = \frac{\epsilon}{2.3026}\int_0^{2\pi}\int_0^1 \frac{\partial h_\lambda}{\partial \log T_{\rm eff}} B Y_l^m(\theta,\phi)e^{-i\omega t}\mu d\mu d\phi. \tag{3.73}$$

$$T_3 = \int (\mu' - \mu)\frac{\partial h_\lambda}{\partial \mu}d\omega_0 + h_\lambda \delta d\omega, \tag{3.74}$$

$$\begin{aligned} T_3 = \int_0^{2\pi}\int_0^1 -(1-\mu^2)\frac{\partial}{\partial\mu}(\epsilon Y_l^m(\theta,\phi)e^{-i\omega t})\frac{\partial h_\lambda}{\partial\mu}(\mu d\mu d\phi) + \\ \int_0^{2\pi}\int_0^1 h_\lambda(-2\epsilon Y_l^m(\theta,\phi)e^{-i\omega t}\mu d\mu d\phi + (1-\mu^2)\frac{\partial}{\partial\mu}(\epsilon Y_l^m(\theta,\phi)e^{i\omega t})d\mu d\phi), \end{aligned} \tag{3.75}$$

$$\begin{aligned} T_3 = -\epsilon\int_0^{2\pi}\int_0^1 (1-\mu^2)\frac{\partial Y_l^m(\theta,\phi)}{\partial\mu}\frac{\partial h_\lambda}{\partial\mu}\mu d\mu d\phi + \\ \epsilon\int_0^{2\pi}\int_0^1 h_\lambda[2Y_l^m(\theta,\phi)\mu + (1-\mu^2)\frac{\partial Y_l^m(\theta,\phi)}{\partial\mu}]d\mu d\phi, \end{aligned} \tag{3.76}$$

$$T_4 = \int \alpha_g \frac{\delta g}{g} h_\lambda d\omega_0. \tag{3.77}$$

In order to simplify this equation, we used the following terms from Stamford and Watson, ( ). They assumed the variations in g is in phase with the variation in p, therefore, they comeup with

$$\frac{\Delta g}{g} = p^*\frac{\Delta p}{p}, \tag{3.78}$$

where, $p^* = (\frac{\partial \log g}{\partial \log p_g})|_{\tau=1}$. Here one can get the value of p^* from stellar model atmosphere that shows the variations in atmospheric gas pressure. Moreover,

$$\frac{\delta p}{p} = -C\frac{\delta r}{r}, \tag{3.79}$$

then,

$$\frac{\delta g}{g} = p^* C\epsilon Y_l^m(\theta,\phi)e^{\omega t}, \tag{3.80}$$

therefore,

$$\int_0^{2\pi}\int_0^1 \alpha_g(-C\epsilon Y_l^m(\theta,\phi)e^{\omega t})h_\lambda(\mu d\mu d\phi), \tag{3.81}$$

$$-\epsilon p^* C\int_0^{2\pi}\int_0^1 \alpha_g h_\lambda Y_l^m(\theta,\phi)\mu d\mu d\phi. \tag{3.82}$$

In a similar fashion, the last term can be written as:

$$T_5 = \frac{1}{2.3026}\int \frac{\partial h_\lambda}{\partial \log g}\frac{\delta g}{g}d\omega_0, \tag{3.83}$$

$$T_5 = \frac{-\epsilon p^* C}{2.3026} \int_0^{2\pi} \int_0^1 \frac{\partial h_\lambda}{\partial \log g} Y_l^m(\theta, \phi) \mu d\mu d\phi. \tag{3.84}$$

For further simplification, if one rotates the coordinate (θ, ϕ) arbitrarily towards the direction of the observer, any spherical harmonics $Y_l^m(\theta, \phi)$ can be written as a linear combination of spherical harmonics of the new polar coordinate. In this case, it is fundamental to notice that both (new and old) coordinates have the same l value (Mathews and Walker, ; Buta and Smith, ; Arfken and Weber,). Then,

$$Y_l^m(\theta, \phi) = \sum_{m'=-l}^{l} C_{mm'}^l Y_l^{m'}(\theta', \phi'), \tag{3.85}$$

where (θ', ϕ') are the angular coordinates of a point on the stellar disk in the coordinate system where the polar axis points towards the observer. The coefficient of the new transformed polar coordinate $(C_{mm'}^l)$, that shows spherical harmonics are orthonormal over the surface of the sphere, can be calculated using:

$$C_{mm'}^l = \int_0^{2\pi} \int_0^{\pi} Y_{lm'}^*(\theta', \phi') Y_l^m(\theta, \phi) \sin\theta' d\theta' d\phi' \tag{3.86}$$

where, $C_{mm'}^l$ depends on the rotation $(\theta, \phi) \rightarrow (\theta', \phi')$ and l, m and m'. Then, the non zero term (C_{m0}^l) can be obtained after integrating the equation which is given by:

$$C_{m0}^l = \sqrt{\frac{4\pi}{2l+1}} Y_l^m(\theta_0, \phi_0), \tag{3.87}$$

where (θ_0, ϕ_0) is the ***subobserver*** angular coordainates in stellar frame (Buta and Smith,). Therefore,

$$Y_l^m(\theta, \phi) = \sqrt{\frac{4\pi}{2l+1}} Y_l^m(\theta_0, \phi_0) Y_l^0(\theta', \phi'), \tag{3.88}$$

$$Y_l^m(\theta, \phi) = Y_l^m(\theta_0, \phi_0) p_l(\mu'), \tag{3.89}$$

where p_l is the Legendere polynomial. Now, the terms introduced earlier T_1, T_2, T_3, T_4 and T_5 can be simplified as follows by using the terminologies introduced previously. Consider the first term T_1:

$$T_1 = \int_0^{2\pi} \int_0^1 \alpha_T B \epsilon Y_l^m(\theta, \phi) \mu d\mu d\phi, \tag{3.90}$$

$$\int_0^1 \alpha_T B \epsilon Y_l^m(\theta_0, \phi_0) p_l(\mu') h_\lambda \mu d\mu, \tag{3.91}$$

finally the equation becomes

$$T_1 = \epsilon Y_l^m(\theta_0, \phi_0) \alpha_T B b_{l\lambda}, \tag{3.92}$$

where, $b_{l\lambda} = \int_0^1 h_\lambda \mu p_l d\mu$ is the weighted limb darkening. The second term T_2 becomes:

$$T_2 = \frac{\epsilon}{2.3026} \int_0^{2\pi} \int_0^1 \frac{\partial h_\lambda}{\partial \log T_{\text{eff}}} B Y_l^m(\theta, \phi) \mu d\mu d\phi, \tag{3.93}$$

$$T_2 = \frac{\epsilon}{2.3026}\int_0^1 \frac{\partial h_\lambda}{\partial \log T_{\text{eff}}} B Y_l^m(\theta_0,\phi_0)\mu d\mu, \tag{3.94}$$

then applying the same definition to the weighted limb darkening, one can get

$$T_2 = \frac{\epsilon Y_l^m(\theta_{0,0})}{2.3026} B \frac{\partial b_{l\lambda}}{\partial \log T_{\text{eff}}}. \tag{3.95}$$

By using the same principles, T_3 becomes:

$$\begin{aligned} T_3 = \epsilon Y_l^m(\theta_0,\phi_0)\Bigg[&\int_0^1 (1-\mu^2)\frac{\partial p_l(\mu')}{\partial \mu}\mu d\mu \\ &+ \int_0^1 2h_\lambda(p_l(\mu')\mu + (1-\mu^2)\frac{\partial p_l(\mu)}{\partial \mu})\Bigg] d\mu, \end{aligned} \tag{3.96}$$

$$T_3 = \epsilon Y_l^m(\theta_0,\phi_0)\left[\int_0^1 (1-\mu^2)\frac{\partial p_l(\mu')}{\partial \mu}\mu d\mu + \int_0^1 2h p_l(\mu')\mu d\mu + \int_0^1 2h_\lambda(1-\mu^2)\frac{\partial p_l(\mu)}{\partial \mu} d\mu\right], \tag{3.97}$$

$$\begin{aligned} T_3 = \epsilon Y_l^m(\theta_0,\phi_0)\int_0^1 (1-\mu^2)\frac{\partial p_l(\mu')}{\partial \mu}\mu d\mu + \epsilon 2 Y_l^m(\theta_0,\phi_0) b_{l\lambda} \\ + \epsilon Y_l^m(\theta_0,\phi_0)\int_0^1 (1-\mu^2)\frac{\partial p_l(\mu)}{\partial \mu} d\mu, \end{aligned} \tag{3.98}$$

$$\begin{aligned} T_3 &= \epsilon Y_l^m(\theta_0,\phi_0)\Bigg[-\int_0^1 (1-\mu^2)\frac{\partial p_l(\mu')}{\partial \mu}\frac{\partial h_\lambda}{\partial \mu}\mu d\mu + 2b_{l\lambda} \\ &\qquad - \int_0^1 (1-\mu^2)h_\lambda \frac{\partial p_l(\mu)}{\partial \mu} d\mu\Bigg], \end{aligned} \tag{3.99}$$

by rearranging the terms above, one can get:

$$\begin{aligned} T_3 = \epsilon Y_l^m(\theta_0,\phi_0)\Bigg[&2b_{l\lambda} - \int_0^1 (1-\mu^2)\frac{\partial p_l(\mu')}{\partial \mu}\frac{\partial h_\lambda}{\partial \mu}\mu d\mu \\ &- \int_0^1 (1-\mu^2)h_\lambda \frac{\partial p_l(\mu)}{\partial \mu} d\mu\Bigg]. \end{aligned} \tag{3.100}$$

Now consider the second term separately and integrate by parts as follows:

$$\int_0^1 (1-\mu^2)\frac{\partial p_l(\mu')}{\partial \mu}\frac{\partial h_\lambda}{\partial \mu}\mu d\mu, \tag{3.101}$$

To solve the integration by parts we let:

- $u = (1-\mu^2)\frac{\partial p_l(\mu')}{\partial \mu}$ $du = -2\mu\frac{\partial p_l(\mu')}{\partial \mu} + (1-\mu^2)\frac{\partial^2 p_l(\mu')}{\partial \mu^2}$,
- $dv = \mu\frac{\partial h_\lambda}{\partial \mu}$, $v = \mu h_\lambda$,

the definition of integration by parts,

$$\int udv = uv - \int vdu, \tag{3.102}$$

therefore,

$$\mu h_\lambda(1-\mu^2)\frac{\partial p_{l(\mu')}}{\partial \mu} - \int \mu h_\lambda\left[-2\mu\frac{\partial p_l(\mu')}{\partial \mu} + (1-\mu^2)\frac{\partial^2 p_l(\mu')}{\partial \mu^2}\right]d\mu. \tag{3.103}$$

From the definition of Legendere differential equation:

$$(1-\mu^2)\frac{\partial^2 p_l}{\partial \mu^2} - 2\mu\frac{\partial p_l}{\partial \mu} + l(l+1)p_l = 0, \tag{3.104}$$

Therefore,

$$T_3 = \epsilon Y_l^m(\theta_0,\phi_0)\left[2b_{l\lambda} - l(l+1)b_{l\lambda} + \mu h_\lambda(1-\mu^2)\frac{\partial P_l}{\partial \mu}d\mu - (1-\mu^2)h_\lambda\frac{\partial p_l(\mu)}{\partial \mu}\right], \tag{3.105}$$

$$T_3 = \epsilon Y_l^m(\theta_0,\phi_0)[2 - l(l+1)b_{l\lambda}], \tag{3.106}$$

then T_3 after a simple algebra becomes:

$$T_3 = \epsilon Y_l^m(\theta_0,\phi_0)[(2+l)(1-l)b_{l\lambda}]. \tag{3.107}$$

The fourth term T_4 of Watson's equation can be simplified as follows:

$$T_4 = -\epsilon P^* C\int_0^{2\pi}\int_0^1 \alpha_g h_\lambda Y_l^m(\theta,\phi)\mu d\mu d\phi, \tag{3.108}$$

$$T_4 = -\epsilon P^* C\int_0^{2\pi}\int_0^1 \alpha_g h_\lambda Y_l^m(\theta_0,\phi_0)p_l(\mu')\mu d\mu, \tag{3.109}$$

$$T_4 = -\epsilon P^* C Y_l^m(\theta_0,\phi_0)b_{l\lambda}\alpha_g. \tag{3.110}$$

The last term T_5 is simplified as the other terms as follows:

$$T_5 = \frac{-\epsilon p^* C}{2.3026}\int_0^1\int_0^{2\pi}\frac{\partial h_\lambda}{\partial \log g}Y_l^m(\theta,\phi)\mu d\mu d\phi, \tag{3.111}$$

$$= \frac{-\epsilon p^* C}{2.3026}\int_0^1\frac{\partial h_\lambda}{\partial \log g}Y_l^m(\theta_0,\phi_0)p_l(\mu)\mu d\mu, \tag{3.112}$$

Therefore,

$$T_5 = \frac{-\epsilon p^* C}{2.3026} \frac{\partial b_{l\lambda}}{\partial \log g} Y_l^m(\theta_0, \phi_0). \tag{3.113}$$

As it is shown in (Watson, ; Watson,), these are the terms introduced to get the observed flux by including some of the factors which contribute to the variations in the surface flux.

Chapter 4

The New Improved Mode Identification Formula

4.1 Introduction

The basic radiative transfer equations and detailed revisions of mode identification techniques for pulsating stars were explained briefly in chapter 2. In this chapter, by considering appropriate physical conditions and mathematical formulations and applying linear perturbations on the radiative transfer equation, we are going to consider the relationship between luminosity pulsation amplitudes for a multilayer atmosphere of an A star. Therefore, the aim in this chapter solely focuses on deriving the new and improved formula for photometric mode identification that is based on the work done by (Watson, ; Watson,) and (Medupe, Christensen-Dalsgaard, and Phorah,). In this chapter, we apply the same approach to Watson's formula derived in chapter 3 but here, we assumed multilayer atmosphere. We also look at the radiative transfer unlike Watson's approach where a semiempirical approach was taken.

4.1.1 Flux Variations

Radiative transfer is the transport of energy by photons in optically thin media and it can also be defined as a change in the intensity I_λ as radiation propagates. The intensity in general changes due to:

- Scattering or Directional change
- Doppler or red shift frequency change
- Absorption
- Emission

In this investigation, we only include the last two effects to derive a new and improved mode identification formula starting from the radiative flux (F) and radiative transfer equations. Here, one can write the radiative flux (F) as:

$$F_\lambda = \int_0^{2\pi} \int_0^1 \mu I_\lambda(\mu, \phi) \sin\theta d\theta d\phi, \tag{4.1}$$

where $\mu = \cos\theta$ is the directional cosine, θ and ϕ are the spherical coordinates of a point in the rest frame of the star. If we apply perturbations on both sides of the equation including the surface normal (μ), we get:

$$F_{\lambda 0} + \delta F_\lambda = \int\int (\mu_0 + \delta\mu)(I_\lambda + \delta I_\lambda) d(\Omega_0 + \delta\Omega), \tag{4.2}$$

where $\delta\mu$ is perturbation in μ. The above equation can be written out as:

$$F_{\lambda 0} + \delta F_\lambda = \int_0^\infty \int_0^1 (\mu_{0\lambda} I_\lambda + I_\lambda \delta\mu + \mu_0 \delta I_\lambda + \delta\mu \delta I_\lambda) d(\Omega_0 + \delta\Omega). \tag{4.3}$$

Since linear approximation is considered the fourth term will be neglected, therefore eqn.(4.3) reduces to:

$$F_{\lambda 0} + \delta F_\lambda = \int_0^\infty \int_0^1 (\mu_0 I_\lambda + I_\lambda \delta\mu + \mu_0 \delta I_\lambda) d(\Omega_0 + \delta\Omega). \tag{4.4}$$

Applying the same principle and neglecting higher order terms and keeping first order terms, we obtain:

$$F_{\lambda 0} + \delta F_\lambda = \int\int \mu_0 I_\lambda d\Omega_0 + \int\int \mu_0 I_\lambda d\delta\Omega + \int\int \mu_0 \delta I_\lambda d\Omega_0, \tag{4.5}$$

the first term is $F_{\lambda 0}$, the unperturbed radiative flux, as the definition given previously. Therefore, equation (4.5) becomes:

$$\delta F = \int_0^\infty \int_0^1 \mu_0 I d\delta\Omega + \int\int \mu_0 \delta I d\Omega_0. \tag{4.6}$$

The first term on the right of the above equation represent perturbation in surface area. The second term represents the perturbation in flux.

Following the above derivations, one can evaluate the two integrals in eqn.(4.6) separately so as to get the required formulation. But before doing so, it is better to have an understanding on the basic concepts that are required for our interpretation of the equations that we are going to solve.

An observer from the ground observes the luminosity of the star:

$$L = AF, \tag{4.7}$$

where F is the energy flux $(erg/cm^2/sec)$ and A is the surface area of the star. By taking linear perturbation on both sides of the above equation we obtain:

$$L + \delta L = (A + \delta A)(F + \delta F), \tag{4.8}$$

or

$$L + \delta L = AF + A\delta F + F\delta A, \tag{4.9}$$

where the first term L is the unperturbed luminosity which cancels with the first term on the right of eqn.(4.9), then we can re-arrange the above equation to:

$$\frac{\delta L}{L} = \frac{\delta F}{F} + \frac{\delta N}{N} + \frac{\delta A}{A}. \tag{4.10}$$

We can rearrange eqn.4.6 to become:

$$\frac{\delta F}{F} = \frac{1}{F}\int_\Omega \mu \delta I_\lambda d\Omega + \frac{1}{F}\int_\Omega \mu I_\lambda d\delta\Omega. \tag{4.11}$$

Here, before going in to details for the derivation, I am going to do the calculations of the two integrals separately.

To evaluate the first integral on the right hand of eqn. (4.11), we begin by writing the radiative transfer equation in a plane parallel atmosphere (Mihalas,) as follows:

$$\mu \frac{dI_\lambda}{d\tau_\lambda} = I_\lambda - S_\lambda, \tag{4.12}$$

where $\mu = \cos\theta$, S_λ is the source function, λ wavelength of radiation, τ_λ is optical depth defined as $d\tau_\lambda = -\kappa_\lambda \rho dr$. Therefore, by substituting these expression of τ_λ, the radiative transfer equation becomes:

$$\mu \frac{dI_\lambda}{-\kappa_\lambda \rho dr} = I_\lambda - S_\lambda. \tag{4.13}$$

For a local thermodynamic equilibrium (LTE) case, the source function equals the Planck's function $B_\lambda = S_\lambda$. This assumption does not imply a complete thermodynamic equilibrium because this assumption would be wrong at the outer layers of the star as it is known that there is a large amount of energy loss at the outer layer. To simplify the radiative transfer equation, we introduce the mass $dm = \rho dr$, leading to eqn.(4.13) to become:

$$\mu \frac{dI_\lambda}{dm} = (B_\lambda - I_\lambda)\kappa_\lambda, \tag{4.14}$$

The radiative transfer equation, after applying linear perturbations on all terms including the μ term, becomes:

$$(\mu + \delta\mu)\frac{d}{dm}(I_\lambda + \delta I_\lambda) = (\kappa_\lambda + \delta\kappa_\lambda)[B_\lambda + \delta B_\lambda - I_\lambda - \delta I_\lambda]. \tag{4.15}$$

This becomes after a simple algebra:

$$(\mu + \delta\mu)\left[\frac{dI_\lambda}{dm} + \frac{d\delta I_\lambda}{dm}\right] = (B_\lambda + \delta B_\lambda - I_\lambda - \delta I_\lambda)(\kappa_\lambda + \delta\kappa_\lambda) \tag{4.16}$$

Ignoring high order terms, one can get from eqn.4.16:

$$\mu\frac{dI_\lambda}{dm} + \mu\frac{d\delta I_\lambda}{dm} + \delta\mu\frac{dI_\lambda}{dm} = \kappa_\lambda B_\lambda + \kappa_\lambda \delta B_\lambda - \kappa_\lambda I_\lambda - \kappa_\lambda \delta I_\lambda + \delta\kappa B_\lambda - \delta\kappa I_\lambda \tag{4.17}$$

Simplifying the equation by noting that $\mu\frac{dI_\lambda}{dm} - B_\lambda\kappa_\lambda + \kappa_\lambda I_\lambda = 0$, we obtain:

$$\mu\frac{d\delta I_\lambda}{dm} + \delta\mu\frac{dI_\lambda}{dm} = \kappa_\lambda \delta B_\lambda - \kappa_\lambda \delta I_\lambda + \delta\kappa B_\lambda - \delta\kappa_\lambda I_\lambda. \tag{4.18}$$

To simplify eqn.(4.18), we divide the whole equation by $-\kappa_\lambda$ and using definition τ_λ we obtain this equation:

$$\delta\mu\frac{dI_\lambda}{d\tau} + \mu\frac{d\delta I_\lambda}{d\tau} = -\delta B_\lambda + \delta I_\lambda - B_\lambda\frac{\delta\kappa_\lambda}{\kappa_\lambda} + I_\lambda\frac{\delta\kappa_\lambda}{\kappa_\lambda}. \tag{4.19}$$

By doing simple algebraic manipulation we end up with:

$$\mu\frac{d\delta I_\lambda}{d\tau_\lambda} = -\delta\mu\frac{dI_\lambda}{d\tau_\lambda} - \delta B_\lambda + \delta I_\lambda + \frac{\delta\kappa_\lambda}{\kappa_\lambda}(I_\lambda - B_\lambda). \tag{4.20}$$

$$\mu\frac{d\delta I_\lambda}{d\tau_\lambda} = \delta I_\lambda - \delta B_\lambda + \frac{\delta\kappa_\lambda}{\kappa_\lambda}(I_\lambda - B_\lambda) - \frac{\delta\mu}{\mu}(I_\lambda - B_\lambda). \tag{4.21}$$

The last term on the right hand side in eqn.(4.21) gives the effect of pulsation on the surface normal. This term is zero for radial oscillation due to the fact that the surface normal does not change direction during radial oscillations. It is also easy to see that the above equation is a first order differential equation with δI_λ as a solution and we will show this in the following section.

4.1.2 Finding the Solution to Radiative Transfer Equation

The radiative transfer equation shown in eqn.(4.21) can be solved as follows. The solution to such type equations can be obtained by using the integrating factor. In this case, the integrating factor is given by $e^{\int \frac{-1}{\mu}d\tau_\lambda}$. Hence,

$$\frac{d\delta I_\lambda}{d\tau_\lambda} - \frac{1}{\mu}\delta I_\lambda = -\frac{1}{\mu}\delta B_\lambda + \frac{1}{\mu}\frac{\delta\kappa_\lambda}{\kappa_\lambda}(I_\lambda - B_\lambda) - \frac{\delta\mu}{\mu^2}(I_\lambda - B_\lambda). \tag{4.22}$$

Then we multiply the whole equation above, eqn.(4.22) by the integrating factor to get the solution of the above differential equation.

Here the quantity $\frac{\tau_\lambda}{\mu}$ is the actual path along the direction μ taken by the radiation. Therefore, in general, as Collins, ( ) stated extinction by scattering or absorption will exponentially diminish the strength of the intensity by $e^{\frac{-\tau_\lambda}{\mu}}$. Multiplying eqn. 4.22 by the integrating factor $e^{\frac{-\tau_\lambda}{\mu}}$ and doing some algebraic manipulations, then eqn.(4.22) will reduce to the following:

$$\frac{d(\delta I_\lambda e^{-\frac{\tau_\lambda}{\mu}})}{d\tau} = \frac{-1}{\mu}\delta B_\lambda e^{\frac{-\tau_\lambda}{\mu}} + \frac{1}{\mu}\frac{\delta\kappa}{\kappa}(I_\lambda - B_\lambda)e^{\frac{-\tau_\lambda}{\mu}} - \frac{\delta\mu}{\mu^2}(I_\lambda - B_\lambda)e^{\frac{-\tau_\lambda}{\mu}}. \tag{4.23}$$

Then, we can rewrite eqn.(4.23) as:

$$d[\delta I_\lambda e^{-\frac{\tau_\lambda}{\mu}}] = \frac{-1}{\mu}\delta B_\lambda e^{-\frac{\tau_\lambda}{\mu}}d\tau_\lambda + \frac{1}{\mu}\frac{\delta\kappa_\lambda}{\kappa_\lambda}(I_\lambda - B_\lambda)e^{-\frac{\tau_\lambda}{\mu}}d\tau_\lambda - \frac{\delta\mu}{\mu^2}(I_\lambda - B_\lambda)e^{-\frac{\tau_\lambda}{\mu}}d\tau_\lambda. \tag{4.24}$$

If we integrate eqn.(4.24) given above from 0 to ∞ in τ_λ:

$$\delta I_\lambda(\infty)e^{-\infty} - \delta I_\lambda(0)e^0 = -\int_0^\infty \delta B_\lambda e^{\frac{-\tau_\lambda}{\mu}}\frac{d\tau_\lambda}{\mu} + \int_0^\infty \frac{\delta\kappa_\lambda}{\kappa_\lambda}(I_\lambda - B_\lambda)e^{-\frac{\tau_\lambda}{\mu}}\frac{d\tau}{\mu} - \int_0^\infty \frac{\delta\mu}{\mu^2}(I_\lambda - B_\lambda)e^{-\frac{\tau_\lambda}{\mu}}d\tau_\lambda, \tag{4.25}$$

$$\delta I_\lambda(0) = \int_0^\infty \delta B_\lambda e^{\frac{-\tau_\lambda}{\mu}}\frac{d\tau_\lambda}{\mu} - \int_0^\infty \frac{\delta\kappa_\lambda}{\kappa_\lambda}(I_\lambda - B_\lambda)e^{-\frac{\tau_\lambda}{\mu}}\frac{d\tau_\lambda}{\mu} + \int_0^\infty \frac{\delta\mu}{\mu^2}(I_\lambda - B_\lambda)e^{-\frac{\tau_\lambda}{\mu}}d\tau_\lambda, \tag{4.26}$$

where eqn.(4.26) gives the perturbed radiative intensity. Since our aim is to get the perturbed radiative flux variation due to non radial pulsation of stars, the next step is to get the radiative surface flux using the radiative intensity. By definition, radiative surface flux at frequency λ is interpreted as the net rate of energy flow through a surface element.

$$\delta F_\lambda = \int_0^{2\pi}\int_0^1 \mu\delta I_\lambda d\mu d\phi \tag{4.27}$$

By applying this definition to eqn.(4.27), the radiative surface flux becomes

$$\delta F_\lambda = \int_0^{2\pi}\int_0^1\int_0^\infty \mu\delta B_\lambda e^{\frac{-\tau_\lambda}{\mu}}\frac{\delta\tau_\lambda}{\mu}d\mu d\phi - \int_0^{2\pi}\int_0^1\int_0^\infty \mu\frac{\delta\kappa_\lambda}{\kappa_\lambda}(I_\lambda - B_\lambda)e^{\frac{-\tau_\lambda}{\mu}}\frac{d\tau_\lambda}{\mu}d\mu d\phi + \int_0^{2\pi}\int_0^1\int_0^\infty \frac{\delta\mu}{\mu}(I_\lambda - B_\lambda)e^{\frac{-\tau_\lambda}{\mu}}\frac{d\tau_\lambda}{\mu}\mu d\mu d\phi \tag{4.28}$$

If we assume the solution of the non radial oscillation to be of the form

$$\frac{\delta r(r,\theta,\phi,t)}{r} = \frac{\delta\tilde{r}(r)}{r}Y_l^m(\theta,\phi)e^{-\omega t} \tag{4.29}$$

$$\delta B_\lambda(r,\theta,\phi,t) = \delta\tilde{B}_\lambda(r)Y_l^m(\theta,\phi)e^{-\omega t} \tag{4.30}$$

$$\frac{\delta\kappa_\lambda}{\kappa_\lambda}(r,\theta,\phi,t) = \frac{\delta\tilde{\kappa_\lambda}(r)}{\kappa_\lambda}Y_l^m(\theta,\phi)e^{-\omega t} \tag{4.31}$$

where Y_l^m is the spherical harmonic function, $\delta\tilde{r}$, δB_λ and $\frac{\delta\tilde{\kappa}_\lambda}{\kappa_\lambda}$ are obtained from a stellar pulsation code and $\frac{\delta r}{r}$ is relative displacement. If we substitute the solutions for the non-radial oscillations given above in eqns.$(4.29 - 4.31)$ into eqn. 4.28 we obtain:

$$\begin{aligned}\delta F_\lambda = &\int_0^{2\pi}\int_0^1\int_0^\infty \delta B_\lambda Y_l^m(\theta,\phi)e^{\frac{-\tau_\lambda}{\mu}}d\tau_\lambda d\mu d\phi \\ &- \int_0^{2\pi}\int_0^1\int_0^\infty \frac{\delta\kappa_\lambda}{\kappa_\lambda}Y_l^m(\theta,\phi)e^{-\omega t}(I_\lambda - B_\lambda)e^{\frac{-\tau_\lambda}{\mu}}d\tau_\lambda d\mu d\phi \\ &+ \int_0^{2\pi}\int_0^1\int_0^\infty \frac{\delta\mu}{\mu}(I_\lambda - B_\lambda)e^{\frac{-\tau_\lambda}{\mu}}d\tau_\lambda d\mu d\phi,\end{aligned} \tag{4.32}$$

As was shown in chapter 3, $\delta\mu$

$$\delta\mu = \frac{(\mu^2-1)}{r_0}\frac{\partial r}{\partial\mu} = (\mu^2-1)\frac{\partial}{\partial\mu}(\frac{\delta r}{r_0}), \tag{4.33}$$

therefore the displacement eigen function is given by:

$$\frac{\delta r}{r} = Y_l^m(\mu,\phi)\frac{\delta\tilde{r}}{r}e^{-i\omega t}, \tag{4.34}$$

here we ignore time dependence for now and the final equation becomes:

$$\frac{\delta\mu}{\mu} = \frac{(\mu^2-1)}{\mu}\frac{\partial Y_l^m(\theta,\phi)}{\partial\mu}\frac{\delta\tilde{r}}{r}. \tag{4.35}$$

By implementing this equation, one can get the following:

$$\begin{aligned}\delta F_\lambda = &\int_0^{2\pi}\int_0^{1}\int_0^{\infty} \delta\tilde{B}_\lambda(r)Y_l^m(\mu,\phi)e^{-\omega t}e^{\frac{-\tau_\lambda}{\mu}}d\tau_\lambda d\mu d\phi \\ &- \int_0^{2\pi}\int_0^{1}\int_0^{\infty} \frac{\delta\tilde{\kappa}_\lambda}{\kappa_\lambda}Y_l^m(\mu,\phi)e^{-\omega t}(I_\lambda - B_\lambda)e^{\frac{-\tau_\lambda}{\mu}}d\tau_\lambda d\mu d\phi \\ &- \int_0^{2\pi}\int_0^{1}\int_0^{\infty} \frac{(1-\mu^2)}{\mu}\frac{\partial Y_l^m}{\partial\mu}\frac{\delta\tilde{r}}{r}e^{-\omega t}(I_\lambda - B_\lambda)e^{\frac{-\tau_\lambda}{\mu}}d\tau_\lambda d\mu d\phi.\end{aligned} \tag{4.36}$$

By applying coordinate transformation to an observer's frame as defined in Arfken and Weber, ( ):

$$Y_l^m(\theta,\phi) = Y_l^m(\theta_0,\phi_0)P_l(\mu), \tag{4.37}$$

where θ_0, ϕ_0 are observer's coordinates and $P_l(\mu)$ is the Legendre polynomial. For simplicity, in this study, the time dependent term $e^{-i\omega t}$ is merged in the integrals of $\delta\tilde{B}_\lambda(r)$, $\frac{\delta\tilde{\kappa}_\lambda}{\kappa_\lambda}$ and $\frac{(1-\mu^2)}{\mu}$. This shows that the variations of these terms are time dependent. Then, we can write the variation in radiative flux as:

$$\begin{aligned}\delta F_\lambda = &\int_0^{2\pi}\int_0^{1}\int_0^{\infty} \delta\tilde{B}_\lambda(r)Y_l^m(\theta_0,\phi_0)e^{\frac{-\tau_\lambda}{\mu}}d\tau_\lambda d\mu d\phi \\ &- \int_0^{2\pi}\int_0^{1}\int_0^{\infty} \frac{\delta\tilde{\kappa}_\lambda}{\kappa_\lambda}Y_l^m(\theta_0,\phi_0)(I_\lambda - B_\lambda)e^{\frac{-\tau_\lambda}{\mu}}d\tau_\lambda d\mu d\phi \\ &- \int_0^{2\pi}\int_0^{1}\int_0^{\infty} \frac{(1-\mu^2)}{\mu}\frac{\partial Y_l^m(\theta_0,\phi_0)}{\partial\mu}\frac{\delta\tilde{r}}{r}(I_\lambda - B_\lambda)e^{\frac{-\tau_\lambda}{\mu}}d\tau_\lambda d\mu d\phi.\end{aligned} \tag{4.38}$$

The lack of ϕ dependence comes from the fact that $Y_l^m(\theta_0,\phi_0)$ is constant and that depends on observers' location, therefore, it comes out of the integrals. Then eqn.(4.38) will after applying coordinate transformation give the following:

$$\begin{aligned}\delta F_\lambda = &2\pi Y_l^m(\theta_0,\phi_0)\int_0^{1}\int_0^{\infty} \mu\delta\tilde{B}_\lambda(r)e^{\frac{-\tau_\lambda}{\mu}}d\tau_\lambda d\mu d\phi P_l(\mu) \\ &- 2\pi Y_l^m(\theta_0,\phi_0)\int_0^{1}\int_0^{\infty} \frac{\delta\tilde{\kappa}_\lambda}{\kappa_\lambda}(I_\lambda - B_\lambda)e^{\frac{-\tau_\lambda}{\mu}}d\tau_\lambda d\mu d\phi P_l(\mu) \\ &- 2\pi Y_l^m(\theta_0,\phi_0)\int_0^{1}\int_0^{\infty} \frac{(1-\mu^2)}{\mu}\frac{\partial P_l(\mu)}{\partial\mu})\frac{\delta\tilde{r}}{r}(I_\lambda - B_\lambda)e^{\frac{-\tau_\lambda}{\mu}}d\tau_\lambda d\mu d\phi P_l(\mu).\end{aligned} \tag{4.39}$$

According to Christensen-Dalsgaard and Frandsen, ( ), it is convenient in the theory of stellar atmosphere to work in terms of moments of radiation field. Therefore, the perturbation in surface flux can be changed to perturbed Eddington flux (δH) by using the following equation:

$$\delta H_\lambda = \frac{1}{4\pi}\oint \mu\delta I_\lambda(r,\lambda)d\Omega, \tag{4.40}$$

where the perturbed Eddington flux is related to flux δF_λ thus:

$$\delta H_\lambda = \frac{\delta F_\lambda}{4\pi} \tag{4.41}$$

In this calculation, we are giving more emphasis in obtaining the solutions for δH_λ and $\delta\kappa_\lambda$, because both δH_λ and $\delta\kappa_\lambda$ are important to calculate the structure of the atmosphere and their spectra. In addition, the two quantities are depth-weighted means of the source function.

The formula for the perturbed relative flux equation can be written as:

$$\begin{aligned}\frac{\delta H_\lambda(0)}{H_\lambda(0)} &= \frac{Y_l^m(\theta_0,\phi_0)}{2H_\lambda(0)}\int_0^1\int_0^\infty \delta\tilde{B}_\lambda(r)P_l(\mu)e^{\frac{-\tau_\lambda}{\mu}}d\tau_\lambda d\mu \\ &- \frac{Y_l^m(\theta_0,\phi_0)}{2H_\lambda(0)}\int_0^1\int_0^\infty \frac{\delta\tilde{\kappa}_\lambda}{\kappa_\lambda}P_l(\mu)(I_\lambda - B_\lambda)e^{\frac{-\tau_\lambda}{\mu}}d\tau_\lambda d\mu \\ &- \frac{Y_l^m(\theta_0,\phi_0)}{2H_\lambda(0)}\int_0^1\int_0^\infty \frac{(1-\mu^2)}{\mu}\frac{dP_l(\mu)}{d\mu}\frac{\delta\tilde{r}}{r}(I_\lambda - B_\lambda)e^{\frac{-\tau_\lambda}{\mu}}d\mu d\tau_\lambda,\end{aligned} \tag{4.42}$$

where $H_\lambda(0)$ is the surface Eddington flux. According to Buta and Smith, ( ), limb darkening law is written in terms of μ to account for changes in the limb darkening due to the surface normal as $\cos\Theta(t) = \hat{n}\cdot\hat{n}_s$. But, in our calculation, the effect of limb darkening is incorporated in the term I_λ. In the above equation, $\frac{\delta H_\lambda}{H_\lambda(0)}$ includes perturbations in temperature and opacity of the gases of the atmosphere of the star. The third term represents the perturbations in the surface normal. Note that the integral in the third term consists of $\frac{\delta\tilde{r}}{r}e^{\frac{-\tau_\lambda}{\mu}}$ which is significant only for surface layers and rapidly approaches zero at $\tau < 1$. Note that the surface normal term differs from the one presented in chapter 3 on Watson's formula in that it includes a factor $\frac{\delta\tilde{r}}{r}e^{\frac{-\tau_\lambda}{\mu}}$. This factor drops rapidly with depth for μ values that are different from 1 for high overtone pulsations ($n \gg 1$). This is demonstrated in the following figures: Let us call the last term on the right hand side of eqn.(4.42), the variation in the normal term T_N:

But, we can show that

$$T_N = \frac{Y_l^m(\theta_0,\phi_0)}{2H(0)}\int_0^1\int_0^\infty (1-\mu^2)\frac{dP_l}{d\mu}\frac{\delta\tilde{r}}{r}\frac{dI}{d\tau}d\mu\tau_\lambda, \tag{4.43}$$

it can be written as:

$$T_N = \frac{Y_l^m(\theta_0,\phi_0)}{2H(0)}\int_0^1 (1-\mu^2)\frac{dP_l}{d\mu}\mu f(\mu)d\mu, \tag{4.44}$$

where,

$$f(\mu) = \int_0^\infty \frac{dI_\lambda}{d\tau}\frac{\delta\tilde{r}}{r}e^{\frac{-\tau}{\mu}}\frac{d\tau}{\mu}. \tag{4.45}$$

But, we can show that,

$$\frac{d}{d\tau}\left[I_\lambda\frac{\delta\tilde{r}}{r}e^{\frac{-\tau}{\mu}}\right] = \frac{dI_\lambda}{d\tau}\frac{\delta\tilde{r}}{r_0}e^{\frac{-\tau}{\mu}} + \frac{d}{d\tau}\left(\frac{\delta\tilde{r}}{r_0}\right)I_\lambda e^{\frac{-\tau}{\mu}} - \frac{1}{\mu}I_\lambda\frac{\delta\tilde{r}}{r}e^{\frac{-\tau}{\mu}}. \tag{4.46}$$

Therefore,

$$f(\mu) = \frac{d}{d\tau}\int_0^\infty I(\tau,\mu)\frac{\delta\tilde{r}}{r}e^{\frac{-\tau}{\mu}} - \int_0^\infty \frac{d}{d\tau}\left(\frac{\delta\tilde{r}}{r_0}\right)I(\tau,\mu)e^{\frac{-\tau}{\mu}}\frac{d\tau}{\mu} + \frac{1}{\mu}\int I(\tau,\mu)\frac{\delta\tilde{r}}{r}e^{\frac{-\tau}{\mu}}\frac{d\tau}{\mu}. \quad (4.47)$$

We show in Chapter 5 that $\frac{\tilde{r}}{r}$ is nearly constant in the atmosphere for low overtone (~ 1) pulsators. This means that in this case $\frac{d}{d\tau}\left(\frac{\delta\tilde{r}}{r}\right) \simeq 0$. Thus, the second term in eqn.(4.47) vanishes for low n pulsation.

If we define,

$$h = \int_0^\infty I(\tau,\mu)\frac{\delta\tilde{r}}{r}e^{\frac{-\tau}{\mu}}\frac{d\tau}{\mu}, \quad (4.48)$$

then,

$$\mu f(\mu) = \mu\frac{dh}{d\tau} + h. \quad (4.49)$$

Note also that for low frequencies,

$$h = \frac{\delta\tilde{r}}{r}\int_0^\infty I(\tau,\mu)e^{\frac{-\tau}{\mu}}\frac{d\tau}{\mu}. \quad (4.50)$$

In Watson's formula, it is known that $\frac{\delta\tilde{r}}{r} = \epsilon$. Therefore,

$$T_N = \epsilon\frac{Y_l^m(\theta_0,\phi_0)}{2H(0)}\int_0^1 (1-\mu^2)\frac{dP_l}{d\mu}\left(\frac{dh}{d\tau} + h\right)d\mu, \quad (4.51)$$

which reduce to:

$$\epsilon Y_l^m(\theta_0,\phi_0)\int_0^1 (1-\mu^2)\frac{dP_l}{d\mu}\left(\frac{dh'}{d\tau} + h'\right)d\mu. \quad (4.52)$$

If we approximate $I \sim B$ and assuming $d\tau \sim d\mu$ then, h' the normalized limb-darkening function . The second assumption is reasonable since the limb-darkening effect suggests that $\tau \sim \mu$. The discussions above can be seen in the following figures:

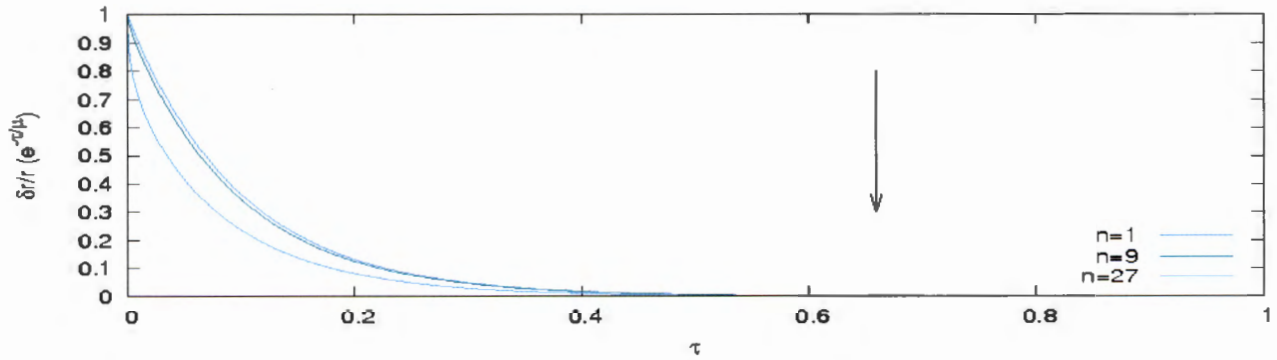

FIGURE 4.1: The variation of the factor $\frac{\delta r}{r}e^{\frac{-\tau_\lambda}{\mu}}$ with τ in the atmosphere of the model with $T_{\text{eff}} = 5778$ K and $\mu = 0.1$. The arrow indicates the location of the photosphere where $\tau = 2/3$.

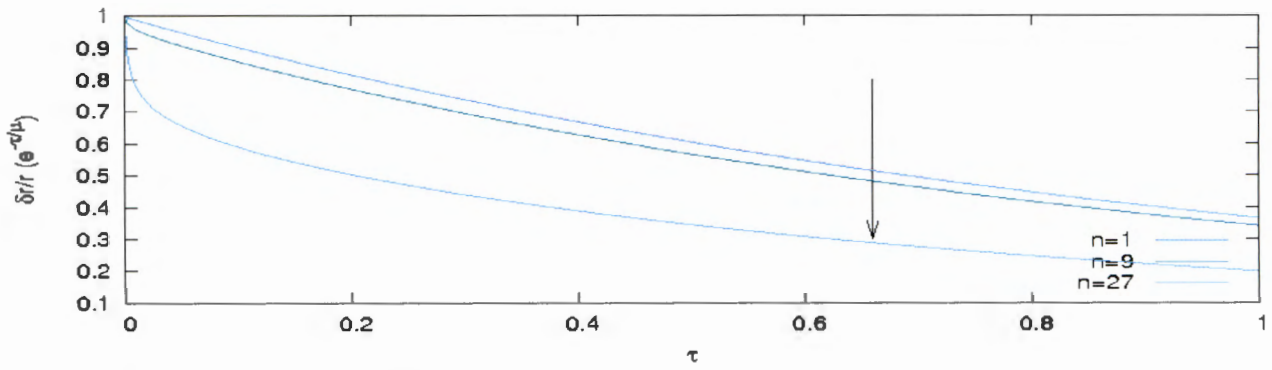

FIGURE 4.2: The variation of the factor $\frac{\delta r}{r} e^{\frac{-\tau_\lambda}{\mu}}$ with τ in the atmosphere of the model with $T_{\text{eff}} = 5778$ K and $\mu = 1$. The arrow indicates the location of the photosphere where $\tau = 2/3$.

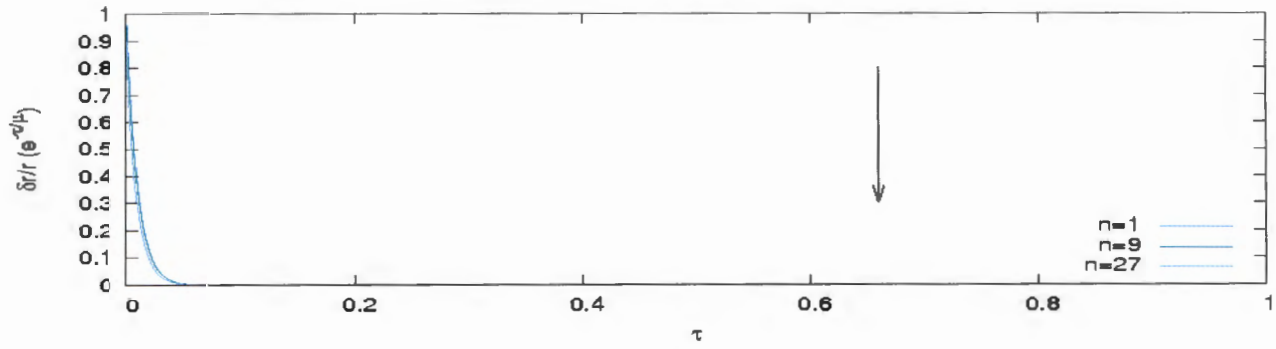

FIGURE 4.3: The variation of the factor $\frac{\delta r}{r} e^{\frac{-\tau_\lambda}{\mu}}$ with τ in the atmosphere of the model with $T_{\text{eff}} = 5778$ K and $\mu = 0.01$. The arrow indicates the location of the photosphere where $\tau = 2/3$.

Fig. 4.1 - Fig. 4.3 show the variation of $\frac{\delta r}{r} e^{\frac{-\tau_\lambda}{\mu}}$ with respect of τ for an equilibrium model with $T_{\text{eff}} = 5778$ K, values of $n = 1, 9, 27$ and $\mu = 0.1, 1, 0.01$ for the three plots from top to bottom respectively. In particular, one can see that for $n = 27$ and $\mu \ll 1$, this factor is near zero for $\tau > 0.1$. The arrow indicates the location of the photosphere where $\tau = 2/3$.

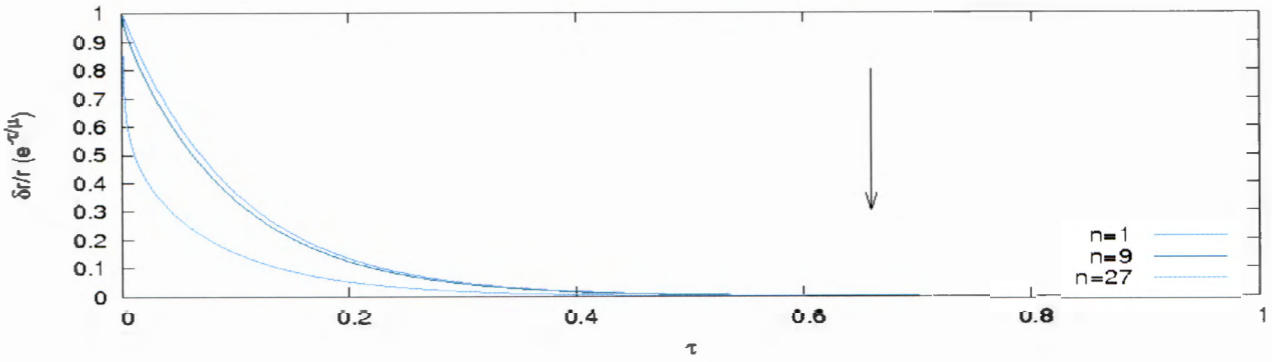

FIGURE 4.4: The variation of the factor $\frac{\delta r}{r} e^{\frac{-\tau_\lambda}{\mu}}$ with τ in the atmosphere of the model with $T_{\text{eff}} = 7512$ K and $\mu = 0.1$. The arrow indicates the location of the photosphere where $\tau = 2/3$.

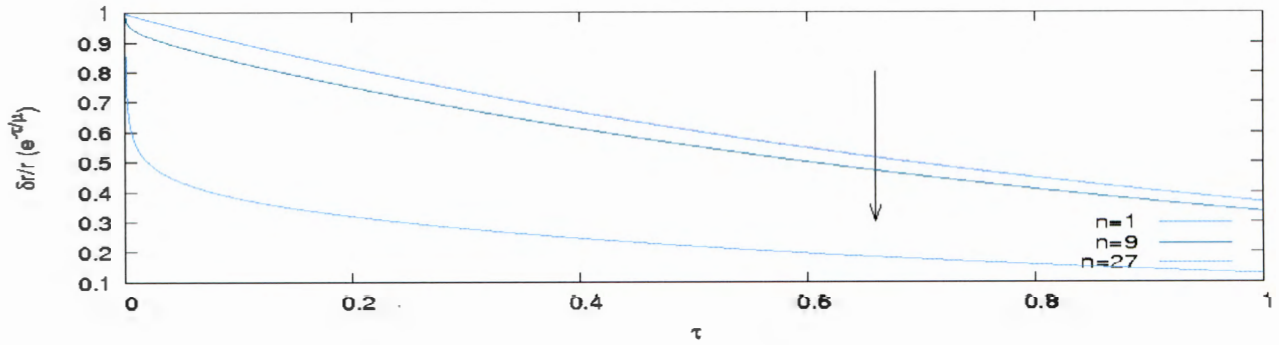

FIGURE 4.5: The variation of the factor $\frac{\delta r}{r} e^{\frac{-\tau_\lambda}{\mu}}$ with τ in the atmosphere of the model with $T_{\text{eff}} = 7512$ K and $\mu = 1$. The arrow indicates the location of the photosphere where $\tau = 2/3$.

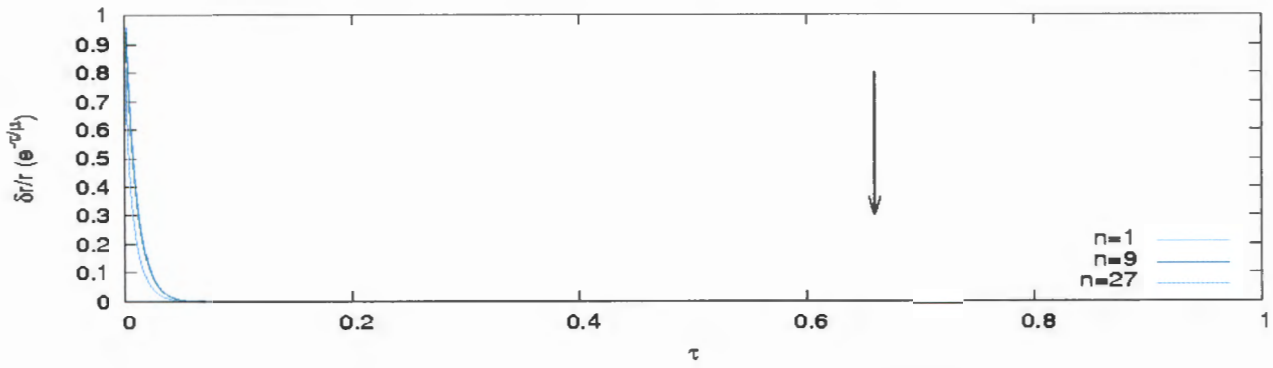

FIGURE 4.6: The variation of the factor $\frac{\delta r}{r} e^{\frac{-\tau_\lambda}{\mu}}$ with τ in the atmosphere of the model with $T_{\text{eff}} = 7512$ K and $\mu = 0.01$. The arrow indicates the location of the photosphere where $\tau = 2/3$.

Fig. 4.4 - Fig. 4.6 show the variation of $\frac{\delta r}{r} e^{\frac{-\tau_\lambda}{\mu}}$ with respect of τ for an equilibrium model with $T_{\text{eff}} = 7512$ K with the values of $n = 1, 9, 27$ and $\mu = 0.1, 1, 0.01$ for the three plots from top to bottom respectively. In particular, one can see that for $n = 27$ and $\mu \ll 1$, this factor is near zero for $\tau > 0.1$. The arrow indicates the location of the photosphere where $\tau = 2/3$.

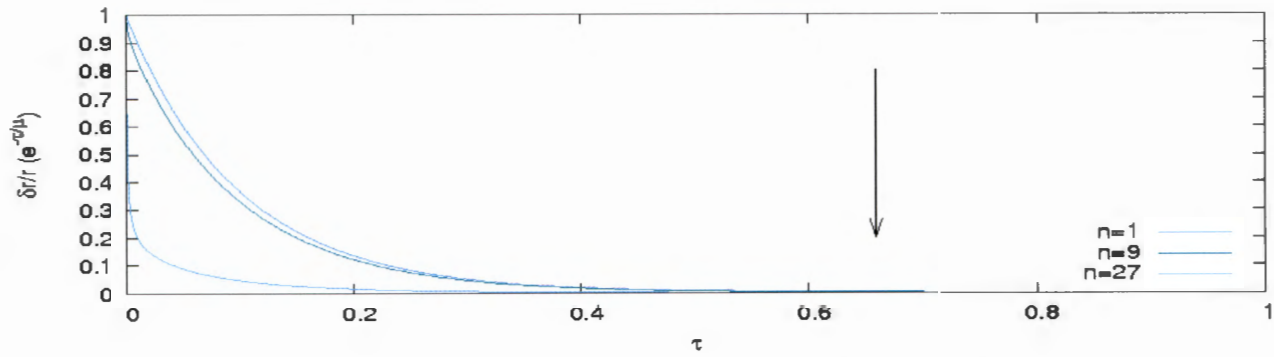

FIGURE 4.7: The variation of the factor $\frac{\delta r}{r} e^{\frac{-\tau_\lambda}{\mu}}$ with τ in the atmosphere of the model with $T_{\text{eff}} = 9440$ K and $\mu = 0.1$. The arrow indicates the location of the photosphere where $\tau = 2/3$.

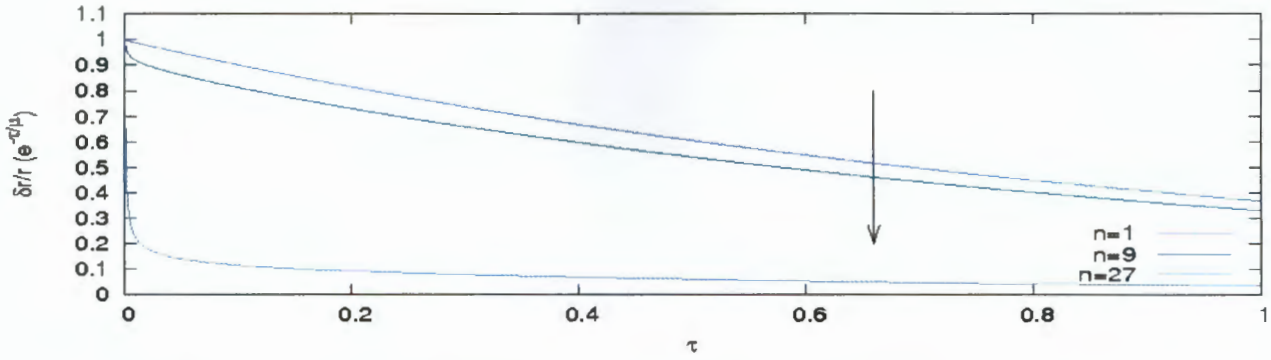

FIGURE 4.8: The variation of the factor $\frac{\delta r}{r}e^{\frac{-\tau_\lambda}{\mu}}$ with τ in the atmosphere of the model with $T_{\text{eff}} = 9440$ K and $\mu = 1$. The arrow indicates the location of the photosphere where $\tau = 2/3$.

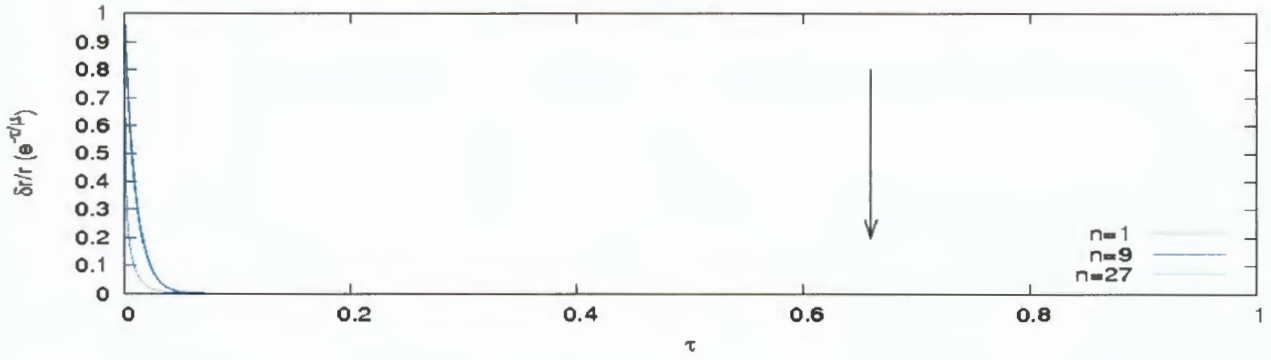

FIGURE 4.9: The variation of the factor $\frac{\delta r}{r}e^{\frac{-\tau_\lambda}{\mu}}$ with τ in the atmosphere of the model with $T_{\text{eff}} = 9440$ K and $\mu = 0.01$. The arrow indicates the location of the photosphere where $\tau = 2/3$.

Fig. - Fig. show the variation of $\frac{\delta r}{r}e^{\frac{-\tau_\lambda}{\mu}}$ with respect of τ for an equilibrium model with $T_{\text{eff}} = 9440$ K with $n = 1, 9, 27$ and $\mu = 0.1, 1, 0.01$ for the three plots respectively. In particular, one can see that for $n = 27$ and $\mu \ll 1$, this factor is near zero for $\tau > 0.1$. The arrow in the plots show the location of the photosphere where $\tau = 2/3$.

4.1.3 Surface Area Variation

In order to complete our calculation, I need to solve the second term in eqn.(4.11), given below:

$$\frac{1}{F}\int\int \mu I_\lambda d\delta\Omega, \tag{4.53}$$

shows one of the effects caused by pulsation of the star, that is, the surface area variation. Therefore, to solve this integral, we need to solve the value of the perturbed solid angle $d\delta\Omega$.

Going back to the beginning of the calculations of the second integral, i.e eqn.(4.11) and substituting the perturbation of the solid angle, calculated in chapter 3 in the integral, then:

$$\int_\Omega \mu I_\lambda d\delta\Omega = -\int_0^{2\pi}\int_0^1 \mu I_\lambda \frac{2\delta r}{r_0}\mu d\mu d\phi + \int_0^{2\pi}\int_0^1 \mu I_\lambda (1-\mu^2)\frac{\partial}{\partial\mu}(\frac{\delta r}{r_0})d\mu d\phi, \tag{4.54}$$

using the coordinate transformation, [see eqn.4.37], used in the calculation of the first integral in the perturbation:

$$\frac{\delta r}{r} = \frac{\delta\tilde{r}}{r}Y_l^m(\theta,\phi)e^{-\omega t}, \tag{4.55}$$

and

$$Y_l^m(\theta,\phi) = Y_l^m(\theta_0,\phi_0)P_l(\mu), \tag{4.56}$$

then, eqn.(4.54) will reduce to:

$$\begin{aligned}\int_\Omega \mu I_\lambda d\delta\Omega = &\int_0^1\int_0^{2\pi} -\mu I_\lambda \frac{2\delta r}{r}Y_l^m(\theta_0,\phi_0)P_l(\mu)\mu d\mu d\phi \\ &+ \int_0^1\int_0^{2\pi} \mu I_\lambda(1-\mu^2)\frac{\partial}{\partial\mu}(\frac{\delta r}{r}Y_l^m(\theta_0,\phi_0)P_l(\mu))d\mu d\phi.\end{aligned} \tag{4.57}$$

Since the integral over ϕ gives the constant 2π, then:

$$\int\int \mu I_\lambda d\delta\Omega = -2\pi Y_l^m(\theta_0,\phi_0)\int_0^1 2\mu I P_l(\mu)\mu\frac{\delta r}{r}d\mu + 2\pi Y_l^m(\theta_0,\phi_0)\int_0^1 \mu I(1-\mu^2)\frac{\partial P_l(\mu)}{\partial\mu}\frac{\delta r}{r}d\mu. \tag{4.58}$$

This expression is equivalent to the third term T_3 of Watson's formula. The difference in the two expressions is T_3 takes the displacement eigen function and other terms by represented as ϵ (amplitude parameter) assumed to be constant whereas here in our calculation, the displacement eigen function is not constant.

$$\begin{aligned}\int_\Omega \mu I_\lambda d\delta\Omega = &-2\pi\int_0^1 \mu I_\lambda 2\frac{\delta\tilde{r}}{r}Y_l^m(\theta_0,\phi_0)P_l(\mu)e^{-i\omega t}\mu d\mu \\ &+ 2\pi\int_0^1 \mu I_\lambda(1-\mu^2)\frac{\partial}{\partial\mu}[\frac{\delta\tilde{r}}{r}Y_l^m(\theta_0,\phi_0)P_l(\mu)e^{-\omega t}]d\mu.\end{aligned} \tag{4.59}$$

But $I(\tau',\mu) = \int_{\tau'}^\infty B_\lambda(\tau)e^{\frac{-\tau}{\mu}}\frac{d\tau}{\mu}$

$$\begin{aligned}&= -2\pi Y_l^m(\theta_0,\phi_0)\int_0^1\int_0^\infty \mu B_\lambda(\tau_\lambda)\frac{\delta\tilde{r}}{r}P_l(\mu)e^{\frac{-\tau_\lambda}{\mu}}e^{-\omega t}d\mu d\tau_\lambda \\ &+ 2\pi Y_l^m(\theta_0,\phi_0)\int_0^1\int_0^\infty B_\lambda(\tau)\mu(1-\mu^2)\frac{\delta\tilde{r}}{r}\frac{\partial P_l(\mu)}{\partial\mu}e^{\frac{-\tau_\lambda}{\mu}}e^{-\omega t}d\tau_\lambda d\mu\end{aligned} \tag{4.60}$$

Therefore, simplifying the equation above as we did before by multiplying it with $\frac{1}{4H_\lambda(0)}$, the equation is simplified as follows:

$$\begin{aligned}\frac{\delta A}{A} = &-\frac{Y_l^m(\theta_0,\phi_0)}{2H_\lambda(0)}\int_0^1\int_{\tau'}^{\infty}\mu B_\lambda(\tau_\lambda)\frac{\delta\tilde{\tau}}{r}P_l(\mu)e^{\frac{-\tau_\lambda}{\mu}}e^{-\omega t}d\mu d\tau_\lambda \\ &+\frac{Y_l^m(\theta_0,\phi_0)}{2H_\lambda(0)}\int_0^1\int_{\tau'}^{\infty}B_\lambda(\tau)\mu(1-\mu^2)\frac{\tilde{\tau}}{r}\frac{\partial P_l(\mu)}{\partial\mu}e^{\frac{-\tau_\lambda}{\mu}}e^{-\omega t}d\tau_\lambda d\mu\end{aligned} \tag{4.61}$$

4.2 The New Formalism

In the previous sections, I derived the very important components of our formalism and going back again to the very definition of luminosity where an observer measures luminosity from a star, we now include surface area effects taking into account the definition and derivation introduced in the previous equation.

We now note that perturbed luminosity of a pulsating star is given by:

$$\frac{\delta L_\lambda}{L_\lambda(0)} = \frac{\delta H_\lambda}{H_\lambda(0)} + \frac{\delta A_\lambda}{A_\lambda} + \frac{\delta N_\lambda}{N_\lambda}, \tag{4.62}$$

where the first term includes, as discussed earlier, radiative surface flux and variation in the surface normal. For $\frac{\delta H_\lambda}{H_\lambda(0)}$, we use first two terms on the right of eqn. (4.42) and for $\frac{\delta A}{A}$ we use eqn.(4.51), $L_\lambda(0)$ is surface luminosity and for $\frac{\delta N_\lambda}{N_\lambda}$, we use the third term of eqn. (4.42).

Now, by substituting all the equations for the different terms, the perturbed luminosity that takes into consideration the multi layered atmosphere is:

$$\begin{aligned}\frac{\delta L_\lambda}{L_\lambda(0)} = &\frac{Y_l^m(\theta_0,\phi_0)}{2H_{\lambda 0}(\lambda)}\int_0^1\int_0^{\infty}\delta\tilde{B}_\lambda(r)P_l(\mu)e^{\frac{-\tau_\lambda}{\mu}}d\tau_\lambda d\mu \\ &-\frac{Y_l^m(\theta_0,\phi_0)}{2H_\lambda(0)}\int_0^1\int_0^{\infty}\frac{\delta\tilde{\kappa}_\lambda}{\kappa_\lambda}P_l(\mu)(I_\lambda-B_\lambda)e^{\frac{-\tau_\lambda}{\mu}}d\tau_\lambda d\mu \\ &-\frac{Y_l^m(\theta_0,\phi_0)}{2H_\lambda(0)}\int_0^1\int_0^{\infty}\frac{(1-\mu^2)}{\mu}\frac{dP_l(\mu)}{d\mu}\frac{\delta\tilde{\tau}}{r}(I_\lambda-B_\lambda)e^{\frac{-\tau_\lambda}{\mu}}d\mu d\tau_\lambda \\ &-\frac{Y_l^m(\theta_0,\phi_0)}{2H_\lambda(0)}\int_0^1\int_{\tau'}^{\infty}2\mu P_l(\mu)B_\lambda(\tau)\frac{\delta\tilde{\tau}}{r}e^{\frac{-\tau_\lambda}{\mu}}d\mu d\tau_\lambda \\ &+\frac{Y_l^m(\theta_0,\phi_0)}{2H_\lambda(0)}\int_0^1\int_{\tau'}^{\infty}(1-\mu^2)B_\lambda(\tau)\frac{dP_l(\mu)}{d\tau}\frac{\delta\tilde{\tau}}{r}e^{\frac{-\tau_\lambda}{\mu}}d\mu d\tau_\lambda.\end{aligned} \tag{4.63}$$

This equation can be arranged in such a way that the observed luminosity becomes the combination of the perturbed radiative transfer equation where it includes variations both in the surface normal as well as variations in the area and temperature. Moreover, eqn. (4.63) also includes the

variation in opacity.

$$\begin{aligned}
\frac{\delta L_\lambda}{L_\lambda(0)} &= \frac{Y_l^m(\theta_0,\phi_0)}{2H_\lambda(0)}\int_0^1\int_0^\infty \delta\tilde{B}_\lambda(r)P_l(\mu)e^{\frac{-\tau_\lambda}{\mu}}d\tau_\lambda d\mu \\
&- \frac{Y_l^m(\theta_0,\phi_0)}{2H_\lambda(0)}\int_0^1\int_0^\infty \frac{\delta\tilde{\kappa}_\lambda}{\kappa_\lambda}P_l(\mu)(I_\lambda - B_\lambda)e^{\frac{-\tau_\lambda}{\mu}}d\tau_\lambda d\mu \\
&- \frac{Y_l^m(\theta_0,\phi_0)}{2H_\lambda(0)}\int_0^1\int_0^\infty (1-\mu^2)\frac{\delta\tilde{r}}{r}\frac{dP_l(\mu)}{d\mu}\frac{dI_\lambda}{d\tau_\lambda}e^{\frac{-\tau_\lambda}{\mu}}d\tau_\lambda d\mu \\
&- \frac{Y_l^m(\theta_0,\phi_0)}{2H_\lambda(0)}\int_0^1\int_{\tau'}^\infty 2\mu P_l(\mu)B_\lambda(\tau)\frac{\delta\tilde{r}}{r}e^{\frac{-\tau_\lambda}{\mu}}d\tau_\lambda d\mu \\
&+ \frac{Y_l^m(\theta_0,\phi_0)}{2H_\lambda(0)}\int_0^1\int_{\tau'}^\infty (1-\mu^2)B_\lambda(\tau)\frac{dP_l(\mu)}{d\tau}\frac{\delta\tilde{r}}{r}e^{\frac{-\tau_\lambda}{\mu}}d\tau_\lambda d\mu,
\end{aligned} \tag{4.64}$$

where we used $\mu\frac{dI_\lambda}{d\tau_\lambda} = I_\lambda - B_\lambda$ from radiative transfer equation.

One can simplify the last three terms of the above equation to show the variations of the surface normal due to pulsation and compare it with the geometric effects from Watson's formula and prove that it vanishes for dipole oscillation $l = 1$, where $l = 0$ refers to radial oscillation. In the following derivation, I will keep the first two terms as it is and simplify the last three terms.

$$\begin{aligned}
\frac{\delta L}{L_{\lambda(0)}} &= \frac{Y_l^m((\theta_0,\phi_0))}{2H_\lambda(0)}\int_0^1\int_0^\infty \delta\tilde{B}_\lambda(r)P_l(\mu)e^{\frac{-\tau_\lambda}{\mu}}d\tau_\lambda d\mu \\
&- \frac{Y_l^m(\theta_0,\phi_0)}{2H_\lambda(0)}\int_0^1\int_0^\infty \frac{\delta\tilde{\kappa}_\lambda}{\kappa_\lambda}P_l(\mu)(I_\lambda - B_\lambda)e^{\frac{-\tau_\lambda}{\mu}}d\tau_\lambda d\mu \\
&- Y_l^m(\theta_0,\phi_0)\Bigg\{\int_0^1 \frac{(1-\mu^2)}{\mu}\frac{dP_l(\mu)}{d\mu}\mu d\mu\int_0^\infty \frac{\delta\tilde{r}}{r}e^{\frac{-\tau_\lambda}{\mu}}\frac{d\tau_\lambda}{2H_\lambda(0)} \\
&+ 2\int_0^1 P_l(\mu)\mu d\mu\int_0^\infty \frac{B_\lambda}{2H_\lambda(0)}\frac{\delta\tilde{r}}{r}e^{\frac{-\tau_\lambda}{\mu}}d\tau_\lambda \\
&- (1-\mu^2)\frac{dP_l(\tau)}{d\tau}d\mu\int_0^\infty \frac{B_\lambda}{2H_\lambda(0)}\frac{\delta\tilde{r}}{r}e^{\frac{-\tau_\lambda}{\mu}}d\tau_\lambda\Bigg\}
\end{aligned} \tag{4.65}$$

By taking the common factor from the last three terms, we can rewrite the above equation as:

$$\begin{aligned}\frac{\delta L}{L_{\lambda(0)}} &= \frac{Y_l^m((\theta_0,\phi_0))}{2H_\lambda(0)}\int_0^1\int_0^\infty \delta\tilde{B}_\lambda(r)P_l(\mu)e^{\frac{-\tau_\lambda}{\mu}}d\tau_\lambda d\mu \\ &- \frac{Y_l^m(\theta_0,\phi_0)}{2H_\lambda(0)}\int_0^1\int_0^\infty \frac{\delta\tilde{\kappa_\lambda}}{\kappa_\lambda}P_l(\mu)(I_\lambda - B_\lambda)e^{\frac{-\tau_\lambda}{\mu}}d\tau_\lambda d\mu \\ &- Y_l^m(\theta_0,\phi_0)\Bigg\{\int_0^1 \frac{(1-\mu^2)}{\mu}\frac{dP_l(\mu)}{d\mu}\frac{dI_\lambda}{d\mu}\mu\int_0^\infty \frac{\delta\tilde{r}}{r}e^{\frac{-\tau_\lambda}{\mu}}\frac{d\tau_\lambda}{2H_\lambda(0)} \\ &+ 2\int_0^1 P_l(\mu)\mu d\mu\int_0^\infty B_\lambda(\tau)\frac{\delta\tilde{r}}{r}e^{\frac{-\tau_\lambda}{\mu}}\frac{d\tau_\lambda}{2H_\lambda(0)} \\ &- \int_0^1(1-\mu^2)\frac{dP_l(\mu)}{d\tau}d\mu\int_0^\infty B_\lambda(\tau)\frac{\delta\tilde{r}}{r}e^{\frac{-\tau_\lambda}{\mu}}\frac{d\tau_\lambda}{2H_\lambda(0)}\Bigg\}\end{aligned} \tag{4.66}$$

By using $\mu\frac{dI_\lambda}{d\mu} = I_\lambda - B_\lambda$ from radiative transfer equation, the above equation becomes:

$$\begin{aligned}\frac{\delta L_\lambda}{L_{\lambda(0)}} &= \frac{Y_l^m(\theta_0,\phi_0)}{2H_\lambda(0)}\int_0^1\int_0^\infty \delta\tilde{B}_\lambda(r)P_l(\mu)e^{\frac{-\tau_\lambda}{\mu}}d\tau_\lambda d\mu \\ &- \frac{Y_l^m(\theta_0,\phi_0)}{2H_\lambda(0)}\int_0^1\int_0^\infty \frac{\delta\tilde{\kappa_\lambda}}{\kappa_\lambda}P_l(\mu)e^{\frac{-\tau_\lambda}{\mu}}\mu\frac{dI_\lambda}{d\tau_\lambda}d\tau_\lambda d\mu \\ &- Y_l^m(\theta_0,\phi_0)\Bigg\{\int_0^1 \frac{(1-\mu^2)}{\mu\cdot}\frac{dP_l}{d\mu}\frac{dI_\lambda}{d\tau_\lambda}\mu d\mu\int_0^\infty \frac{\delta\tilde{r}}{r}e^{\frac{-\tau_\lambda}{\mu}}\frac{d\tau_\lambda}{2H_\lambda(0)} \\ &+ 2\int_0^1 P_l(\mu)\mu d\mu\int_0^\infty B_\lambda(\tau)\frac{\delta\tilde{r}}{r}e^{\frac{-\tau_\lambda}{\mu}}\frac{d\tau_\lambda}{2H_\lambda(0)} \\ &- \int_0^1(1-\mu^2)\frac{dP_l(\mu)}{d\tau}d\mu\int_0^\infty B_\lambda(\tau)\frac{\delta\tilde{r}}{r}e^{\frac{-\tau_\lambda}{\mu}}\frac{d\tau_\lambda}{2H_\lambda(0)}\Bigg\}.\end{aligned} \tag{4.67}$$

We can further simplify the above equation by combining the last two terms as follows:

$$\begin{aligned}\frac{\delta L_\lambda}{L_{\lambda(0)}} &= \frac{Y_l^m(\theta_0,\phi_0)}{2H_\lambda(0)}\int_0^1\int_0^\infty \delta\tilde{B}_\lambda(r)P_l(\mu)e^{\frac{-\tau_\lambda}{\mu}}d\tau_\lambda d\mu \\ &- \frac{Y_l^m(\theta_0,\phi_0)}{2H_\lambda(0)}\int_0^1\int_0^\infty \frac{\delta\tilde{\kappa_\lambda}}{\kappa_\lambda}P_l(\mu)e^{\frac{-\tau_\lambda}{\mu}}\mu\frac{dI_\lambda}{d\tau_\lambda}d\tau_\lambda d\mu \\ &- Y_l^m(\theta_0,\phi_0)\Bigg\{\int_0^1 \frac{(1-\mu^2)}{\mu}\frac{dP_l}{d\mu}\mu d\mu\int_0^\infty \frac{\delta\tilde{r}}{r}e^{\frac{-\tau_\lambda}{\mu}}\frac{d\tau_\lambda}{2H_\lambda(0)}\frac{dI_\lambda}{d\tau_\lambda} \\ &+ \int_0^\infty \frac{\delta\tilde{r}}{r}\frac{B_\lambda(\tau)}{2H_\lambda(0)}e^{\frac{-\tau_\lambda}{\mu}}d\tau_\lambda\left[\int_0^1 2P_l(\mu)\mu - \int_0^1(1-\mu^2)\frac{dP_l(\mu)}{d\mu}\right]d\mu\Bigg\}.\end{aligned} \tag{4.68}$$

Now, if we define two new functions from the last calculation $f(\mu)$ and $g(\mu)$ as:

$$f(\mu) = \int_0^\infty \frac{\delta\tilde{r}}{r}\frac{dI_\lambda}{d\tau_\lambda}e^{\frac{-\tau_\lambda}{\mu}}\frac{d\tau_\lambda}{2H_\lambda(0)}, \tag{4.69}$$

and

$$g(\mu) = \int_0^\infty \frac{\delta\tilde{r}}{r}\frac{B_\lambda}{2H_\lambda(0)}e^{\frac{-\tau_\lambda}{\mu}}d\tau_\lambda. \tag{4.70}$$

Substituting both functions defined above, back to the previous equation, eqn.(4.95), the perturbed luminosity becomes:

$$\begin{aligned}\frac{\delta L_\lambda}{L_\lambda(0)} &= \frac{Y_l^m(\theta_0,\phi_0)}{2H_\lambda(0)}\int_0^1\int_0^\infty \delta\tilde{B}_\lambda(r)P_l(\mu)e^{\frac{-\tau_\lambda}{\mu}}d\tau_\lambda d\mu \\ &- \frac{Y_l^m(\theta_0,\phi_0)}{2H_\lambda(0)}\int_0^1\int_0^\infty \frac{\delta\tilde{\kappa}_\lambda}{\kappa_\lambda}P_l(\mu)\frac{dI_\lambda}{d\tau_\lambda}e^{\frac{-\tau_\lambda}{\mu}}d\tau_\lambda\mu d\mu \\ &- \frac{Y_l^m(\theta_0,\phi_0)}{2H_\lambda(0)}\left(\int_0^1\frac{1-\mu^2}{\mu}\frac{dP_l}{d\mu}f(\mu)\mu d\mu + \left[\int_0^1 2P_l(\mu)\mu - (1-\mu^2)\frac{dP_l}{d\mu}\right]g(\mu)d\mu\right).\end{aligned} \tag{4.71}$$

For $\tau\epsilon[0,1]$, the exponential term can be expanded using Taylor expansion as:

$$e^{\frac{-\tau_\lambda}{\mu}} \simeq 1 - \frac{\tau_\lambda}{\mu} + \frac{1}{2!}\frac{\tau_\lambda^2}{\mu^2} - \frac{1}{3!}\frac{\tau_\lambda^3}{\mu^3} + \frac{1}{4!}\frac{\tau_\lambda^4}{\mu^4} + ... \tag{4.72}$$

Using the above Taylor expansion and only considering first order terms, the two functions defined earlier becomes:

$$f(\mu) = \int_0^\infty \frac{\delta\tilde{r}}{r}\frac{dI_\lambda}{d\tau_\lambda}(1-\frac{\tau_\lambda}{\mu})\frac{d\tau_\lambda}{2H_\lambda(0)}, \tag{4.73}$$

and the second function reduces to:

$$g(\mu) = \int_0^\infty \frac{\delta\tilde{r}}{r}\frac{B_\lambda}{2H_\lambda(0)}(1-\frac{\tau_\lambda}{\mu})d\tau_\lambda, \tag{4.74}$$

Substituting these back to the original equation shown above, the observed variation in luminosity for pulsating stars becomes:

$$\begin{aligned}\frac{\delta L}{L_\lambda(0)} &= \frac{Y_l^m(\theta_0,\phi_0)}{2H_\lambda(0)}\int_0^1\int_0^\infty \delta\tilde{B}_\lambda(r)P_l(\mu)\Big(1-\frac{\tau_\lambda}{\mu}\Big)d\tau_\lambda d\mu \\ &- \frac{Y_l^m(\theta_0,\phi_0)}{2H_\lambda(0)}\int_0^1\int_0^\infty \frac{\delta\tilde{\kappa}_\lambda}{\kappa_\lambda}P_l(\mu)\Big(1-\frac{\tau_\lambda}{\mu}\Big)\frac{dI_\lambda}{d\tau_\lambda}d\tau_\lambda\mu d\mu \\ &- \frac{Y_l^m(\theta_0,\phi_0)}{2H_\lambda(0)}\left\{\int_0^1\frac{1-\mu^2}{\mu}\frac{dP_l}{d\mu}f(\mu)\mu d\mu + \left[\int_0^1 2P_l(\mu)\mu - (1-\mu^2)\frac{dP_l}{d\mu}\right]g(\mu)d\mu\right\}.\end{aligned} \tag{4.75}$$

For radially oscillating stars where $l = 1$, the geometric term (the term in the square bracket)

in the above equation, the variation in the surface normal vanishes as Watson, ( ) and Watson, ( ) shows. The final equation for observed luminosity is given above where it shows all the variations during non radial pulsation including the variation in the surface normal, where this term vanishes for radial pulsation, variation in the surface area and temperature. More over the two functions, $f(\mu)$ and $g(\mu)$ are as defined before. Both functions show the integral over the displacement eigen function, where it was assumed constant during Watson, ( ) and Watson, ( ) publications. Moreover, the two functions demonstrates how the displacement eigen function $\frac{\delta\vec{r}}{r}$ behaves and varies in the atmosphere of a pulsating star. In previous works, as mentioned before, the displacement eigen function was treated as constant and their calculations were based at a particular point in the atmosphere with a value of $\tau = 2/3$. Both $f(\mu)$ and $g(\mu)$ are integrals of the displacement eigen function with respect to optical depth. This variation in the displacement eigen function for different equilibrium models of variable stars is presented in the upcoming chapter. Moreover, the two integrals demonstrates the integrals of intensity with respect to optical depth as well as how B_λ (Planck function) and H_λ (surface Eddington flux) behave with respect to optical depth.

If one compares Watson's equations introduced in chapter 3 term by term with our calculations, one can see that the contribution of the geometrical effect (T_3) will be ignored for $l = 1$ in (Watson,) case. But the effect of geometry in contributing for the observed flux should be significant as it is known that during pulsation, the shape of the star change which in turn affects the observed flux. Moreover, the derivation of the mode identification formula is done by considering the atmosphere of the star as a distinct individual layer and calculated at a particular optical depth $\tau = \frac{2}{3}$. But in our calculation, we treated the atmosphere of the star as multilayered so as to treat as a whole by varying the integral of the optical depth from the surface to deep inside the star, to include the effect of the atmosphere by varying the integral of the optical depth from 0 to ∞. The variation in the observed flux can be caused by any physical changes occurring inside the atmosphere of the star. Not at a particular point as suggested by (Watson,).

Chapter 5

Results and Discussion

The derivations we did in chapter 4 is an improved photometric mode identification formula for pulsating stars derived from the combination of radiative transfer equation and the radiative flux emanating from pulsating stars. The formalism introduced is based on non-grey approximation where the pulsation equations and opacity depends on the depth and frequency of observation. Moreover, in the new formalism introduced in this thesis, the effects of local temperature, geometry, pressure, surface normal and limb darkening effects are included, where they contribute to the variation in the observed flux.

Some of the parameters in our calculations such as $\frac{\delta T}{T}$, $\frac{\delta P}{P}$ are obtained from pulsation code obtained from Medupe, Christensen-Dalsgaard, and Phorah, ( ). In addition, by using an equilibrium model as an input I_ν, B_ν, τ_ν, it is easy to get the opacity table $\kappa_\nu(T, P, \nu)$ using model atmosphere ATLAS9 where (Kurucz and Bell,) included convection based on the mixing length theory (MLT). In this approximation, he used the mixing length parameter $l/H_p = 1.25$.

Hence by using the model stellar atmosphere, opacity tables were constructed. Moreover, by using the outputs (the opacity tables) the following three dimensional opacity contours of $\log P$, $\log T$ and κ_ν are plotted.

The three dimensional plots ($logP, logT, \kappa_\nu$) shown in figures 5.1 to 5.6 show two humps which are caused by hydrogen ionization. The opacity contours shows an opacity bump for frequency and wavelength of 1.216×10^5 and 2.46×10^2 respectively. Moreover, the second raw also shows ($logP, logT$, $opacity$ (κ_ν)) for $f = 397549 \times 10^{14}$ and $\lambda = 3.57 \times 10^2$. In this particular plot, it is easy to note that the bump is due to hydrogen ionization where the region of the star both temperature and pressure are high leading to high opacity.

In addition, all the figures show the opacity (κ_ν), $\log P$ and $\log T$ three dimensional plots where the bump shows hydrogen ionization zone. Parameters from our calculations such as $\alpha_T(\lambda)$, $\alpha_g(\lambda)$ and $p^* = (\frac{\partial \log g}{\partial \log P_g})_{\tau=1}$ are obtained from model atmospheres using ATLAS9.

The fundamental differences we introduced in this study is the derivation of photometric amplitude in a plane parallel atmosphere where the derivation is based from perturbation of radiative transfer where we got the flux perturbation. In addition, the variation in luminosity includes the derived variation in the surface normal and in area by considering a spherical, hydrostatic equilibrium star.

Researches in the derivation of the flux variation $(\frac{\Delta F_\nu}{F_\nu})$ was done by Toutain and Gouttebroze, ( ) with an assumption of a star with radius R_0 where their integral, mostly for a rotating star (the Sun), to obtain the observed flux across the disk. In their calculation, they included the radiative transfer equation in the photosphere of the sun and the opacity perturbation as a result of non radial pulsation. Toutain, Berthomieu, and Provost, ( ) tried to improve the formalism and calculated and derived analytical equation for the amplitudes of non radial pulsation by considering the photosphere as a sphere. They calculated the intensity perturbation by using both Eulerian and Lagrangian formalism (for the Sun) for low degree p and g solar modes. Both Lagrangian and

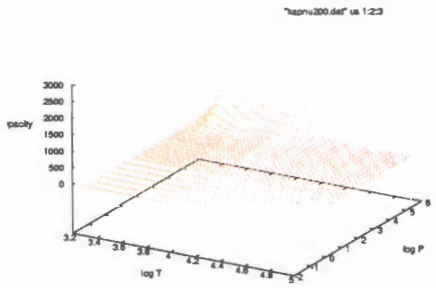

FIGURE 5.1: Three dimensional contour showing how opacity behaves inside a star, where the two bumps demonstrate the hydrogen ionization zone.

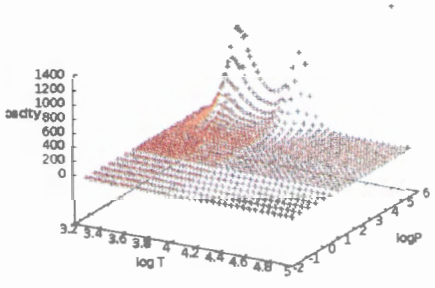

FIGURE 5.2: Opacity contour demonstrating how opacity behaves inside a star. The two bumps around log T=3.6-log T=3.8 and log P=4-log P=5shows regions inside the star where hydrogen ionizes and large variation in opacity is observed

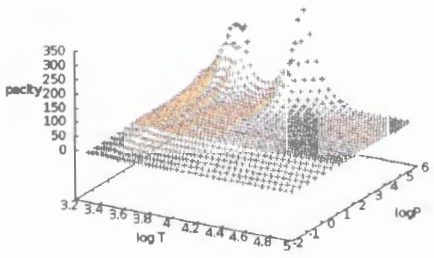

FIGURE 5.3: Three dimensional contour showing how opacity behaves inside a star. The two humps show region of a star where hydrogen ionization dominates.

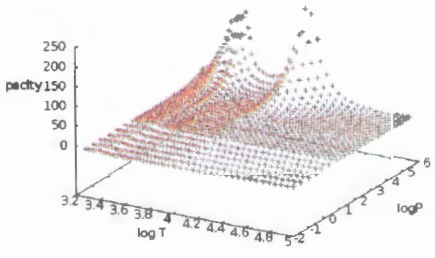

FIGURE 5.4: Opacity contour demonstrating how opacity behaves inside a star.The humps in the plot shows the how hydrogen ionization affects opacity.

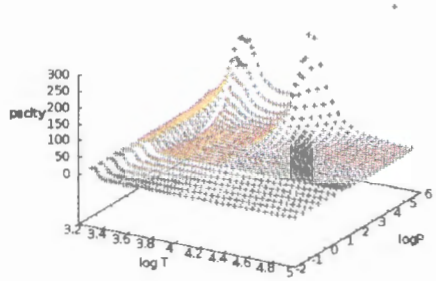

FIGURE 5.5: Three dimensional contour showing how opacity behaves inside a star, where the humps shows hydrogen ionization zone.

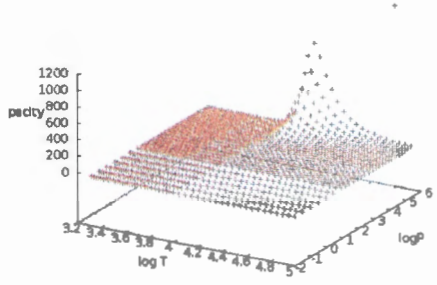

FIGURE 5.6: Opacity contour demonstrating how opacity behaves inside a star.The sharp rise in opacity is shown in the figure where hydrogen ionizes.

Eulerian expressions for plane parallel approximation give rise to the same value and obtained the same outputs as previous works. In addition, Toutain, Berthomieu, and Provost, (1999) checked both formalisms numerically. But for numerical calculation it came out that the Lagrangian formalism is more suited than the Eulerian form due to the fact that convection is ignored in this form. Moreover, their analytical expression is derived based on grey atmosphere assumption. Toutain, Berthomieu, and Provost, (1999) also compared their analytical equation flux perturbation and intensity for non radial pulsation both in the spherical and plane parallel assumptions. During their analytical calculation, they treated the atmosphere as a layer and integrated over the visible disc. Since its inception, calculation of flux variation due to non radial pulsation, a lot of progress has been made and our contribution in this regard will play fundamental role in progressing mode identification and studying the internal structure of the stars. In this study, we introduced and treated the atmosphere of the star as a continuous state and integrated from outside to deep into the core which is completely different from the analysis presented by Watson, (1987) and Watson, (1988)'s treatment as a single layer and calculated at an optical depth of $\tau = 2/3$.

The quantity in our photometric amplitude calculation $(I_\lambda - B_\lambda)$ has a value of zero for isothermal atmosphere $(\tau > 2/3)$ whereas it is non zero near the surface of the star. Our photometric amplitude, calculated by assuming plane parallel atmosphere, shows the contribution from the different layers of the atmosphere (from inside to outside of the atmosphere) which is different from Watson, (1987) and Watson, (1988), where he calculated the atmosphere as a single layer. The calculation we did showed an integration over the optical depth from 0 to ∞ which is completely different from the understanding presented by different authors. Their calculation is not wrong but valid only for low frequency oscillating stars. The equation that we introduced, as the new photometric amplitude, which helps us to use as a mode identification formula, incorporates almost all the ingredients that contribute to the variation in the observed luminosity (intensity). Those parameters are briefly discussed and their analytic formalism are extensively derived in chapter 4. Watson, (1987) and Watson, (1988) formalism introduced limb darkening by writing normalized limb darkening in a quadratic form where as the equation we introduced here assumes the limb darkening introduced in the variation in the surface normal. Moreover, his formula is solely calculated on the basis of intensities formulated from a boundary condition (at optical depth $\tau = \frac{2}{3}$)

defined at the photosphere. In addition, the atmosphere is treated as a single layer, by assuming the eigen function as constant.

When a pulsating star is observed, there is a manifestation of changes in brightness. The observed brightness changes are caused due to changes from geometric effects (distortion in the surface area, for non radial pulsation, variation in the surface normal). Other changes that causes variation in brightness are thermodynamical changes which are associated with optical depth perturbations and $(I_\lambda - B_\lambda)$. Hence, our calculations are developed by taking into account the variations or changes mentioned. As discussed above, Watson, ( ) and Watson, ( ) developed his equations assuming that the atmosphere as a single layer which implies there is no integration over the optical depth and displacement eigen function $\frac{\delta\tilde{r}}{r}$. He also assumed constant eigen functions in the stellar atmosphere but the displacement eigen function is not constant and the luminosity observed comes from all layers of the atmosphere of a pulsating star where the outer layer contribution is dominant during pulsation. Therefore, to include and show the non constant shape eigen function, we assumed a plane parallel atmosphere, where the solution for the radiative transfer equation is given by:

$$I_\lambda(\mu, \tau_\lambda = 0) = \int_0^\infty B_\lambda(\tau_\lambda) e^{\frac{-\tau_\lambda}{\mu}} \frac{d\tau_\lambda}{\mu}. \tag{5.1}$$

In our calculation of photometric mode identification formula, one can easily see that for a given stellar model, the observed luminosity variation caused by stellar pulsation is caused by temperature perturbation, perturbation in opacity, displacement eigen function and departure from thermodynamical (radiative) equilibrium $(I_\lambda - B_\lambda)$.

5.1 Analysis of the Theoretical equation using Equilibrium Models

The photometric mode identification formula introduced in chapter 4 is given below:

$$\begin{aligned}\frac{\delta L}{L_\lambda(0)} = & \frac{Y_l^m(\theta_0,\phi_0)}{2H_\lambda(0)} \int_0^1 \int_0^\infty \delta\tilde{B}_\lambda(r) P_l(\mu)\Big(1 - \frac{\tau_\lambda}{\mu}\Big) d\tau_\lambda d\mu \\ & - \frac{Y_l^m(\theta_0,\phi_0)}{2H_\lambda(0)} \int_0^1 \int_0^\infty \frac{\delta\tilde{\kappa}_\lambda}{\kappa_\lambda} P_l(\mu)\Big(1 - \frac{\tau_\lambda}{\mu}\Big) \frac{dI_\lambda}{d\tau_\lambda} d\tau_\lambda \mu d\mu \\ & - \frac{Y_l^m(\theta_0,\phi_0)}{2H_\lambda(0)} \left\{ \int_0^1 \frac{1-\mu^2}{\mu} \frac{dP_l}{d\mu} f(\mu) \mu d\mu + \left[\int_0^1 2P_l(\mu)\mu - (1-\mu^2)\frac{dP_l}{d\mu} \right] g(\mu) d\mu \right\}.\end{aligned} \tag{5.2}$$

where,

$$f(\mu) = \int_0^\infty \frac{\delta\tilde{r}}{r} \frac{dI_\lambda}{d\tau_\lambda} (1 - \frac{\tau_\lambda}{\mu}) \frac{d\tau_\lambda}{2H_\lambda(0)} \tag{5.3}$$

and

$$g(\mu) = \int_0^\infty \frac{\delta\tilde{r}}{r} \frac{B_\lambda}{2H_\lambda(0)} (1 - \frac{\tau_\lambda}{\mu}) d\tau_\lambda. \tag{5.4}$$

Where $P_{l=0} = 1$ therefore $\frac{dP_{l=0}}{d\mu} = 0$.

For a radially pulsating star, the variation in the surface normal becomes zero as there is no change in the direction of the surface normal, refer to the fourth term in eqn. (5.2). To demonstrate how this equation works, we studied equilibrium stellar models and their atmosphere and analyze the properties of the eigen functions (Pressure, temperature, opacity and displacement eigen functions). The following table shows the equilibrium stellar models used in this analysis. We implemented a FORTRAN code called *naledi* introduced by Medupe, Christensen-Dalsgaard, and Kurtz, ( ) and Medupe, Christensen-Dalsgaard, and Phorah, ( ) to check the improved mode identification formula using the following equilibrium models.

TABLE 5.1: Equilibrium models used in this study Medupe, Christensen-Dalsgaard, and Kurtz, ( ) and Medupe, Christensen-Dalsgaard, and Phorah, ( ).

Model No.	T_{eff}	log g
1	5778	4.43
2	6164	4.41
3	6430	4.35
4	7072	4.29
5	7512	4.30
6	7900	4.30
7	8340	4.31
8	9088	4.32
9	9440	4.32

The table above shows the stellar equilibrium models with the respective T_{eff}, frequency of pulsation ranging between $n = 1$ and $n = 30$ with a step of 3 and $log\, g$. The values of $log\, g$ presented in the table are obtained from our model atmosphere calculations. These models are typically A-type variable stars. Their effective temperature ranges between $6000 - 11,500$K, where in our model atmosphere the effective temperatures are chosen in such a way that they cover the temperature range of A-type stars. This work is to study their atmosphere and pulsation based on Medupe, Christensen-Dalsgaard, and Phorah, ( ).

Here, we treat the models by introducing a new formula where its derivation is shown in chapter 4. The analysis here shows the variation in the temperature eigen function, displacement eigen function, opacity, temperature, pressure and displacement $(\frac{r}{R})$ in the variable star.

Medupe, Christensen-Dalsgaard, and Phorah, ( ) presented a theoretical equation that relates perturbation in the surface flux, opacity and temperature. The theoretical analysis presented here uses a FORTRAN program called $naledi.f$ using $ifort$ compiler, where the program takes all equilibrium models and gives iterated values for acoustic cutoff frequency. When one compiles $naledi.f$, it gives several options to load equilibrium models, do iterations, create eigen frequency spectrum and more. But for this particular work, we load the equilibrium models followed by doing iterations by giving range of frequencies manually. Since the solutions for pulsation equations are complex, we provided both (real and complex parts of the solution) to the program. But in this work we focused and presented the real part of the solution. Moreover, the program gives the freedom to calculate the damping rate for several frequencies, but in this work we did not give emphasis on damping. $naledi.f$ also provides an option to calculate the eigen values and eigen frequencies and create eigen value spectrum. In this process, we demonstrated how the temperature eigen function $\frac{\delta T}{T}$, the displacement eigen function $\frac{\delta \vec{r}}{r}$, opacity eigen function and other physical

parameters vary in the star especially in the atmosphere. In the upcoming sections, we demonstrate the outputs of $naledi.f$.

5.1.1 Eigen Values and Eigen Functions

Eigen frequencies are natural vibrations or frequencies where stars normally pulsate. The solution to pulsation equations for grey atmosphere is complex where it has real and imaginary solutions. The following are some of the real solutions plotted with respect to depth ($logP$), optical depth τ and other physical parameters which can significantly vary throughout the star, especially the atmosphere of the star. In most calculations and plots, one can see that the Eigen solutions are higher in the atmosphere of a pulsating star and becomes smaller as one traces deep into the core of the star. The models in this study are based on studying their atmosphere and envelope; the point where the two meet is known to be the matching point. The interference of the waves that we mentioned earlier is caused due to the medium change in the star (atmosphere/ envelope). Here, the atmosphere is treated as purely radiative and constructed from several layers, where energy transport is dominated by radiation and the focus is to solve radiative transfer equations by considering different assumptions as solved in chapter 4.

5.1.2 Equilibrium Model with T_{eff} = 5778 K and log g = 4.43

The equilibrium model with T_{eff} = 5778 is tested for various pulsation frequencies ranging from $n = 1 - 30$, where the frequency range is A-type stars pulsate. The solution to the pulsation equation gives both real and imaginary solutions where in this analysis we focus on the real solutions. The imaginary solutions shows that the displacement gets smaller and smaller or higher and introduces damping and phase difference but it is not our interest here.

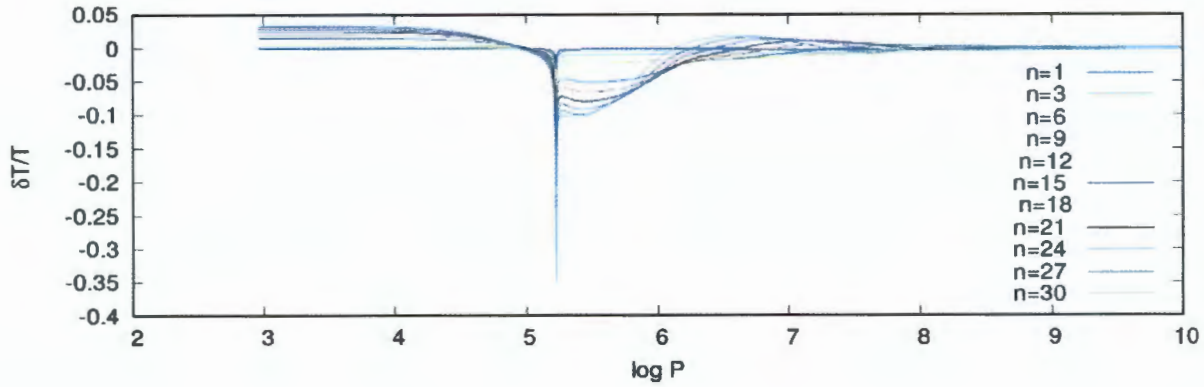

FIGURE 5.7: The real part of temperature eigen function with respect to depth $(logP)$.

The temperature eigen function is shown in Fig. 5.7. The eigen functions shows variations in the atmosphere of the star where hydrogen ionization dominates in a region between $log\, P = 5$ and $log\, P = 6$. The temperature eigen function $\frac{\delta T}{T}$ as shown here demonstrates great variability for different n values, where n is associated with frequency; especially those equilibrium models with high frequency shows tremendous variability close to the surface. It is easy to notice from Fig. that $\frac{\delta T}{T}$ shows variation up to $log\, P = 8$. But as one traces deep in the star, the temperature eigen function becomes constant. All frequency models have constant temperature eigen function close to the surface but dramatically changes around the hydrogen ionization zone.

Fig. demonstrates the real part of the temperature eigen function as a function of optical depth τ. The temperature eigen function $(\frac{\delta T}{T})$ shows great variability in the atmosphere; even going deep in the star it shows variability. Near the surface of the star $\frac{\delta T}{T}$ remains constant but as one traces in the atmosphere, $\frac{\delta T}{T}$ shows variation for all the models. These variations continue through the atmosphere of the star. Deep in the star, on the other hand, $\frac{\delta T}{T}$ becomes constant for all models.

The variation in the displacement eigen function shown in Fig. 5.9 shows great variability in the atmosphere and becomes maximum $(\frac{\delta r}{r} = 1)$ near the surface of the star for all n values. The position where variation in the displacement eigen function corresponds to the position where variation of temperature eigen function occurs. Various frequencies shows significantly different displacement eigen functions in the atmosphere of the star. The positions correspondence between the temperature eigen function and displacement eigen function shows that the displacement eigen function responds very well to the effect of the temperature eigen function. Low frequency eigen functions are nearly constant in the atmosphere. $\frac{\delta r}{r}$ with respect to depth $(log\, P)$ between $log\, P =$

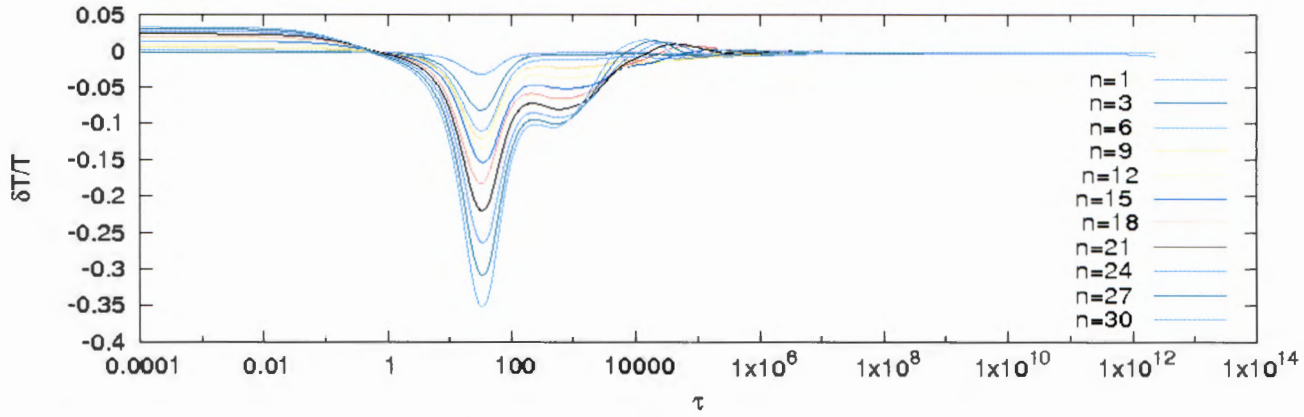

FIGURE 5.8: The real part of temperature eigen function with respect to optical depth τ.

6 and $log\, P = 8$ show great variability. Deep in the star $\frac{\delta r}{r}$ becomes constant except $n = 1$ and $n = 3$.

Another quantity that we studied using this model is the properties of the displacement eigen function as a function of optical depth τ shown in Fig. 5.10. Near the surface, the displacement eigen function becomes maximum with a value of 1 regardless of the frequency used in the equilibrium model. Those with lower values of n appears to have constant $\frac{\delta r}{r}$ deep in the star whereas the equilibrium models with higher values of n show variation across τ. Near the surface, those with high values of $n = 21 - 30$ show sharp decrement in the displacement eigen function as compared to lower n-values ($n = 1 - 9$).

More analysis is done in this model with regard to opacity variation. The variation in the opacity eigen function is shown in Fig. 5.11. Lower frequency models shows that the opacity eigen function is constant near the surface of the star whereas those with high frequency demonstrates that the opacity eigen function increases from the surface to the atmosphere and vary greatly in the hydrogen ionization zone, where the cause for opacity fluctuation occurs. It is also easy to notice form the figure that the dip in the perturbation of opacity varies with frequency. Moreover, some samples with high frequency also shows variation even near the surface and shows some bumps in the atmosphere of the star. These small bumps are visible between $log\, P = 3$ and $log\, P = 4$. Furthermore, the variation in $\frac{\delta \kappa}{\kappa}$ continues even deeper between $log\, P = 6$ and $log\, P = 7$. Deep in the star $\frac{\delta \kappa}{\kappa}$ becomes constant for all values of n.

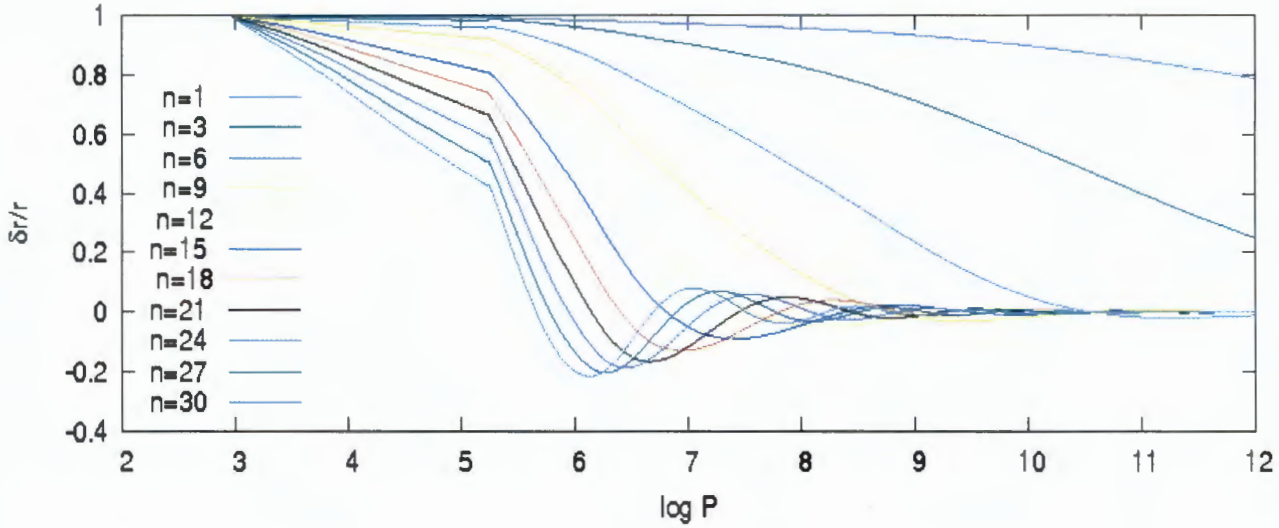

FIGURE 5.9: The real part of the displacement eigen function with respect to depth ($logP$).

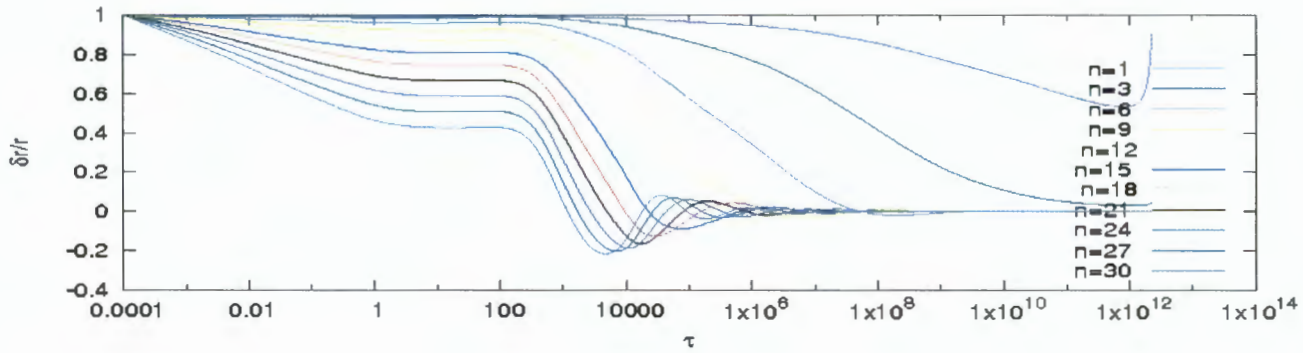

FIGURE 5.10: The displacement eigen function as a function of τ (optical depth).

5.1.3 Equilibrium Model with T_{eff} = 6164 K and log g = 4.41

As we did in the previous equilibrium model, $T_{eff} = 5778$ K, the test was done for a range of frequencies similar to the ones presented earlier. From the temperature eigen function with respect to depth ($log\ P$), one can see that the higher the frequency the more the perturbation in the temperature eigen function. Moreover, as compared to the previous equilibrium model, $T_{eff} = 5778$ K, the dip in the perturbation moves towards the surface. The effect of the perturbation is happening in the first hydrogen ionization zone. A close observation, close to $log\ P = 5$ in the plot shows that the high frequency pulsation causes a greater dip in the first hydrogen ionization zone as shown in Fig. and the variation continues up to $log\ P = 7$.

From Fig. , it is easy to note that all models show constancy of temperature eigen function near the surface.

The temperature eigen function ($\frac{\delta T}{T}$) is also studied as a function of optical depth. In a similar

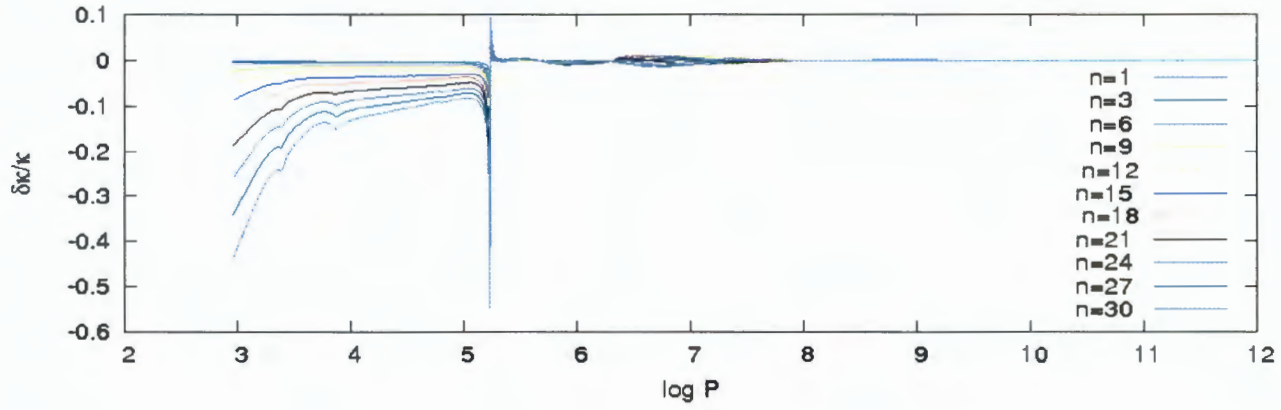

FIGURE 5.11: The real part of the variations in opacity with respect to depth

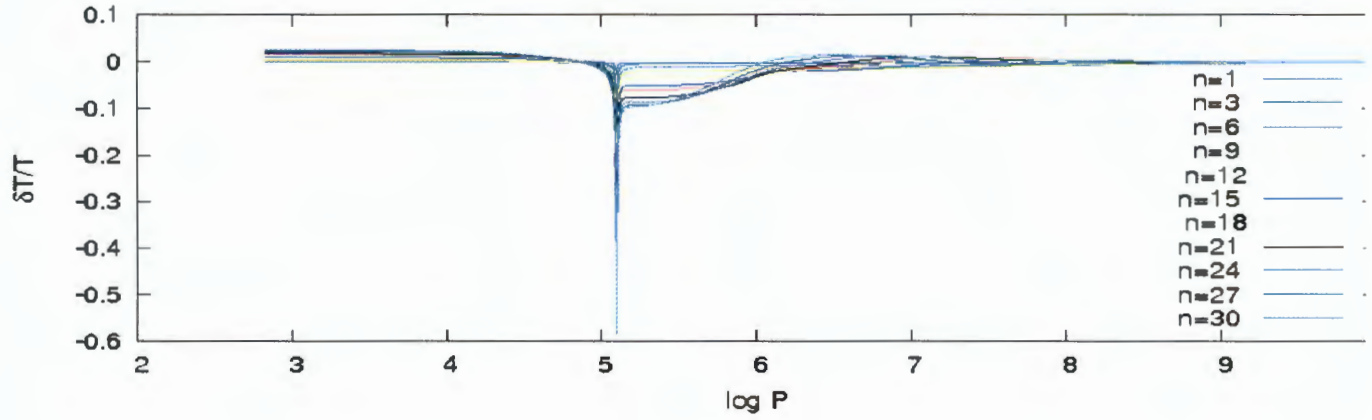

FIGURE 5.12: The real part of the temperature eigen function as a function of depth.

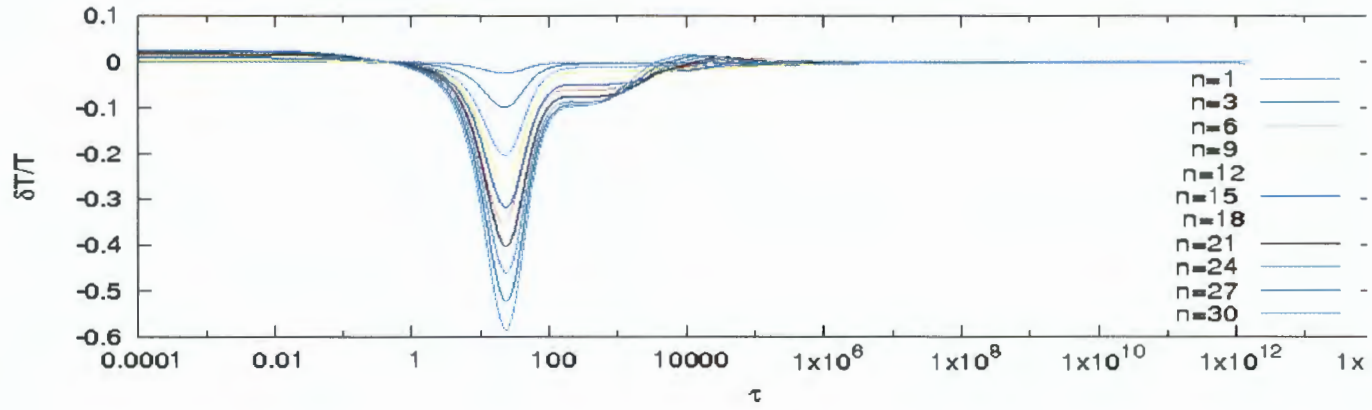

FIGURE 5.13: The real part of the temperature eigen function as a function of optical depth τ.

way as before, the temperature eigen function demonstrates variability in the atmosphere. In addition, one can see from Fig. 5.13 that the variability moves toward the surface as compared to the lower temperature model T_{eff} = 5778. All models near the surface have constant $\frac{\delta T}{T}$.

The displacement eigen function, on the other hand, has a slight variation in the hydrogen ionization zone where its variation is observed in the area where temperature eigen function also varies. It also shows that the displacement eigen function reacts quickly to most frequency ranges presented in the hydrogen ionization zone except the lowest frequency. The displacement eigen function as a function of depth is presented in Fig. 5.14. The displacement eigen function for smaller n value ($n = 1$) is constant up to $log\ P = 7$. If one traces deep in the star the displacement eigen function for $n = 1$ shows slight deviation.

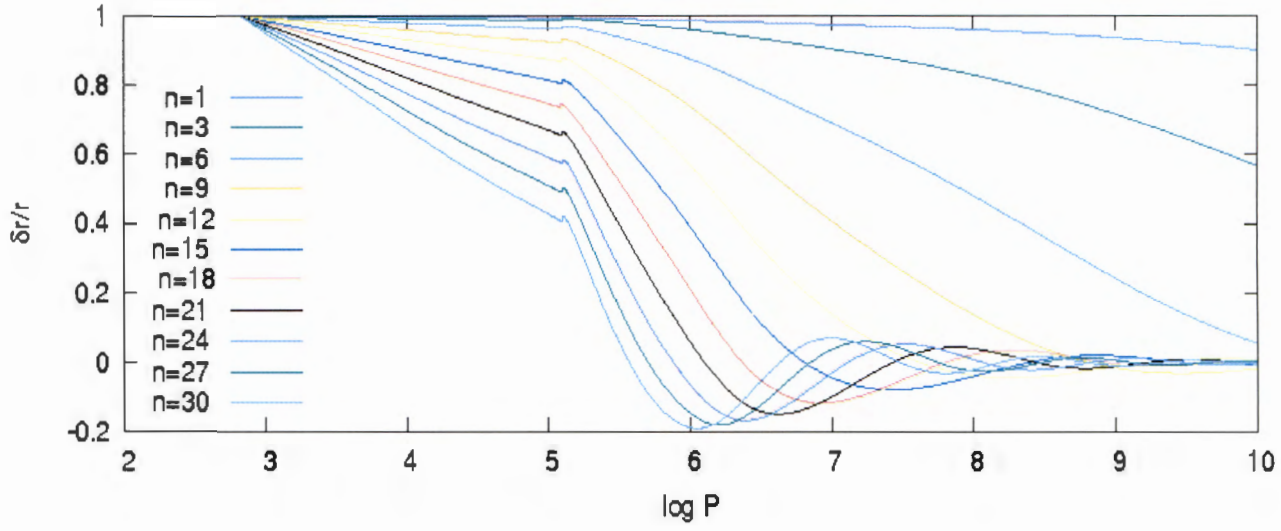

FIGURE 5.14: The displacement eigen function as a function of ($log\ P$) depth.

Analysis in the variation in the displacement eigen function $\frac{\delta r}{r}$ with respect to optical depth (τ) appears to be constant for small n values or lower frequencies as shown in Fig. 5.15. $\frac{\delta r}{r}$ attains its maximum value of 1 at $\tau = 0$ as shown in fig. 5.15 regardless of the frequency used. Those with high frequency shows variation as one goes deep in the star with the highest value of $n = 30$ shows a larger negative slope.

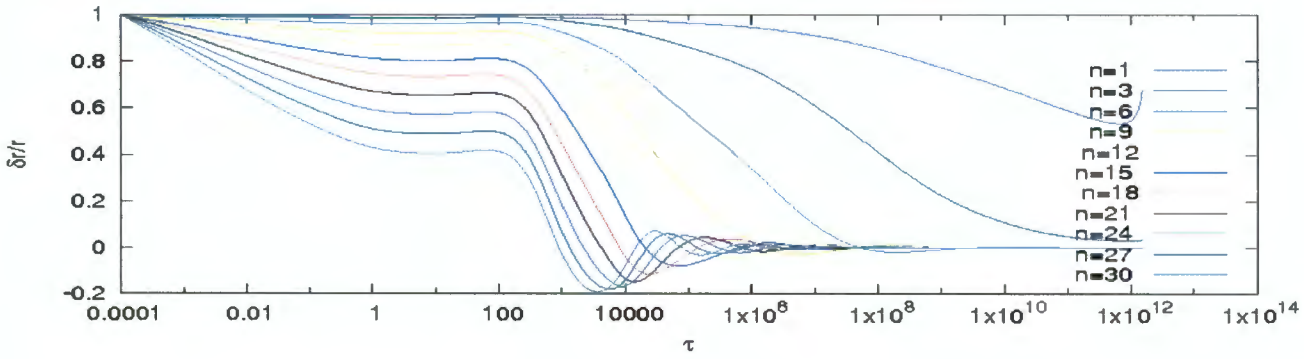

FIGURE 5.15: The displacement eigen function as a function of optical depth τ.

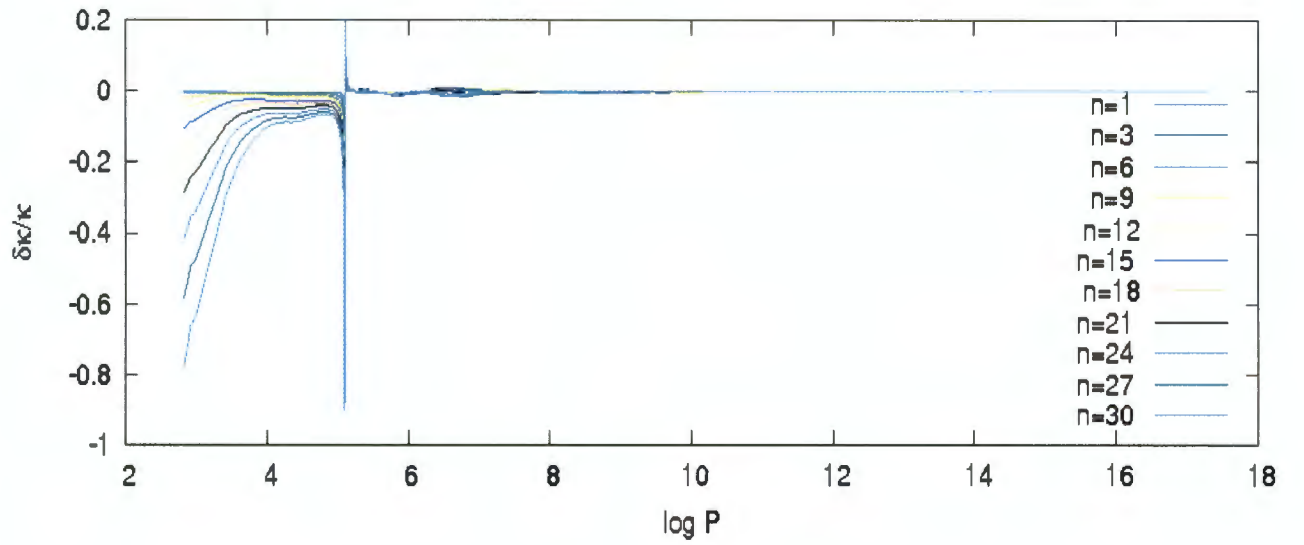

FIGURE 5.16: The opacity eigen function as a function of depth.

From fig. 5.16, it can be seen that the variation in the eigen function of opacity as a function of depth and its variation is clear in the first hydrogen ionization zone in the atmosphere of the star. It is also noticeable that the equilibrium model with higher frequency significantly shows variation and greater dip. On the other hand, the lower frequency models shows a slight dip or variation but still their change or variation discards the premise suggested by Watson, (1987) and Watson, (1988). Higher n values show sharp increase with slight humps in the atmosphere and great variability in the atmosphere. Moreover, deeper in the star though very small there is still variation in $\frac{\delta\kappa}{\kappa}$ around $logP = 6.3$. Deep in the star the opacity eigen function becomes constant.

One can also see that the position where the variation in $\frac{\delta\kappa}{\kappa}$ occurs moves closer to the surface as compared to the lower temperature model ($T_{\text{eff}} = 5778$K) presented in the previous section.

5.1.4 Equilibrium Model with T_{eff} = 6430 K and log g = 4.35

For the equilibrium model with $T_{\text{eff}} = 6430$K, the same analysis was done as before. The temperature eigen function have larger or bigger depth as compared to the lower temperature models. Moreover, the dip in the hydrogen ionization zone moves to the left, that is towards the surface of the star. For different frequencies, the temperature eigen function as shown in Fig. 5.17 behaves differently with the higher frequencies with a larger dip, at $log\ P = 5$, as compared to the lower frequency ones. Near the surface of the star, all frequency models, display constant temperature eigen function. All frequency models shows great variability in the temperature eigen function between $log\ P = 5$ and $log\ P = 7$. Moreover, the temperature eigen function shows disparity when one traces deep in the star up to a region where $log\ P = 7$. Deep in the star, the temperature eigen function becomes constant. This manifests that the temperature eigen function is affected mostly in the atmosphere of the star.

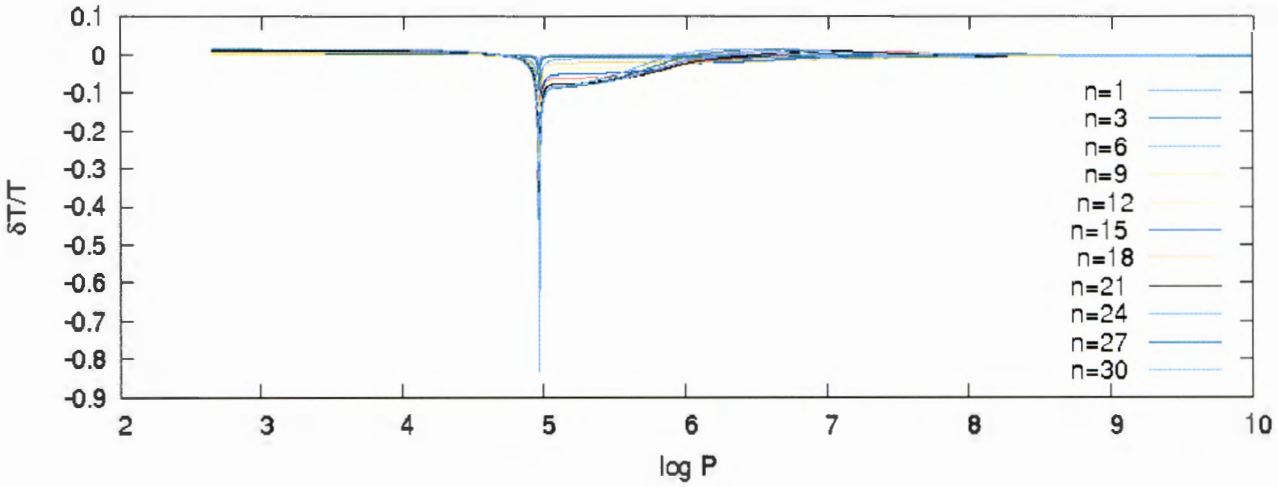

FIGURE 5.17: The temperature eigen function as a function of depth ($log\ P$).

The temperature eigen function is also studied on how it behaves with respect to optical depth and is presented in Fig. 5.18. From the figure, one can see the behavior of the temperature eigen function from two positions. The first position is near the surface of the star, where all models show no variability in $\frac{\delta T}{T}$ and the other one is in the atmosphere of the star, in the region between $log\ P = 4.7$ and $log P = 7.5$, where greater variability is observed. For lower n values $\frac{\delta T}{T}$ shows a very small variation in the first hydrogen ionization zone but deep in the star it becomes constant. It is clear that the place where variability in $\frac{\delta T}{T}$ dominates move towards the surface as compared to the lower temperature models $T_{\text{eff}} = 5778$ K and $T_{\text{eff}} = 6164$ K.

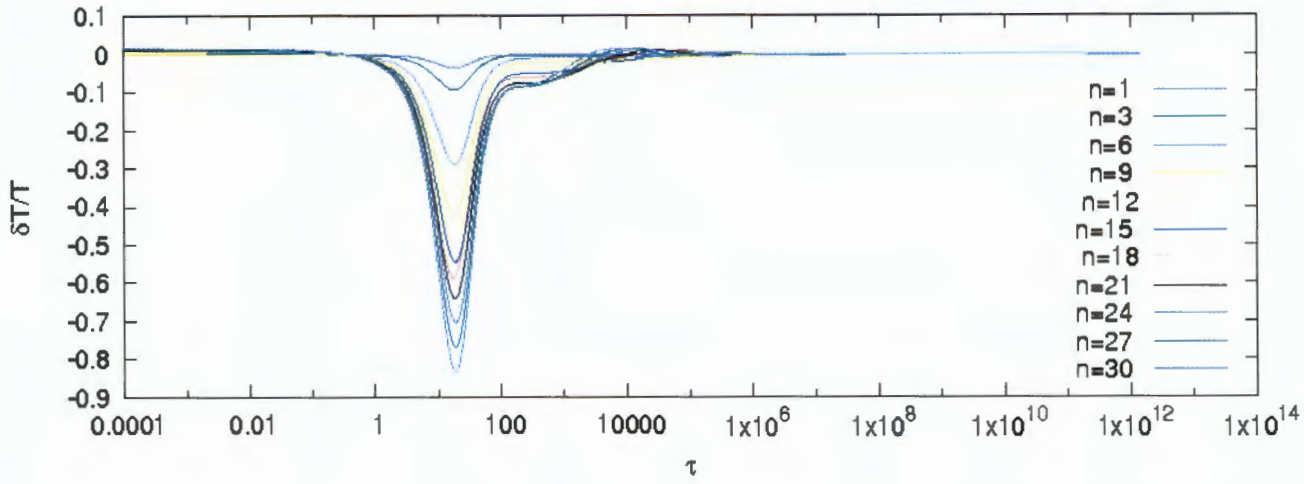

FIGURE 5.18: The temperature eigen function as a function of optical depth (τ).

The same can be said regarding the displacement eigen function as compared to the other models considered. The higher frequency models have high gradient as compared to the lower frequency models. The displacement eigen function picks the maximum value near the surface of the star regardless of frequency used as clearly seen in Fig. 5.19. For $n = 1$, $\frac{\delta r}{r}$ shows constancy up to $log\ P = 7$ then deep in the star, $\frac{\delta r}{r}$ shows slight deviation. The significant variation in $\frac{\delta r}{r}$ is observed for all the models considered starting from $log\ P = 5$. At $log\ P = 5$, $\frac{\delta r}{r}$ behaves uniquely due to hydrogen ionization. Moreover, in the region between $log\ P = 5$ and $log\ P = 8$ significant variations in $\frac{\delta r}{r}$ is observed. As in the previous models, T_{eff} = 5778 K and T_{eff} = 6164 K, deep in the star $\frac{\delta r}{r}$ becomes constant except for the first three lower n values.

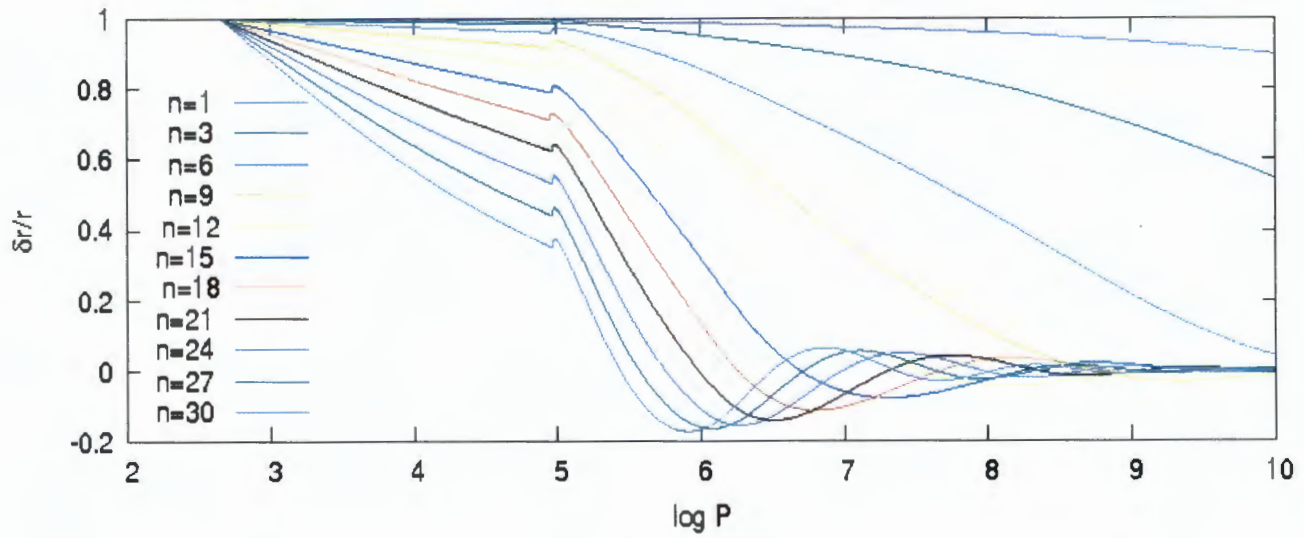

FIGURE 5.19: The displacement eigen function as a function of depth.

We also investigated the displacement eigen function $\frac{\delta r}{r}$ as a function of optical depth to study

how the displacement eigen function behaves inside the star. As presented in Fig. 5.20, $\frac{\delta r}{r}$ looks constant for equilibrium models with lower frequency up to a certain region but it behaves differently deep in the star (purple line in the plot). The displacement eigen function has a maximum value near the surface. The higher frequency models, on the other hand, show deviation from constancy. The high frequency model $n = 30$ deviates the most from constancy across the optical depth. Fig. 5.20 also shows the highest value of $\frac{\delta r}{r} = 1$ near the surface of the star.

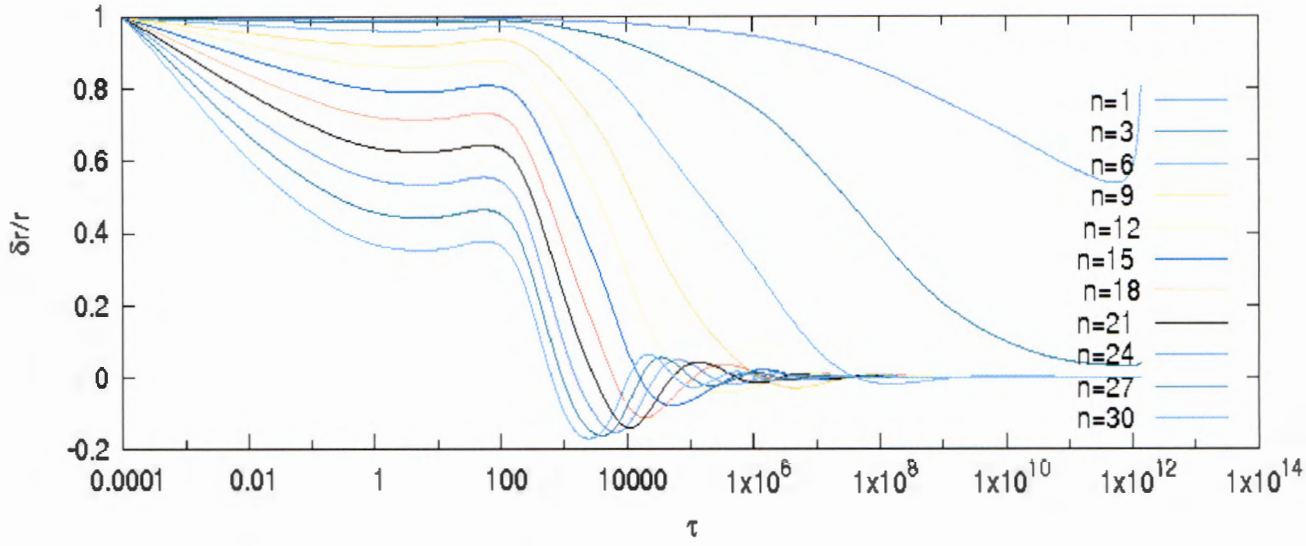

FIGURE 5.20: The displacement eigen function as a function of optical depth.

The variation in opacity eigen function in this particular model is different from the previous models, e.g. $T_{eff} = 6430$K, considered except the dip in the perturbation is higher for this model as compared to the lower temperature models. The implication is that the higher the effective temperature the higher the temperature eigen function ($\frac{\delta T}{T}$) to respond for perturbation in the atmosphere of the star as shown in Fig 5.21. Around $logP = 6$, there is also a small variation in $\frac{\delta r}{r}$ that might be caused by second hydrogen ionization zone. Deep in the star, $\frac{\delta \kappa}{\kappa}$ becomes constant for all n values. One can also see that the position where significant variability in $\frac{\delta \kappa}{\kappa}$ observed moves towards the surface.

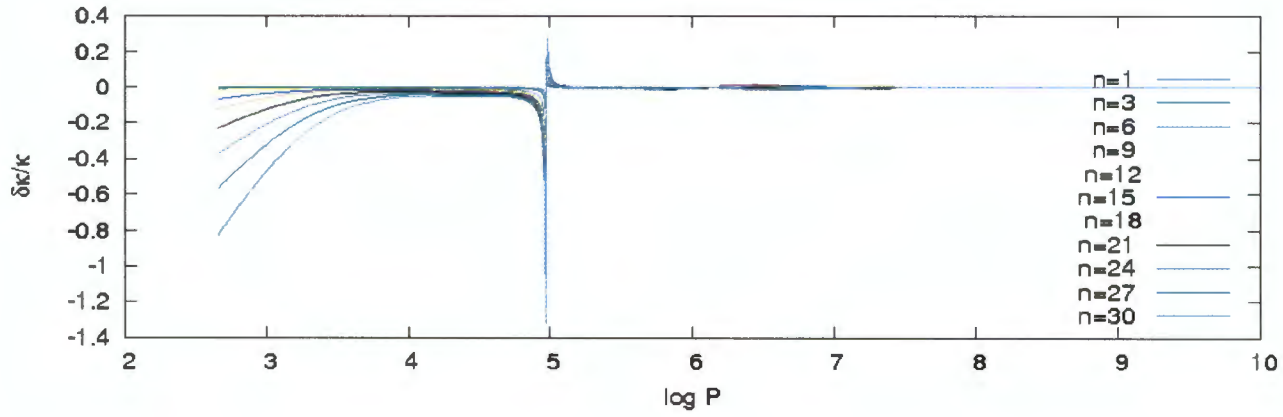

FIGURE 5.21: Variation in opacity $\frac{\delta\kappa}{\kappa}$ as a function of depth.

5.1.5 Equilibrium Model with T_{eff} = 7072 K and log g = 4.292

As discussed in the previous equilibrium model stars (T_{eff} = 5778 K, T_{eff} = 6164 K and T_{eff} = 6430 K), the temperature eigen function with respect to $log\ P$ (referring to depth) is depicted in Fig. . The depth or perturbation is deep for lower frequency equilibrium models ($n = 6, 9, 12$) and the dip in this model moves towards the surface. The dip in $\frac{\delta T}{T}$ is observed in the hydrogen ionization zone and this might be caused as a result of change in opacity.

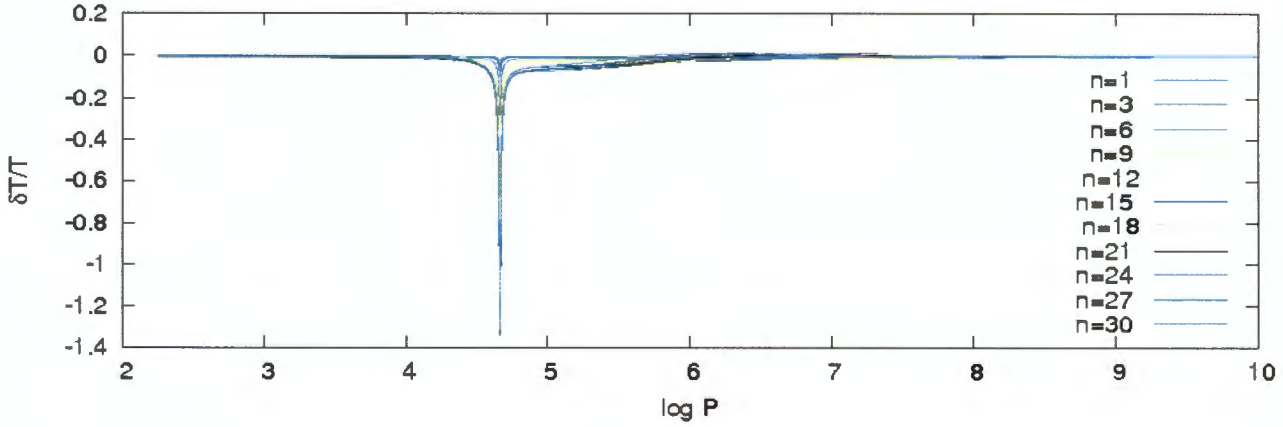

FIGURE 5.22: The temperature eigen function as a function of depth ($log\ P$).

All n value models show constant temperature eigen function close to the surface. Deep in the star the variation in the temperature eigen function becomes constant.

The temperature eigen function ($\frac{\delta T}{T}$) as a function of optical depth is presented in Fig. . As the previous models, the temperature eigen function shows variation in the atmosphere. The variability also moves towards the surface with lower n value models show slight variation in $\frac{\delta T}{T}$.

Fig. shows the dependence of displacement eigen function in depth ($log\ P$) of the star. One can clearly see that the displacement eigen function is large at the surface of the star for $n = 1$. The gradient of the displacement eigen function is different for different values of n. The dip in the displacement eigen function occurs in the same position as the temperature eigen function where

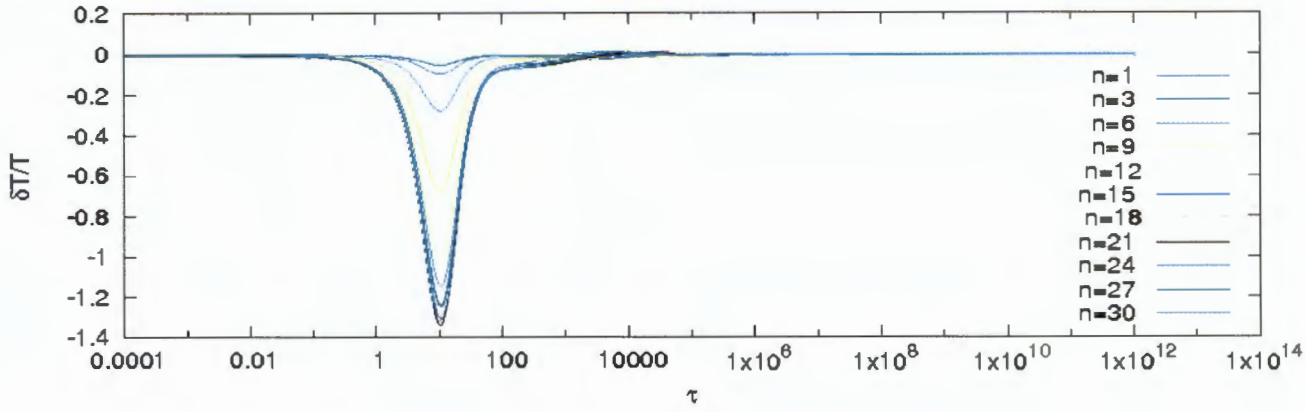

FIGURE 5.23: The temperature eigen function as a function of optical depth (τ).

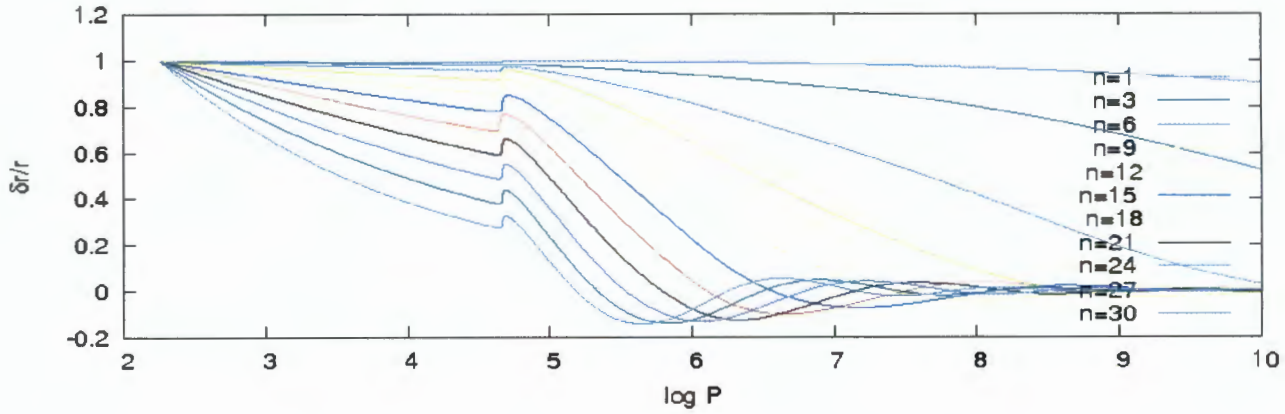

FIGURE 5.24: The displacement eigen function as a function of $log\ P$ (depth).

opacity fluctuation occurs. The variation in $\frac{\delta r}{r}$ show different gradient with higher frequency ones having high gradient. Between $log\ P = 4$ and $log\ P = 5$, $\frac{\delta r}{r}$ shows unique variation, visible hump. For low n values, $\frac{\delta r}{r}$ looks constant with a slight deviation around $log\ P = 9$.

The displacement eigen function is also tested with respect to optical depth (τ) and one can see how it behaves near the surface of the star as presented in Fig. 5.25. In the atmosphere, $\frac{\delta r}{r} = 1$ and it is the largest value regardless of the n values and T_{eff}. For smaller values of n, $\frac{\delta r}{r}$ with respect to τ displaying constancy and those with high n values show larger deviation from being constant deep in the star.

This model is also tested to check the opacity eigen function $\frac{\delta \kappa}{\kappa}$ with respect to $log\ P$ and is presented in Fig. .

The dip in the opacity eigen function $\frac{\delta \kappa}{\kappa}$ occurs in the hydrogen ionization zone shown in Fig. . High frequency equilibrium model pulsation stars behave in a different way as compared to low frequency ones. Higher values of n spikes in the hydrogen ionization zone. Equilibrium models with n values ($n = 9, 12, 15, 18$) have greater depth as compared to low n values. Moreover, around $logP = 6$ there is a slight variability displayed in $\frac{\delta \kappa}{\kappa}$. One can also see that near the surface, those models with low n-values are constant and the other models with high n

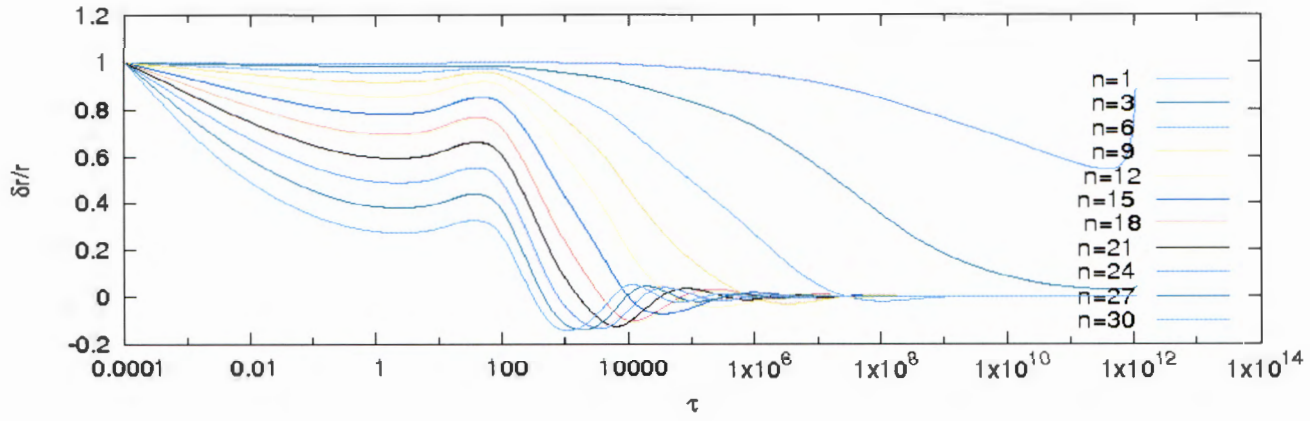

FIGURE 5.25: The displacement eigen function as a function of optical depth (τ).

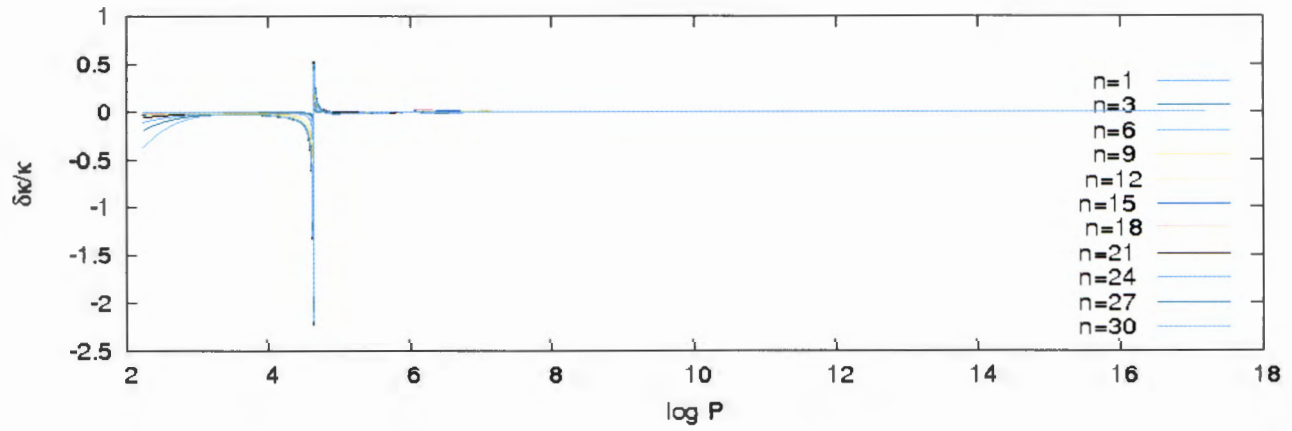

FIGURE 5.26: The opacity eigen function as a function of *log P* (depth).

values demonstrate a positive slope up to $logP = 3$. Between $logP = 3$ and $logP = 4.5$, $\frac{\delta\kappa}{\kappa}$ looks constant. In addition, the deeper one goes in $logP$, except between $logP = 4$ and $log\,P = 6$, $\frac{\delta\kappa}{\kappa}$ becomes constant.

5.1.6 Equilibrium Model with T_{eff} = 7512 and log g = 4.301

The high temperature equilibrium model with T_{eff} = 7512K is presented in this section. The temperature eigen function as a function of $log\ P$ (referring depth in this case) behaves in the same way as the previous model (T_{eff} = 7072 K). The variations occur in the first hydrogen ionization zone around $logP = 4.5$. As compared to the previous models presented, the position where this variation occurs moves toward the surface.

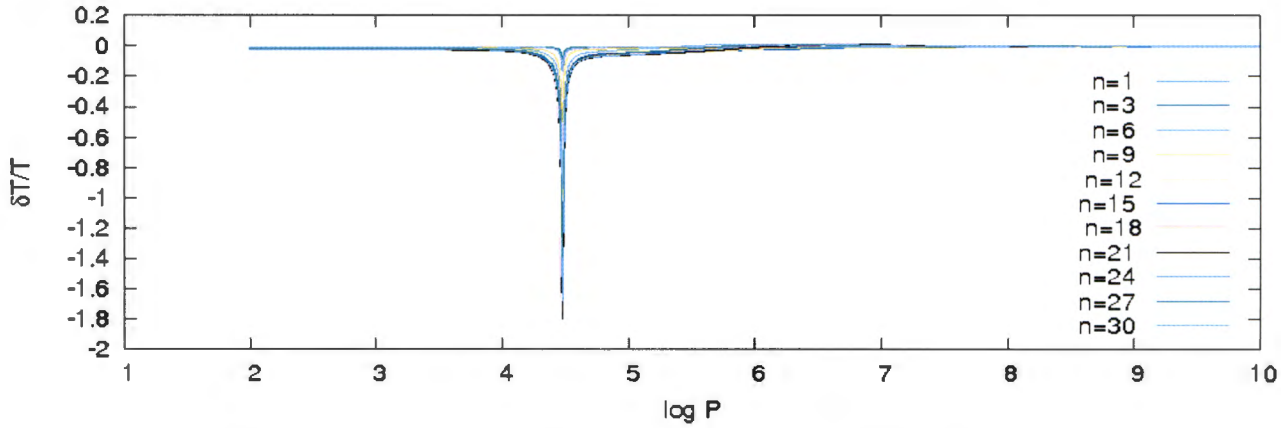

FIGURE 5.27: The temperature eigen function as a function of depth ($log\ P$).

A closeup investigation of the depth shows a slight deviation or change in position towards the surface towards $log\ P = 4$ as compared to the lower temperature models. This model has a larger depth in the temperature eigen function as shown in Fig. 5.27. Moreover, there is a slight variation in the temperature eigen function between $logP = 5$ and $logP = 6$. Deep in the star, $\frac{\delta T}{T}$ becomes constant. Once again the temperature eigen function is tested with respect to optical depth and is presented in Fig. 5.28. From the figure, it is easy to see how $\frac{\delta T}{T}$ behaves inside the star and the variation is clearly seen in the atmosphere. In addition, one can see that the lowest n value models show a very small variability in the temperature eigen function as compared to the higher n values.

Fig. 5.29 shows the displacement eigen function as a function of depth ($log\ P$). The position where the depth created in the displacement eigen function plot is the place where the temperature eigen function also varies, which is the hydrogen ionization zone. Moreover, it is easy to notice from the displacement eigen function plot that those equilibrium models with n- values (high frequency) ($n = 21, 24, 27, 30$) have higher gradient than the low frequency models ($n = 1, 3, 6, 9$). In addition, one can see that the displacement eigen function becomes larger ($\frac{\delta r}{r} = 1$) close to the surface. One can also see the feature (hump) between $log\ P = 4$ and $log\ P = 5$ which is caused by hydrogen ionization.

More analysis on $\frac{\delta r}{r}$ was also done with respect to optical depth (τ) and near the surface regardless of the n values and T_{eff}, $\frac{\delta r}{r}$ has a maximum value of 1. The displacement eigen function $\frac{\delta r}{r}$ for lower n values is constant across τ except deep in the star as shown in Fig. 5.30. For higher values of n, the displacement eigen function shows variability across τ.

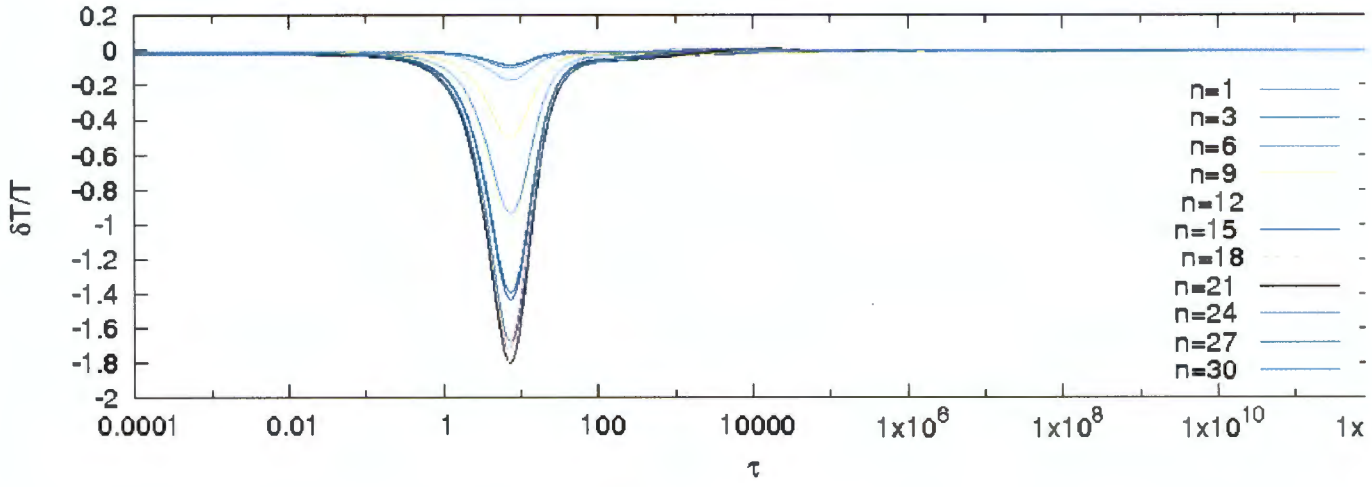

FIGURE 5.28: The temperature eigen function as a function of optical depth (τ).

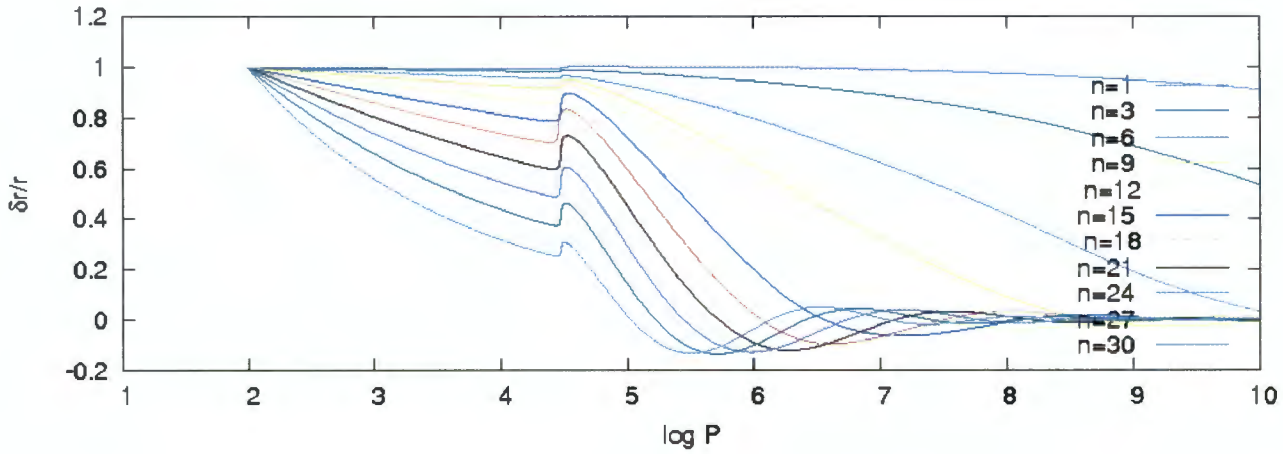

FIGURE 5.29: The displacement eigen function as a function of depth ($log\ P$).

The opacity eigen function, on the other hand, shows variation between $log\ P = 4$ and $logP = 5$, where the variation is caused due to first hydrogen ionization zone. The second variation around $log\ P = 6$, which is smaller as compared to the first variation, is the second hydrogen ionization zone as shown in Fig. . Deep in the star, on the other hand, $\frac{\delta\kappa}{\kappa}$ becomes constant.

Near the surface, almost all n values show constant $\frac{\delta\kappa}{\kappa}$ except the two highest n values. Again, here the position where $\frac{\delta\kappa}{\kappa}$ shows great variation moves towards the surface between $logP = 4$ and $logP = 5$.

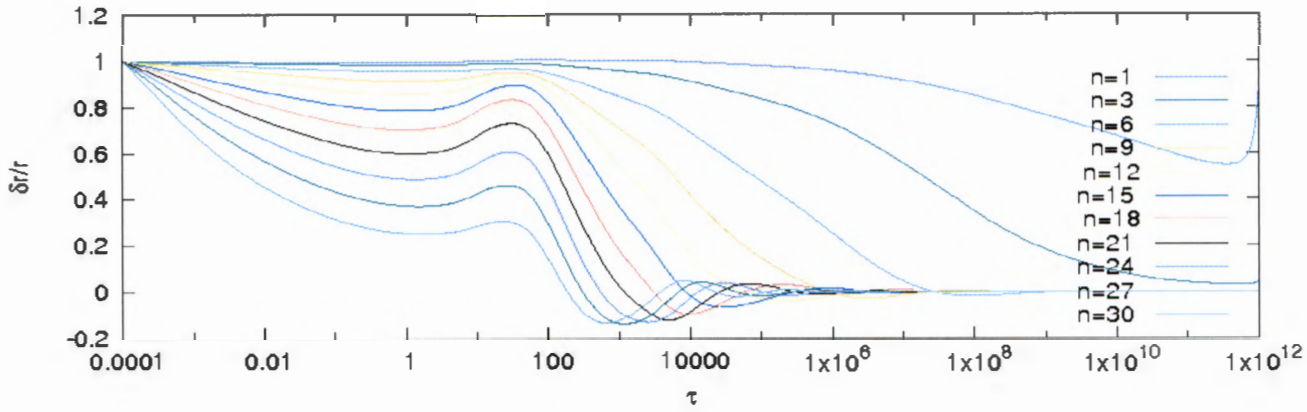

FIGURE 5.30: The displacement eigen function as a function of optical depth (τ).

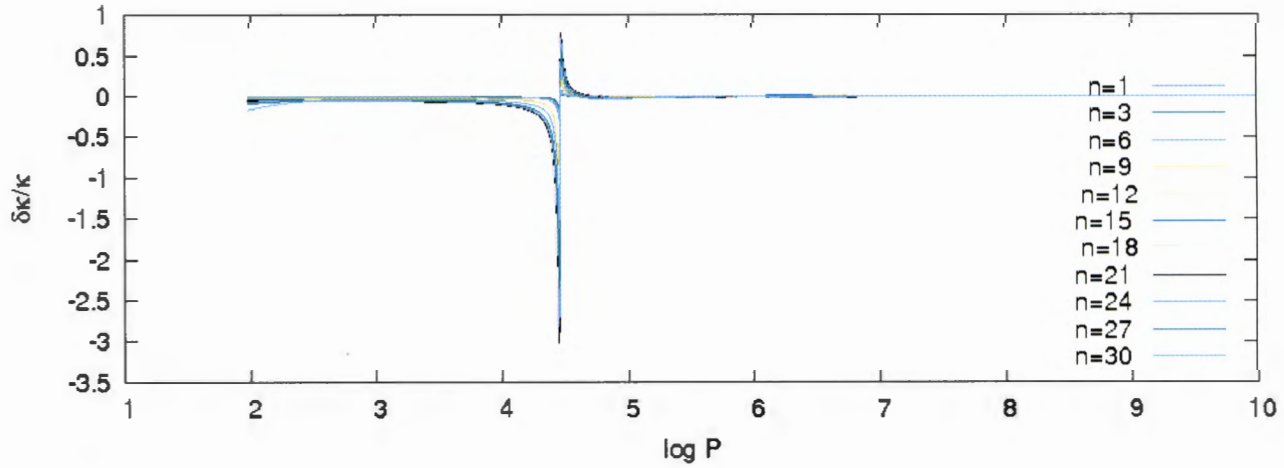

FIGURE 5.31: The variation in the eigen function of opacity as a function of depth ($log\ P$).

5.1.7 Equilibrium Model with T_{eff} = 7900 K and log g = 4.3

The temperature eigen function as a function of $log\ P$ (depth) for an equilibrium model with $T_{\text{eff}} =$ 7900K is presented in Fig. 5.32.

In this figure, the equilibrium models with low frequency creates a sharp dip close to $log\ P =$ 4 and the others shows the variability in the region where hydrogen ionization dominates. As compared to the lower temperature models mentioned before, the hydrogen ionization zone moves towards the surface. The trend one can notice in the temperature eigen function is that, as the temperature for the equilibrium model increases, $\frac{\delta T}{T}$ near the surface becomes more flat or constant. Deeper in the star, $\frac{\delta T}{T}$ becomes constant.

Further studies in the temperature eigen function is presented in Fig. 5.33 ;and significant variations can be seen in the atmosphere of the star. As compared to the previous models, the variability moves towards the surface of the star. Near the surface, $\frac{\delta T}{T}$ becomes constant for all models under consideration. When one traces through the atmosphere of the star, those models with high

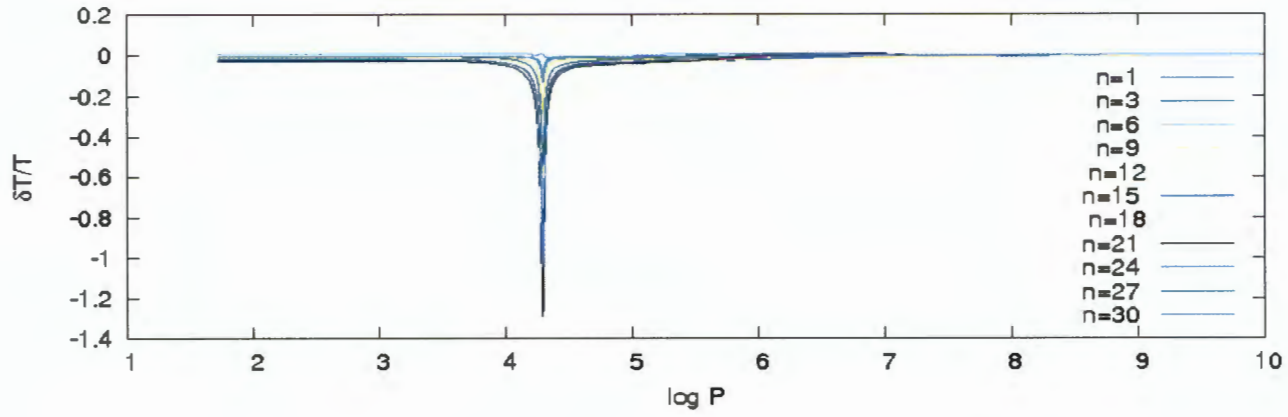

FIGURE 5.32: Plot showing the real part of the temperature eigen function as a function of $log\ P$ inside the star.

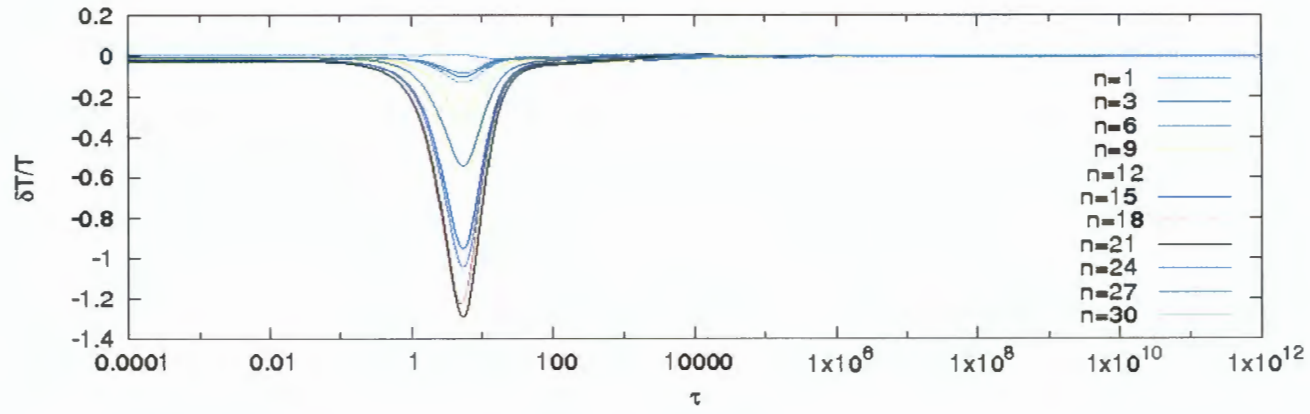

FIGURE 5.33: Plot showing the temperature eigen function as a function of optical depth τ.

n-values creates a hump in the hydrogen ionization zone but the remaining models create various depths depending on their n-values. Deeper in the star, on the other hand, $\frac{\delta T}{T}$ becomes constant.

As in the previous models mentioned in previous sections, the displacement eigen function as a function of $log\ P$ is presented in Fig. 5.34. Low frequency equilibrium models have low gradient and shows a small bump around the region where hydrogen ionization dominates.

As n (frequency) increases, the gradient increases and the bumps become clearer. The displacement eigen function becomes constant starting from $log\ P = 8$, that is, deep in the star except the low frequency one $n = 1$ that behaves differently. The gradient for $n = 1, 3, 6$ increases rapidly.

Fig. 5.35 shows how the displacement eigen function behaves inside the star as a function of optical depth. As shown in the figure, near the surface of the star the displacement eigen function becomes higher and has a value of 1. For lower values of n between $1 - 6$, $\frac{\delta r}{r}$ tracing through the atmosphere it looks constant. But the high frequency models behave differently deep inside the star. For such models, $\frac{\delta r}{r}$ show huge deviation with negative slope. Deep inside the star, $\frac{\delta r}{r}$ becomes constant. One should notice from the plot of $\frac{\delta r}{r}$ with respect to τ that, $\frac{\delta r}{r}$ has the highest value for all models regardless of the n values and T_{eff}.

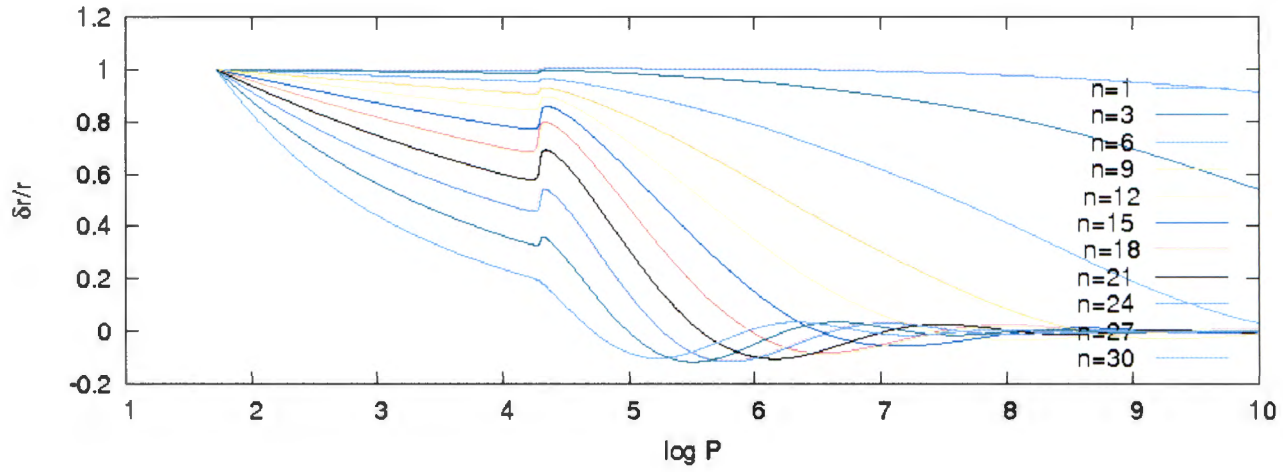

FIGURE 5.34: An illustration showing the displacement eigen function as a function of $log\ P$ inside the star.

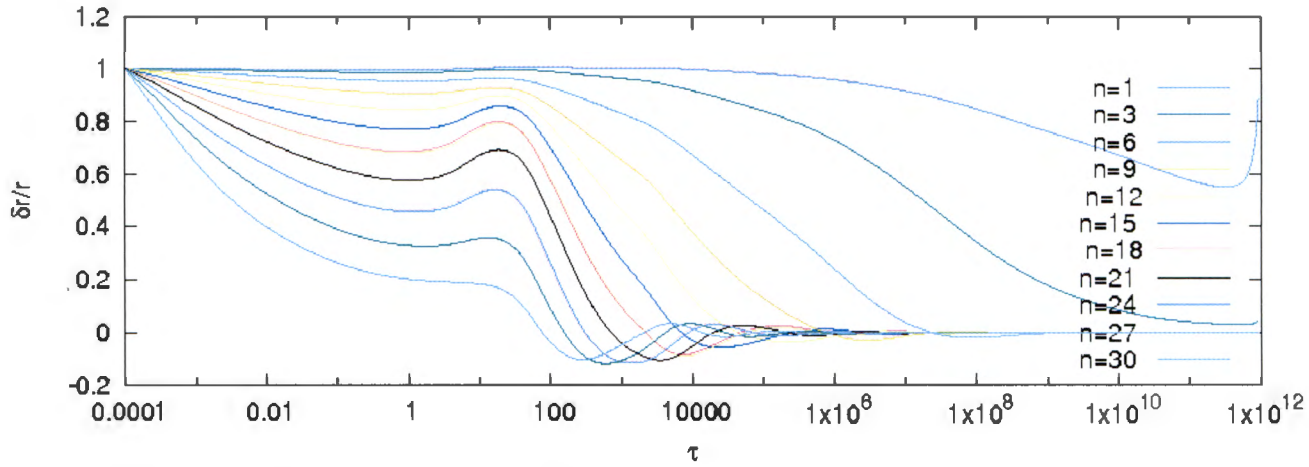

FIGURE 5.35: The displacement eigen function as a function of optical depth.

Fig. 5.36 demonstrates the variation in opacity as a function of depth where the significant variation occur very close to $log\ P = 4$, the region where the opacity fluctuation is caused due to hydrogen ionization zone. The variation in the temperature eigen function, the displacement eigen function and opacity fluctuations occur almost at the same position around $log\ P = 4$. As compared to lower T_{eff} models ($T_{eff} = 5778K$, $T_{eff} = 6164K$, $T_{eff} = 6430K$), the position where the opacity variation occurs moves towards the surface. In addition, all the n values, except one, have constant $\frac{\delta\kappa}{\kappa}$ near the surface. Both the spike and the dip are large as compared to the previous models. Deep in the star, $\frac{\delta\kappa}{\kappa}$ becomes constant regardless of the n-values considered.

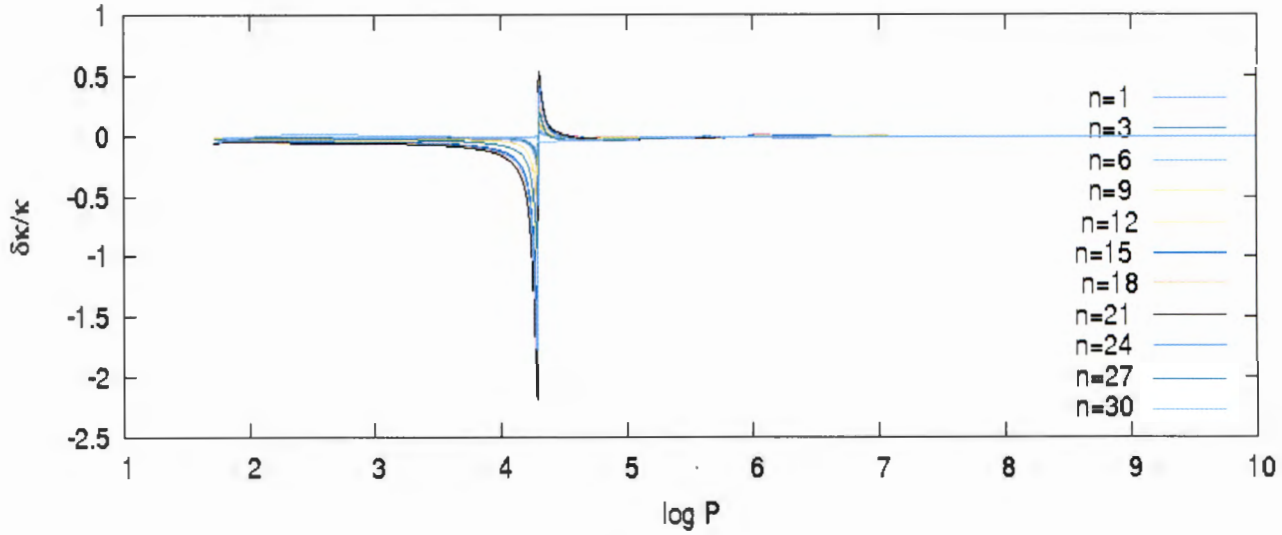

FIGURE 5.36: Opacity eigen function as a function of *log P* inside the star.

5.1.8 Equilibrium Model with T_{eff} = 8340 K and log g = 4.3185

The temperature eigen function as a function of *log P* is presented in Fig. 5.37. The striking difference between this model and the previous models discussed in the previous sections is that some frequencies creates a sharp spike and the rest creates larger depth. But near the surface and deep in the star, the temperature eigen function remains constant.

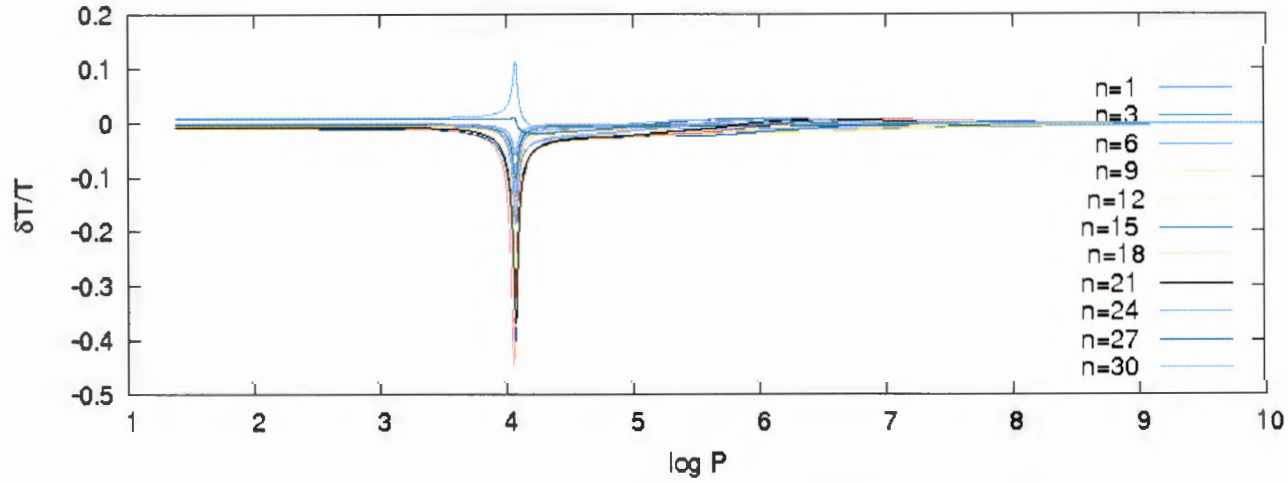

FIGURE 5.37: Figure showing how the temperature eigen function behaves in the star.

Again the position where the perturbation happens, moves towards the surface as compared to the previous models.

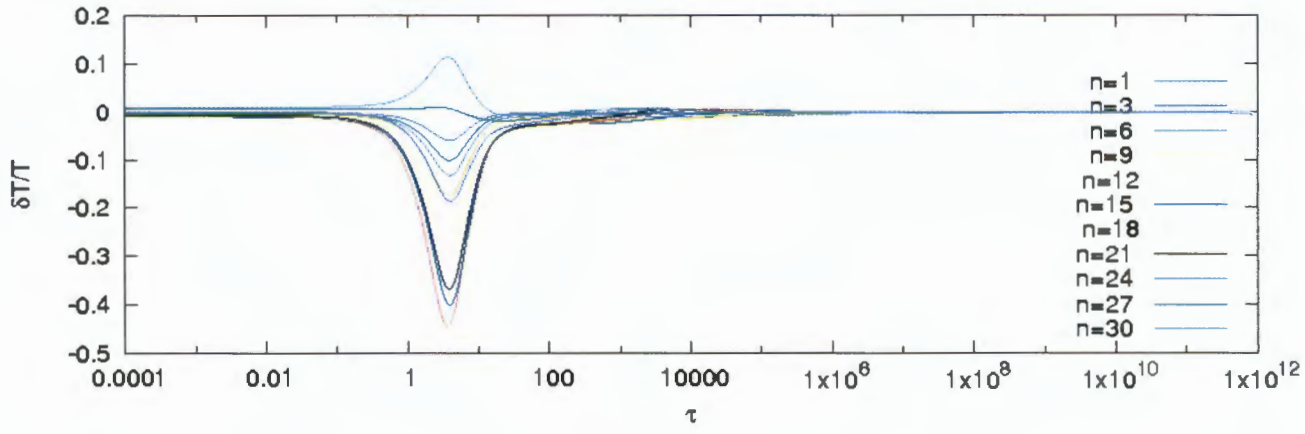

FIGURE 5.38: Plot showing how the temperature eigen function behaves in the star with respect to optical depth τ.

Further study of $\frac{\delta T}{T}$ with respect to optical depth (τ) is shown Fig. 5.38 which demonstrates high variability in the atmosphere of the star. Near the surface and deep in the star the temperature eigen function is constant with respect to optical depth (τ). The unique feature in the variation in the temperature eigen function, $\frac{\delta T}{T}$, is that higher frequency models ($n = 27$ and $n = 30$) shows significant hump in the atmosphere of the star.

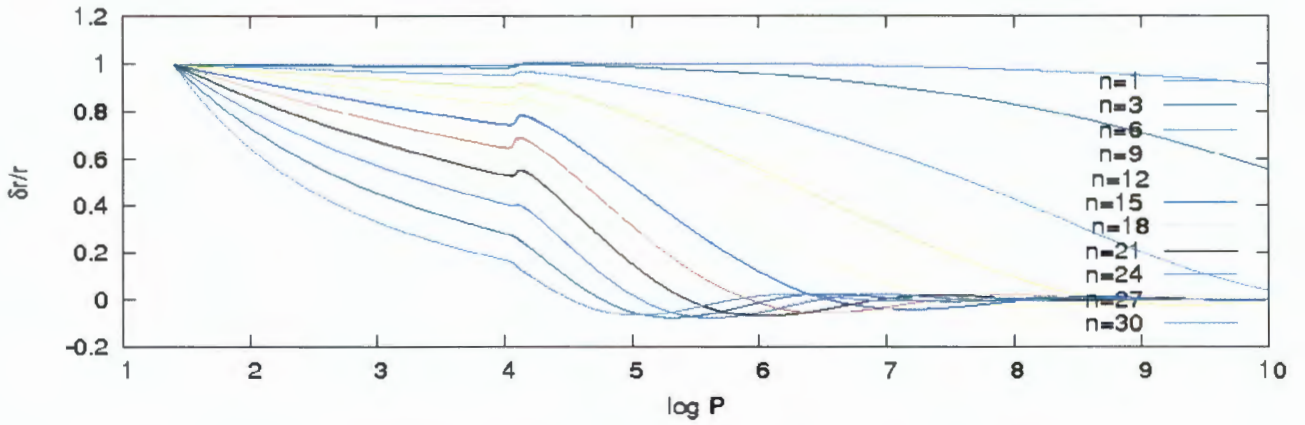

FIGURE 5.39: An illustration showing how the displacement eigen function behaves in the star with respect to log P.

Fig. 5.39 demonstrates the behavior of the displacement eigen function as a function of $log\ P$ (depth). This model, with high temperature, shows larger gradient with high n values and low gradients for small values of n. In the hydrogen ionization zone, with high n values, the bumps are clearer. For lower values, $n = 1$, the displacement eigen function behaves differently deep inside the star. But regardless of the frequency used, the displacement eigen function attains its maximum value towards the surface. Further studies in the displacement eigen function are presented in Fig. 5.40. Lower frequency models show constant $\frac{\delta r}{r}$ with slight deviation deep in the star. Between $log\ P = 4$ and $log\ P = 5$, the hydrogen ionization zone, $\frac{\delta r}{r}$ shows clear hump and variation. In addition, as in all the previous models discussed in previous sections, $\frac{\delta r}{r}$ attains maximum value

in the atmosphere of the star. Those with high $n = 30$ value demonstrates that $\frac{\delta r}{r}$ shows large deviation. As one traces deep in the star, the variation in $\frac{\delta r}{r}$ decreases and approaches 0.

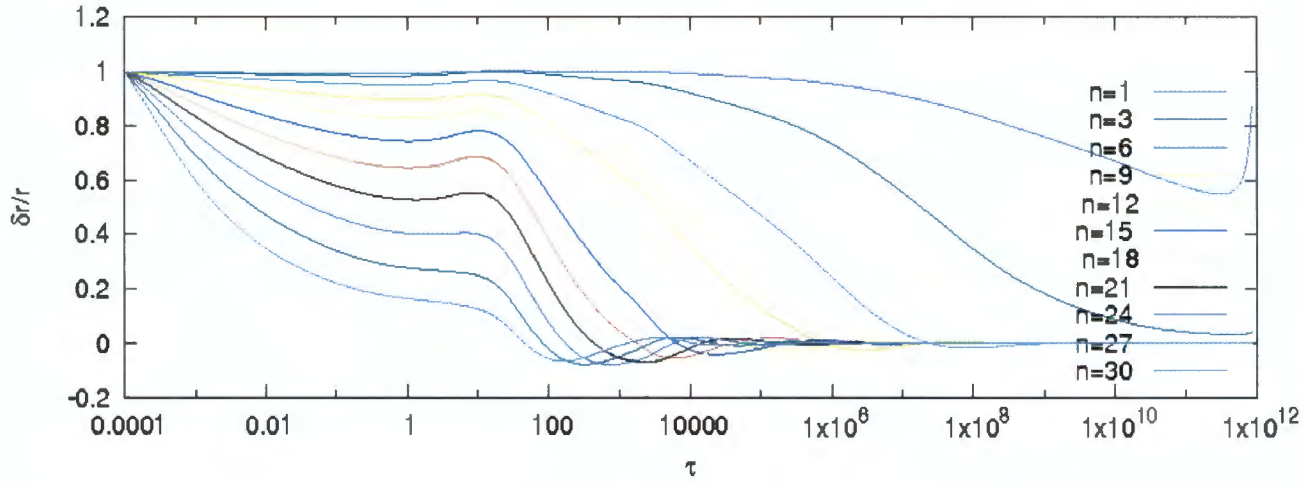

FIGURE 5.40: An illustration showing how the displacement eigen function behaves in the star with respect to optical depth τ.

Regarding the perturbation in opacity, Fig. 5.41 demonstrates how opacity varies inside the star.

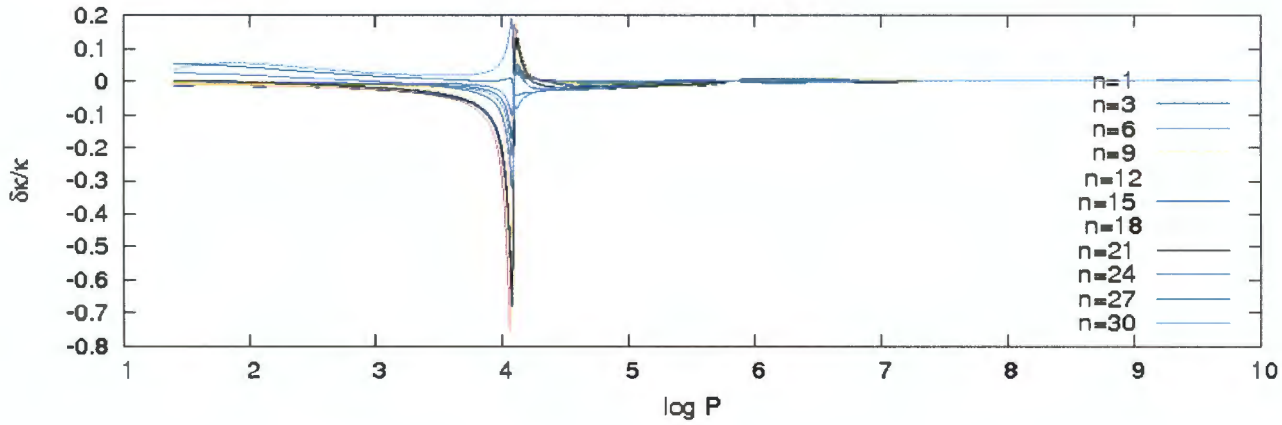

FIGURE 5.41: Figure showing how the opacity eigen function behaves in the star.

The three highest n values $n = 24, 27, 30$ shows variation in opacity near the surface of the star. In the atmosphere, where hydrogen ionization is assumed to be the cause for opacity variation. Despite the fact that we used different frequencies, all models shows significant variability around $log\, P = 4$. Deep in the star, between $logP = 5$ and $logP = 6$, though it is small, there is still change in the opacity but not as significant as the first hydrogen ionization zone. Deep in the star, the opacity variation becomes constant implying that there is a very small chance of noticing opacity perturbation in the center of the star.

5.1.9 Equilibrium Model with T_{eff} = 9088 K and log g = 4.327

The temperature eigen function for this model behaves differently as compared to the previous low temperature models discussed in the previous sections. Near the surface of the star some of the models with a particular range of n values looks constant up to the hydrogen ionization zone, which moves towards the surface of the star in comparison to the previous models. Higher n value models have a variable temperature eigen function near the surface. It also has more deviation and variation in the hydrogen ionization, that causes opacity fluctuation. Moreover, $\frac{\delta T}{T}$ continues to vary up to a certain depth around $log\, P = 5$, $logP = 6$ and $logP = 7$ then it becomes constant deep in the star. These variations can be seen in Fig. 5.42. Near the surface, $\frac{\delta T}{T}$ shows different behavior; some have constant $\frac{\delta T}{T}$ and others have a negative slope.

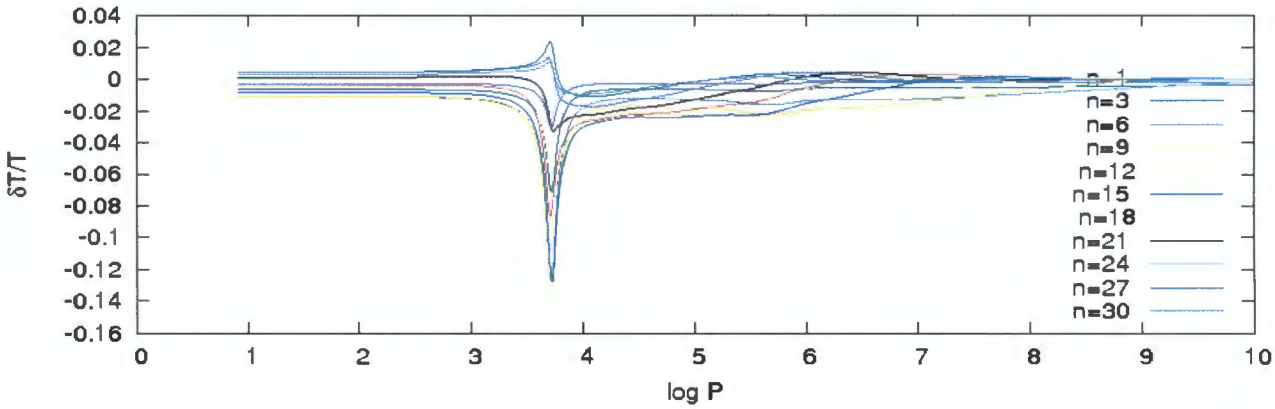

FIGURE 5.42: The real part of the temperature eigen function as a function of depth $log\, P$.

Additional studies conducted to study the behavior of $\frac{\delta T}{T}$ with respect to optical depth are shown in Fig. 5.43. As the temperature T_{eff} for the equilibrium model increases, the variation moves towards the atmosphere. Deeper in the star, $\frac{\delta T}{T}$ becomes constant. But in this particular model, the variation in the temperature eigen function is unique.

The displacement eigen function as a function of $log\, P$ (depth) is presented in Fig. 5.44. It is easy to notice the significant differences between this model and the previous models, T_{eff} = 5778K, T_{eff} = 6164K, T_{eff} = 6430K, with the same frequency but different effective temperature. Higher n values demonstrate higher gradient and greater variability. In this particular model, the plot of $\frac{\delta r}{r}$ shows the vanishing humps in Fig. 5.44 as compared to the previous models discussed in the previous sections.

The other physical quantity studied here is the displacement eigen function as a function of optical depth (τ). Fig. 5.45 shows $\frac{\delta r}{r}$, the displacement eigen function, as a function of τ. Low n value models demonstrate that $\frac{\delta r}{r}$ is constant across the star. On the other hand, the higher values of n near the surface show negative slope and deeper in the star those with high values of n shows larger deviation with negative slope and approach 0. One can also notice from Fig. 5.45 that $\frac{\delta r}{r}$ attains the maximum value of 1 near the surface at $\tau = 0$.

The stellar models with smaller values of n shows that the displacement eigen function has a low gradient (constant) approximately zero. Those with high values of n have higher gradient (negative).

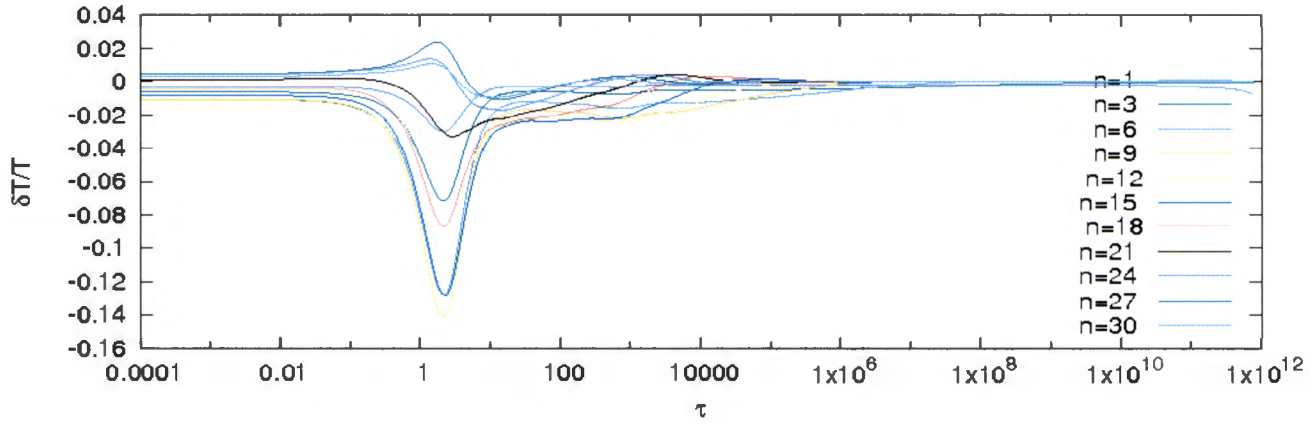

FIGURE 5.43: An illustration showing how the temperature eigen function behaves as a function of optical depth.

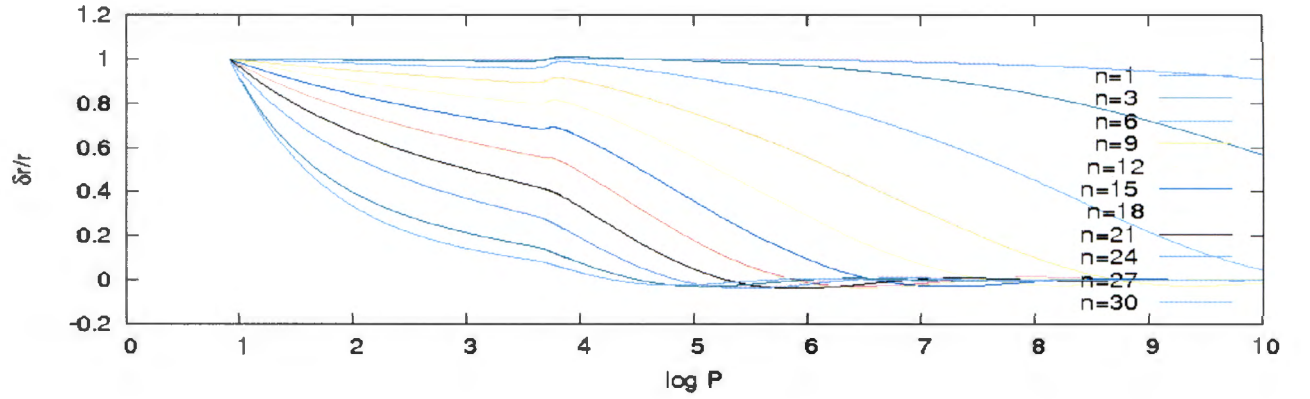

FIGURE 5.44: The real part of the displacement eigen function and how it behaves as a function of $log\ P$ (depth).

Fig. 5.46 shows the effect of opacity eigen function $\frac{\delta\kappa}{\kappa}$ as a function of depth. To begin with, the position where these variabilities are observed, moved closer to the surface. For certain n values, the opacity eigen function looks constant near the surface of the star whereas higher n values shows non constant $\frac{\delta\kappa}{\kappa}$ near the surface of the star. $\frac{\delta\kappa}{\kappa}$ shows great variability close to $logP = 4$ where hydrogen ionization dominates, that causes opacity fluctuation. Moreover, between $logP = 5$ and $logP = 6$ there is a small variability in $\frac{\delta\kappa}{\kappa}$ that is not as dominant as the previous one. Deep in the star, on the other hand, $\frac{\delta\kappa}{\kappa}$ becomes constant. In between $logP = 3$ and $logP = 4$, all models, regardless of the frequency used, they show high variability.

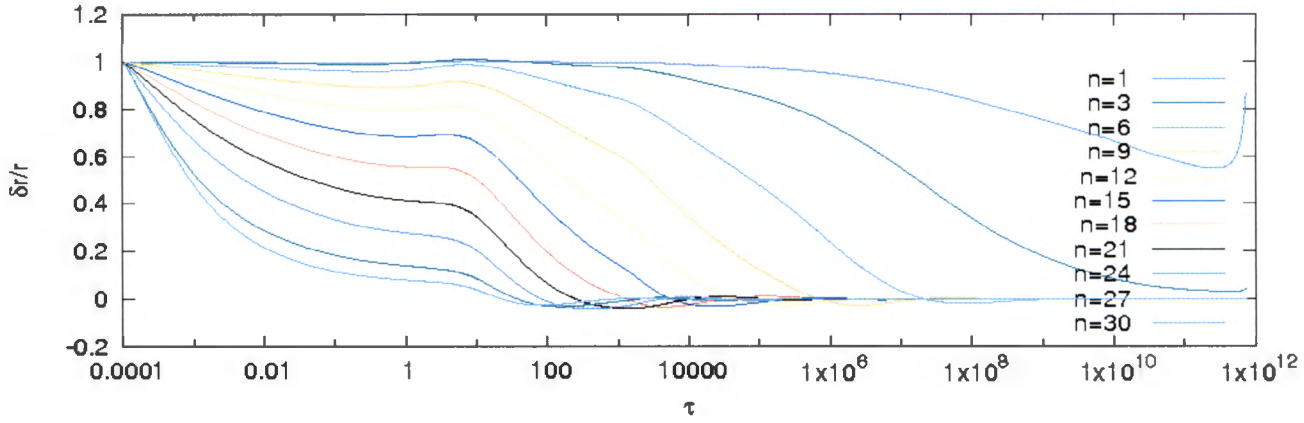

FIGURE 5.45: An illustration showing how the displacement eigen function behaves as a function of optical depth (τ).

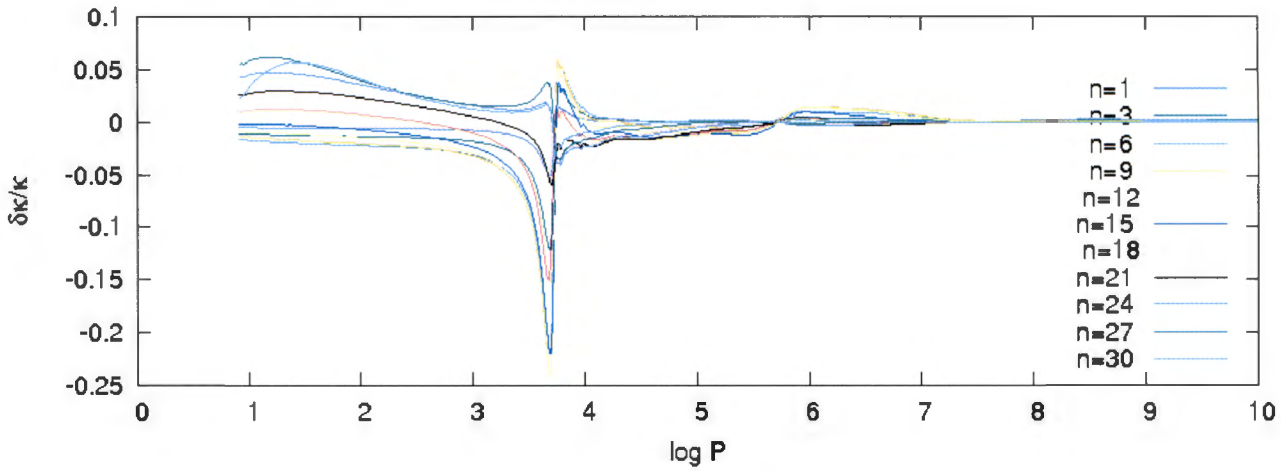

FIGURE 5.46: Figure showing how the opacity eigen function behaves as a function of $log\ P$ (depth).

5.1.10 Equilibrium Model with T_{eff} = 9440 K and log g = 4.327

An equilibrium model with high temperature $T_{\text{eff}} = 9440$ K is used to investigate the theoretical work presented in this work. As in the previous models, we tested the temperature eigen function as a function of $log\ P$ (depth). $\frac{\delta T}{T}$ demonstrates large variability near the surface, for some n values, and constant for others. But inside the atmosphere it demonstrates a huge variability, assumed to be the hydrogen ionization zone, shown in Fig. 5.47. Lower values of n show no variation near the surface but between $logP = 3$ and $logP = 4$.

The variability in $\frac{\delta T}{T}$ continues to be significant even deeper in the star up to $logP = 7$. Then the temperature eigen function becomes constant deep in the star. One can easily notice from the temperature eigen function Vs $log\ P$ plot that, as the effective temperature of the equilibrium model increases, the position where the variability occurs move towards the surface (atmosphere).

More analysis in the variation in the temperature eigen function is performed with respect

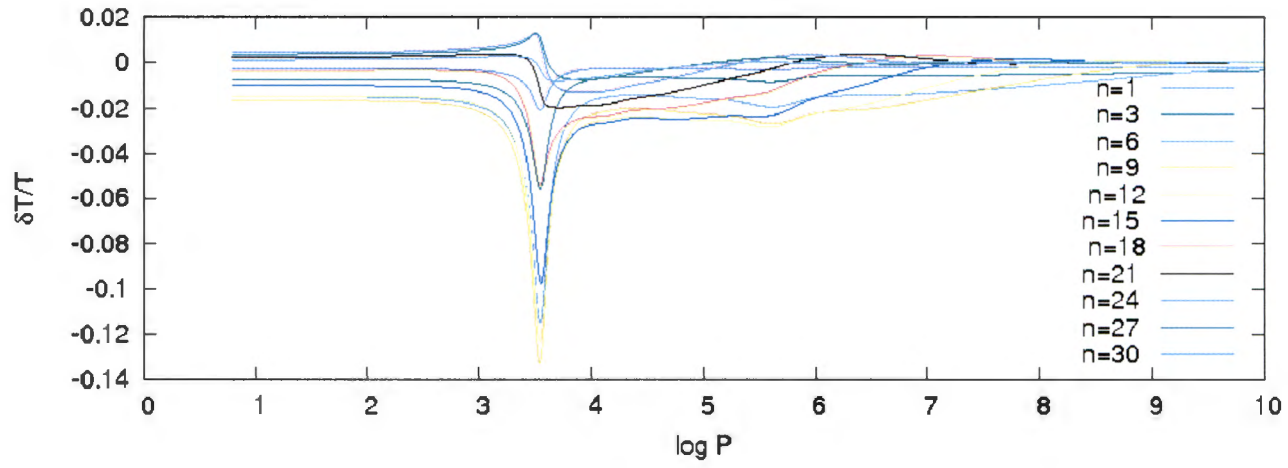

FIGURE 5.47: The real part of the temperature eigen function showing how it behaves inside a star.

to optical depth and is presented in Fig. 5.48. From the figure, one can see the variation in the temperature eigen function happening in the atmosphere. Near the surface $\frac{\delta T}{T}$ is constant.

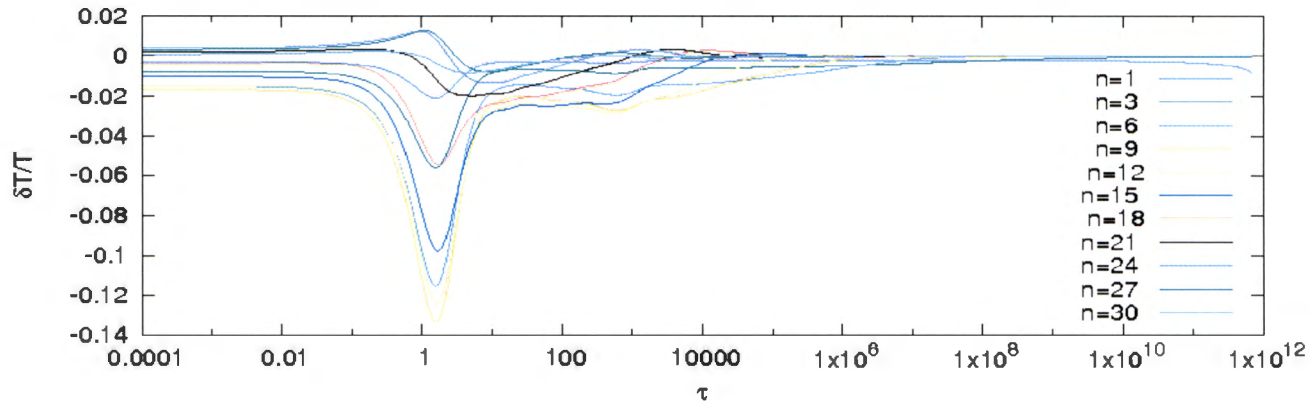

FIGURE 5.48: An illustration showing how the temperature eigen function as a function of optical depth (τ) inside a star.

The displacement eigen function $\frac{\delta r}{r}$ as a function of $log\ P$ is presented in Fig. 5.49.

From the figure, it is easy to see that the displacement eigen function $\frac{\delta r}{r}$ attains maximum value near the surface of the star. Moreover, the gradient of the displacement eigen function becomes higher for higher values of n. The hump in the hydrogen ionizion zone which was visible in the previous models disappear. The smallest value of $n = 1$ behaves differently inside the star. On the other hand, the displacement eigen function for most n values show variation with negative slope and deep inside the star becomes constant and approaches zero.

Further analysis in the displacement eigen function is presented in Fig. 5.50. As shown in the figure, those with smaller values of n shows that $\frac{\delta r}{r}$ looks constant in the atmosphere. Deep in the star, for high values of n, the displacement eigen function shows deviation with negative slope.

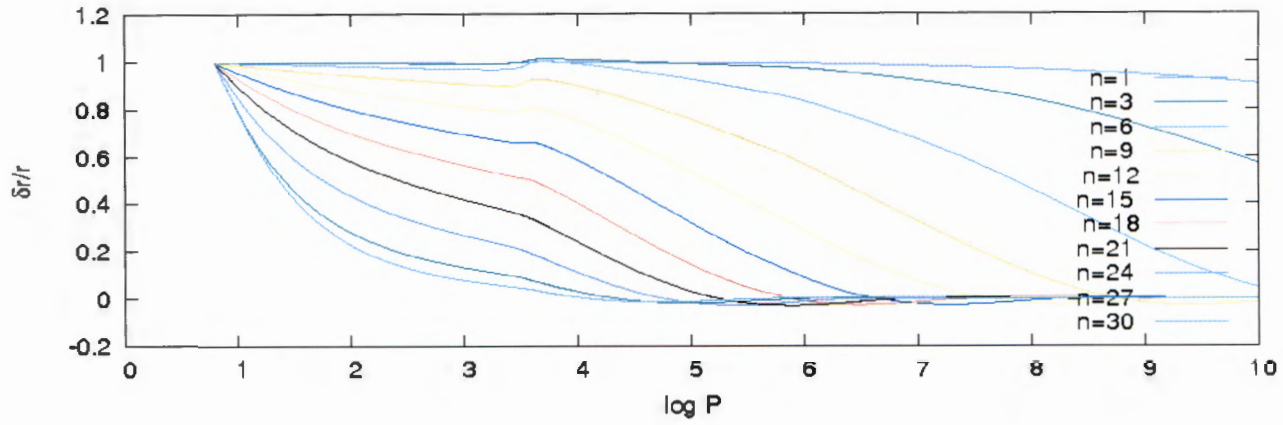

FIGURE 5.49: A plot showing Displacement eigen function as a function of depth.

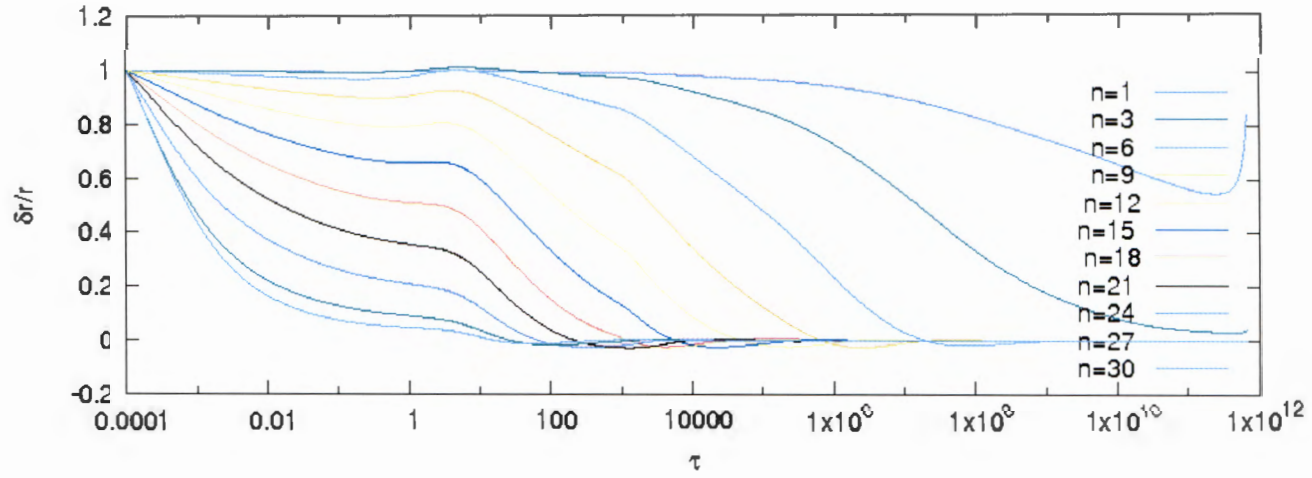

FIGURE 5.50: A plot showing Displacement eigen function as a function of optical depth.

Moreover, deep inside the star, $\frac{\delta r}{r}$ drops sharply and approaches to *zero.* Despite the fact that we used different n values for this equilibrium model, $\frac{\delta r}{r}$ reach the highest value near the atmosphere $\tau = 1$.

For this high temperature model, opacity eigen function is tested with respect to $log\ P$ (depth) and its behavior is studied. Near the surface of the star, all n value models show variation in the opacity eigen function. The variability near the surface as compared to the previous models discussed ($T_{\text{eff}} = 5778$ K, $T_{\text{eff}} = 6164$ K, $T_{\text{eff}} = 6430$ K, $T_{\text{eff}} = 7072$ K) is significant and none of the n value models show constancy near the surface. In the hydrogen ionization zone, all n models happens to show great variability in $\frac{\delta \kappa}{\kappa}$. More variability or perturbation in the opacity eigen function can be seen around $log\ P = 6$. But these variations are not as dominant as the perturbations that happened in the atmosphere between $log\ P = 3$ and $log\ P = 4$ as shown in Fig. 5.51.

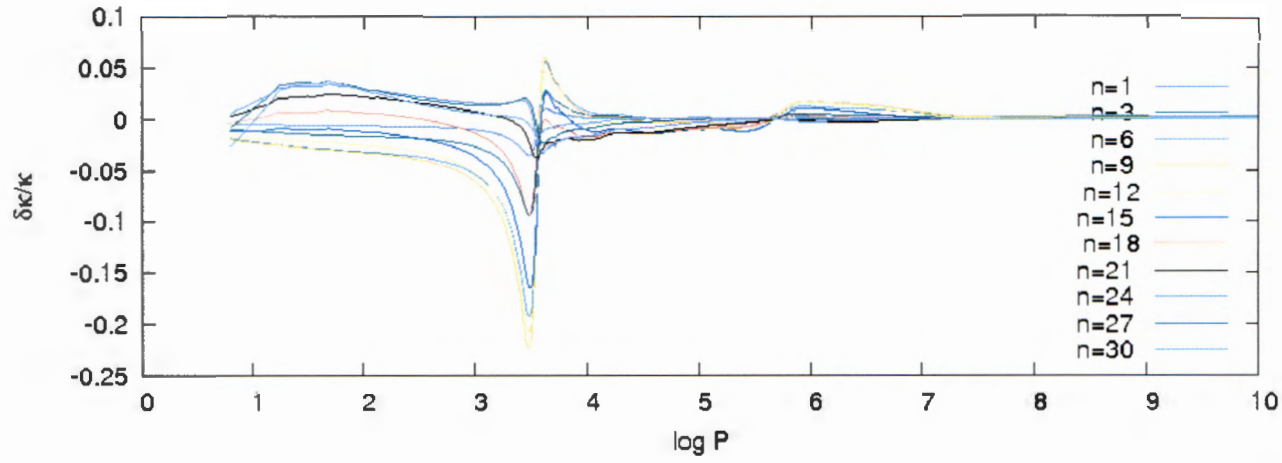

FIGURE 5.51: Figure showing opacity eigen function as a function of depth.

If one compares this model to the previous models discussed in this work, the hydrogen ionization zone moves towards the surface (atmosphere) and the premise made before regarding the constancy of the opacity eigen function can be disproved by studying Fig. 5.51. As compared to the previous models presented in this thesis, the variation in opacity eigen function is high and significant for higher temperature model.

5.2 Comparison between our formula with Watson's formula

Watson's formula has five terms T_1, T_2, T_3, T_4 and T_5 essentially describe the effects of flux perturbations on the luminosity perturbations. T_2 and T_5 account for the perturbations in limb-darkening. Therefore, in order to compare our formula with the Watson's formula we need to compare $T_1 + T_2 + T_4 + T_5$ with the first two terms of our formula, namely:

$$\frac{Y_l^m(\theta_0,\phi_0)}{2H(0)}\left\{\int_0^1\int_0^\infty \delta\tilde{B}(\tau)P_l(\mu)e^{\frac{-\tau}{\mu}}d\tau d\mu + \int_0^1\int_0^\infty \frac{\delta\tilde{\kappa}}{\kappa}(\tau)P_l(\mu)(I_\lambda - B_\lambda)e^{\frac{-\tau}{\mu}}d\tau_\lambda d\mu\right\}. \quad (5.5)$$

T_3 is equivalent to:

$$\begin{aligned} &= Y_l^m(\theta_0,\phi_0)\left\{\int_0^1 2\mu P_l(\mu)h'_\lambda(\mu)d\mu - \int_0^1(1-\mu^2)\frac{dP_l}{d\mu}h_\lambda(\mu)\right. \\ &\left. - \int_0^1(1-\mu^2)\frac{dP_l(\mu)}{d\mu}\mu\left[\frac{dh'}{d\tau} - \int_0^\infty\left(\frac{\delta\tilde{r}}{r}\right)I_\lambda(\tau,\mu)e^{\frac{-\tau}{\mu}}\frac{d\tau}{\mu} + \frac{1}{\mu}h'\right]\right\}. \end{aligned} \quad (5.6)$$

We have shown that for low frequencies, the above expression becomes T_3 exactly.

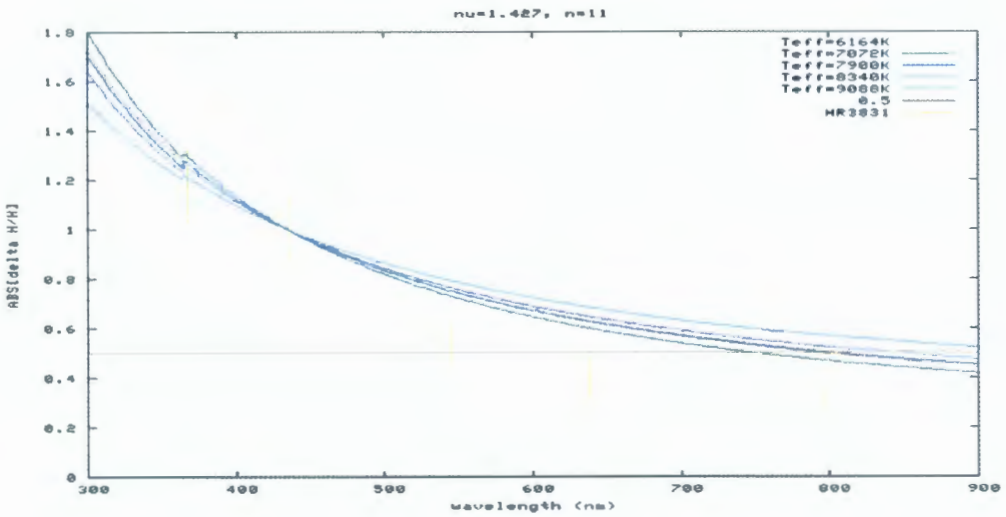

FIGURE 5.52: The first two terms of our formalism fitted with HR3831. and $roAp$ stars.

For the equilibrium models T_{eff} = 6164K, T_{eff} = 7072K, T_{eff} = 7900K, T_{eff} = 8340K and T_{eff} = 9088K, we tested the first two terms of our formula, with a real data HR3831 and $roAp$ stars. Our equation does not fit well to $roAp$ stars, as discussed earlier we neglected the presence of the magnetic field. The yellow bars show HR3831 as presented in Fig. 5.52.

Chapter 6

Conclusions

In this thesis, we have achieved the following:

1. We have derived an equation that models the impact of radiation and p-modes on the light output of a star taking into consideration the several layers of the atmosphere.
2. We have shown that our derived equation is consistent with Watson, ( ) and Watson, ( ) formula for a single layered atmosphere at low overtone frequencies. At those low frequencies, the eigen functions are nearly constant in the atmosphere.
3. Furthermore, our formalism includes the effects of opacity fluctuation on the emergent flux in the atmosphere of A stars.

This was shown to be a significant contributor to the flux of A stars by Medupe, Christensen-Dalsgaard, and Phorah, ( ). They found that the opacity fluctuations result in a sharp 'dip' in the temperature eigen function just below the photospheric layer. They also showed that opacity fluctuations can also introduce a phase difference between flux perturbations and temperature perturbations.

We acknowledge that our formula was based on radiation energy transport only. We neglected convection, this is the limitation to our formalism because sub-surface convection plays important role in exciting pulsations in Solar-like stars. It is also important in cooler A and F stars. Another limitation of our formula is in the neglect of magnetic fields and rotation. Thus, it is likely not suitable for solving the problem of fitting multi-color photometric amplitudes data as outlined in Medupe, Christensen-Dalsgaard, and Phorah, ( ). Furthermore, Cunha, ( ) showed that magnetic pressure is of the same magnitude as gas pressure in the atmosphere of $roAp$ stars.

We however believe our new formula could still be useful for studies of mode identification in high overtone pulsators. A suggestion for comparison with data is to compute the eigen functions using a code that includes consistent treatment of radiative transfer and convection presented in Porah (2008). This code combines code by Houdek, ( ) and Houdek et al., ( ) with the code Medupe, Christensen-Dalsgaard, and Kurtz, ( ).

The formalism introduced in this work is based on non-grey approximation where the pulsation equations and opacity depends on the depth and frequency of observation. We also showed that for a given stellar model, in general, luminosity variation due to pulsation is due to temperature, opacity perturbations, departure from radiative equilibrium ($I_\lambda - B_\lambda$). Moreover, the atmosphere of a pulsating star with high overtone, all layers above the photosphere contribute towards the variation in observed luminosity. In addition, the upper layer of the atmosphere significantly contributes to the observed luminosity. The contribution from geometric effects depends on the temperature structure of the star and the shape of the displacement eigen function and the weight factor $e^{\frac{-\tau_\lambda}{\mu}}$.

In addition, since our assumption to derive our formalism is a multilayered atmosphere in pulsating stars, the contribution towards the observed luminosity from different layers is different where the upper most layers contribute the most whereas deeper layers contribute less. In a deeper layer, for example, if there exists a node, its contribution towards the geometry effect, that is

surface normal variation and variation in the surface area, is *insignificant or none*. But nodes close to the surface layer play a significant role in affecting the geometric effect which in turn affect the observed luminosity. We demonstrated these contributions and the effects of the eigen functions towards luminosity variations.

References

Aerts, C. (1996a). "Mode identification of pulsating stars from line-profile variations with the moment method: a more accurate discriminant." In: 314, pp. 115–122.

— (1996b). "Mode identification of pulsating stars from line-profile variations with the moment method: a more accurate discriminant." In: 314, pp. 115–122.

Aerts, C., J. Christensen-Dalsgaard, and D. W. Kurtz (2010). *Asteroseismology*.

Aerts, C., M. de Pauw, and C. Waelkens (1992). "Mode identification of pulsating stars from line profile variations with the moment method. an example - The Beta Cephei star Delta Ceti". In: 266, pp. 294–306.

Aerts, C. and L. Eyer (2000a). "Mode Identification from Line-Profile Variations". In: *Delta Scuti and Related Stars*. Ed. by M. Breger and M. Montgomery. Vol. 210. Astronomical Society of the Pacific Conference Series, p. 113. eprint: `astro-ph/0002349`.

— (2000b). "Mode Identification from Line-Profile Variations". In: *Delta Scuti and Related Stars*. Ed. by M. Breger and M. Montgomery. Vol. 210. Astronomical Society of the Pacific Conference Series, p. 113. eprint: `astro-ph/0002349`.

Aizenman, M. L. (1980). "The stability of the beta Cephei stars". In: *Nonradial and Nonlinear Stellar Pulsation*. Ed. by H. A. Hill and W. A. Dziembowski. Vol. 125. Lecture Notes in Physics, Berlin Springer Verlag, pp. 76–95.

Alexander, D. R. et al. (2003). "Opacities of Molecules and Dust". In: *Stellar Atmosphere Modeling*. Ed. by I. Hubeny, D. Mihalas, and K. Werner. Vol. 288. Astronomical Society of the Pacific Conference Series, p. 289.

Arfken, G. B. and H. J. Weber (2005). *Mathematical methods for physicists 6th ed.*

Baglin, A. et al. (2002). "COROT: asteroseismology and planet finding". In: *Stellar Structure and Habitable Planet Finding*. Ed. by B. Battrick et al. Vol. 485. ESA Special Publication, pp. 17–24.

Baker, N. and R. Kippenhahn (1962). "The Pulsations of Models of δ Cephei Stars. With 17 Figures in the Text". In: 54, p. 114.

Balmforth, N. J., D. O. Gough, and W. J. Merryfield (1990). "Pulsations of model Mira variables". In: *From Miras to Planetary Nebulae: Which Path for Stellar Evolution?* Ed. by M. O. Mennessier and A. Omont, pp. 85–87.

Balmforth, N. J. et al. (2000). "Excitation Mechanism in roAp Stars". In: *IAU Colloq. 176: The Impact of Large-Scale Surveys on Pulsating Star Research*. Ed. by L. Szabados and D. Kurtz. Vol. 203. Astronomical Society of the Pacific Conference Series, pp. 453–454.

— (2001). "On the excitation mechanism in roAp stars". In: 323, pp. 362–372.

Balona, L. A. (1986a). "Mode identification from line profile variations". In: 219, pp. 111–129.

— (1986b). "Mode identification from line profile variations. II - A quantitative least-squares algorithm". In: 220, pp. 647–656.

— (2010). *Challenges In Stellar Pulsation*.

— (2013). "Long periods in two Kepler roAp stars". In: 436, pp. 1415–1421.

Balona, L. A., K. Krisciunas, and A. W. J. Cousins (1994). "Gamma-Doradus - Evidence for a New Class of Pulsating Star". In: 270, p. 905.

Balona, L. A. and R. S. Stobie (1979a). "The effect of radial and non-radial stellar oscillations on the light, colour and velocity variations". In: 189, pp. 649–658.

— (1979b). "Wesselink radii of double-mode cepheids". In: 189, pp. 659–666.

Balona, L. A. et al. (2011a). "Kepler observations of the variability in B-type stars". In: 413, pp. 2403–2420. arXiv: 1103.0644 [astro-ph.SR].

Balona, L. A. et al. (2011b). "The Kepler view of γ Doradus stars". In: 415, pp. 3531–3538.

Balona, L. A. et al. (2013). "Kepler observations of the open cluster NGC 6819". In: 430, pp. 3472–3482.

Bautista, M. A. (1997). "Atomic data from the IRON Project. XX. Photoionization cross sections and oscillator strengths for Fe I". In: 122.

Bedding, T. R. (2014). "Solar-like oscillations: An observational perspective". In: *Asteroseismology*. Ed. by P. L. Pallé and C. Esteban, p. 60.

Bedding, T. R. and H. Kjeldsen (2003). "Solar-like Oscillations". In: 20, pp. 203–212. eprint: astro-ph/0305425.

Bedding, T. R. et al. (1998). "Mode switching in the nearby Mira-like variable R Doradus". In: 301, pp. 1073–1082. eprint: astro-ph/9808322.

Bedding, T. R. et al. (2010). "Solar-like Oscillations in Low-luminosity Red Giants: First Results from Kepler". In: 713, pp. L176–L181. arXiv: 1001.0229 [astro-ph.SR].

Bersier, D., G. Burki, and M. Burnet (1994). "Fundamental parameters of Cepheids. I. Photometric data in the Geneva system." In: 108, pp. 9–24.

Bigot, L. and W. A. Dziembowski (2002). "The oblique pulsator model revisited". In: 391, pp. 235–245.

Bond, H. E., R. Ciardullo, and S. D. Kawaler (1993). "Asteroseismology of planetary nebula nuclei". In: 43, pp. 425–430.

Bond, H. E. and M. G. Meakes (1990). "The pulsating nucleus of the planetary nebula Longmore 4". In: 100, pp. 788–792.

Bono, G. and M. Marconi (1997). "RR Lyrae variables." In: *IAU Symposium*. Ed. by T. R. Bedding, A. J. Booth, and J. Davis. Vol. 189. IAU Symposium, pp. 305–310.

Borucki, W. J. and D. G. Koch (2011). "Kepler mission highlights". In: *IAU Symposium*. Ed. by A. Sozzetti, M. G. Lattanzi, and A. P. Boss. Vol. 276. IAU Symposium, pp. 34–43.

Bouabid, M.-P. et al. (2010). "Theoretical study of γ Doradus pulsations in pre-main sequence stars". In: *Astronomische Nachrichten* 331, p. 1044. arXiv: 1007.2746 [astro-ph.SR].

Brassard, P. et al. (2001). "Discovery and Asteroseismological Analysis of the Pulsating sdB Star PG 0014+067". In: 563, pp. 1013–1030.

Breger, M. (1972). "Pre-Main Stars. I. Light Variability, Shells, and Pulsation in NGC 2264". In: 171, p. 539.

— (1979). "Delta Scuti and related stars". In: 91, pp. 5–26.

— (1995). "Astrophysical Applications of Delta Scuti Stars". In: *IAU Colloq. 155: Astrophysical Applications of Stellar Pulsation*. Ed. by R. S. Stobie and P. A. Whitelock. Vol. 83. Astronomical Society of the Pacific Conference Series, p. 70.

— (2000). "Amplitude Variability of Delta Scuti Stars: 4 CVn". In: *IAU Colloq. 176: The Impact of Large-Scale Surveys on Pulsating Star Research*. Ed. by L. Szabados and D. Kurtz. Vol. 203. Astronomical Society of the Pacific Conference Series, pp. 421–425.

Buta, R. J. and M. A. Smith (1979). "The light variations of nonradial pulsators - Theory and application to the line profile variable 53 Persei". In: 232, pp. 213–235.

Buzasi, D. L. (2000). "Experiment Design and Data Reduction for Seismology: Lessons Learned from WIRE". In: *The Third MONS Workshop: Science Preparation and Target Selection*. Ed. by T. Teixeira and T. Bedding, p. 9.

Campos, A. J. and M. A. Smith (1980a). "Pulsational mode-typing in line profile variables. I - Four Beta Cephei stars". In: 238, pp. 250–265.

— (1980b). "Pulsational mode-typing in line profile variables. II - rho Puppis and delta Scuti". In: 238, pp. 667–673.

Carbon, D. F. and O. Gingerich (1969). "The Grid of Model Stellar Atmospheres from 4000deg *to*10, 000deg In: *Theory and Observation of Normal Stellar Atmospheres*. Ed. by O. Gingerich, p. 377.

Cardona, O., E. Simonneau, and L. Crivellari (2009). "Method for Calculating the Opacity of the Atomic Lines in Stellar Atmospheres". In: 690, pp. 1378–1385.

Carson, T. R. (1976). "Stellar opacity". In: 14, pp. 95–117.

Castelli, F. (2005). "ATLAS12: how to use it". In: *Memorie della Societa Astronomica Italiana Supplementi* 8, p. 25.

Castelli, F. and R. L. Kurucz (2004). "New Grids of ATLAS9 Model Atmospheres". In: *ArXiv Astrophysics e-prints*. eprint: astro-ph/0405087.

Castor, J. I. (1968). "A Simplified Picture of the Cepheid Phase Lag". In: 154, p. 793.

— (1971). "On the Calculation of Linear, Nonadiabatic Pulsations of Stellar Models". In: 166, p. 109.

Catelan, M. and H. A. Smith (2015). *Pulsating Stars*.

Catelan, M. and H.A. Smith (2015). *Pulsating Stars*. Wiley. ISBN: 9783527655205. URL: https://books

Chapellier, E. et al. (1998). "53 Persei: a slowly pulsating B star". In: 331, pp. 1046–1050.

Chaplin, W. J. and A. Miglio (2013). "Asteroseismology of Solar-Type and Red-Giant Stars". In: 51, pp. 353–392. arXiv: 1303.1957 [astro-ph.SR].

Chaplin, W. J. et al. (2010). "The Asteroseismic Potential of Kepler: First Results for Solar-Type Stars". In: 713, pp. L169–L175. arXiv: 1001.0506 [astro-ph.SR].

Charpinet, S. et al. (2005). "The Asteroseismic Analysis of the EC14026 Star PG 0014+067 Revisited". In: *14th European Workshop on White Dwarfs*. Ed. by D. Koester and S. Moehler. Vol. 334. Astronomical Society of the Pacific Conference Series, p. 619.

Chiosi, C. (1990). "The evolution of the Cepheid stars". In: *Confrontation Between Stellar Pulsation and Evolution*. Ed. by C. Cacciari and G. Clementini. Vol. 11. Astronomical Society of the Pacific Conference Series, pp. 158–192.

Chiosi, C., G. Bertelli, and A. Bressan (1992). "New developments in understanding the HR diagram". In: 30, pp. 235–285.

Christensen-Dalsgaard, J. and S. Frandsen (1983a). "Radiative transfer and solar oscillations /Invited review/". In: 82, pp. 165–204.

— (1983b). "Radiative transfer and solar oscillations /Invited review/". In: 82, pp. 165–204.

Christensen-Dalsgaard, J., H. Kjeldsen, and J. A. Mattei (2001). "Solar-like Oscillations of Semiregular Variables". In: 562, pp. L141–L144. eprint: astro-ph/0110475.

Christy, R. F. (1966). "Pulsation Theory". In: 4, p. 353.

Clayton, G. (1996a). "Observational properties of dust shells of R Coronae Borealis stars". In: *Hydrogen Deficient Stars*. Ed. by C. S. Jeffery and U. Heber. Vol. 96. Astronomical Society of the Pacific Conference Series, p. 63.

— (2009a). "The Evolutionary History of the R Coronae Borealis Stars". In: *APS Southeastern Section Meeting Abstracts*, H3.

Clayton, G. C. (1996b). "The R Coronae Borealis Stars". In: 108, p. 225.

Clayton, G. C. (2009b). "The Evolution of R Coronae Borealis Stars". In: *Journal of the American Association of Variable Star Observers (JAAVSO)* 37, p. 195.

— (2012). "What Are the R Coronae Borealis Stars?" In: *Journal of the American Association of Variable Star Observers (JAAVSO)* 40, p. 539. arXiv: 1206.3448 [astro-ph.SR].

Clayton, G. C., B. A. Whitney, and W. A. Lawson (1995). "Pulsations and Dust Formation in R Coronae Borealis Stars". In: *IAU Colloq. 155: Astrophysical Applications of Stellar Pulsation*. Ed. by R. S. Stobie and P. A. Whitelock. Vol. 83. Astronomical Society of the Pacific Conference Series, p. 433.

Collins, G. W. (1989). *The fundamentals of stellar astrophysics*.

Cousins, A. W. J. and P. R. Warren (1963). "Variable Stars Observed During the Cape Bright Star Programme". In: *Monthly Notes of the Astronomical Society of South Africa* 22, p. 65.

Cox, A. N. (1965). "Stellar Opacities". In: *Leaflet of the Astronomical Society of the Pacific* 9, p. 297.

— (1974a). "Recent progress in linear and non-linear calculations of radial stellar pulsation". In: *Stellar Instability and Evolution*. Ed. by P. Ledoux, A. Noels, and A. W. Rodgers. Vol. 59. IAU Symposium, pp. 39–46.

Cox, A. N. and J. N. Stewart (1962). "Effects of Bound-Bound Absorption on Stellar Opacities." In: 67, p. 113.

— (1965). "Radiative and Conductive Opacities for Eleven Astrophysical Mixtures." In: 11, p. 22.

— (1970a). "Rosseland Opacity Tables for Population i Compositions". In: 19, p. 243.

— (1970b). "Rosseland Opacity Tables for Population II Compositions". In: 19, p. 261.

Cox, A. N., J. N. Stewart, and D. D. Lilers (1965). "Effects of Bound-Bound Absorption on Stellar Opacities." In: 11, p. 1.

Cox, A. N. and J. E. Tabor (1976). "Radiative opacity tables for 40 stellar mixtures". In: 31, pp. 271–312.

Cox, J. P. (1963). "On Second Helium Ionization as a Cause of Pulsational Instability in Stars." In: 138, p. 487.

— (1974b). "Pulsating stars". In: *Reports on Progress in Physics* 37, pp. 563–698.

— (1974c). "Pulsating stars." In: *Reports on Progress in Physics* 37, pp. 356–698.

— (1975). "Stellar oscillations, stellar stability and application to variable stars". In: *Memoires of the Societe Royale des Sciences de Liege* 8, pp. 129–159.

— (1980). *Theory of stellar pulsation*.

Cox, J. P. and C. A. Whitney (1963). "Comments on Zhevakin's Paper, "One Common Error in the Theory of Stellar Variability"". In: 7, p. 139.

Cugier, H. (2012). "Testing the opacity and equation of state of LTE and non-LTE model atmospheres with OPAL and OP data for early-type stars". In: 547, A42, A42.

Cugier, H., W. A. Dziembowski, and A. A. Pamyatnykh (1994). "Nonadiabatic observables in beta Cephei models". In: 291, pp. 143–154.

Cunha, M. S. (2002a). "A theoretical instability strip for rapidly oscillating Ap stars". In: 333, pp. 47–54.

— (2002b). "Pulsations in roAp Stars (invited paper)". In: *IAU Colloq. 185: Radial and Nonradial Pulsationsn as Probes of Stellar Physics*. Ed. by C. Aerts, T. R. Bedding, and J. Christensen-Dalsgaard. Vol. 259. Astronomical Society of the Pacific Conference Series, p. 272.

Cunha, M. S. et al. (2007). "Asteroseismology and interferometry". In: 14, pp. 217–360. arXiv: 0709.4613.

Daszyńska-Daszkiewicz, J., W. A. Dziembowski, and A. A. Pamyatnykh (2003). "Constraints on stellar convection from multi-colour photometry of delta Scuti stars". In: 407, pp. 999–1006. eprint: astro-ph/0305539.

De Cat, P. (2001). "An observational study of bright southern slowly pulsating B stars". PhD thesis. Institute of Astronomy, Katholieke Universiteit Leuven, Belgium.

De Cat, P. et al. (2005). "A study of bright southern slowly pulsating B stars. III. Mode identification for singly-periodic targets in spectroscopy". In: 432, pp. 1013–1024.

De Cat, P. et al. (2006). "A spectroscopic study of southern (candidate) γ Doradus stars. I. Time series analysis". In: 449, pp. 281–292. eprint: astro-ph/0511207.

de Pauw, M., C. Aerts, and C. Waelkens (1993a). "Mode identification of pulsating stars from line profile variations with the moment method. A theoretical study of the accuracy of the method". In: 280, pp. 493–507.

— (1993b). "Mode identification of pulsating stars from line profile variations with the moment method. A theoretical study of the accuracy of the method". In: 280, pp. 493–507.

De Ridder, J., C. Aerts, and M.-A. Dupret (2004). "Mode identification using photometry and spectroscopy". In: *IAU Colloq. 193: Variable Stars in the Local Group*. Ed. by D. W. Kurtz and K. R. Pollard. Vol. 310. Astronomical Society of the Pacific Conference Series, p. 466.

De Ridder, J. et al. (2004). "Asteroseismology of the β Cephei star ν Eridani - III. Extended frequency analysis and mode identification". In: 351, pp. 324–332.

Dolez, N. and D. O. Gough (1982). "On the Problem of Interpreting Rapidly Oscillating Ap-Stars". In: *Pulsations in Classical and Cataclysmic Variable Stars*. Ed. by J. P. Cox and C. J. Hansen, p. 248.

Dupret, M.-A. et al. (2002). "Influence of non-adiabatic temperature variations on line profile variations of slowly rotating beta Cep stars and SPBs. I. Non-adiabatic eigenfunctions in the atmosphere of a pulsating star". In: 385, pp. 563–571.

Dupret, M.-A. et al. (2003a). "A photometric mode identification method, including an improved non-adiabatic treatment of the atmosphere". In: 398, pp. 677–685. eprint: astro-ph/0211395.

Dupret, M.-A. et al. (2003b). "An Improved Method of Photometric Mode Identification: Applications to Slowly Pulsating B, β Cephei, δ Scuti and γ Doradus Stars". In: 284, pp. 129–132.

Dupret, M.-A. et al. (2006). "Theoretical Aspects of g-mode Pulsations in gamma Doradus Stars". In: 77, p. 366.

Dziembowski, W. (1977). "Light and radial velocity variations in a nonradially oscillating star". In: 27, pp. 203–211.

Dziembowski, W. and P. R. Goode (1985). "Frequency splitting in AP stars". In: 296, pp. L27–L30.

Dziembowski, W. A. and S. Cassisi (1999). "Nonradial Modes in RR LYR Stars". In: 49, pp. 371–382. eprint: astro-ph/9907414.

Dziembowski, W. A. and P. R. Goode (1996). "Magnetic Effects on Oscillations in roAp Stars". In: 458, p. 338.

Dziembowski, W. A., P. Moskalik, and A. A. Pamyatnykh (1993). "The Opacity Mechanism in B-Type Stars - Part Two - Excitation of High-Order G-Modes in Main Sequence Stars". In: 265, p. 588.

Dziembowski, W. A. and A. A. Pamiatnykh (1993). "The opacity mechanism in B-type stars. I - Unstable modes in Beta Cephei star models". In: 262, pp. 204–212.

Eddington, A. S. (1917). "The pulsation theory of Cepheid variables". In: *The Observatory* 40, pp. 290–293.

— (1918a). "Stars, Gaseous, On the pulsations of a gaseous star". In: 79, pp. 2–22.

Eddington, A. S. (1918b). "Stars, Gaseous, On the pulsations of a gaseous star". In: 79, pp. 2–22.
— (1919). "The problem of the Cepheid variables". In: 79, p. 177.
— (1926). *The Internal Constitution of the Stars*.
Edgar, J. A. (1933). "The pulsation theory of Cepheid Variables". In: 93, pp. 422–441.
Feast, M., P. Whitelock, and J. Menzies (2002). "Globular clusters and the Mira period-luminosity relation". In: 329, pp. L7–L12. eprint: astro-ph/0111108.
Feast, M. W. (1975). "The R Coronae Borealis type variables". In: *Variable Stars and Stellar Evolution*. Ed. by V. E. Sherwood and L. Plaut. Vol. 67. IAU Symposium, pp. 129–141.
Fox-Machado, L. and E. Pérez Pérez (2017). "A seismic analysis of the δ Scuti star KIC 6951642 observed with KEPLER". In: *Revista Mexicana de Astronomia y Astrofisïca Conference Series*. Vol. 49. Revista Mexicana de Astronomia y Astrofisica Conference Series, pp. 87–87.
Garrido, R. (2000). "Photometric Modal Discrimination in δ Scuti and γ Doradus Stars". In: *Delta Scuti and Related Stars*. Ed. by M. Breger and M. Montgomery. Vol. 210. Astronomical Society of the Pacific Conference Series, p. 67. eprint: astro-ph/0001064.
Garrido, R., E. Garcia-Lobo, and E. Rodriguez (1990). "Modal discrimination of pulsating stars by using Stromgren photometry". In: 234, pp. 262–268.
Gautschy, A. (1997). "The development of the theory of stellar pulsations". In: *Vistas in Astronomy* 41, pp. 95–115.
Gautschy, A. and H. Saio (1995). "Stellar Pulsations Across The HR Diagram: Part 1". In: 33, pp. 75–114.
— (1996a). "Stellar Pulsations Across the HR Diagram: Part 2". In: 34, pp. 551–606.
— (1996b). "Stellar Pulsations Across the HR Diagram: Part 2". In: 34, pp. 551–606.
Gautschy, A., H. Saio, and H. Harzenmoser (1998). "How to drive roAp stars". In: 301, pp. 31–41. eprint: astro-ph/9806290.
Gingold, R. A. (1976). "The evolutionary status of Population II Cepheids". In: 204, pp. 116–130.
Goode, P. R. and L. H. Strous (1996). "Observation of the excitation of solar oscillations". In: *Bulletin of the Astronomical Society of India* 24, p. 223.
Grauer, A. D. and H. E. Bond (1984). "The pulsating central star of the planetary nebula Kohoutek 1-16". In: 277, pp. 211–215.
Green, E. M. et al. (2003). "Discovery of A New Class of Pulsating Stars: Gravity-Mode Pulsators among Subdwarf B Stars". In: 583, pp. L31–L34.
Grigahcène, A. et al. (2010). "Kepler observations: Light shed on the hybrid γ Doradus - δ Scuti pulsation phenomenon". In: *Astronomische Nachrichten* 331, p. 989.
Gustafsson, B. et al. (1975). "A grid of model atmospheres for metal-deficient giant stars. I". In: 42, pp. 407–432.
Guzik, J. A. et al. (2000a). "Driving g-mode Pulsations in Gamma Doradus Variables". In: *IAU Colloq. 176: The Impact of Large-Scale Surveys on Pulsating Star Research*. Ed. by L. Szabados and D. Kurtz. Vol. 203. Astronomical Society of the Pacific Conference Series, pp. 445–446.
— (2000b). "Driving the Gravity-Mode Pulsations in γ Doradus Variables". In: 542, pp. L57–L60.
Handler, G. (1999). "The domain of γ Doradus variables in the Hertzsprung-Russell diagram". In: 309, pp. L19–L23.
— (2005). "Five New beta Cephei Stars Revealed in ASAS Photometry". In: *Information Bulletin on Variable Stars* 5667, p. 1.
— (2006). "Observational aspects of asteroseismology". In: *Communications in Asteroseismology* 147, pp. 31–39.

Handler, G. and R. R. Shobbrook (2002). "On the relationship between the δ Scuti and γ Doradus pulsators". In: 333, pp. 251–262. eprint: astro-ph/0202152.

Handler, G. et al. (1997). "Variable central stars of young planetary nebulae. I. Photometric multi-site observations of IC 418." In: 320, pp. 125–135.

Hareter, M. et al. (2008). "MOST discovers a multimode δ Scuti star in a triple system: HD 61199". In: 492, pp. 185–195. arXiv: 0810.3529.

Heynderickx, D. and U. Haug (1994). "A new frequency analysis of photometric observations of the β Cephei star IL Velorum". In: 106, pp. 79–85.

Heynderickx, D., C. Waelkens, and P. Smeyers (1994). "A photometric study of β Cephei stars. II. Determination of the degrees L of pulsation modes". In: 105, pp. 447–480.

Hine III, B. P. and R. E. Nather (1987). "A search for pulsations in planetary nebulae nuclei". In: *IAU Colloq. 95: Second Conference on Faint Blue Stars*. Ed. by A. G. D. Philip, D. S. Hayes, and J. W. Liebert, pp. 619–621.

Hoffleit, D. (1997). "History of the Discovery of Mira Stars". In: *Journal of the American Association of Variable Star Observers (JAAVSO)* 25, pp. 115–136.

Holdsworth, D. L. et al. (2014). "KIC 7582608: a new Kepler roAp star with frequency variability". In: 443, pp. 2049–2062. arXiv: 1406.7680 [astro-ph.SR].

Houdek, G. (1996). "Pulsation of Solar-type stars". PhD thesis. "Ph.D. Thesis, Formal- und Naturwisseschaftliche Fakult"at der Universität Wien, (1996)".

— (2003). "Excitation Mechanisms in roAp Stars". In: *Magnetic Fields in O, B and A Stars: Origin and Connection to Pulsation, Rotation and Mass Loss*. Ed. by L. A. Balona, H. F. Henrichs, and R. Medupe. Vol. 305. Astronomical Society of the Pacific Conference Series, p. 45.

— (2012). "Excitation of Stellar Pulsations". In: *Progress in Solar/Stellar Physics with Helio- and Asteroseismology*. Ed. by H. Shibahashi, M. Takata, and A. E. Lynas-Gray. Vol. 462. Astronomical Society of the Pacific Conference Series, p. 7. arXiv: 1201.0194 [astro-ph.SR].

Houdek, G. and D. O. Gough (2007). "An asteroseismic signature of helium ionization". In: 375, pp. 861–880. eprint: astro-ph/0612030.

Houdek, G. et al. (1999a). "Amplitudes of stochastically excited oscillations in main-sequence stars". In: 351, pp. 582–596. eprint: astro-ph/9909107.

— (1999b). "Amplitudes of stochastically excited oscillations in main-sequence stars". In: 351, pp. 582–596. eprint: astro-ph/9909107.

Hubeny, I. (1997). "Stellar Atmosphers Theory: an Introduction". In: *Stellar Atmospheres: Theory and Observations*. Ed. by J. P. De Greve, R. Blomme, and H. Hensberge. Vol. 497. Lecture Notes in Physics, Berlin Springer Verlag, p. 1.

Hubeny, I. and D. Mihalas (2014). *Theory of Stellar Atmospheres: An Introduction to Astrophysical Non-Equilibrium Quantitative Spectroscopic Analysis*. Princeton University Press. Princeton University Press. ISBN: 9780691163291. URL: https://books.google.co.za/books?id=lQ

Hutton, R. G. and R. H. Mendez (1993). "The central stars of He 2-131 and He 2-138 - Photometric variations". In: 267, pp. L8–L10.

Iglesias, C. A., F. J. Rogers, and B. G. Wilson (1987). "Reexamination of the metal contribution to astrophysical opacity". In: 322, pp. L45–L48.

— (1992). "Spin-orbit interaction effects on the Rosseland mean opacity". In: 397, pp. 717–728.

Ita, Y. et al. (2006). "Search for SiO masers in nearby Miras pulsating in the first overtone mode ." In: 77, p. 85. eprint: astro-ph/0511024.

Joshi, S. and Y. C. Joshi (2015). "Asteroseismology of Pulsating Stars". In: *Journal of Astrophysics and Astronomy*.

Jurcsik, J. et al. (2006). "The triple-mode pulsating variable V823 Cassiopeiae". In: 445, pp. 617–625. eprint: astro-ph/0508646.

Kaler, J. B. (1983). "A photometric survey of compact and selected planetary nebulae". In: 264, pp. 594–598.

Karoff, C. et al. (2007). "Identification of Variable Stars in COROT's First Main Observing Field (LRc1)". In: 134, pp. 766–777. arXiv: 0909.4797 [astro-ph.SR].

Kawaler, S. D. et al. (1986). "The helium shell game - Nonradial g-mode instabilities in hydrogen-deficient planetary nebula nuclei". In: 306, pp. L41–L44.

Kaye, A. B. et al. (1999a). "Gamma Doradus Stars: Defining a New Class of Pulsating Variables". In: 111, pp. 840–844. eprint: astro-ph/9905042.

Kaye, A. B. et al. (1999b). "HD 62454 and HD 68192: Two New γ Doradus Variables". In: 118, pp. 2997–3005.

Kennelly, E. J. et al. (1998). "The Oscillations of Tau Pegasi". In: 495, pp. 440–457.

Kerschbaum, F. and J. Hron (1992). "Semiregular variables of types SRa and SRb - Basic properties in the visual and the IRAS-range". In: 263, pp. 97–112.

Kilkenny, D. et al. (1997). "A new class of rapidly pulsating star - I. EC 14026-2647, the class prototype". In: 285, pp. 640–644.

King, D. S. and J. P. Cox (1968). "Pulsating Stars". In: 80, p. 365.

Kiriakidis, M., M. F. El Eid, and W. Glatzel (1992). "Heavy element opacities and the pulsations of Beta Cepheid stars". In: 255, 1P–5P.

Kjeldsen, H. and T. R. Bedding (1995). "Amplitudes of stellar oscillations: the implications for asteroseismology." In: 293, pp. 87–106. eprint: astro-ph/9403015.

Koch, D. et al. (2010a). "The Kepler Mission and Early Results". In: *38th COSPAR Scientific Assembly*. Vol. 38. COSPAR Meeting, p. 2513.

Koch, D. G. et al. (2010b). "Kepler Mission Design, Realized Photometric Performance, and Early Science". In: 713, L79, pp. L79–L86. arXiv: 1001.0268 [astro-ph.EP].

Kolenberg, K. et al. (2010a). "First Kepler Results on RR Lyrae Stars". In: 713, pp. L198–L203. arXiv: 1001.0417 [astro-ph.SR].

— (2010b). "First Kepler Results on RR Lyrae Stars". In: 713, pp. L198–L203. arXiv: 1001.0417 [astro-ph.SR].

Kuczawska, E. and S. Zola (1995). "Pulsations in the Nucleus of Planetary Nebula IC 418?" In: *IAU Colloq. 155: Astrophysical Applications of Stellar Pulsation*. Ed. by R. S. Stobie and P. A. Whitelock. Vol. 83. Astronomical Society of the Pacific Conference Series, p. 443.

Kurtz, D. W. (1982). "Rapidly oscillating AP stars". In: 200, pp. 807–859.

— (1990a). "Oscillations in roAp Stars". In: *Progress of Seismology of the Sun and Stars*. Ed. by Y. Osaki and H. Shibahashi. Vol. 367. Lecture Notes in Physics, Berlin Springer Verlag, p. 373.

— (1990b). "Rapidly oscillating AP stars". In: 28, pp. 607–655.

— (2006). "Stellar Pulsation: an Overview". In: *Astrophysics of Variable Stars*. Ed. by C. Aerts and C. Sterken. Vol. 349. Astronomical Society of the Pacific Conference Series, p. 101.

Kurtz, D. W. and F. Marang (1995). "The discovery of delta Scuti pulsational variability in the pre-main-sequence Herbig AE star, HR 5999, and the discovery of rotational light variability in the remarkable He-weak BP star, HR 6000". In: 276, pp. 191–198.

Kurucz, R. L. (1970b). *Atlas: A computer program for calculating model stellar atmospheres*.

— (1970a). "Atlas: a Computer Program for Calculating Model Stellar Atmospheres". In: *SAO Special Report* 309.

— (1979). "Model atmospheres for G, F, A, B, and O stars". In: 40, pp. 1–340.

Kurucz, R. L. and B. Bell (1995). *Atomic line list*.

LeBlanc, F. (2010). *An Introduction to Stellar Astrophysics.*

Lebzelter, T. and M. Obbrugger (2009). "How semiregular are irregular variables?" In: *Astronomische Nachrichten* 330, p. 390. arXiv: 0902.4096 [astro-ph.SR].

Li, Y. (1992a). "Bisystem Oscillation Theory of Stars - Part Two - Excitation Mechanisms". In: 257, p. 145.

— (1992b). "Bisystem oscillation theory of stars. I - Linear theory. II - Excitation mechanisms". In: 257, pp. 133–152.

Liakos, A. and P. Niarchos (2016). "Poetry in Motion: Asteroseismology of Delta Scuti Stars in Binaries using Kepler Data". In: *ArXiv e-prints*. arXiv: 1606.08638 [astro-ph.SR].

Madore, B. F. (1977). "The frequency of Cepheids with companions: a photoelectric approach." In: 178, pp. 505–511.

Magic, Z. et al. (2013). "The Stagger-grid: A grid of 3D stellar atmosphere models. I. Methods and general properties". In: 557, A26, A26. arXiv: 1302.2621 [astro-ph.SR].

Mantegazza, L. (2000). "Mode Detection from Line-Profile Variations". In: *Delta Scuti and Related Stars*. Ed. by M. Breger and M. Montgomery. Vol. 210. Astronomical Society of the Pacific Conference Series, p. 138.

Martinez, P. and D. W. Kurtz (1990). "Two New Southern Rapidly Oscillating Ap Stars - HD 193756 and HD 218495". In: *Information Bulletin on Variable Stars* 3509, p. 1.

Mathews, J. and R. L. Walker (1970). *Mathematical methods of physics.*

Matthews, J. (2005). "A suitcase full of astrophysics: The MOST microsat and opportunities for low-cost space astronomy". In: *Astrometry in the Age of the Next Generation of Large Telescopes*. Ed. by P. K. Seidelmann and A. K. B. Monet. Vol. 338. Astronomical Society of the Pacific Conference Series, p. 297.

Matthews, J. M. (1988). "A possible mechanism for exciting pulsation in cool AP stars". In: 235, 7P–11P.

— (2007). "One small satellite, so many light curves: Examples of δ Scuti asteroseismology from the MOST space mission^1". In: *Communications in Asteroseismology* 150, p. 333.

Medupe, R., J. Christensen-Dalsgaard, and D. W. Kurtz (2002). "Applications of Non-Adiabatic Radial Pulsation Equations to roAp Stars". In: *IAU Colloq. 185: Radial and Nonradial Pulsationsn as Probes of Stellar Physics*. Ed. by C. Aerts, T. R. Bedding, and J. Christensen-Dalsgaard. Vol. 259. Astronomical Society of the Pacific Conference Series, p. 296.

Medupe, R., J. Christensen-Dalsgaard, and M. Phorah (2009). "Radial Pulsations in A Stars: the Effects of Opacity Fluctuations in their Atmospheres". In: *American Institute of Physics Conference Series*. Ed. by J. A. Guzik and P. A. Bradley. Vol. 1170. American Institute of Physics Conference Series, pp. 506–511.

Medupe, R., D. W. Kurtz, and J. Christensen-Dalsgaard (2000). "Studies of Non-adiabatic Effects on Radial Pulsations in the Atmospheres of Rapidly Oscillating Ap Stars". In: *IAU Colloq. 176: The Impact of Large-Scale Surveys on Pulsating Star Research*. Ed. by L. Szabados and D. Kurtz. Vol. 203. Astronomical Society of the Pacific Conference Series, pp. 451–452.

Mendez, R. H., A. D. Verga, and A. Kriner (1983). "The Photometric and Radial Velocity Variations of the Central Star of the Planetary Nebula IC4187". In: 8, p. 175.

Mihalas, D. (1978). *Stellar atmospheres /2nd edition/.*

— (2001). "Fifty Years of Research on Stellar Atmospheres". In: 18, pp. 311–316.

Milne, E. A. (1929). "Bakerian Lecture: The Structure and Opacity of a Stellar Atmosphere". In: *Philosophical Transactions of the Royal Society of London Series A* 228, pp. 421–461.

Moskalik, P. (1995). "Cepheid Variables: Period Ratios and Mass Determination". In: *Astrophysical Applications of Powerful New Databases*. Ed. by S. J. Adelman and W. L. Wiese. Vol. 78. Astronomical Society of the Pacific Conference Series, p. 225.

Moskalik, P. and W. A. Dziembowski (1992). "New opacities and the origin of the Beta Cephei pulsation". In: 256, pp. L5–L8.

Nordlund, Å., R. F. Stein, and M. Asplund (2009). "Solar Surface Convection". In: *Living Reviews in Solar Physics* 6.

Olech, A. and P. Moskalik (2009). "Double mode RR Lyrae stars in Omega Centauri". In: 494, pp. L17–L20. arXiv: 0812.4173.

Olech, A. et al. (1999). "RR Lyrae Variables in the Globular Cluster M55. The First Evidence for Nonradial Pulsations in RR Lyrae Stars". In: 118, pp. 442–452. eprint: astro-ph/9812302.

Osaki, Y. (1971). "Non-Radial Oscillations and the Beta Canis Majoris Phenomenon". In: 23, p. 485.

Pamyatnykh, A. A. (1999). "Pulsational Instability Domains in the Upper Main Sequence". In: 49, pp. 119–148.

Patriarchi, P. and M. Perinotto (1997). "Wind variability in central stars of planetary nebulae. II." In: 126, pp. 385–391.

Percy, J. R. (2007). *Understanding Variable Stars*.

Pesnell, W. D. (1987). "A new driving mechanism for stellar pulsations". In: 314, pp. 598–604.

Petersen, J. O. (1973). "Masses of double mode cepheid variables determined by analysis of period ratios." In: 27, pp. 89–93.

Petersen, J. O. and J. Christensen-Dalsgaard (1999). "Pulsation models of delta Scuti variables. II. delta Scuti stars as precise distance indicators". In: 352, pp. 547–554.

Poretti, E. et al. (2002a). "Asteroseismology from space: The delta Scuti star theta ^{2} Tauri monitored by the WIRE satellite". In: 382, pp. 157–163. eprint: astro-ph/0111361.

— (2002b). "Asteroseismology from Space: WIRE Monitoring of the δ Sct Star ^{2} Tauri". In: *IAU Colloq. 185: Radial and Nonradial Pulsationsn as Probes of Stellar Physics*. Ed. by C. Aerts, T. R. Bedding, and J. Christensen-Dalsgaard. Vol. 259. Astronomical Society of the Pacific Conference Series, p. 624.

Prialnik, D. (2000). *An Introduction to the Theory of Stellar Structure and Evolution*.

Prša, A. et al. (2011). "Kepler Eclipsing Binary Stars. I. Catalog and Principal Characterization of 1879 Eclipsing Binaries in the First Data Release". In: 141, 83, p. 83. arXiv: 1006.2815 [astro-ph.SR].

Querci, F., M. Querci, and T. Tsuji (1974). "Model Atmospheres for C Type Stars". In: 31, p. 265.

Randall, S. K. et al. (2005). "The Potential of Multicolor Photometry for Pulsating Subdwarf B Stars". In: 161, pp. 456–479. eprint: astro-ph/0507607.

Rauer, H. et al. (2014). "The PLATO 2.0 mission". In: *Experimental Astronomy* 38, pp. 249–330. arXiv: 1310.0696 [astro-ph.EP].

Rogers, F. J. and C. A. Iglesias (1994). "Astrophysical Opacity". In: *Science* 263, pp. 50–55.

— (1998). "Opacity of Stellar Matter". In: 85, pp. 61–70.

Rosseland, S. (1925a). "No. 296. The theory of the stellar absorption coefficient." In: *Contributions from the Mount Wilson Observatory / Carnegie Institution of Washington* 296, pp. 1–19.

— (1925b). "The Theory of the Stellar Absorption Coefficient". In: 61, p. 424.

— (1950). "On the luminosity-velocity relation of Cepheids". In: 110, p. 440.

Russell, H. N. (1914a). "Relations Between the Spectra and other Characteristics of the Stars. I. Historical". In: 93, pp. 227–230.

— (1914b). "Relations Between the Spectra and other Characteristics of the Stars. III." In: 93, pp. 281–286.

Saio, H. and J. P. Cox (1980). "Linear, nonadiabatic analysis of nonradial oscillations of massive near main sequence stars". In: 236, pp. 549–559.

Schuh, S. et al. (2006). "Exciting new features in the frequency spectrum of the EC 14026 star HS 0702+6043. Simultaneous g-modes and p-modes in a sdB pulsator". In: 77, p. 480. eprint: astro-ph/0510832.

Seaton, M. J. et al. (1994). "Opacities for Stellar Envelopes". In: 266, p. 805.

Shibahashi, H. (1983). "Magnetic overstability as an excitation mechanism of the rapid oscillations of AP stars". In: 275, pp. L5–L9.

Shibahashi, H. and M. Takata (1995). "Oblique Pulsator Model for the Blazhko Effect of RR Lyrae Stars". In: *IAU Colloq. 155: Astrophysical Applications of Stellar Pulsation*. Ed. by R. S. Stobie and P. A. Whitelock. Vol. 83. Astronomical Society of the Pacific Conference Series, p. 42.

Simon, N. R. (1982). "A plea for reexamining heavy element opacities in stars". In: 260, pp. L87–L90.

Smalley, B. et al. (2015). "KIC 4768731: a bright long-period roAp star in the Kepler field". In: 452, pp. 3334–3345. arXiv: 1507.01516 [astro-ph.SR].

Smith, M. A. (1977). "Nonradial pulsations in early to mid-B stars". In: 215, pp. 574–583.

Smith, M. A. et al. (1984). "Stable nonradial pulsations in 53 Persei from 1977 to 1983". In: 282, pp. 226–235.

Stamford, P. A. and R. D. Watson (1977). "Observational characteristics of simple radial and non-radial Beta Cephei models". In: 180, pp. 551–565.

— (1981). "Baade-Wesselink and related techniques for mode discrimination in nonradial stellar pulsations". In: 77, pp. 131–158.

Stankov, A. and G. Handler (2005). "Catalog of Galactic β Cephei Stars". In: 158, pp. 193–216. eprint: astro-ph/0506495.

Starrfield, S. et al. (1985). "An analysis of nonradial pulsations of the central star of the planetary nebula K1-16". In: 293, pp. L23–L27.

Starrfield, S. G. et al. (1983). "The discovery of nonradial instability strips for hot, evolved stars". In: 268, pp. L27–L32.

Stellingwerf, R. F. (1978). "Helium ionization driving in Beta Cephei stars". In: 83, pp. 1184–1189.

Stello, D. et al. (2010). "Detection of Solar-like Oscillations from Kepler Photometry of the Open Cluster NGC 6819". In: 713, pp. L182–L186. arXiv: 1001.0026 [astro-ph.SR].

Stibbs, D. W. N. (1950). "A study of the spectrum and magnetic variable star HD 125248". In: 110, p. 395.

Stothers, R. (1977). "On the rapid variability of central stars of planetary nebulae". In: 213, pp. 791–793.

Telting, J. H. and C. Schrijvers (1997). "Line-profile variations of non-radial adiabatic pulsations of rotating stars. II. The diagnostic value of amplitude and phase diagrams derived from time series of spectra." In: 317, pp. 723–741.

Toutain, T., G. Berthomieu, and J. Provost (1999). "Light perturbation from stellar nonradial oscillations: an application to solar oscillations". In: 344, pp. 188–198.

Toutain, T. and C. Froehlich (1992). "Characteristics of solar p-modes - Results from the IPHIR experiment". In: 257, pp. 287–297.

Toutain, T. and P. Gouttebroze (1993). "Visibility of solar p-modes". In: 268, pp. 309–318.

Trampedach, R. et al. (2013). "A Grid of Three-dimensional Stellar Atmosphere Models of Solar Metallicity. I. General Properties, Granulation, and Atmospheric Expansion". In: 769, 18, p. 18. arXiv: 1303.1780 [astro-ph.SR].

Ulrich, R. K. (1970). "The Five-Minute Oscillations on the Solar Surface". In: 162, p. 993.

Vögler, A., J. H. M. J. Bruls, and M. Schüssler (2004). "Approximations for non-grey radiative transfer in numerical simulations of the solar photosphere". In: 421, pp. 741–754.

Vogt, N. et al. (2016). "Determination of Pulsation Periods and Other Parameters of 2875 Stars Classified as MIRA in the All Sky Automated Survey (ASAS)". In: 227, 6, p. 6. arXiv: 1609.05246 [astro-ph.SR].

Waelkens, C. (1991). "Slowly pulsating B stars". In: 246, pp. 453–468.

Wallerstein, G. and A. N. Cox (1984). "The Population II Cepheids". In: 96, pp. 677–691.

Warner, P. B., A. B. Kaye, and J. A. Guzik (2003). "A Theoretical γ Doradus Instability Strip". In: 593, pp. 1049–1055.

Watson, R. D. (1987). "Colour changes in mid-B star variables". In: *Proceedings of the Astronomical Society of Australia* 7, pp. 38–41.

— (1988). "Contributing factors to flux changes in nonradial stellar pulsations". In: 140, pp. 255–290.

Whitelock, P. A. (1990). "Pulsating red variables". In: *Confrontation Between Stellar Pulsation and Evolution*. Ed. by C. Cacciari and G. Clementini. Vol. 11. Astronomical Society of the Pacific Conference Series, pp. 365–378.

Wood, P. R. (1995). "Mira Variables: Theory versus Observation". In: *IAU Colloq. 155: Astrophysical Applications of Stellar Pulsation*. Ed. by R. S. Stobie and P. A. Whitelock. Vol. 83. Astronomical Society of the Pacific Conference Series, p. 127.

Wood, P. R. and D. M. Zarro (1981). "Helium-shell flashing in low-mass stars and period changes in mira variables". In: 247, pp. 247–256.

Yungelson, L. R. and A. V. Tutukov (1997). "Family links between Planetary Nebulae, nuclei and cataclysmic variables, binary white dwarfs, R CrB stars and SNe IA (Invited Review)". In: *Planetary Nebulae*. Ed. by H. J. Habing and H. J. G. L. M. Lamers. Vol. 180. IAU Symposium, p. 85.

Zalewski, J. (1993). "Pulsational properties of post-AGB stars". In: 43, pp. 431–440.

Zhevakin, S. A. (1963). "Physical Basis of the Pulsation Theory of Variable Stars". In: 1, p. 367.

Zijlstra, A. A. and T. R. Bedding (2002). "Period Evolution in Mira Variables". In: *Journal of the American Association of Variable Star Observers (JAAVSO)* 31, pp. 2–10.

Zima, W. (2006). "A new spectroscopic mode identification method". In: *Communications in Asteroseismology* 147, pp. 56–60.

Zima, W. et al. (2006). "A new method for the spectroscopic identification of stellar non-radial pulsation modes. II. Mode identification of the δ Scuti star FG Virginis". In: 455, pp. 235–246. eprint: astro-ph/0606515.

Zwintz, K. et al. (2013). "γ Doradus pulsation in two pre-main sequence stars discovered by CoRoT". In: 550, A121, A121. arXiv: 1301.0991 [astro-ph.SR].

(2000). In: *Variable Stars as Essential Astrophysical Tools*. Ed. by Cafer İbanoğlu. Vol. 544. NATO Science Series. ISBN: 978-0-7923-6084-1.